Metal Complexes of Di(N-heterocyclic carbene) Ligands

Dissertation

der Mathematisch-Naturwissenschaftlichen Fakultät

der Eberhard Karls Universität Tübingen

zur Erlangung des Grades eines

Doktors der Naturwissenschaften

(Dr. rer. nat.)

vorgelegt von

M. Sc. Kim S. Flaig

aus Nürtingen

Tübingen

2018

Gedruckt mit Genehmigung der Mathematisch-Naturwissenschaftlichen Fakultät der Eberhard Karls Universität Tübingen.

Tag der mündlichen Qualifikation: 12.02.2019

Dekan: Prof. Dr. Wolfgang Rosenstiel

1. Berichtserstatter: Prof. Dr. Doris Kunz

2. Berichtserstatter: Prof. Dr. Reiner Anwander

Die vorliegende Arbeit entstand im Zeitraum von September 2015 bis Dezember 2018 am Institut für Anorganische Chemie der Eberhard Karls Universität Tübingen unter Anleitung von Frau Prof. Dr. Doris Kunz.

Mein besonderer Dank gilt Frau Prof. Dr. Doris Kunz für die Möglichkeit, diese Arbeit in Ihrem Arbeitskreis angefertigt haben zu dürfen, die hervorragenden Arbeitsbedingungen und die sehr gute Betreuung.

Der Ursprung der Wissenschaft liegt im Wissen, daß wir nichts wissen.

Fernando Pessoa

Quelle: Die Stunde des Teufels

For my parents

Abstract (german)

Die Dissertation handelt von der Synthese von Metallkomplexen mit zwei unterschiedlichen Di(N-heterocyclischen Carben)-Liganden vegi^{R} und mani^{R} (R = *t*Bu, *n*Pr).

Im ersten Teil wird der Gebrauch von metallhaltigen und metallfreien Basen zur Deprotonierung von vegi$^{R} \cdot 2HPF_6$ untersucht. Werden alkalimetallhaltige Basen verwendet führt dies zu den entsprechenden Alkalimetallkomplexen (Li, Na und K) aufgrund des starken chelatisierenden Charakters des Liganden. Die Zugabe der entsprechenden Kronenether zu den Alkalimetallkomplexen führte nur im Fall des labilsten Komplexes, des Kaliumkomplexes, zur Freisetzung des freien Dicarbens. Im Fall von Lithium vegi$^{t\mathrm{Bu}}$ wurde ein Gleichgewicht zwischen einem heteroleptischen- und homoleptischen Komplex beobachtet. Die Bildung des homoleptischen Komplexes wird durch Dispersionswechselwirkungen erklärt. Die Synthese der freien Dicarbene konnte durch die sehr starke metallfreie Phosphazenbase P_4-*t*Bu realisiert werden.

Im nächsten Kapitel wird eine neue Syntheseroute von dinuklearen Ag(I) und Au(I) vegi$^{t\mathrm{Bu}}$ Komplexen via Transmetallierung des *in situ* gebildeten Li-Komplexes mit $AgBF_4$ oder [AuCl(SMe_2)] aufgezeigt. Die Geometrie des dinuklearen Cu(I)-vegi$^{t\mathrm{Bu}}$-Komplexes konnte durch eine Kristalltrukturanalyse aufgeklärt werden.

Der dritte Teil beschäftigt sich mit der Synthese von Gruppe 10 Metallkomplexen der vegi$^{t\mathrm{Bu}}$ und vegi$^{n\mathrm{Pr}}$ Liganden. Paramagnetische Ni(II)-Komplexe und diamagnetische Ni(0)-Komplexe mit einer ungewöhnlichen Koordination an das Rückgrat des Liganden wurden hergestellt. In ersten Versuchen wurde der Ni(0)-Komplex als Katalysator in der Vinylcyclopropan-Umlagerung getestet. Die Synthese von quadratisch planaren Dimethyl- und Dichloridokomplexen der Metalle Palladium und Platin wird beschrieben.

Im letzten Teil der Arbeit geht es um die Reaktivität von mani$^{R} \cdot 2HPF_6$ gegenüber Li-, Na- und K-Basen. Zusätzlich wird die Generierung von [Pt(CH_3)$_2$(mani$^{n\mathrm{Pr}}$)$_2$] beschrieben.

Abstract (english)

This thesis deals with the synthesis of metal complexes of two different di(N-heterocyclic carbene) ligands vegi^{R} und mani^{R} (R = *t*Bu, *n*Pr).

In the first part the use of metal bases and metal-free bases to deprotonate vegi$^{R}\cdot 2HPF_6$ was investigated. Using alkali-metal (Li, Na and K) bases to deprotonate vegi$^{R}\cdot 2HPF_6$ the corresponding alkali-metal complexes form due to the strongly chelating character of the ligand. Adding the respective crown ethers to the alkali complexes led to the liberation of the free dicarbene only for the most instable complex, the potassium complex. In the case of lithium vegi^{tBu} an equilibrium between the heteroleptic and the homoleptic complex is observed. The formation of the homoleptic complex can be explained by dispersion interactions. The free dicarbenes can be generated using the strong metal-free phosphazene base P_4-*t*Bu.

The next part deals with a new synthesis route of known dinuclear Ag(I) and Au(I) vegi^{tBu} metal complexes via transmetalation of the *in situ* generated Li complexes with $AgBF_4$ or [$AuCl(SMe_2)$]. The geometry of the dinuclear Cu(I) vegi^{tBu} complex was elucidated by X-ray analysis.

The third part deals with the synthesis of group 10 metal complexes of vegi^{tBu} and vegi^{nPr}. Paramagnetic Ni(II) complexes and diamagnetic Ni(0) complexes with an unusual binding mode to the backbone of the vegi ligand are obtained. The Ni(0) was tested in first experiments as a catalyst in the vinylcyclopropane rearrangement. The synthesis of square planar dimethyl and dichlorido platinum- and palladium complexes are described.

In the last part the reactivity of mani$^{R}\cdot 2HPF_6$ toward Li, Na and K bases are presented as well as the generation of [$Pt(CH_3)_2$(mani^{nPr})$_2$].

Contents

1 Introduction

1.1 N-heterocyclic Carbenes

Carbenes are neutral compounds with a divalent carbon atom. The carbon atom is electron-deficient with only six electrons in its valence shell including two nonbonding electrons and no formal charge. Therefore, carbenes are reactive intermediates which usually are generated *in situ*. Dichlorocarbene (CCl_2), for example, can be synthesized via deprotonation of chloroform followed by an α-elimination.[1] The first free stable carbene, a phosphinocarbene, was isolated by *Bertrand et al.* in 1988.[2]

In NHCs (N-heterocyclic carbenes) - a special subgroup of carbenes - the carbene atom is part of a nitrogen containing heterocyclus. Pioneering work was carried out independently by *Öfele* as well as *Wanzlick* and *Schönherr* in the 60ies who first synthesized metal–N-heterocyclic carbene complexes in 1968.[3,4] Subsequent works by *Lappert et al.* examined the coordination properties and organometallic chemistry of these ligands.[5,6] A major breakthrough came from the *Arduengo* group with the isolation of "free" IAd (1,3-di(adamantyl)imidazol-2-ylidene).[7] Since then NHCs have become one of the most important classes of ligands in organometallic chemistry.[8–10]

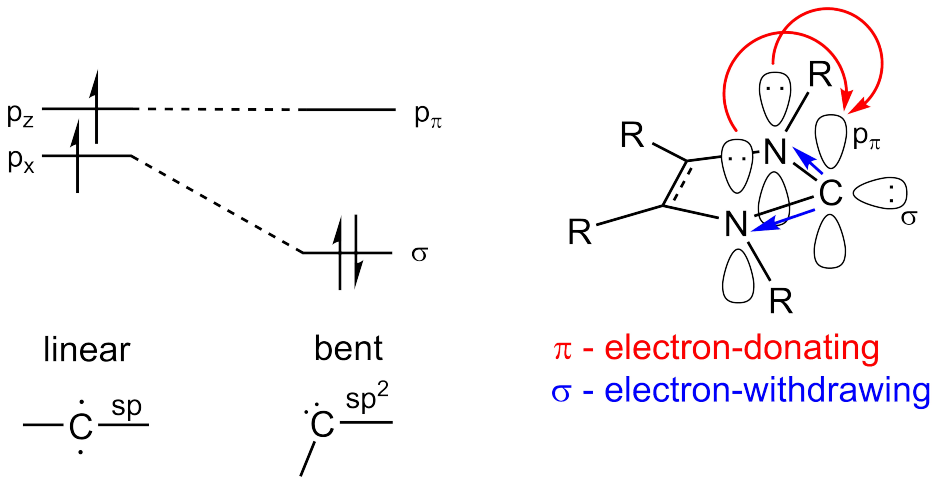

Figure 1: Left: Relationship between the carbene bond angle and the nature of the frontier orbitals.[11] Right: Ground-state electronic structure and stabilization principle of imidazol-2-ylidene.[12]

In general the geometry at a carbene carbon atom can be linear or bent (Figure 1: left). The linear geometry is based on an sp-hybridized carbon that has two energetically degenerated p orbitals (p_x,p_z), which leads to a triplet ground state. This geometry constitutes an extreme case. The degeneration of the π-orbital breaks in the bent carbene structure which contains an sp^2-hybridized carbon atom. The free p_π-orbital remains constant in energy while the former p_x-orbital has sp^2-character and gets strongly stabilized.[11] NHCs are nucleophilic carbenes because the empty π-orbital lies relatively high as well as the occupied σ-orbital.[10] The electronic situation of an NHC can be seen in Figure 1 on the right. The adjacent nitrogen atoms stabilize the singlet state of the NHC by π-electron donating and σ-electron withdrawing effects. In other words, the state is stabilized by both, inductively by lowering the energy of the occupied σ-orbital and mesomerically by donating electron density into the empty p-orbital, which leads to a four-π-electron 3-center system. The partially empty p-orbital can provide π acceptor character while the electron lone pair at the carbene functions as the donor. Additionally, unsaturated NHCs are stabilized by aromaticity.[13] Unsaturated NHCs are 25 kcal/mol more stable than the corresponding saturated NHCs.[14] Due to the large HOMO-LUMO gap, NHCs have a singlet ground-state with the HOMO best described as a formally sp^2-hybridized lone pair (σ orbital) and the LUMO as an unoccupied p-orbital at the carbene carbon atom. Due to their stronger σ-donor character compared to phosphines, NHCs can be used to create more electron-rich-metal "centers". NHCs have a stronger metal-bond in complexes then phosphines.[8,15] Interest in the design- and synthesis of novel NHCs and their metal complexes ensued following their application in homogenous catalysis by *Herrmann et al.* in 1995.[16]

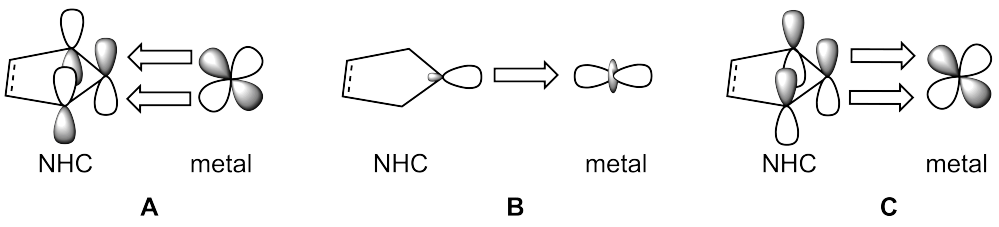

Figure 2: Schematical frontier orbital interactions between the NHC and a transition metal (nitrogen atoms in the NHC moiety are not shown).[17]

The interactions between an NHC and a transition metal center can be seen as a simplified diagram in Figure 2. The electronic interaction in the M-NHC bond contains three main components.[13] Electron density can be accepted by the NHC from the filled d-orbitals of the metal center (M $\rightarrow$ NHC π^*-backdonation; A). The main contribution is the donation of electron density from the NHC σ-orbital to an empty orbital on the metal center which is shown in red (NHC $\rightarrow$ M σ-donation; B). Another component is the π-donating bond of the NHC to the metal (NHC $\rightarrow$ M π-donating; C). Especially in bonds with electron-deficient metals, the NHC can donate electron density from its filled π orbitals to the empty d-orbitals of the metal.
NHC ligands are often formed by the deprotonation of an *N*,*N*'-disubstituted imidazolium or other azolium salts. As a result of the high-lying HOMO of free NHCs, binding of the C2-atom of the NHC to a transition metal leads to the formation of a very strong metal-carbon bond. The transition metal complexes can be synthesizeded via different ways, the most common ones are:[9]

- Synthesis of the free carbene and addition of a metal precursor.
- *In situ* deprotonation of the imidazolium salt with a base and addition of a metal precursor.
- Deprotonation of the imidazolium salt with a basic metal precursor.
- Transmetalation of a Ag- or Cu-NHC complex with a metal precursor.

1.2 Bis(N-heterocyclic Carbene)

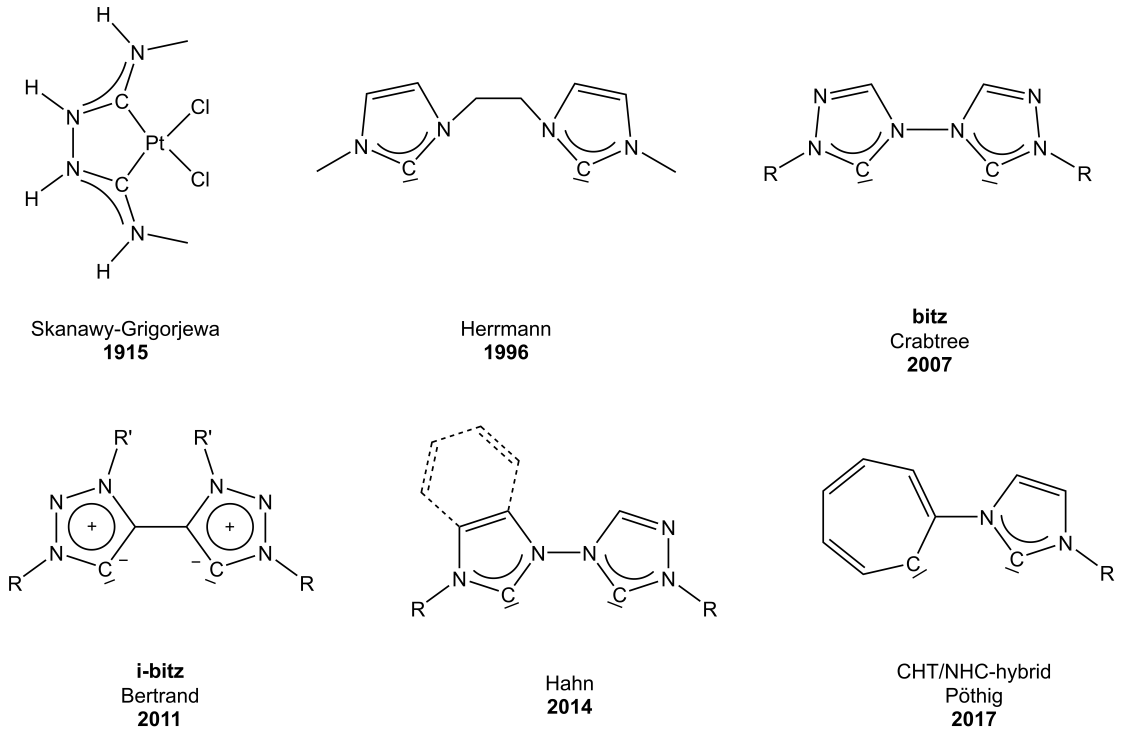

Figure 3: Selection of literature known biscarbene ligands.

The first synthesis of a dicarbene complex occurred in the early 20th century, when *Skanawy-Grigorjewa* followed a suggestion from *Tschugajeff* adding isonitrile, hydrazine and tetrachloroplatinate with hydrochloric acid.[18,19] Unfortunately, they did not have the required spectroscopic techniques at that time to reveal the formation of the first dicarbene complex and thought they had obtained a Pt-hydrazine complex. Years later *Balch*[20], *Rouschias*, and *Shaw* clarified independently the formation of an N-N connected Pt-dicarbene complex.[21] The first free isolated bis(NHC) was generated by *Herrmann* in 1996 with two imidazol-moieties bridged by an ethylene-group.[22] In 2007 an N-N connected dicarbene with triazole moieties was published, which shows free rotation around the N-N bond.[23] This so called bitz ligand is very flexible and coordinates in a chelating or bridging fashion. The attempt of isolating the free dicarbene resulted in a rearrangement, but its Rh, Ru and Pd complexes were synthesized.[23,24] An isomer of the bitz ligand is the C-C connected i-bitz ligand from *Bertrand*.[25] A 1,4-

difunctional mixed combination of a triazolinylidene and an imidazolinylidene is also known and was reported by *Hahn*.[26] Recently, *Pöthig* presented palladium complexes bearing a 1,4-dicarbene ligand which is a hybrid of a cycloheptatrienylidene (CHT) and an NHC.[27,28]

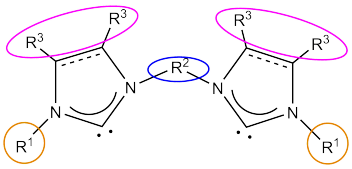

Figure 4: The modular structure of a dicarbene.

In bidentate carbene ligands two donor centers can coordinate to the metal atom in a chelating or bridging fashion. The electron density at the metal can be increased efficiently in the chelate complexes due to binding to the two NHC moieties. The properties of dicarbene ligands can be tuned by variation of the substitutents R^1, R^2 and R^3. R^1 mainly regulates the steric influence of the ligand. R^2 is the linker and has a major influence on the bite angle. The sterics and bite angle of the ligand regulate whether a chelating or bridging complex is obtained. If small R^1 substituents are used with a long linker then chelation is favored. Conversely, when long linkers and bulky steric R^1 groups are used chelation is avoided. Most bis-NHCs are designed to preferentially bind to the metal center in a chelating fashion. The design of non-chelating bis-NHCs is, however, also of great interest, as they can result in bimetallic structures that may lead to advances in the development of electronic materials.[29]

1.3 The dicarbene vegi

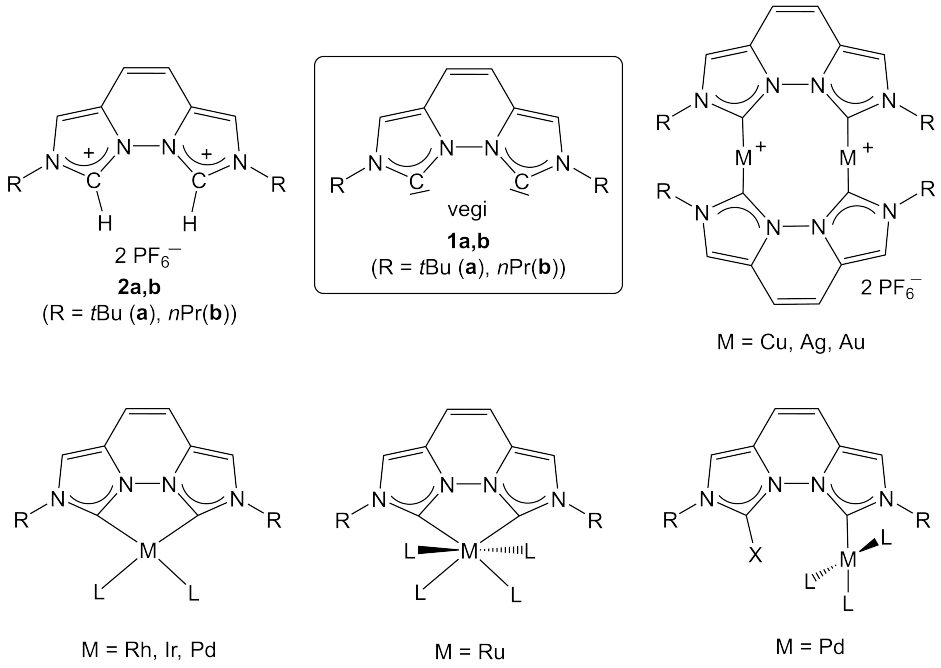

Figure 5: The bisimidazolium salt **2**, the dicarbene vegi **1** and known metal complexes with the vegi ligand.[30–35]

The synthesis of the bisimidazolium salts **2a,b** was first achieved by *Verena Gierz* in the *Kunz* group. The free dicarbene (**1a** and **1b**) was named vegi due to the first two letters of her name.[30,32] The ligand is an N,N-connected planar π-conjugated 1,4-dicarbene that can be regarded as an analogue of 1,10-phenanthroline and can be visualized as a merging of two monopyrido moieties. The empty π-orbital at the carbene carbon is part of the conjugated 14π-electron system of the vegi dicarbene and is therefore well stabilized. There is a variety of substituents known at the nitrogen atoms such as methyl-[36], *n*-propyl-[30], *tert*-butyl-[30,33], benzyl-[30,37] and phenyleth-1-yl[38]. In coinage metal complexes the vegi ligand adopts a bridging coordination mode. Also heterobimetallic complexes Cu-Ag and Ag-Au are known.[33] In all other known transition metal complexes the vegi ligand binds in a chelating fashion. In the Rh(I) and Pd(II) complexes the coordination geometry at the metal is square planar.[30,32] The Rh(I) complex is an active catalyst in transfer hydrogenation reactions of various ketones.[30,31] The Ru(II) complex obtains an octahedral coordination geometry at the

metal center.[30] The Ir(I) complex bis(NHC)(COD)-Ir undergoes an acid-catalysed COD isomerisation.[35] Unsymmetric Pd(II) complexes are also known with the vegi ligand prepared from a monochlorinated vegi-species with DBU and a Pd(II) precursor, but not fully structurally characterized.[34] Despite its rigid geometry, the vegi-ligand is still so flexible that it can not only act as a chelating, but also as a bridging ligand.

2 Purpose and Motivation

One goal was to exchange the counteranion from PF_6^- in the known bis(imidazolium) salt **2a**[30,32] to Cl^-. This ligand precursor would be advantageous in the generation of the free dicarbene **1**. Deprotonation reactions with alkali-metal bases could lead to the formation of alkali-chloride salts of low solubility and the desired dicarbene **1**. Another benefit from a ligand precursor with chloride anions would be the generation of dichlorido vegi metal complexes without adding an additional chloride source. Another goal was the isolation and crystallization of the free dicarbene **1a**. This would open new possibilities for the synthesis of other vegi metal complexes by simple coordination of the carbene to the metal instead of transmetalation. The π-acceptor ability of **1a** should be determined by the synthesis of selenium adducts. Due to the strong chelating character of **1a** and **1b** the deprotonation of **2a** and **2b** with cesium bases was of interest as well as to see whether the very first cesium NHC complex could be obtained.

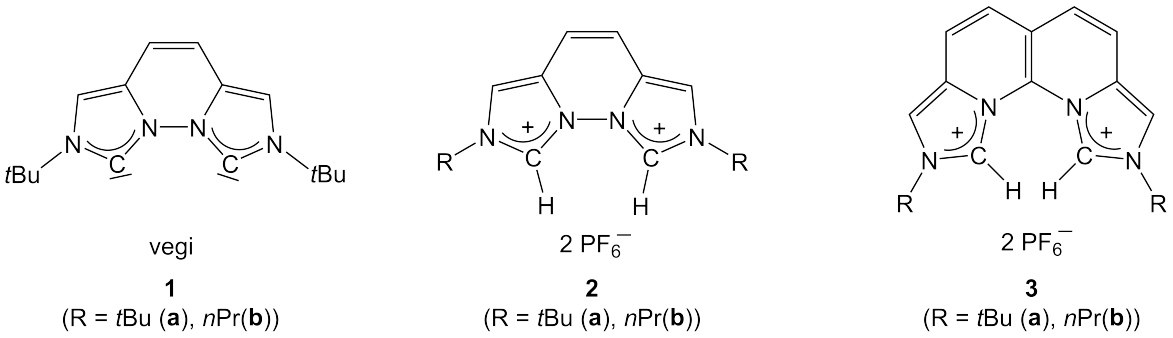

Figure 6: The ligand precursors **2a,b** and **3a,b** and the free dicarbene **1a,b** used in this work.

In the next chapter a new synthesis route of the known dinuclear Ag(I) and Au(I) vegi^{tBu} complexes was targeted and transferred to the synthesis of heterobimetallic complexes. The dinuclear Ag(I) complex was further tested in transmetalation reactions. Elucidation of the molecular structure of the dinuclear Cu(I)**1a** complex was another issue to compare its geometry with that of the other coinage metal complexes.

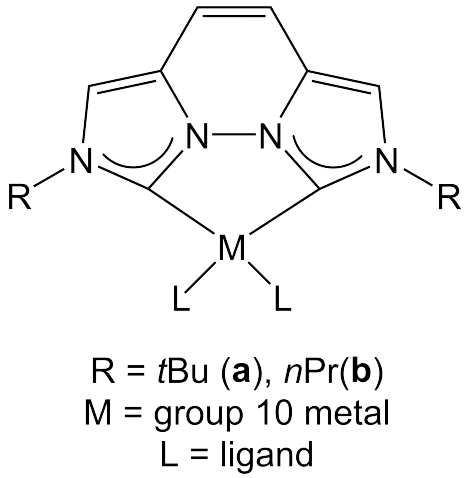

Figure 7: The general structure of chelating group 10 metal metal vegi complexes.

Another emphasis was put on the synthesis of chelating group 10 metal complexes of vegi^{R} (Figure 7). Especially the synthesis of a Ni(0) vegi^{R} complex, a potential catalyst in the vinylcyclopropane rearrangement was of interest. Furthermore, finding access to palladium- and platinum vegi^{R} complexes with dimethyl- and dichlorido ligand was of interest.

In the last part the reactivity of the mani^{R} ligand precursor **3a,b** should be investigated towards deprotonation with alkali-metal and metal-free bases in comparison to vegi^{R}. The generation of mono- or dinuclear Ag(I) mani^{R} complexes was of interest as well.

3 Ligand precursors

3.1 Bis(imidazolium) salts

In this work two different bis(imidazolium) salt systems were used as ligand precursors. The synthesis of the bis(imidazolium) salt vegi$^{R} \cdot 2HPF_6$ was developed by *Gierz* in our research group in 2010.[39,40] The other bis(imidazolium) salt mani$^{R} \cdot 2HPF_6$ (**3a,b**) was synthesized in 2017 by *Steimann* in our research group. This anellated naphthyridine based bis(imidazolium) salt with 18π-electrons also contains PF_6^- counterions.
In this work **2a** and **2b** were synthesized by me, while the mani$^{t\mathrm{Bu}}$ and mani$^{n\mathrm{Pr}}$ ligand precursors **3a** and 3**b** had been synthesized by *Steimann* and were only used by me as ligand precursors.[41]

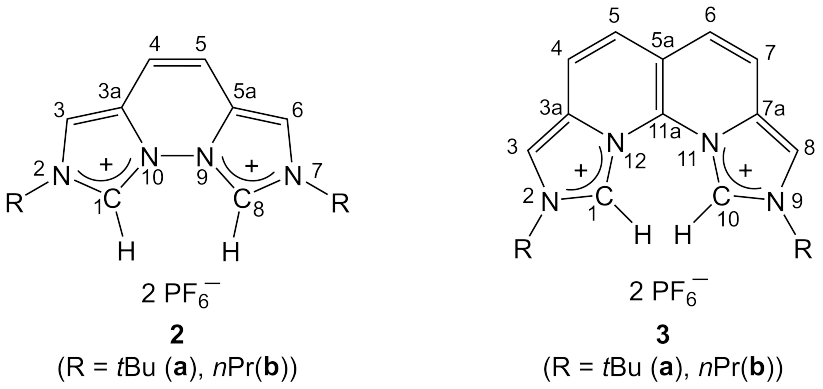

Figure 8: The bis(imidazolium) salts vegi^{R} **2** and mani^{R} **3** used in this work.

3.2 Synthesis of the bis(imidazolium) salts according to *Gierz*

The synthesis of vegi$^{R} \cdot 2HPF_6$ (R = *n*Pr (**2b**), Bn) was published in 2010.[39,40] The sterically more hindered *tert*-butyl groups (**2a**) were also introduced to obtain the vegi$^{t\mathrm{Bu}}$ ligand which was first synthesized by *Gierz* as well.[30,42]

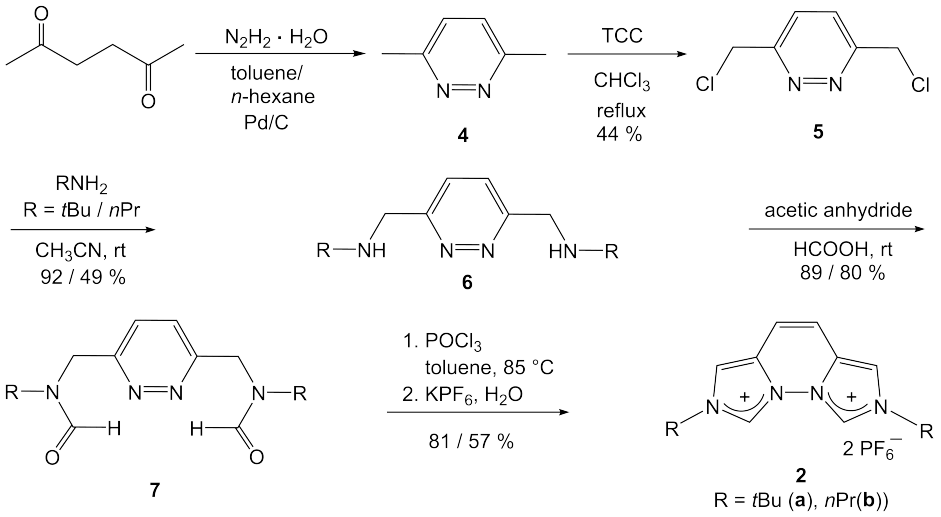

Figure 9: Synthesis of the bis(imidazolium) salts **2a** and **2b**.

The starting material 3,6-dimethylpyridazine (**4**) can be synthesized from 2,5-hexanedione and hydrazine hydrate via a condensation reaction followed by a dehydrogenation with palladium on activated carbon. The synthesis was carried out according to *Wiley*[43,44] with a modification by *Raible*.[45]

The next four-step synthesis of the bis(imidazolium) salt **2a,b** was developed by *Gierz*[31] and starts with the formation of 3,6-bis(dichloromethyl)pyridazine (**5**). In an electrophilic chlorination with trichloroisocyanuric acid, the regioselective formation of the bischlorinated product **5** was achieved. It is important to use amylene stabilized chloroform as a solvent instead of ethanol stabilized chloroform. Byproducts of differently chlorinated species must be separated by column chromatography. A 44 % yield of the chlorinated product **5** can be isolated as colorless crystals.

In the next step, 3,6-bis(chlormethyl)pyridazine (**5**) was reacted with an excess of the corresponding amine (*tert*-butylamine or *n*-propylamine) in acetonitrile to obtain the corresponding diamine **6a,b** via a nucleophilic substitution. The straightforward reaction led to the clean formation of the desired product as a beige solid. Then 3,6-bis(*tert*-butylaminomethyl)pyridazine (**6a**) is formylated with a 1:1 mixture of acetic anhydride and formic acid to obtain 3,6-bis(*tert*-butylformamidomethyl)pyridazine (**7a**) in 89 %

yield. Due to hindered rotation of the amide bond three conformers are obtained in the case of the *n*-propyl substituted product. In case of the *tert*-butyl groups only one conformer forms.

The final product can be synthesized by cyclization of **7a,b** with $POCl_3$ in a Bischler-Napieralski type-reaction in toluene at 80 °C. In the last step, the counterion is exchanged to PF_6^- by addition of KPF_6 to an aqueous solution of the raw material. The products were isolated as beige solids with an overall yield of 20 % for **2a** and 10 % for **2b**.

The ^{1}H NMR data of vegi$^{t\mathrm{Bu}} \cdot 2HPF_6$ and vegi$^{n\mathrm{Pr}} \cdot 2HPF_6$ are summarized in Table 1 and are in agreement with the literature.[31] Although the bisimidazolium salts **2a** and **2b** are poorly soluble in THF-d_8, analyzable ^{1}H NMR spectra were obtained. The chemical shifts in THF-d_8 are helpful as a control for further reactions. The signals for the hydrogen atoms 1/8 are in the down-field region for both bis(imidazolium) salts, indicating an acidic character of these hydrogen atoms. This indicates that deprotonation reactions take place at H-1/8. The signals H-1/8 and H-3/6 show a ^4J-coupling depending on the solvent.

Table 1: ^{1}H NMR data of the literature known bis(imidazolium) salts. The chemical shifts in THF-d_8 is new data.

	solvent	^{1}H NMR [ppm]					
		H-1/8	H-3/6	H-4/5	R		
vegi$^{t\mathrm{Bu}} \cdot 2HPF_6$	DMSO-d_6	10.64 (d)	8.79 (d)	7.71	1.76		
	CD_3CN	9.7 (d)	8.22 (d)	7.54	1.79		
	THF-d_8	10.22	8.35	7.46	1.79		
vegi$^{n\mathrm{Pr}} \cdot 2HPF_6$	DMSO-d_6	10.57	8.51 (d)	7.76	4.55	1.95	0.95
	CD_3CN	9.72	8.06	7.57	4.47	2.01	1.00
	THF-d_8	10.05 (d)	8.19 (d)	7.54	4.48	2.06	1.06

Before the anion exchange from Cl^- to PF_6^- anion, the counterion $PO_2Cl_2^-$ is also

present in the mixture. Therefore, it is advantageous to exchange the anion from Cl^- to PF_6^- with KPF_6 in an aqueous solution of the raw material at 50 °C to easily remove all undesired counterions first.

At the beginning of my work, the goal was to obtain a vegi^{tBu}· 2HCl (**8**) ligand precursor, as the deprotonation with alkali-bases would then lead straightforwardly to the free dicarbene by precipitation of the alkali-metal chlorides. Another benefit would be the generation of dichlorido complexes without adding an additional chloride source.

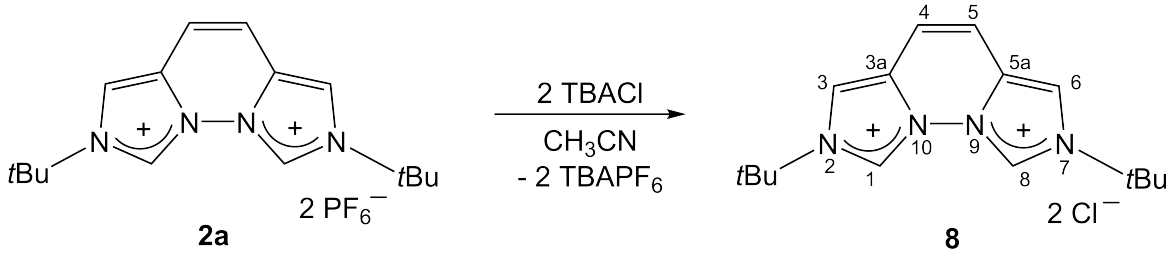

Figure 10: Anion exchange from **2a** to **8**.

The vegi^{tBu} · 2HPF$_6$ was tested in the anion exchange from PF_6^- to Cl^-. **2a** and tetrabutylammonium chloride (TBACl) were suspended in acetonitrile. **2a** is soluble in acetonitrile whereas TBACl is poorly soluble. The suspension was stirred for 2.5 h at room temperature. The mixture was then concentrated and filtered. The residue and the filtrate were dried separately. The residue was washed with acetonitrile and dried, it contained the bis(imidazolium) salt vegi^{tBu}· 2HCl as a white-off solid in a 18 % yield. The ^{1}H NMR spectrum shows the signal for the acidic protons H-1/8 at 13.09 ppm which is shifted 3.35 ppm down-field compared to that of **2a**. The other signals are only affected by less than 0.04 ppm. The ^{1}H NMR spectrum of the filtrate also shows the signals for vegi^{tBu}· 2HCl. This explains the low yield of 18 % of the residue because the salt is soluble in acetonitrile and additional signals for the tetrabutylammonium cation are present. The ^{31}P NMR spectrum of the filtrate shows the septet of the PF_6^- anions at -144.6 ppm ($^1J_{PF}$ = 706 Hz). In the ^{31}P{^{1}H} NMR spectrum of the washed residue only the middle peak of the septet is visible. Therefore, only small amounts of PF_6^- from TBAPF$_6$ or **2a** are still present in the mixture of vegi^{tBu}· 2HCl after workup.

The ESI mass spectrum shows a signal at m/z = 271.1 (100) [M-2Cl$^-$+PF_6^-]$^+$ and two small signals at m/z = 307.1 (0.3) [M-Cl$^-$]$^+$ and m/z = 416.9 (0.5) [M-2Cl$^-$+PPF_6^-]$^+$ of the PF_6^- anion containing products.

Other solvents must be used to synthesize vegi^{tBu}· 2HCl (**8**) to obtain a higher yield. A possible solution is a reaction of the mixture after the cyclization before the PF_6^- exchange.
Therefore, after the cyclisation with $POCl_3$, the residue was washed with diethyl ether. The ^{1}H NMR spectrum indicates the formation of **2a**. The residue is suspended in acetonitrile and filtered off and the solution is stored at -28 °C (fraction 1). A solid starts to crystallize which was filtered off (fraction 2) and the solution was again stored at -28 °C. Again a solid formed (fraction 3). In all three fractions **2a** was confirmed by NMR spectroscopy. Also the chloride was detected with $AgNO_3$ in all three fractions. In the ESI mass spectrum of fraction 1 a signal at m/z 307.2 can be detected for [M-Cl]$^+$. In fraction 2 this signal is missing whereas the signal for $PO_2Cl_2^-$ at m/z = 132.8 is found. In all three fractions three signals are detected in the ^{31}P{^{1}H} NMR spectrum, which are comparable to $PO_2Cl_2^-$.[46] Crystallization experiments failed because the solids were only soluble in H_2O and DMSO. To remove all phosphorus containing species three experiments were done. The species were hydrolyzed to phosphate, hydrogenphosphate or dihydrogenphosphate. Afterwards a saturated aqueous $CaCl_2$ solution was used to separate the anions by precipitation of $Ca_3(PO_4)_2$. It was necessary to add DBU as a base for full precipitation. In every reaction a solid formed, the precipitate was filtered off and the filtrate concentrated to dryness. The ^{1}H NMR spectra showed many unknown signals, and additional DBU signals. Therefore, a strong basic anion exchanger (Cl^- from Amberlite® IRA-402, Merck, 0.6-0.75 mm) was used. A mixture of **8**/**2a** was filtered over a column charged with the anion exchanger. The measured ^{31}P{^{1}H} NMR spectrum from the filtrate also showed the typical signal for PF_6^-.

2a was used for further experiments, because the synthesis of **8** was not straightforward. The experiment with the anion exchanger was carried out once. This experiment could

be repeated with different solvents to possibility obtain pure **8**.

3.3 Selenium Adducts

Although NHCs were initially believed to be mainly σ-donor ligands, studies show that they can accept electron density via π-back donation from the metal, which contributes to the overall strength of the metal-carbene bond.[13]

Different methods have been used to determine the π-accepting ability of NHCs.[47,48] *Ganter* employed ^{77}Se NMR spectroscopy (I = 1/2, 7.5% natural abundance) of selenium carbene adducts (selenoureas). The chemical shifts of the adducts correlate with the π-acceptor character of the respective carbene. The higher the π-acidity, the more downfield shifted is the signal. The selenoureas were synthesized using KHMDS as a base to deprotonate the bis(imidazolium) salts at -78 °C in presence of elemental selenium.[49] Works by *Nolan* demonstrate the use of KO*t*Bu as a base at room temperature to generate the selenium carbene adducts.[50,51]

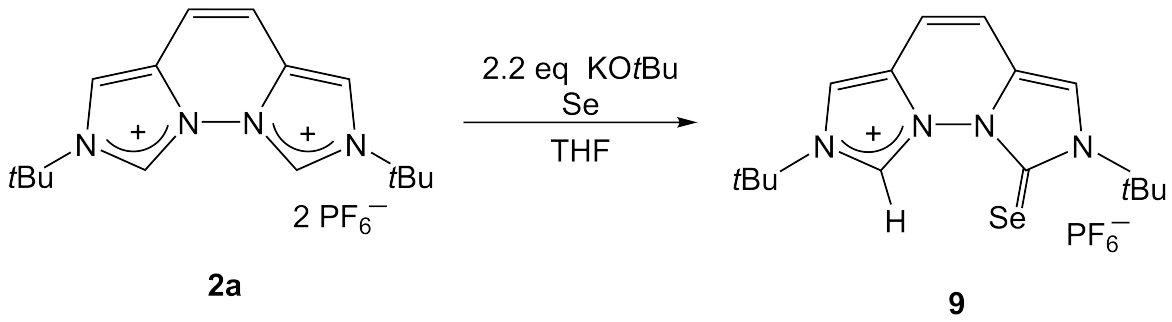

Figure 11: Synthesis of **9**.

Selenium adducts of the vegi$^{t\mathrm{Bu}}$ ligand were synthesized according to *Buck* from our research group.[52] Therefore, the bis(imidazolium) salt vegi$^{t\mathrm{Bu}} \cdot 2\mathrm{HPF}_6$ (**2a**) was suspended in THF and elemental selenium was added. The suspension was cooled to - 35 °C. Then a solution of KO*t*Bu in THF was added. After the mixture had been stirred for 30 min at -35 °C it was heated slowly to room temperature and stirred overnight. All volatile species were removed under vacuum. Dichloromethane was added to the grey residue and the suspension filtered over Celite®. The yellow fil-

trate was dried. If only one equivalent of KO*t*Bu and one equivalent of selenium was used, then **9** was obtained. The H-1 signal shifts down-field to 13.02 ppm in the ^{1}H NMR spectrum. The ^{77}Se NMR shows a signal at 250 ppm. In comparison, IMes (1,3-dimesitylimidazol-2-ylidene) has a shift of 35 ppm and has a poor π-acceptor ability. SIMes (1,3-bis(2,4,6-trimethylphenyl)-4,5-dihydroimidazol-2-ylidene) has a signal at 116 ppm and is a stronger π-acceptor. In comparison the down-field shifted signal of **9** indicates a relatively strong π-acceptor character. However, an interaction between the selenium atom and the proton could lead to a distortion of the selenium signal in the ^{77}Se NMR spectrum as indicated by the strong down-field shift of the proton signal. Using two equivalents of selenium led to the formation of one symmetric species in the ^{1}H NMR spectrum with signals at 1.72, 5.86 and 7.28 ppm in CD_3CN.

4 Alkali-metal vegi^{R} complexes

The pK_a values of the 2-position of the conjugate acid of imidazol-2-ylidene derived structures lie between 16-24.[53–56] Stable NHCs[7] usually can be synthesized by deprotonation of the respective imidazolium salts with strong alkali-metal bases such as alkyllithium, lithium amides and sodium hydride, potassium *tert*-butoxide or medium-strong bases such as potassium *tert*-butanolate and even sodium acetate. After removal of the metal salts by filtration or by distillation, the free carbenes can be isolated.[7,9,11,57–59] All mentioned pK_a values for the used bases in the next chapter are from the *Evans* and *Bordwell* tables and refer to the corresponding acids.[60,61]

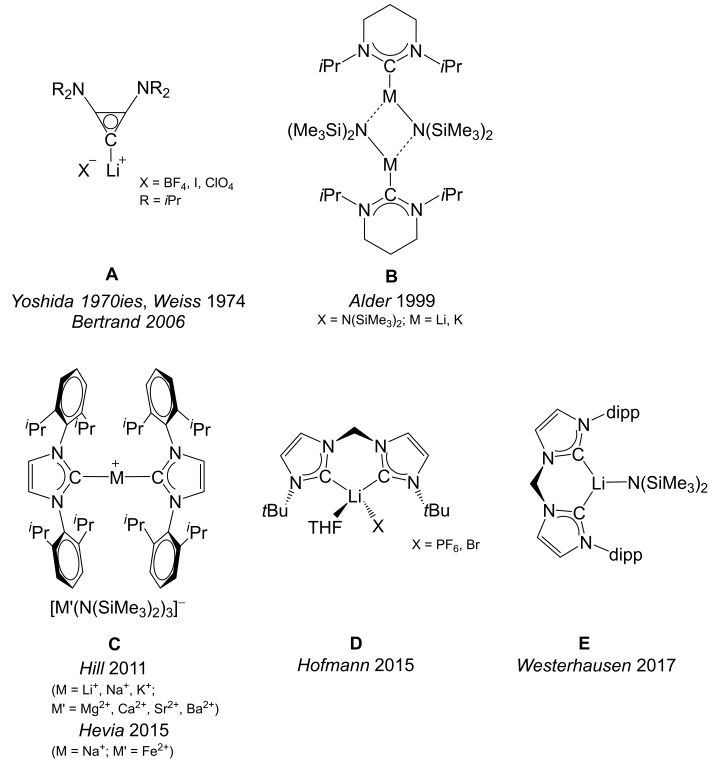

Figure 12: Selection of literature known alkali-metal NHC complexes.

In some literature known examples, the alkali-metal ions from the used base remain coordinated to the carbene during the synthesis resulting in the corresponding alkali-metal complexes.[62] An example is the so-called Weiss-Yoshida carbene **A**. The three-membered-ring isomer of an imidazolinylidene was first isolated and described as its lithium complex in the 70ies.[63–65] It was not even possible to liberate the carbene with [12]-crown-4 and the coordination of the lithium atom is independed of its counterion which was shown by *Bertrand* in 2006. With bases containing the softer Lewis-acidic potassium cation, the free carbene could be isolated.[66,67] The intended synthesis of alkali-metal bases can be achieved by adding alkali-metal salts to the free carbene as demonstrated by *Alder*.[68] In comparison to lithium NHC complexes, sodium and potassium NHC complexes are very rare. They can be generated from the free carbene by the addition of an excess of potassium salts or potassium hexamethyldisilazide (example **B**).[68,69] They can also be synthesized by a transfer reaction of the HMDS anion to a more strongly coordination counterion (example **C**).[70–72] Chelation of lithium ions with a second NHC moiety was shown by *Hofmann et al.* with a dicarbene

ligand. The deprotonation with potassium bases lead to the free dicarbene.[73] The dicarbene **E** only acts as a chelating ligand with the small and hard lithium ion. With NaHMDS or KHMDS dinuclear structures are obtained.[69] As NHCs are relatively strong σ-donors, they seem to be promising ligands for the complexation of s-block metal ions.

The general synthesis of alkali-metal complexes will be discussed in the following. In Figure 13 the reaction pathway is shown.

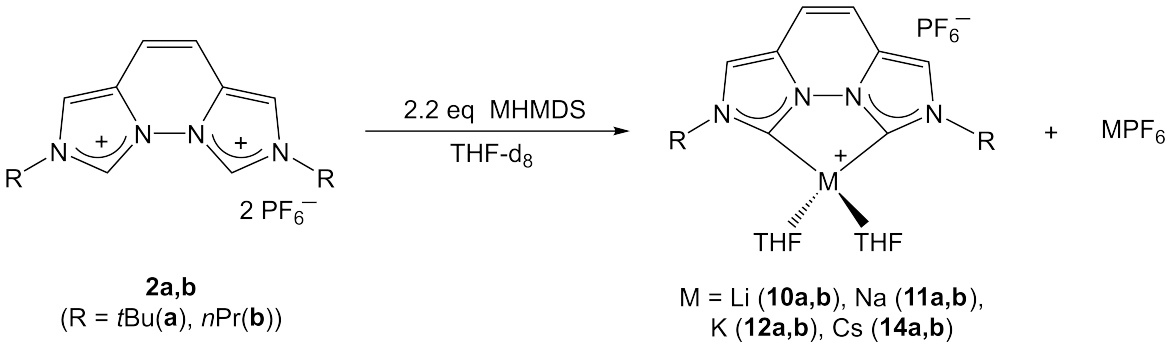

Figure 13: Formation of the alkali-metal complexes.

4.1 Synthesis of Lithium vegi^{R} complexes

The generation of the Li complexes was carried out *in situ* without any further workup. Therefore, $LiPF_6$, hexamethyldisilazane (HMDS) and traces of lithium hexamethyldisilazide (LiHMDS) are present in the reaction mixture. They could not be removed and were thus part of the NMR spectroscopic studies of the equilibrium in solution.

4.1.1 Deprotonation of the *N*-*n*-propyl-substituted bis(imidazolium) salt 2b

The deprotonation of *N*-*n*-propyl-substituted bis(imidazolium) salt **2b** with two equivalents methyllithium (MeLi, pK_a = 48 (H_2O), 56 (DMSO)) in THF-d_8 at -30 °C (to generate the free dicarbene) led to the absence of the signal for the imidazolium protons. It was initially assumed by *Gierz* that the free carbene was formed.[40] A ^{1}H NMR

spectrum after one hour at room temperature showed only signals of decomposition products.[31,40] The deprotonation reaction was repeated by *Raible*.[45] He showed that a slight excess of the base is required to fully deprotonate vegi$^{n\mathrm{Pr}} \cdot 2\mathrm{HPF}_6$. He could also deprotonate **2b** with *n*-BuLi (pK_a = 56 (DMSO)) at -78 °C in THF or toluene. Extraction experiments with diethyl ether, toluene or *n*-pentane to remove the vegi-species from the lithium salts were unsuccessful. This was an early indication that the formed species was not the free dicarbene, which should be soluble in nonpolar solvents. The carbene signal was detected at 185.4 ppm at room temperature. This chemical shift is atypical for a free unsaturated carbene, whose signals are usually found between 206-220 ppm,[34,68,74,75] and points to predict the formation of a lithium adduct. Organolithium compounds tend to form oligomeric structures[76] therefore, different structures of a formed lithium adduct could be possible. The formation of a heteroleptic lithium vegi$^{n\mathrm{Pr}}$ complex with two THF molecules and one vegi ligand coordinating to the lithium atom and of a homoleptic lithium complex with two vegi ligands are the most probable structures. DFT calculations by *Raible* on the vegi$^{\mathrm{Me}}$ ligand also support the formation of a lithium adduct. The calculated ^{13}C-carbene signals (188.5 ppm for the homoleptic (H-) Li complex and 185.7 ppm for the heteroleptic lithium complex) for the proposed lithium structures are close to the experimental value for vegi$^{n\mathrm{Pr}}$ at 185.4 ppm. *Raible* did not observe the abstraction of the lithium atom from the carbene after adding [12]-crown-4 to the reaction mixture, indicating a chelating coordination of the vegi$^{n\mathrm{Pr}}$ ligand and a strong coordination.[45]

The deprotonation reactions were repeated with MeLi and *n*-BuLi and also with LiHMDS (pK_a = 26 (THF), 30 (DMSO)). A brown-red suspension formed after adding LiHMDS to the beige suspension of the vegi$^{n\mathrm{Pr}} \cdot 2\mathrm{HPF}_6$ salt in THF. For all deprotonation reactions a slight excess of the base (around 2.2 equivalents) was used due to the impurity of the base, and the observation by *Raible*. After the bis(imidazolium) salt **2b** was reacted with 2.2 equivalents of LiHMDS in THF no imidazolium peaks and the presence of two broad signals at 7.03 ppm for the pyridazo (H-4/5) and at 7.56 ppm for the imidazo protons (H-3/6) were detected in the ^{1}H NMR spectrum. In the ^{13}C{^{1}H} NMR spectrum a carbene signal was detected as a singlet at 185.3 ppm.[42]

All chemical shifts matched those of *Raible*.

4.1.2 Deprotonation of the *N*-*tert*-butyl-substituted bis(imidazolium) salt 2a

Then the bulkier *tert*-butyl-substituted salt **2a** was used for deprotonation reactions to see if the steric has any additional effect. The deprotonation reaction takes place in THF-d_8 with Li-bases such as LiHMDS, *n*-BuLi or MeLi and leads to the same products. In the following the deprotonation reaction with LiHMDS is discussed. After adding the base to the beige suspension of **10a** in THF-d_8 a brown-red solution forms. In the ^{1}H NMR spectrum the formation of not only one new signal set but also a second set in a 1:1 ratio was observed. The aromatic backbone signals (H-4/5 and H-3/6) are not baseline separated but the *tert*-butyl signals are separated by 0.17 ppm and are at 1.51 ppm and 1.68 ppm.

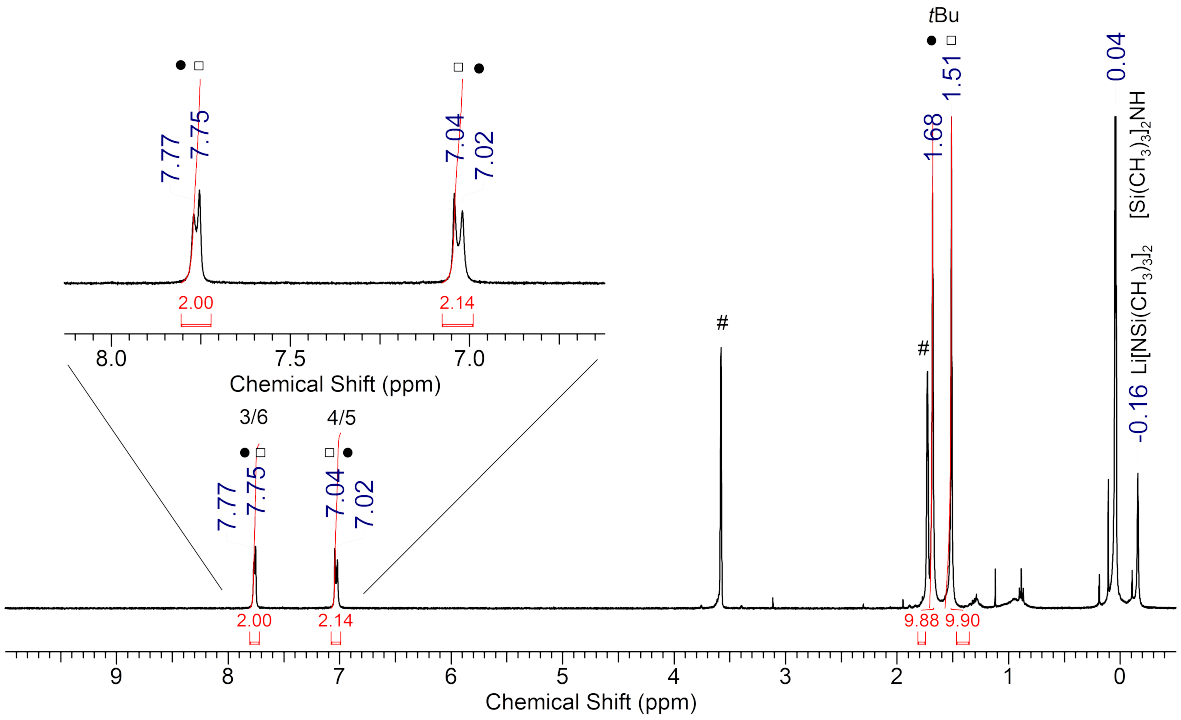

Figure 14: ^{1}H NMR spectrum at room temperature of Li-vegi^{tBu} complexes (square = **10a-H**, circle = **10a**).

Such a strong change of the environment around the *tert*-butyl groups could result

from a species in which two carbene ligands are coordinated to the lithium atom, and the *tert*-butyl groups would be affected by the aromatic deshielding effect of the second ligand. The other Li complex could be a heteroleptic complex with two THF molecules and one vegi$^{t\mathrm{Bu}}$ ligand coordinated to the lithium atom. To clarify their structures further NMR experiments of both formed Li-species in solution were conducted.[42]

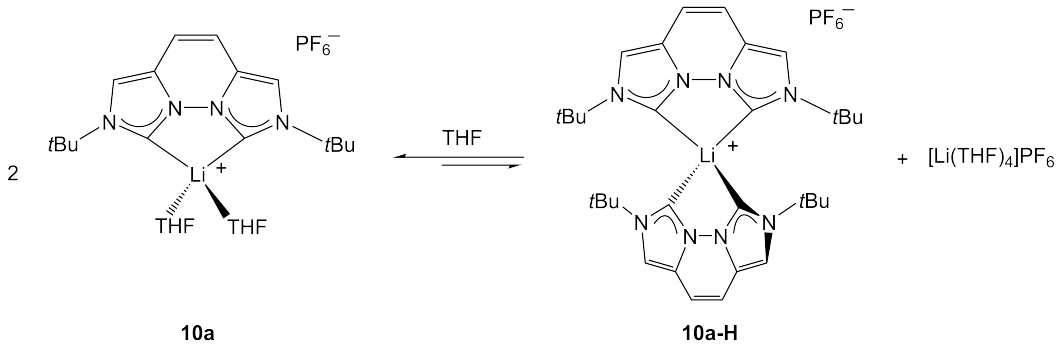

Figure 15: The equilibrium reaction between **10a** and **10a-H**.

The mixture was cooled down to -80 °C and a ^{1}H NMR spectrum was measured. The low temperature led to sharp signals. The ratio of the signal pairs changed to 1:0.8, which confirms the presence of two species in equilibrium. Upon warming, the coalescence of the signals H-3/6 (8.0 ppm) and of the signals H-4/5 (7.18 ppm) is observed at 60 °C, while the *tert*-butyl signals still remain separated. Thermodynamically, complex **10a** is favored.

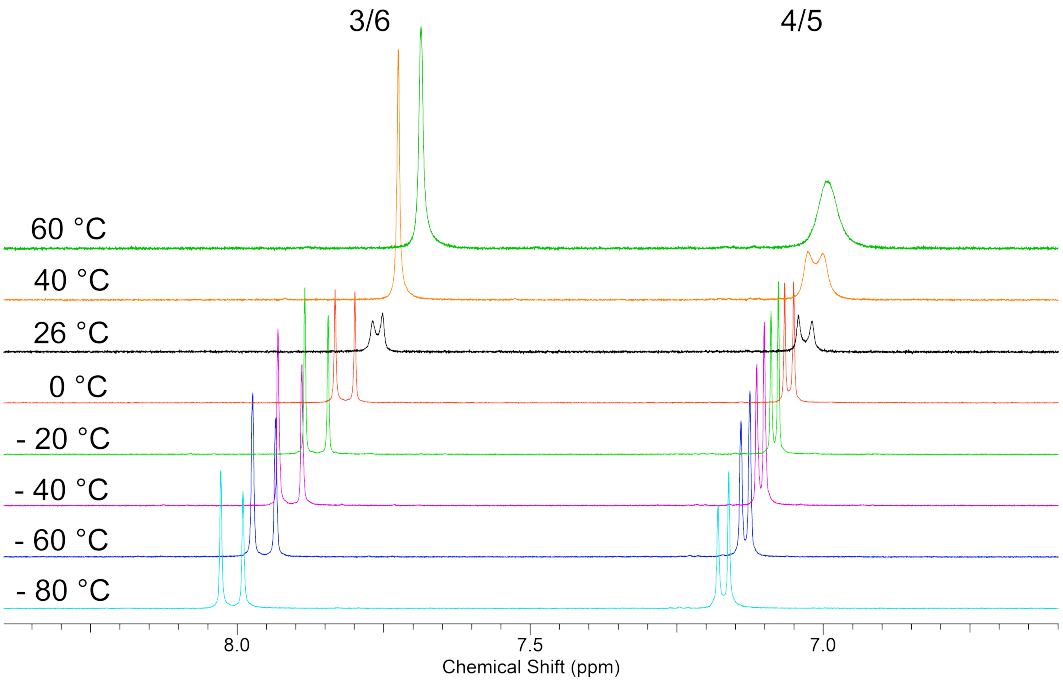

Figure 16: VT ^{1}H NMR spectra (detail, -80 °C to +60 °C) showing two signal sets that begin to coalesce at 40 °C of **10a** and **10a-H**.

The ^{7}Li NMR spectrum (I = 3/2, 92.4% natural abundance) shows one relatively sharp peak at 3.2 ppm and two broad peaks at 1.5 ppm (smaller) and 0.4 ppm (larger) at room temperature. Upon cooling to -80 °C all peaks become sharp and baseline separated. The integrals of the peaks at 3.16 ppm, 1.51 ppm, 0.16 ppm, and -0.40 ppm show a ratio of 0.4:1:0.3:1.9. The peak at -0.40 ppm results from $LiPF_6$ and the peak at 0.16 ppm from traces of LiHMDS. Lithium compounds with these chemical shifts are considered solvent-separated ion pairs, whereas higher chemical shifts indicate a more covalent character of the lithium-carbon bond.[77]

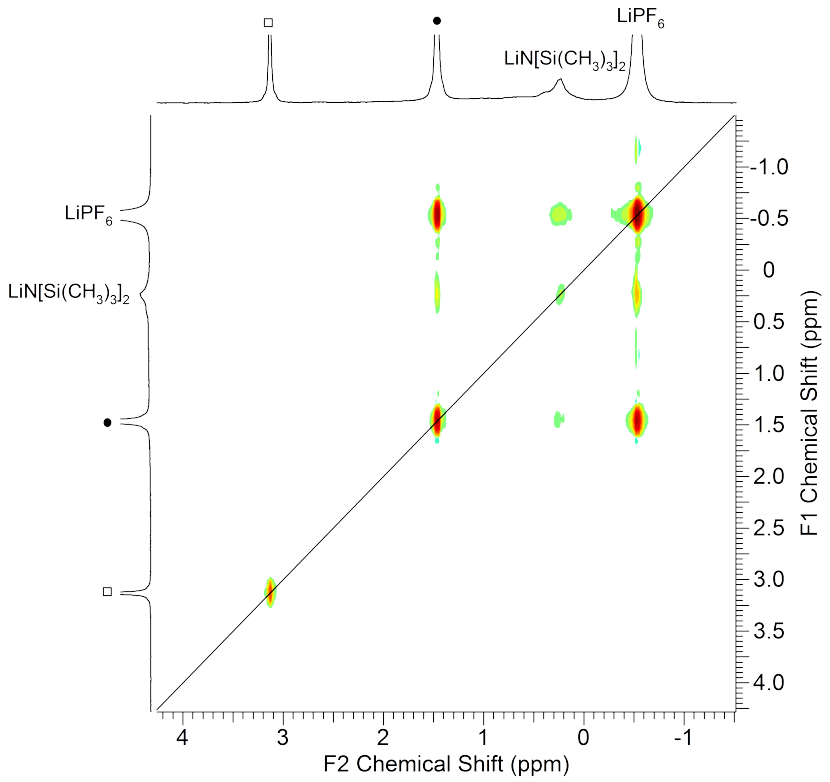

Figure 17: ^{7}Li,^{7}Li EXSY NMR spectrum (-40 °C).

The connection of the 0.4:1 ratio of the ^{7}Li NMR signals at 3.16 and 1.51 ppm with the respective 1:0.8 ratio observed for the ^{1}H NMR signals at 1.68 and 1.51 ppm, is indicative of the formation of complex **10a** which contains one vegi$^{t\mathrm{Bu}}$ ligand with the ^{1}H NMR *tert*-butyl signal at 1.68 ppm and the ^{7}Li NMR signal at 1.51 ppm and of a second homoleptic complex **10a-H** containing two vegi$^{t\mathrm{Bu}}$ ligands with the ^{1}H NMR *tert*-butyl signal at 1.51 ppm and the ^{7}Li NMR signal at 3.16 ppm. A complex ratio of 1:0.4 results (**10a** and **10a-H**). The theoretical amount of $LiPF_6$ formed is 1 equivalent of $LiPF_6$ per **10a** and 1.5 equivalent of $LiPF_6$ per complex **10a-H**, so that a total integral of $1 + 0.6 = 1.6$ is expected, which fits to the observed value of 1.9.

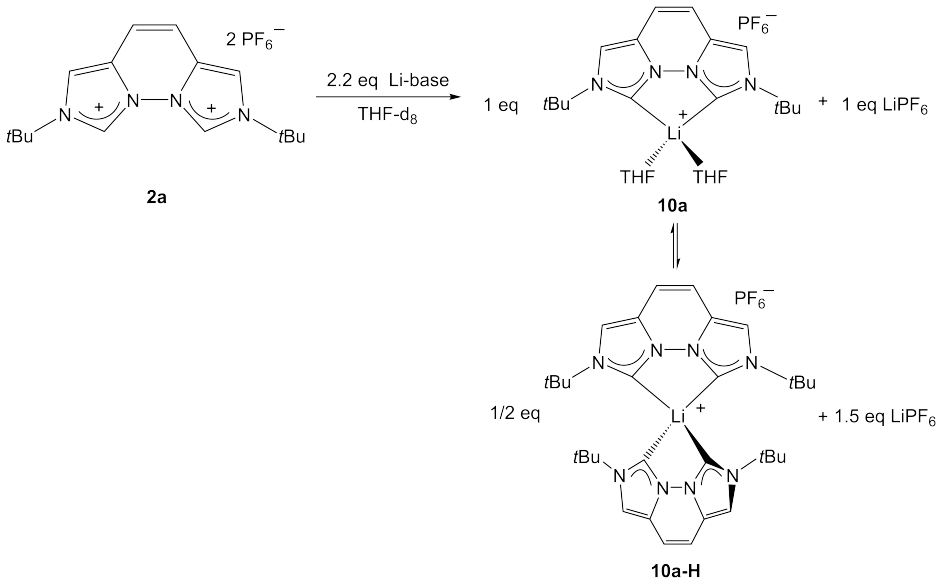

Figure 18: The equilibrium reaction of the Li-complexes.

A ^{7}Li,^{7}Li EXSY NMR experiment at -40 °C reveals that **10a** is the more dynamic complex and undergoes a fast exchange, with residual LiHMDS and $LiPF_6$ while no exchange on the NMR time scale is observed for the Li ion of the homoleptic complex **10a-H** containing two vegi$^{t\mathrm{Bu}}$ ligands.

The ^{13}C NMR spectrum measured at -80 °C confirms the formation of two carbene Li complexes by the two carbene signals found at the characteristic chemical shifts of 184.3 ppm (**10a-H**) and 182.2 ppm (**10a**) (assignment by 2D ^{1}H, ^{13}C{^{1}H} NMR experiments) in which the direct Li-C coupling of $^{1}J_{\mathrm{CLi}}$ = 22.7 Hz (**10a-H**) and 24.2 Hz (**10a**) leading to a 1:1:1:1 quartet for each carbene signal is resolved (see Figure 19). At room temperature only the carbene signal of **10a-H** shows a Li-C coupling ($^{1}J_{\mathrm{CLi}}$ = 22.2 Hz), while the signal of the more dynamic complex **10a** (see Figure 17) is detected as a broad singlet. Recently, *Braunstein* and *Danopoulos* reported the only example of a direct LiC coupling in an NHC complex (an amide PNC pincer complex with an imidazolin-2-ylidene moiety) with a coupling constant of $^{1}J_{\mathrm{CLi}}$ = 32.0 Hz for the ^{13}C NMR signal at 198.6 ppm.[78] There are no other known examples of direct observed Li-C couplings in NHC complexes. The observable Li-C coupling for the complexes **10a** and **10a-H** is a clear evidence for a covalent contribution to the Li-C bond, which is supported by the rather low-field ^{7}Li NMR signals at 3.16 and 1.51 ppm.

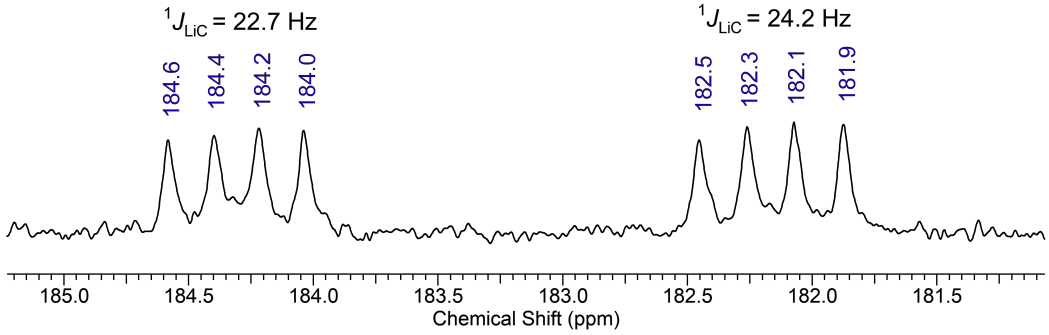

Figure 19: $^{13}C\{^{1}H\}$ NMR spectrum in THF-d_8 (detail): carbene signals at -80 °C.

Further evidence for the formation of the two species **10a** and **10a-H** was obtained from DFT calculations of the NMR chemical shifts. For complex **10a-H**, two minimum structures (D2 and C2 symmetry) of similar energy were found (*vide infra*) that might both be present and interconvert in solution. More information about the DFT calculations which were done by *Kunz* can be found in the corresponding publication.[79]

Colorless single crystals suitable for X-ray crystallography were obtained by slow diffusion of benzene into a concentrated solution of the THF-mixture at ambient temperature. The X-ray structure analysis reveals coordination of the PF_6^- counterion to the lithium atom, in accordance with observations from *Hofmann* for complex **E**.[73] Two independent molecules are in the asymmetric unit, one of which shows a stronger disorder of the PF_6^- counterion. As the geometries of both independent complexes are identical within the standard deviation, only the geometry of the non-disordered complex is discussed in the following. The carbene-Li distances of 2.22-2.23 Å match those of complex **D**[73] but are longer than those typically reported for NHC-Li complexes (2.09-2.20 Å).[80] The bite angle C1-Li-C8 is 80.1°[79], and is in the range of other vegi^{R} complexes.[31,35,40] The C1-C8 carbene distance of 2.89 Å is only slightly shorter than the value for the bis(imidazolium) salt **2b** (3.04 Å) and the calculated value (DFT) for the free carbene vegi^{Me} (2.97 Å)[40]. It lies right within the broad range of 2.67-3.26 Å which has previously been observed for this ligand system. The shortest distance was

found in an Ir-chelate complex and the longest in a dichloroimidazolium salt.[81] The Li atom does not lie in the bisecting line of the N-C-N angles. It is distorted 24° towards the center of the molecule. Due to the large s character of the carbene σ-orbital, which can be concluded from the very acute NCN angles (average 100.6°) of **10a'** as well as of the free carbene vegi^{Me} (calculated 100.6°), this deviation should only require small amounts of energy. In summary, no significant geometric reorientation of the carbene is necessary to complex the lithium cation, a situation that was observed earlier for monodentate NHC lithium complexes.[62] The $^{19}F\{^{1}H\}$ NMR spectrum in THF-d_8 at -80 °C shows only one signal at 73.34 ppm (d, $^{1}J_{PF} = 710.8$ Hz). The existence of the structure **10a'** is therefore only present in the solid-state and in solution there is an exchange of the coordinating PF_6^- anion with THF.[79]

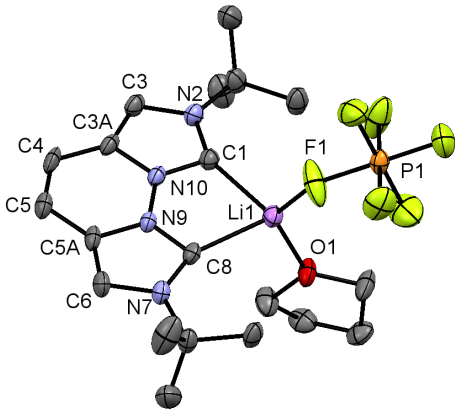

Figure 20: Molecular structure of the Li vegi^{tBu} complex **10a'**. Atoms are shown with anisotropic atomic displacement parameters at the 50% probability level. Hydrogen atoms as well as two cocrystallized benzene molecules and a second independent molecule of **10a'** (showing disorder) are omitted for clarity. Selected bond lengths (Å) and angles (deg): Li1-C1 2.230(5), Li1-C8 2.223(5), O1-Li1 1.920(5), Li1-F1 1.902(5), N9-N10 1.386(3), C5-C4 1.347(4), C1-C8 2.892, C1-Li-C8 80.99(18), O1-Li1-F1 121.2(2), N2-C1-N10 100.7(2), N9-C8-N7 100.4(2), C3-C3A-C4 137.8(3), C5-C5a-C6 136.9(3).

Crown-ether was added to the Li-vegi^{tBu} complexes to attempt the liberation of the dicarbene. The ^{1}H NMR spectrum after deprotonation showed the two species in the ratio 2:1 (**10a**:**10a-H**). In the first experiment 2.4 equivalents of [12]-crown-4 was added

to the solution. The ratio changed to 1:1.2 (**10a**:**10a-H**) in favor of complex **10b-H** as expected according to the principle of Le Chatelier by removing free lithium ions. The $^{13}C\{^{1}H\}$ NMR spectrum still shows a broad singlet at 184.1 ppm for the carbene signal of **10a** and a quartet (1:1:1:1) at 185.7 ppm with a $^{1}J_{LiC}$ coupling of 22.5 Hz for complex **10a-H**. This reveals that, despite complexation of $LiPF_6$ by [12]-crown-4, the Li^+ exchange in complex **10a** is still fast on the NMR time scale. The free dicarbene could not be liberated. This is in accordance with observations made by *Bertrand et al.* for the Weiss-Yoshida carbene complex **A**, which was isolated as its crown ether complex.[66] The same result was obtained by using 4.8 equivalents. The double amount of crown ether was added because 2:1 complexes of alkali-metal ions are known. The lithium complexes **10a** and **10a-H** remain stable under addition of excess of the crown ether.

Another reaction was tested to see whether the Li atom could be abstracted. 2.2 equivalents of TBACl were added to a mixture of the Li-vegi^{tBu} complexes to see if LiCl precipitates in THF and the carbene is freed. In the ^{1}H NMR spectrum three main signals are obtained at 1.51 ppm, 7.07 ppm and 7.83 ppm which are all very broad. The formation of the free dicarbene can be excluded. The coordination of chloride to the homo- or heteroleptic Li complex could take place and result in signal broadening. Especially the calculated structure of the homoleptic complex with dispersion interactions shows that there is enough space for a chloride ligand to coordinate.

4.1.3 Investigation of the Equilibrium

Non coordinating solvents like benzene-d_6 and toluene-d_8 were used to see whether the equilibrium between the two Li complexes could be shifted to the side of the homoleptic Li-complex. The formation of two species by deprotonation of **10a** in benzene-d_6 and toluene-d_8 at room temperature was observed. However, as THF-d_8 is not present, the nature of the complex **10a** must be different, while **10a-H** could still be formed.

Table 2: NMR data of the lithium complexes (*measured at -80 °C).

	solvent	^{1}H NMR [ppm]					^{7}Li NMR	^{13}C NMR
		H-3/6	H-4/5	R				
Li(**1a**)	THF-d_8	7.77	7.02	1.68			1.51*	184.1 br s
		7.75	7.04	1.51			3.16*	185.7 q
	benzene-d_6	6.64	6.37	1.22			1.43 br s	
		6.34	6.06	1.36				
	toluene-d_8	6.66	6.38	1.23			2.94 br s	
		6.43	6.15	1.37			1.28 br s	
	CD_3CN	7.57	6.95/6.99	1.64				
Li(**1b**)	THF-d_8	7.58	7.03	4.19	190-1.95	0.95		185.3
	benzene-d_6	5.97	5.87	3.99	1.54-1.58	1.26		
	toluene-d_8	6.05	5.95	3.99	1.59-1.58	1.26		
		6.20 br s		3.69-3.77	1.34-1.36	0.86-0.87		

Indeed, the two observed species vary not only in the chemical shift of the *tert*-butyl groups but also in the ligand backbone signals, which is not the case in THF (Table 2). Therefore, the species **10a"** is postulated, which could contain coordinated PF_6^- solvent, or HMDS (formed during the reaction). In both cases a larger amount of **10a-H** is formed (ratios **10a"**:**10a-H** = 1:0.5 (benzene-d_6) and 1:1.4 (toluene-d_8)). It is not clear whether the increased concentration of **10b-H** is due to the reduced stability of species **10a"** or to the low solubility of the formed $LiPF_6$ in the nonpolar solvent. The stronger coordinating solvent acetonitrile was also used as a solvent during the deprotonation reaction. This solvent favors the formation of the heteroleptic complex **10a"** in a 7:1 ratio. Single crystals suitable for X-ray diffraction are needed to determine the structure of complex **10a"**.

4.1.4 Reasons for the formation of the homoleptic complex

The formation of the homoleptic lithium complex is ascribed to London dispersion that should be enhanced in the case of *tert*-butyl-substituents. These interactions were shown to contribute particularly to the stability of sterically demanding organic molecules and metal complexes.[82–85] DFT calculations reveal the formation of a homoleptic complex **10a-H** where the two ligand planes show an orthogonal arrangement.

Calculations with dispersion correction by Grimme[86] reveal a rotation of one ligand about the C2 axis by 9° where one *tert*-butyl group is close to the vegi^{tBu} ligand in the optimized geometry. This is not the case for the vegi^{Me} ligand. The difference of the standard reaction enthalpies of the dispersion is 45 kJ/mol (298 K, 1 bar). The energetic contribution of the dispersion was calculated via an isodesmic reaction. All calculations have been made by *Kunz*.[42]

Initially the formation of the homoleptic vegi^{R} carbene complex seems to be limited to the *N*-*tert*-butyl-substituted vegi ligand in the lithium complex. A closer examination of the *n*-propyl-substituted species reveals at -80 °C a ^{7}Li NMR signal at 2.42 ppm with a ratio of only 5 % in comparison to the Li signal of complex **10b** at 1.47 ppm. In analogy to the analytical data of complex **10a-H** this signal can be assigned to the homoleptic complex **10b-H**. The EXSY spectrum at -40 °C reveals that in contrast to the complex **10a-H** the lithium ion of this complex also undergoes a fast exchange with complex **10b** and $LiPF_6$. The lower concentration and the faster exchange rate can be explained by a higher energy of this species.

4.1.5 Deprotonation of 2a in toluene-d$_8$ and benzene-d$_6$ with methyllithium

Table 3: ^{1}H NMR data of Li vegi^{tBu} in toluene-d$_8$.

	solvent	^{1}H NMR [ppm]		
		H-3/6	H-4/5	*t*Bu
vegi^{tBu}	benzene-d$_6$	6.23	6.00	1.30
	toluene-d$_8$	6.35	6.07	1.32

With MeLi as the base, only one symmetric compound was generated when treating vegi^{tBu} in toluene-d$_8$ or benzene-d$_6$. In both reactions grey suspensions formed. If a ^{1}H NMR spectrum is measured immediately only the solvent signals can be detected. Is the measurement repeated on the next day (grey solid and colorless solution) then three signals are obtained. The signals are different from the signals obtained for both vegi^{tBu}

dicarbenes and for the Li-species obtained using LiHMDS in toluene-d_8 or benzene-d_6. The formed Li complex here must be a complex with either PF_6 or solvent molecules coordinating to the lithium cation and it must be different from that obtained with LiHMDS as the base.

The Li-vegi$^{t\mathrm{Bu}}$ complexes **10a** and **10a-H** can also be generated by the deprotonation of **2a** with P_4-*t*Bu (Schwesinger's base) in THF-d_8 and the addition of $LiPF_6$. If 0.5 equivalents of $LiPF_6$ are used, the ^{1}H NMR spectrum shows one single set of broad signals, situated between those of the complexes **10a** and **10a-H**. Using one equivalent of $LiPF_6$ (instead of only 0.5 equivalents) led to the formation of **10a** and **10a-H** in a 0.5:1 ratio. The signals remain broad which might be explained by a fast equilibrium. Applying 1.5 equivalents of $LiPF_6$ showed only one signal set in the ^{1}H NMR spectrum which lies between the signal sets of **10a** and **10a-H**. In benzene-d_6 the complexes **10a** and **10a-H** could not be generated via this reaction, which can be explained by the poor solubility of $LiPF_6$ in benzene-d_6.

4.2 Synthesis of sodium vegi^{R} complexes

The deprotonation of vegi$^{t\mathrm{Bu}} \cdot 2HPF_6$ with sodium hexamethyldisilazide (NaHMDS) in THF-d_8 led to an orange solution and the formation of a Na-vegi$^{t\mathrm{Bu}}$ complex. The signals in the ^{1}H NMR spectrum are shifted high-field compared to the signals for the Li-vegi$^{t\mathrm{Bu}}$ complexes. The carbene signal of the Na-vegi$^{t\mathrm{Bu}}$ complex is detected at 189.3 ppm. In benzene-d_6 the Na-vegi$^{t\mathrm{Bu}}$ complex was also generated. A grey suspension formed after the base had been added.

Table 4: NMR data of the sodium complexes.

	solvent	^{1}H NMR [ppm]					^{13}C NMR
		H-3/6	H-4/5	R			
11a	THF-d_8	7.65	6.92	1.64			189.3
	benzene-d_6	6.39	6.08	1.35			
11b	THF-d_8	7.43	6.91	4.17	1.88	0.93	191.9
	benzene-d_6	6.04	5.97	3.81	1.60	0.80	
	toluene-d_8	6.14	6.06	3.93	1.68-1.72	0.87	

With vegi$^{n\mathrm{Pr}}$ a Na complex can also be generated by the addition of NaHMDS to a grey suspension of **2b** in THF-d_8 leading to a light brown suspension. The carbene signal of the complex is detected at 191.9 ppm. The Na-vegi$^{n\mathrm{Pr}}$ complex was also prepared in benzene-d_6 and toluene-d_8 leading to a brown-red suspension.

The corresponding crown ether was added to the Na-vegi^{R} complexes **11a,b** in an attempt to liberate the free carbene. 2 and 4 equivalents of [15]-crown-5 were added to the sodium complexes. The Na complexes appeared stable and no free dicarbene was formed. From a reaction mixture with 4 equivalents of the crown ether, colorless single crystals were formed and analyzed by X-ray structure analysis. The analysis reveals the formation of [Na([15]-crown-5)]PF_6. As the published data[87] contains strong disorders, the X-ray data was published[42] and can also be found in the spectroscopic data section of this thesis.

4.3 Synthesis of potassium vegi^{R} complexes

2a was deprotonated with potassium hexamethyldisilazide (KHMDS) in THF-d_8. A ^{1}H NMR measurement of the brown solution confirms the deprotonation of the bis(imidazolium) salt. The carbene signal is detected at 195.2 ppm which is shifted downfield compared to the signal for the Li or Na complexes. This clearly indicates the formation of the potassium complex **12a**. **2a** was also deprotonated with KHMDS in toluene-d_6 and benzene-d_8. In all cases one symmetric potassium complex formed. In acetonitrile the deprotonation did not work, many small signals of unkown products were obtained. But the generated complex **12b** in THF-d_8 could be dried and measured in CD_3CN. The spectrum shows three singlets. Benzyl potassium (pK_a = 43) or potassium *tert*-butoxide (pK_a = 17 (H_2O), 29 (DMSO)) were also used in THF-d_8 as bases to obtain the K-vegi$^{t\mathrm{Bu}}$ complex. **2b** was also deprotonated with KHMDS in THF-d_8 and benzene-d_6 forming the K-vegi$^{n\mathrm{Pr}}$ complex **12b**. The carbene signal is detected at 196.3 ppm. Both bis(imidazolium) salts **2a** and **2b** were successfully deprotonated with potassium *tert*-butoxide in THF-d_8.

Table 5: NMR data of the potassium complexes (* = generated in THF-d_8 and measured in CD_3CN).

	solvent	^{1}H NMR [ppm]					^{13}C NMR
		H-3/6	H-4/5	R			
K(**1a**)	THF-d_8	7.57	6.85	1.65			195.2
	CD_3CN*	7.52	6.89	1.62			
	benzene-d_6	6.54	6.18	1.43			
	toluene-d_8	6.55	6.18	1.42			
K(**1b**)	THF-d_8	7.37	6.86	4.16	1.89	0.95	196.3
	benzene-d_6	6.10	6.02	3.90	1.63	0.82	

From a saturated THF solution colorless single crystals formed. Due to the low crystal quality, the structure only serves as a connectivity proof (Figure 21). The bigger size of the potassium ion allows three vegi^{tBu} ligands coordinate to the metal center in an octahedral fashion.

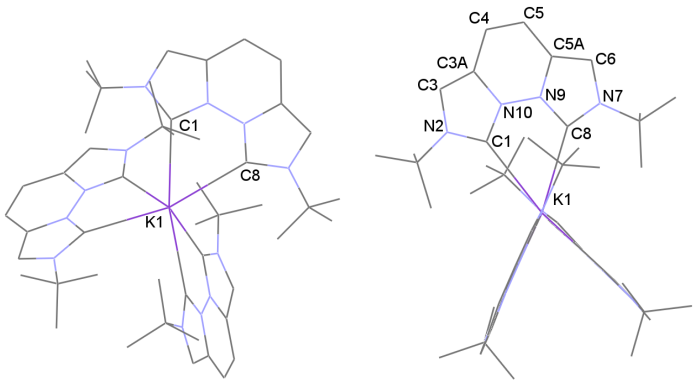

(a) The view from above. (b) The view from the side.

Figure 21: Molecular structure of **12a**. Hydrogen atoms, PF_6^- anion as well as two cocrystallized THF molecules are omitted for clarity.

Complex **12a** can also be generated via the reaction of the free dicarbene **1a** with one equivalent or more KPF_6 in THF-d_8.

4.4 Synthesis of cesium vegi^{R} complexes

No Cs(NHC) complexes were found in literature.[88] Therefore, the medium strong base cesium carbonate was initially used ($pK_a = 10$ (H_2O)) to deprotonate **2a**.

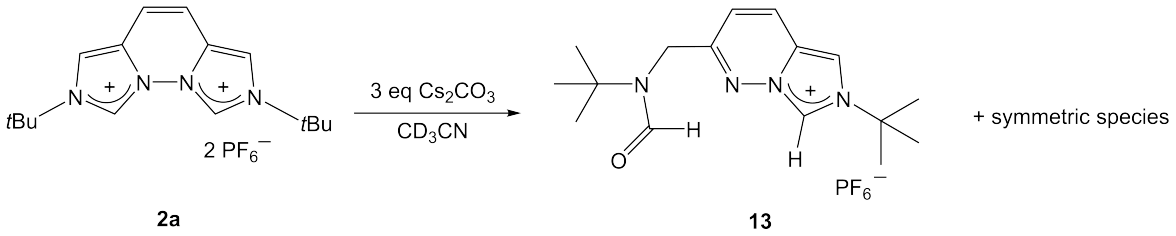

2a **13**

Figure 22: Synthesis of the unsymmetric compound **13**.

Using 2.2 equivalents of Cs_2CO_3 and one equivalent of vegi$^{tBu} \cdot 2HPF_6$ lead to the formation of an unsymmetric species **13** and a symmetric complex in a ratio of 1:2.5.

Table 6: Ratios of the unsymmetric versus symmetric complexes in acetonitrile.

equivalents of base	**2a**	**13**	symmetric complex
1.1	1.7	1	0
2.2	-	1	2.5
3	-	1	1.7
6	-	1	2.5
8	-	1	5

If the ^{1}H NMR was measured after 1 h only the unsymmetric species was left. The monodeprotonated product **13** is stable for 11 days in an acetonitrile solution. The symmetric species shows three singlet signals at 1.72 ppm, 7.21 ppm and 7.83 ppm. Deprotonation with only 1.1 equivalent of Cs_2CO_3 in acetonitirile gives the unsymmetric species and the bis(imidazolium) salt **2a** in a ratio of 1:1.7. The use of six equivalents of Cs_2CO_3 leads to the formation of the unsymmetric species and a symmetric species in a ratio of 1:2.5. The ratio can further be shifted to the symmetric side by using up to eight equivalents of base.

The symmetric species is not a Cs-NHC complex. Therefore, the backbone signals have

to be in the region between the K-vegi$^{t\mathrm{Bu}}$ complex **12a** and the free carbene **1a**. In contrast, the signals of the unknown symmetric species are low-field shifted.

The experiment was repeated with three equivalents of Cs_2CO_3 in acetonitrile which led to a ratio of 1:1 for a symmetric complex and the unsymmetric complex. After 4 h the signals for the symmetric species in the ^{1}H NMR are almost gone. After 8 h total reaction time only the unsymmetric species is left. The measured NMR spectra and ESI mass spectrum reveal the formation of the unsymmetric complex **13** where one imidazolium ring became hydrolyzed under formation of the aldehyde (Figure 22). Most likely OH^- is formed which induces the ring opening.

The formation of a Cs complex or the free dicarbene via the transmetalation reaction of the Li complexes and the addition of two equivalents of CsF could not be realized. The signals for the Li complexes are still detected and the equilibrium shifts to the side of complex **10a-H**. Also after the addition of an excess (total 2.5 equivalents) the signals of the Li-complexes remain.

A cesium base which does not form OH^- or H_2O was needed to deprotonate the vegi^{R} ligands without side reactions. Therefore, cesium hexamethyldisilazide (CsHMDS) was prepared following a literature known synthesis via the cesium halide route avoiding the use of cesium metal. Anhydrous cesium fluoride and LiHMDS were dissolved in *n*-hexane to undergo a salt metathesis reaction (Figure 23). After refluxing overnight, the solvent was removed *in vacuo* and toluene was added to extract only CsHMDS. After filtering off LiF the product could be obtained as a white solid which was sublimed at 200 °C.[89]

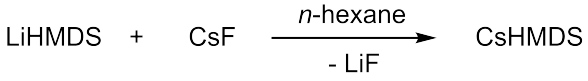

Figure 23: Literature known synthesis of cesium hexamethyldisilazide.

Using 2.2 equivalents of CsHMDS in THF-d_8 to deprotonate **2a** or **2b** leads to the

formation of either the dicarbene or a Cs-complex.

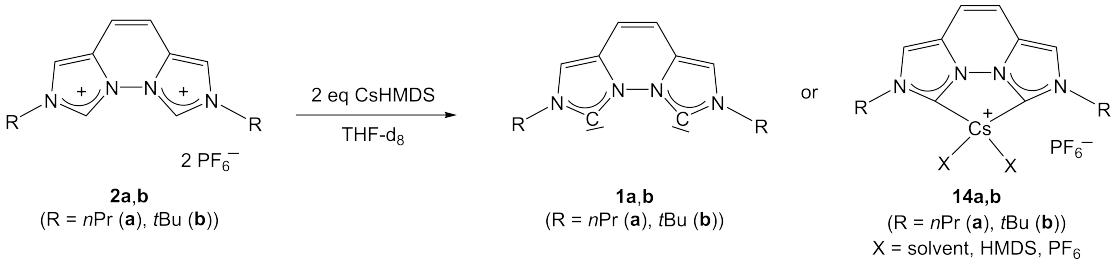

Figure 24: Synthesis of the dicarbene via CsHMDS.

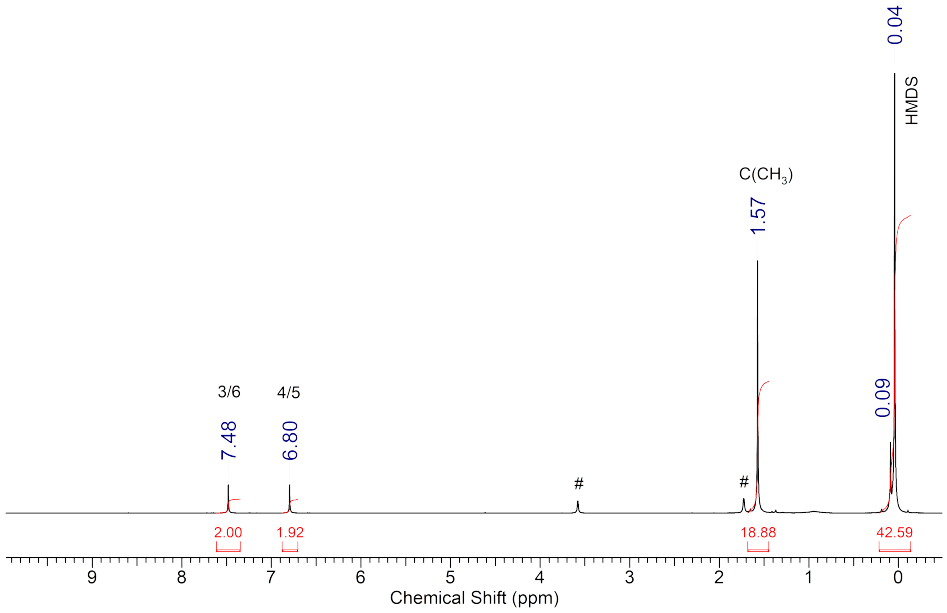

Figure 25: ^{1}H NMR spectrum of the reaction of **2a** with CsHMDS. (THF-d$_8$, #).

In case of vegi$^{n\mathrm{Pr}}$ a dark brown suspension formed in THF-d$_8$ after adding CsHMDS whereas with vegi$^{t\mathrm{Bu}}$ a light brown suspension formed. The ^{1}H NMR spectrum of the reaction with vegi$^{t\mathrm{Bu}}$ and CsHMDS in THF-d$_8$ is shown in Figure 25. As expected, the backbone signals are observed in between the signals for the K-vegi^{R} complex and the free dicarbene (7.47 ppm, 6.77 ppm and 1.64 ppm). The backbone signals are however, very similar to the signals for the dicarbene. Therefore, a ^{13}C{^{1}H} NMR spectrum was measured. The carbene signal at 201.7 ppm is also observed in between the values for the K-vegi^{R} complex and the free dicarbene (195.2 ppm (**12a**) and 202.6 ppm (**14a**)).

The signal lies, however, again closer to that of the dicarbene. With these NMR measurements no clear evidence can be given. The formation of a Cs-vegi$^{t\mathrm{Bu}}$ complex is more likely because the carbene signal differs between **14a** and **1a**. In the literature an example of an NHC-stannocene complex (216.9 ppm (C_6D_6)[90]) shows also only a small high-field shift of 2.8 ppm of the signal of the carbene atom compared to the signal of the free carbene (1,3-dimesitylimidazol-2-ylidene, 219.7 ppm (THF-d_8)[74]).

The deprotonation reaction of **2a** with CsHMDS also worked in benzene-d_6 and toluene-d_8. Using nonploar solvents, such as benzene, the precipitation of $CsPF_6$ and its removal via filtration would be possible. A first isolation experiment was carried out in toluene. To a suspension of **2a** in toluene-d_8 2.2 equivalents CsHMDS were added. After 1.5 h the mixture was filtered over Celite®. The obtained yellow filtrate was concentrated to dryness. A ^{1}H NMR of the obtained brown-red oil was measured. The signals do not match with the signals obtained from the NMR experiment in toluene. In this case four signals were obtained in toluene-d_8 which could be assigned to 3,6-bis(*tert*-butylformamidomethyl)pyridazine (**7a**). No NMR data of compound **7a** for comparison in toluene exists. The filtration over Celite® could induce the hydrolysis of the product.

Table 7: NMR data of the formed Cs-vegi^{R} complexes.

	solvent	^{1}H NMR [ppm]					^{13}C{^{1}H} NMR [ppm]
		H-3/6	H-4/5	R			
Cs-vegi$^{t\mathrm{Bu}}$	THF-d_8	7.48	6.80	1.57			201.7
	benzene-d_6	6.61	6.25	1.45			
	toleuene-d_8	6.61	6.23	1.44			
Cs-vegi$^{n\mathrm{Pr}}$	THF-d_8	7.27	6.79	4.10	1.89	0.93	202.8

If the reaction with CsHMDS led to a Cs-vegi^{R} complex, this would be the first Cs NHC complex known so far. Experiments in toluene and THF of **2a** with CsHMDS took place and were filtered over a syringe filter. The resulting filtrates were stored at -30 °C for crystallization. An X-ray diffraction measurement of a single crystal

would verify the formation of a Cs complex, but so far, no suitable single crystals have formed.

4.5 Deprotonation reactions with metal-free bases

While deprotonation with metal bases leads to the corresponding metal complex, due to the strong chelating character of the vegi ligand metal free bases are used in the following to obtain the free dicarbene. The stability of free NHCs has received much attention. It is known from theoretical studies that the stability of free NHCs is mainly attributed to the p_π-p_π delocalization of the nitrogen lone pairs. Steric effects also contribute to the stability of NHCs but to a smaller extent.[91,92]

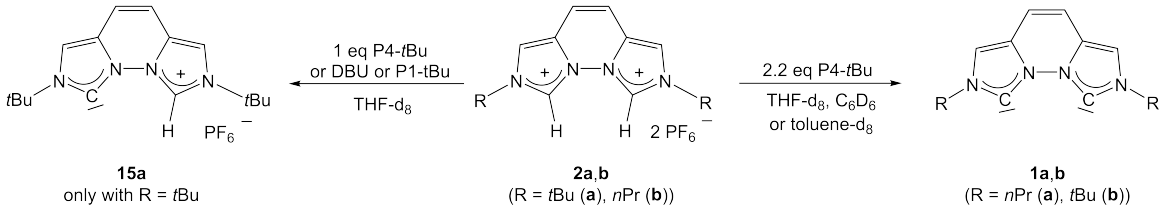

Figure 26: Synhtesis of monocarbene (**15a**) and dicarbene (**1a,b**).

Starting with the weaker organic base *N*,*N*-diisopropylethylamine (DIPEA), pK_a = 11 (H_2O)), the deprotonation of vegi$^{t\mathrm{Bu}}$ and vegi$^{n\mathrm{Pr}}$ with 2.4 equivalents DIPEA in CD_3CN did not lead to a deprotonation of the bis(imidazolium) salts, because the base is too weak.

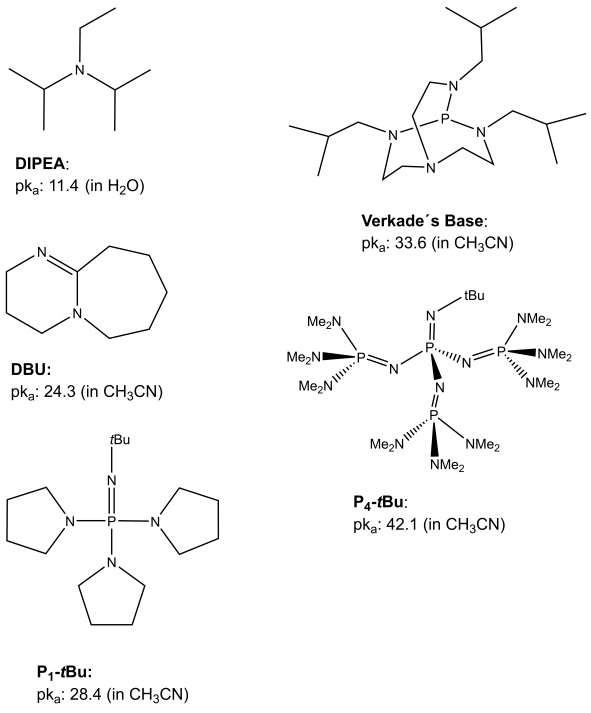

Figure 27: The used metal-free bases.

The use of 2.2 equivalents of 1,8-diazabicyclo[5.4.0]undec-7-ene (DBU) as a non-nucleophilic base and stronger base (pK_a = 24.3 (CH_3CN), pK_a = 12 (H_2O)) - in THF-d_8 only showed the formation of the monocarbene. Even the use of 4.2 equivalents of DBU only led to the formation of the monocarbene vegi$^{t\mathrm{Bu}}$ **15a**. The monocarbene shows a broad singlet signal at 10.50 ppm with an integral of two (instead of one) and singlets at 8.15 ppm (2H, sharp), 7.30 ppm (2H, sharp) and 1.75 ppm (18H, $C(CH_3)_3$). Only half of the expected signal set of an unsymmetric compound is observed. This indicates a fast exchange of the imidazolium protons between the carbene moiety in **15a**.

Stronger metal-free bases were needed to fully deprotonate the salts **2a** and **2b**. Phosphazene bases are extremely strong bases. They contain a basic nitrogen center which is double bonded to a pentavalent phosphorus. Starting with the weakest phosphazene base P$_1$-*t*Bu (*tert*-butylimino-tri(pyrrolidino)phoshorane, pK_a = 28.4) only led to the formation of the monocarbene **15a** (using 2.2 and 4.2 equivalents of P$_1$-*t*Bu) with half of the integral for the acidic proton.

The monocarbene can also be generated with the azaphosphatrane (2,8,9-triisobutyl-2,5,8,9-tetraaza-1-phosphabicyclo[3.3.3]undecane) which is also referred as Verkade's base. This strong nonionic Brønsted base was also not able to deprotonate **2a** and **2b** fully. Using 2.2 equivalents of the Verkade's base in THF in the case of vegi$^{t\mathrm{Bu}}$ only led to the monocarbene **12a**. In case of vegi$^{n\mathrm{Pr}}$ many signals are obtained of unkown side products.

Therefore, the Schwesinger superbase P$_4$-*t*Bu (1-*tert*-butyl-4,4,4-tris(dimethylamino)-2,2-bis[tris(dimethylamino)-phosphoranylidenamino]-2λ 5,4λ 5-catenadi(phosphazene)) was used. This base is one of the strongest metal free bases (p$K_a = 42.1$) and a very weak nucleophile due to its very high steric hindrance. The base is extremely hydroscopic but is stable toward hydrolysis.[93,94] With 2.2 equivalents of P$_4$-*t*Bu the carbenes vegi$^{t\mathrm{Bu}}$ (**1a**) and vegi$^{n\mathrm{Pr}}$ (**1b**) can be generated. In both cases a dark brown THF-solution formed.

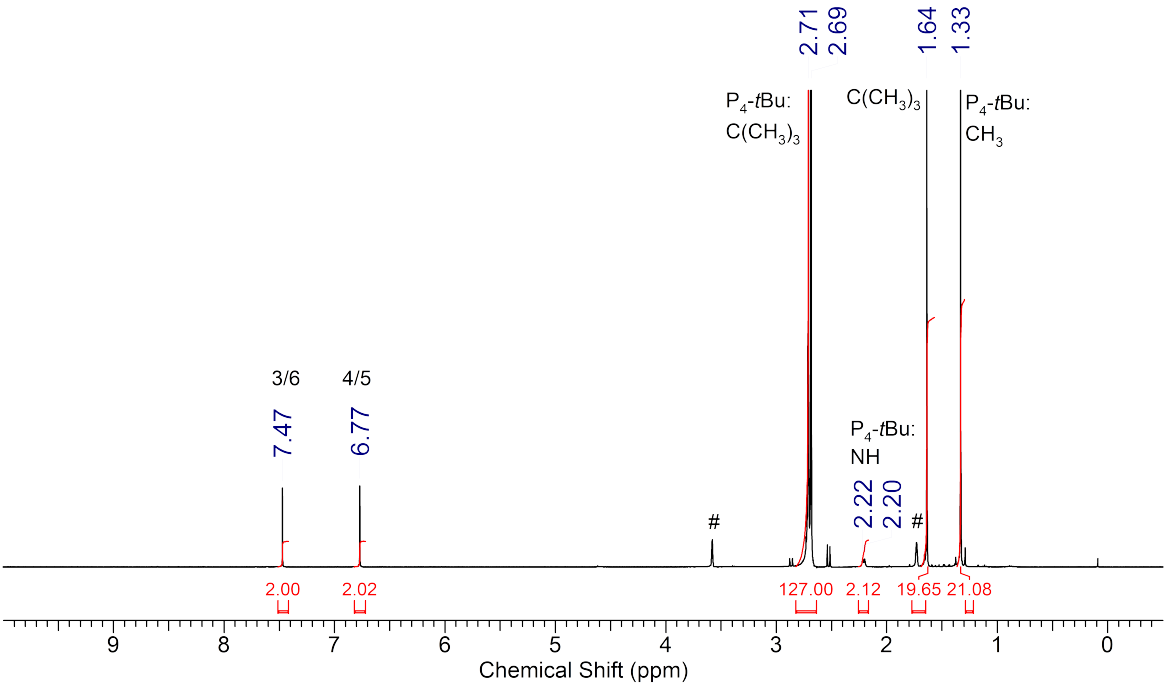

Figure 28: ^{1}H NMR spectrum of **1a** (THF, #).

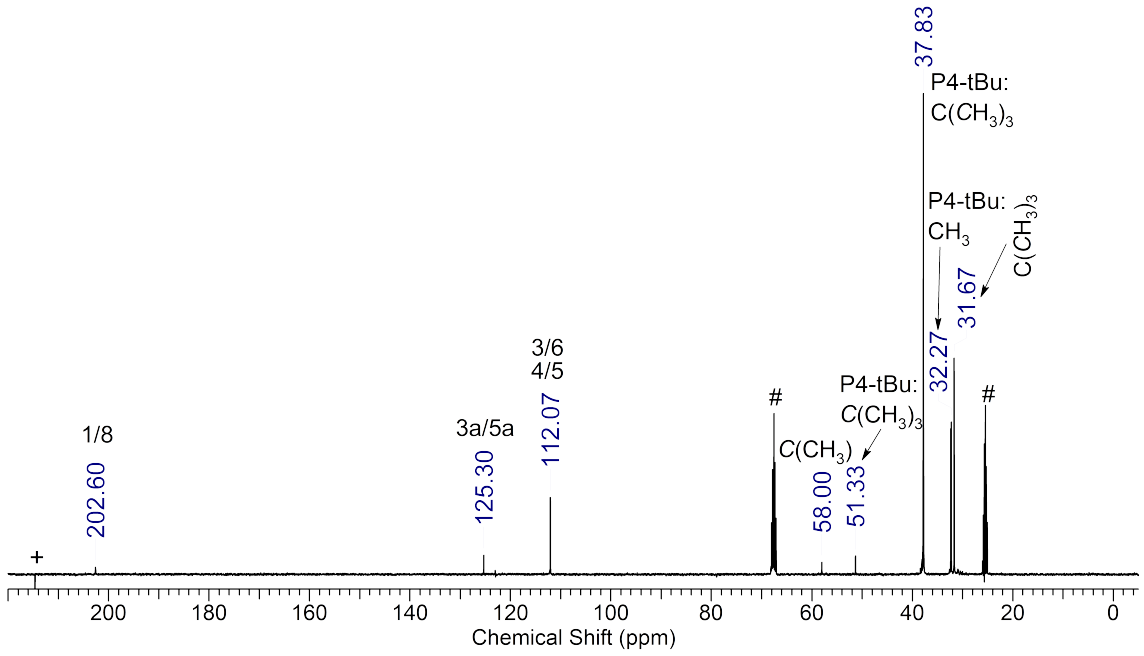

Figure 29: $^{13}C\{^{1}H\}$ NMR spectrum of **1a** (THF, #; + artefact).

The deprotonation reaction of **2a** and **2b** with P_4-*t*Bu was also carried out in benzene-d_6. In both cases the formation of a dark brown oil was observed. While in toluene-d_6 the reaction of **2a** with P4-*t*Bu led to an almost colorless solution containing the fully deprotonated species, the reaction with **2b** and P_4-*t*Bu led to a dark brown oil. The ^{1}H NMR spectrum also shows the formation of a fully deprotonated species. All NMR data of the dicarbenes **1a,b** in different solvents are summarized in table Table 8.

Table 8: Generation of the dicarbens **1a,b** with 2.2 equivalents of P_4-*t*Bu ([a]generated and measured in these solvents).

	solvent	^{1}H(NMR) [ppm]					^{13}C{^{1}H}(NMR) [ppm]
		H-3/6	H-4/5	R			
vegi$^{t\mathrm{Bu}}$	THF-d_8	7.47	6.77	1.64			202.6
	C_6D_6	6.71	6.33	1.49			
	toluene-d_8	6.71	6.31	1.48			
vegi$^{n\mathrm{Pr}}$	THF-d_8	7.33	6.79	4.10	1.90	0.94	204.5
	C_6D_6	6.36	6.25	3.83	1.64	0.71	
	toluene-d_8	6.37	6.25	3.81	1.67	0.74	

The use of only one equivalent of P_4-*t*Bu also led to the monocarbene **15**. This monocarbene **15** is stable in solution for a few days. The ^{1}H NMR spectrum shows a signal at 10.05 with a integral of one and signals at 8.15 ppm and 7.30 ppm for the backbone protons (4/5 and 3/6) each with an integral of two. The signal for the *tert*-butyl group is at 1.75. Cooling the THF-d_8 solution down to -80 °C resulted in a splitting of the signals into two sets for H-3/6 to 8.14 ppm and 8.36 ppm and H-4/5 to 7.22 ppm and 7.48 ppm and the *tert*-butyl groups are found at 1.74 ppm and 1.81 ppm. This means that the monocarbene **15a** exists as a static molecule (on the NMR timescale) at low temperatures. At room temperature the imidazolium proton shows a fast exchange. There is no equilibrium between the bis(imidazolium) salt and the dicarbene, as at -80 °C a carbene signal at 197.7 ppm for the monocarbene is obtained. Not all signals could be assigned. The generation of the monocarben of vegi$^{n\mathrm{Pr}}$ was attempted, but the reaction mixture contained impurities of unkown sideproducts. This confirms the observation of *Raible* and *Gierz* that the vegi$^{n\mathrm{Pr}}$ carbene is not stable when generated with a substoichiometric amount of base.

Table 9: NMR data of the monocarbene (* The chemical shift of this signal varies, concentration and solvent dependent).

	solvent	^{1}H NMR [ppm]						^{13}C{^{1}H} NMR
		H-3/6	H-4/5		R			
15a	THF-d_8	10.05*	8.15	7.30	1.75			197.7
15b	THF-d_8	10.67	8.21	7.57	4.49	2.06	1.04	-

The isolation of the free dicarbene **1a,b** would be an improvement for the synthesis of metal complexes. The free carbene could be added to the desired metal precursor and via simple coordination of the carbene to the metal, instead of transmetalation, the desired metal complex could be obtained. The isolation of the formed metal complexes would be easier since no or less salts need to be removed.

Isolation experiments for the dicarbene vegi$^{t\mathrm{Bu}}$ were carried out. The dicarbene was generated with 2.2 equivalents P_4-*t*Bu in THF. The dark brown suspension was dried and an oily dark brown solid was formed. The residue is extracted with a 1:1 mixture of toluene/*n*-pentane. The orange solution was filtered off and dried. The ^{1}H NMR spectrum shows decomposition. No signals of the dicarbene are obtained. Instead, many signals of unkown products are detected.

The reaction was repeated in THF and the brown suspension was cocentrated to dryness after 50 min. Then a sublimation at room temperature followed ($7{\cdot}10^{-5}$ mbar). As nothing started to sublime, the oil bath was heated up to 70 °C in 20 °C steps. No sublimation was observed.

Another reaction was tested with **2a** and P_4-*t*Bu in toluene in which a dark oil was formed as a second phase. The light colored upper phase was separated and analyzed. The ^{1}H NMR spectrum shows signals of the dicarbene and [P_4-*t*BuH]PF_6. Acetonitrile was added to wash out all polar compounds. A dark oily solution resulted. The ^{1}H NMR spectrum shows many signals of unkown products.

The formed corresponding acid [P_4-*t*BuH]PF_6 is highly soluble and therefore challenging to remove during the work up of the dicarbenes **1a** and **1b**.

The use of only 1.1 equivalents of LiHMDS in THF-d_8 with vegi$^{tBu} \cdot 2HPF_6$ (**2a**) yields the monodeprotonated species **15a**. The ^{1}H NMR spectrum also shows a signal at 10.02 ppm with an integral of one and two broad singlets at 8.11 ppm and 7.27 ppm each with an integral of two. The *tert*-butyl signal is detected at 1.74 ppm. The $^{31}P\{^1H\}$ spectrum shows a septet at -144.13 ppm ($^1J_{PF}$ = 709 Hz) and the $^{19}F\{^1H\}$ a signal at -74.11 ppm ($^1J_{PF}$ = 709 Hz) for the counterion. The mixture was also cooled down to -80 °C. The H-3/6 signal at 8.11 ppm splits into two signals at 8.12 ppm and 8.31 ppm and also the signal at 7.27 ppm splits into signals at 7.20 ppm and 7.46 ppm. The *tert*-butyl signal splits into signals at 1.74 ppm and 1.81 ppm. The carbene signal at -80 °C is detected at 197.8 ppm. Overall the VT NMR measurement is in line with the experiment of the monocarbene generated with P_4-*t*Bu in THF-d_8. The monocarbene shows a fast exchange of the imidazolium proton at room temperature and therefore two broad singlets are detected for the four backbone protons. The ^{7}Li NMR spectrum at -80 °C of the monocarbene and $LiPF_6$ mixture shows a larger signal at -2.14 ppm and a small signal at 0.15 ppm. The signal at -2.14 ppm is assigned to $LiPF_6$ and the small signal at 0.15 ppm to residual LiHMDS.

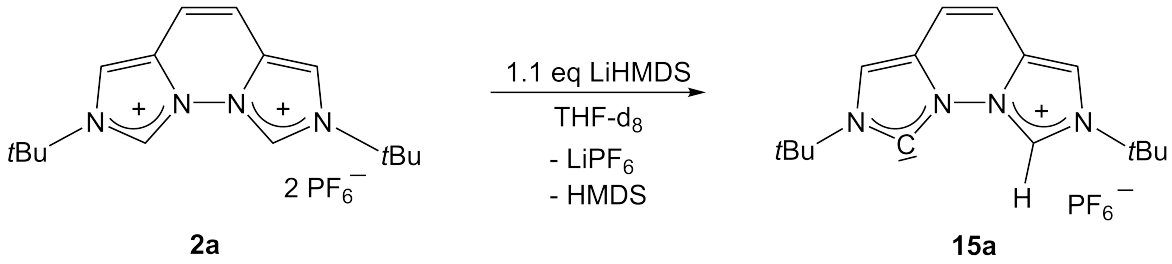

2a **15a**

Figure 30: Synthesis of the monocarbene **15a**.

In conclusion the deprotonation of the bis(imidazolium) salts **2a** and **2b** with lithium, sodium or potassium bases did not result in formation of the free dicarbenes, but in formation of the respective alkali-metal carbene complexes, which can be easily

derived from the ^{13}C NMR spectra of the compounds. The high-field shift of the carbene signal is characteristic for the coordination of the carbene to metal ions as its shielding is increased.[75,88] The trend of the chemical shifts of the carbene signals also follows the decrease in Lewis acidity of the metals and the covalent contribution to the metal-carbene bond, and thus the expected bond strength of the primarily electrostatic carbene-metal bonds. The ^{13}C{^{1}H} NMR resonances of the carbene carbon atoms of the metal complexes increase towards that of the free carbenes as the size of the cation increases.

Therefore, the signal of the Li complexes is most high-field shifted and the signal of the free dicarbene the strongest low-field shifted (see Table 10). The observation of direct Li-C couplings in the ^{13}C{^{1}H} NMR and the low-field chemical shifts of the ^{7}Li NMR signals point to an enhanced covalent contribution in the Li-carbene bond. The lithium and sodium complexes are very stable and even withstand chelation by the respective crown ethers.

Table 10: ^{13}C NMR data of the carbene signals of the alkali-metal complexes and the dicarbenes.

	^{13}C{^{1}H} NMR [ppm]	
	vegi$^{t\mathrm{Bu}}$	vegi$^{n\mathrm{Pr}}$
Li	184.1/185.7	185.4
Na	189.3	191.9
K	195.2	196.3
Cs	201.7	202.8
NHC	202.6	204.5

The signals of the backbone protons in the ^{1}H NMR spectra for the Li, Na and K complexes and the free dicarbene are shown in Figure 31. The Li complexes show the strongest low-field shift of the heteroaromatic proton signals in comparison with the Na, K and Cs complexes and the heteroaromatic proton signals are most high-field shifted for the free dicarbene. The same order is obtained for the complexes with the vegi$^{n\mathrm{Pr}}$ ligand.[75,95]

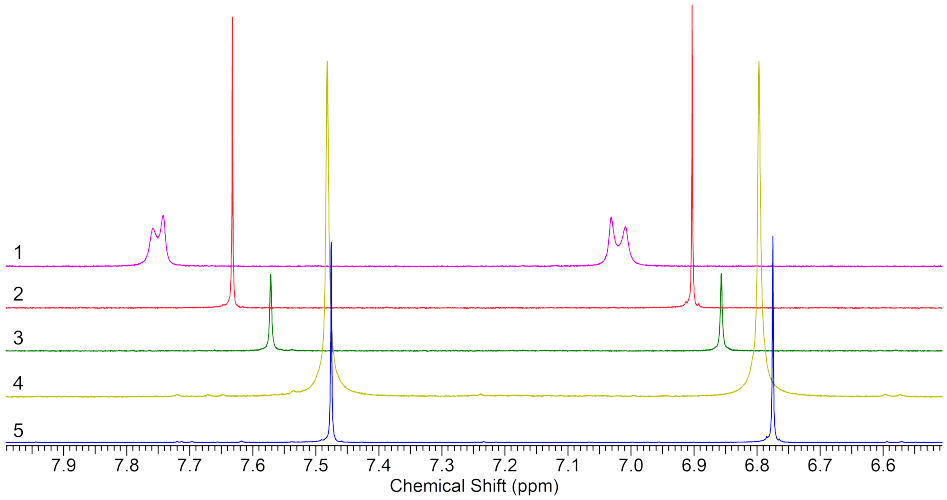

Figure 31: ^{1}H NMR (detail) spectra: Backbone signals H-3/6 and H-4/5 in THF-d_8. 1) Li vegi$^{t\mathrm{Bu}}$ complexes **10a/10a-H**; 2) Na vegi$^{t\mathrm{Bu}}$ complex **11a**; 3) K vegi$^{t\mathrm{Bu}}$ complex **12a**; 4) Cs vegi$^{t\mathrm{Bu}}$ complex **14a**; 5) dicarbene vegi$^{t\mathrm{Bu}}$ **1a**.

5 Coinage metal vegi^{R} complexes

5.1 Homodinuclear coinage metal vegi^{R} complexes

Coinage metal NHC complexes have been investigated for their diverse structural properties and their variable applications.[96] Since the first report of a Ag-NHC complex by *Arduengo* in 1993[97] a lot of articles regarding Ag-NHCs have been published. They are mainly used as NHC transfer reagents[96,98,99], homogenous catalysts, luminescence materials[8,100,101] and also indicate to have antimicrobial potential.[102] The respective Au-NHC complexes were found to be active in various cyclization reactions.[103,104] Cu(I)(NHC) complexes are potential catalysts for various reactions, including [2+3] cycloadditions,[105,106] nitrene and also carbene transfer reagents.[107] The formation of dinuclear coinage metal complexes containing NHCs ligands[108,109] is of interest to study metal-metal interactions.

The coinage metal-carbene bond strength follows the order Au-C > Cu-C > Ag-C and the bond length increases in the order Cu-C < Au-C < Ag-C.[110] Calculations (density functional theory) predict that the NHC-metal bond is mostly of electrostatic nature with minor covalent interactions which are largely σ-bonding.[111] The synthesis of transition metal complexes bearing NHCs ligands by carbene transfer from Ag- or Cu-NHC complexes represents a useful alternative to the synthetic methods involving highly unstable free carbenes.[96]

The synthesis of silver carbene complexes is straightforward and can be conducted in polar solvents such as acetonitrile, dichloromethane and dioxane with silver(I) oxide as the basic metal precursor.[100] Copper NHC complexes can be prepared via transmetalation from the respective silver NHC complexes[112] or directly from the imidazolium salt with basic copper(I) oxide.[113] Gold NHC complexes are mostly prepared by transmetalation of the respective silver NHC complex.[112] The driving force of both transmetalation reactions are the stronger metal-NHC bond in the product compared to the weaker Ag-NHC bond, which is confirmed by theoretical calculations.[110]

The synthesis of dinuclear coinage-NHC complexes with vegi$^{n\mathrm{Pr}}$ and vegi$^{\mathrm{Bn}}$ ligands has been reported by our group in 2012.[37] Dinuclear coinage metal complexes can also be synthesized with the bulkier *tert*-butyl groups attached to the nitrogen atoms at the vegi ligand.[30,33] The optimized syntheses by *Denninger* from our group were repeated.[33]

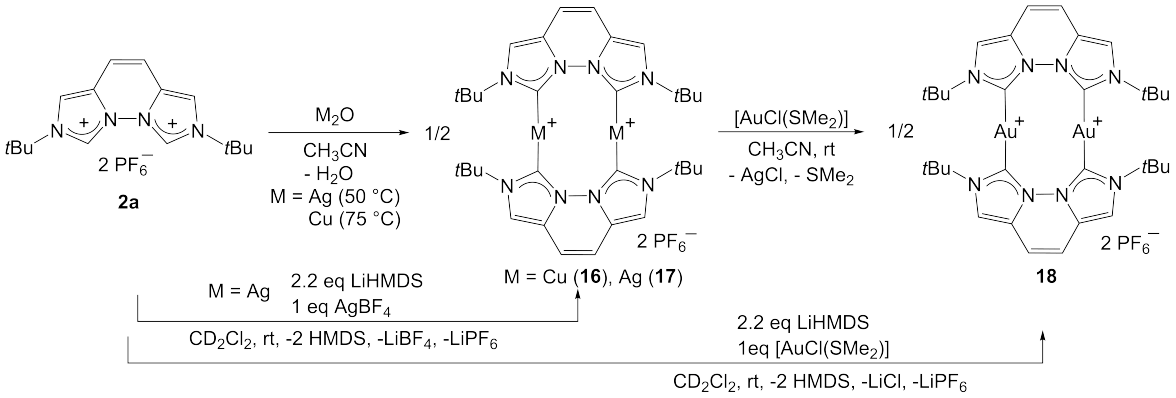

Figure 32: Synthesis of the coinage metal complexes **16**, **17** and **18**.

The Ag complex **17** can be synthesized with basic Ag_2O and **2a** in acetonitrile at 50 °C overnight in the dark. The ^{1}H NMR spectrum in acetonitrile shows three signals at 1.74 (singlet, *tert*-butyl groups), 7.18 (singlet, H-4/5) and at 7.92 ppm (singlet, superimposed by a doublet, H-3/6) indicating a symmetric complex. The coupling pattern at 7.92 ppm results from an exchange of one of the silver ions, which leads to a doublet for the coupling from H-3/6 to the Ag atom (I = 1/2) and a decoupled signal (singlet). In comparison with the bisimidazolium salt **2a**, the respective signals are shifted upfield, which is typical for transition metal NHC complexes.[75] In the ^{13}C{^{1}H} NMR spectrum the signal for the C-carbene atom is at 168.1 ppm also showing couplings with the silver isotopes (^{107}Ag/^{109}Ag). Three doublets and one broad singlet are obtained due to the exchange of the silver isotopes. The Ag complex **17** shows a dynamic behavior which was studied by NMR techniques and is published in my master thesis. VT NMR experiments reveal a silver-silver exchange process in complex **17**.[114]

The Ag complex **17** can also be generated via transmetalation of the *in situ* syn-

thesized Li complexes **10a**/**10a-H** with an excess of 2.4 equivalents of $AgBF_4$ in dichloromethane. The ^{1}H NMR spectrum shows full conversion into complex **17**. Generally the synthesis and handling of complex **17** was conducted with the exclusion of light, to prevent its decomposition and formation of elemental Ag.

The corresponding synthesis of the Cu complex is carried out at 75 °C overnight. $CuPF_6$ can also be removed by filtration over Celite®. The backbone signals (H-3/6 and -4/5) and the *tert*-butyl-group signal of **16** are shifted high-field in the ^{1}H NMR spectrum in comparison with the spectrum of silver complex **17**. In the ^{13}C{^{1}H} NMR spectrum the signal for the C-carbene atom can be detected at 163.1 ppm, upfield shifted in comparison with the respective silver complex **17**.

The dinuclear gold complex **18** was obtained by transmetalation of the *in situ* generated silver complex **17** with 1.05 equivalents of [AuCl(SMe_2)] at room temperature in acetonitrile. The backbone signals (H-3/6 and -4/5) are shifted upfield while the *tert*-butyl group signal is shifted down-field in the ^{1}H NMR spectrum of **18** in comparison with the spectrum of silver complex **17**. In the ^{13}C{^{1}H} NMR spectrum the signal for the C-carbene atom can be detected at 172.2 ppm, down-field shifted in comparison with the respective silver complex **17**.

The vegi$^{n\mathrm{Pr}}$ and vegi$^{\mathrm{Bn}}$ ligands act as bridging ligands with all monovalent coinage metal ions forming homoleptic complex as well. While the silver complex vegi$^{\mathrm{Bn}}$ (and also vegi$^{n\mathrm{Pr}}$) features a coplanar orientation of the ligands, the ligand planes are oriented in a 31° angle in the Au complex and in a 70° angle in the Cu complex, which can be explained by steric hindrance due to the decreasing metal-C bond lengths in this order.[37]
It was of interest to see whether the steric bulk of the vegi$^{t\mathrm{Bu}}$ ligand has an influence on the geometry of the coinage metal complexes. *Denninger* obtained single crystals suitable for X-ray diffraction of the Au vegi$^{t\mathrm{Bu}}$ complex **18**, which shows an angle between the ligand planes of 77°. In my master thesis I elucidated the molecular structure of the Ag complex **17**. It shows a perpendicular arrangement of both vegi$^{t\mathrm{Bu}}$ ligand planes to

each other. The single crystals were unfortunately not of optimal quality, but the X-ray structure analysis confirms the structure of the bridging dinuclear silver complex **17**. The accuracy of the metal-metal bond in the molecular structure is good enough to be discussed. The Ag-Ag distance of 2.693 Å and is in the lowest among those complexes bearing neutral ligands[115] and it is shorter than the metal-metal distance in metallic silver (2.88 Å).[116] The Ag-Ag distance is also considerably shorter than the sum of the van der Waals radii for Ag (3.44 Å)[117] implying weak d^{10}-d^{10} interactions.[118,119] Compared to the dinuclear silver vegi^{Bn} (2.7391 Å) and vegi$^{n\mathrm{Pr}}$ (2.7405 Å) complexes this distance is significantly shorter. Colorless single crystals of the Cu complex **16** were obtained from a saturated acetonitrile solution at -30 °C and were suitable for X-ray diffraction (Figure 33). All three coinage metal vegi$^{t\mathrm{Bu}}$ complexes can now be compared. The ligand planes are orientated in a 69° angle in the Cu complex **16**. In this case the degree of tilting does not follow the metal-C bond lengths. This geometry change can probably be explained by London dispersion of the *tert*-butyl groups. The shorter the metal-carbene bond length are, the stronger these interactions should be.

The crystals of **16** belong to the orthorhombic space group *Pbca*. The asymmetric unit contains one molecules of **16**, one acetonitrile and one dichloromethane molecule as well as the two PF_6^- counterions.

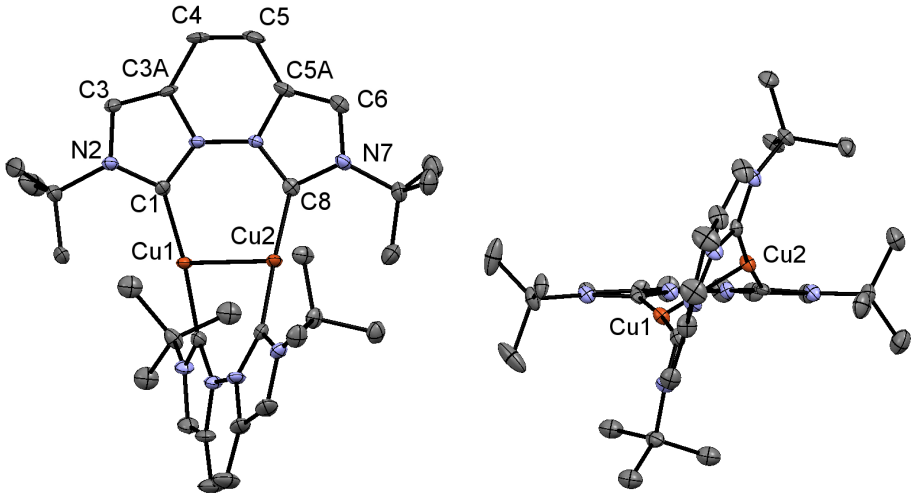

(a) The view from the side. (b) The view from above.

Figure 33: Molecular structure of the Cu complex **16**. Atoms are shown with anisotropic atomic displacement parameters at the 50% probability level. Hydrogen atoms as well as one cocrystallized acetonitrile molecule, one cocrystallized dichloromethane molecule and two PF_6^- anions are omitted for clarity. Selected bond lengths (Å) and angles (deg): Cu1-Cu2 2.451(3), C1-Cu1 1.905(6), C8-Cu2 1.897(6), N9-N10 1.382(6), C4-C5 1.318(9), C1-C8 3.02, C8-Cu2 1.896(6), N10-C1-N2 101.6(4), N9-C8-N7 102.4(4), C3-C3A-C4 134.5(5), C6-C5A-C5 134.9(5), N10-C1-Cu1 126.8(4), N2-C1-Cu1 130.4(4).

The Cu-Cu distance of 2.451(3) Å is short compared to the Cu-Cu distance in elemental copper (2.56 Å) and the the sum of the van der Waals radii of two Cu atoms (2.8 Å).[115] The distance is also shorter than the Cu-Cu distance in the vegi^{Bn} Cu complex (2.4923 Å)[37] and in literature known dinuclear Cu(NHC) complexes bearing neutral ligands.[109,120]. The Cu-carbene bond lies almost perfectly on the bisecting line of the NCN carbene angles. This can be explained by the strong electron donating character of the ligand that reduces the Coulomb repulsion. This was also observed in the vegi^{Bn} Cu complex.[37] The tricyclic pyridazine moiety is twisted by 17.63° to maintain an almost linear coordination at the copper atoms (174.3(2) and 172.2(2)°. The average Cu-C(carbene) distance measures 1.90 Å, which is shorter then the Au-Carbene distance in the Au complex (2.02 Å) and the Ag-Carbene distance (2.20 Å). The N9-N10 bond length is rather long (1.382(6) Å) compared to the C4-C5 distance (1.318(9) Å)

which is often observed in the chelating vegi complexes. The NCN angles of 101.6(4)° (N10-C1-N2) and 102.4(4)° (N9-C8-N7) are slightly smaller than those found in the respective Au complexes.

From the reaction of silver complex **17** with 1.1 equivalents of $AuClSMe_2$ the gold complex **19** as the main product and another unsymmetric complex in a ratio of 1:0.25 were obtained. At -30 °C single crystals were formed from an acetonitrile/diethyl ether solution of the gold complex **19**. The molecular structure reveals the formation of an unsymmetric gold complex. The formation of compound **19** was also confirmed by ^{1}H NMR spectroscopy.

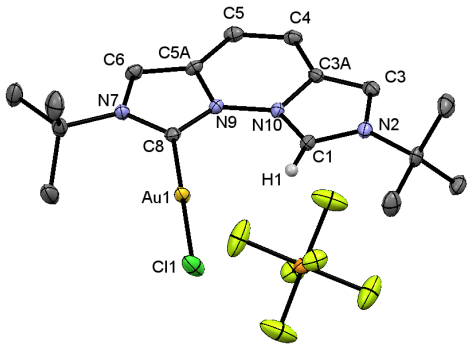

Figure 34: Molecular structure of the Au complex **19**. Atoms are shown with anisotropic atomic displacement parameters at the 50% probability level. Hydrogen atoms (except H-1) are omitted for clarity. Selected bond lengths (Å) and angles (deg): Au1-C8 1.982(3), Au1-Cl1 2.2758(7), C1-H1 0.9500, C4-C5 1.344(4), H1-Cl1 3.705, N9-N10 1.385(3), C8-Au1-Cl1 179.08(8), N10-C1-N2 106.9(2), N9-C8-N7 102.7(2), C3-C3A-C4 135.2(2), C6-C5A-C5 134.9(2).

The C3-C3A-C4 and C6-C5A-C5 angles are almost identical (135.2(2) and 134.9(2)°). The N10-C1-N2 angle measures 106.9(2)° in the imidazole moiety while the angle decreases upon coordination to the gold atom to 102.7(2)° (N9-C8-N7). The C8-Au1-Cl1 angle is almost linear (179.08(8)). The Au1-Cl1 bond length is longer (2.2758(7) Å) than the Au1-C8 bond length (1.982(3) Å) which is comparable to known Au(I)NHC

complexes.[121,122] Complex **19** is an interesting compound in the perspective of synthesizing heterobimetallic complexes. A sequential reaction with this complex by deprotonation of H-1 and adding another metal precursor could lead to a heterobimetallic complex.

5.2 Heterodinuclear coinage metal vegi^{R} complexes

The synthesis of heterodinuclear NHC complexes is of great interest to study metal-metal bonding interactions. The combination of two metals in one molecule can produce synergistic catalytic activity which could lead to novel catalysts. Different examples of heterobimetallic complexes containing NHC are shown in Figure 35. A heterodinuclear pincer-type bis-NHC complex containing Ag and Au **I** is known and generated via a postsynthetic modification.[123] Other examples are complex **II** by *Catalano*[124] or complex **III**, a linear Au and Ag NHC complex stabilized by a diphosphanyl ligand, which was published by *Braunstein*.[125]

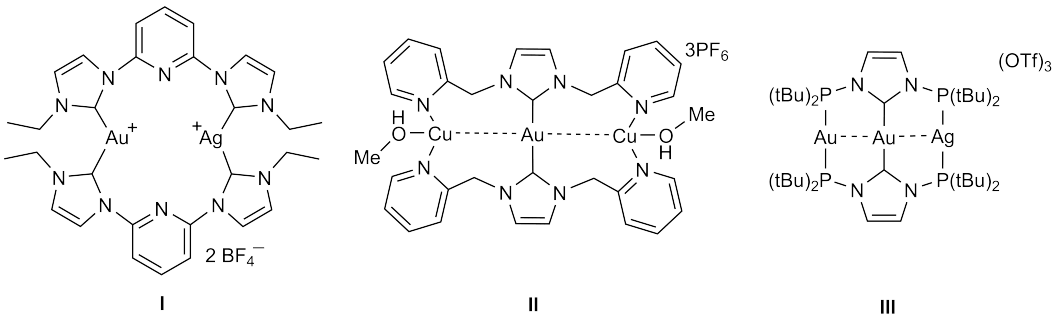

Figure 35: Selected literature examples of heterobimetallic complexes containing NHC ligands.

The synthesis of heterobimetallic complexes with the vegi$^{t\mathrm{Bu}}$ ligand has been reported by *Denninger*.[33] All the experiments were repeated and carried out under different conditions to confirm the system to be at equilibrium state.

5.2.1 Generation of the Ag-Au complex 20

A heterodinuclear Ag-Au-NHC complex **20** was *in situ* synthesized from one equivalent of Ag-NHC complex **17** with one equivalent of [AuCl(SMe_2)] in CD_3CN (Figure 36, route A). After a short time an equilibrium reaction takes place through transmetalation. Signals for both the homodinuclear complexes **17** and **18** and also the mixed Ag-Au NHC complex **20** occur in the ^1H NMR spectrum. To verify the mixture to be at equilibrium, the complex **20** was also generated *in situ* by metal ion exchange combining one equivalent of the Ag-NHC complex **17** with one equivalent of the Au-Au complex **18** in CD_3CN (route B).

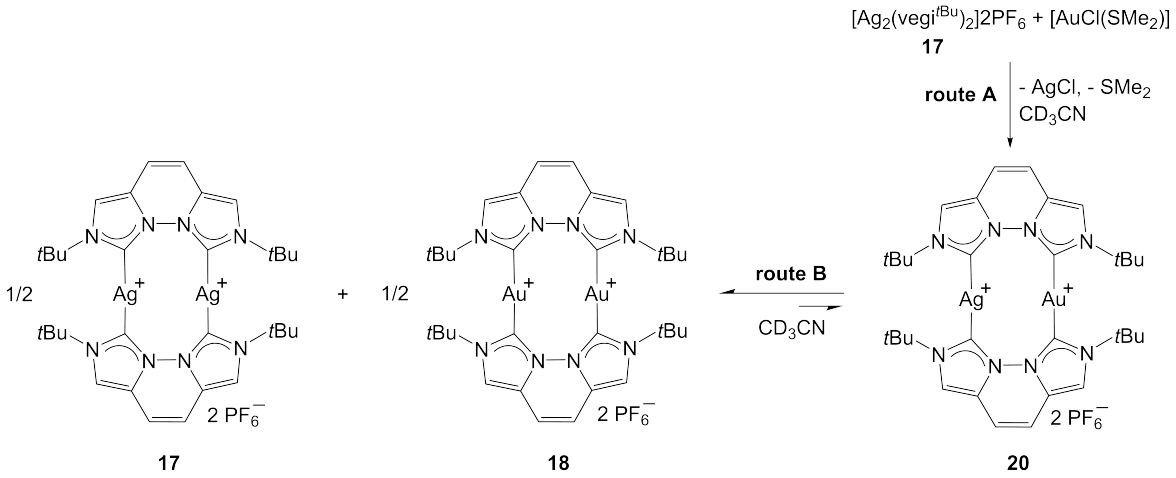

Figure 36: Synthesis of **17**, **18** and **20**.

It is important to mention that if very pure complexes **17** and **18** were used to generate the mixed complex **20** it is necessary to add catalytic amounts of $AgBF_4$ (< 0,5 mg) to form the mixed Au-Ag-NHC complex **20**. Hence, some free silver ions as a catalyst are essential in the mixture to overcome kinetic inhibition and to get into the thermodynamic equilibrium sate.

Table 11: ^{1}H NMR data of complexes **17**, **18** and **20** in CD_3CN.

	^{1}H (NMR) [ppm]		
	H-3/6	H-4/5	*t*Bu
Ag complex **17**	7.92, "t", $^{4}J_{AgH} = 1.7$	7.18, s	1.74, s
Au complex **18**	7.87, s	7.14, s	1.83, s
Ag-Au complex **20**	7.90, s	7.17, s	1.75, s
	7.88, d, $^{6}J_{AgH} = 1.5$	7.16, s	1.83, s

Both synthetic routes A and B lead to the same ^{1}H NMR spectrum. The ^{1}H NMR spectral data of complexes **17**, **18** and **20** are summarized in Table 11. The signals in the ^{1}H NMR spectrum for the mixed Ag-Au complex **20** lie in between the signals for the mononuclear complexes **17** and **18**. Because the mixed complex **20** has reduced symmetry four signals for H-4-, H-5-, H-3- and H-6 are expected. The same compound was obtained by *Denninger* and is also reported in my master thesis.[33] In addition *Denninger* could confirm the formation of the mixed Ag Au complex **20** by mass spectrometry. The signal at m/z 989.203765 (cald 989.204170) for the $[[AgAu(vegi^{tBu})_2]PF_6]^+$ fragment is observed and also the signals for the homodinuclear complexes **17** and **18**. Based on the ^{1}H NMR spectrum the amount of the mixed Ag-Au-NHC complex **20** at the equilibrium state is lower than that of the homodinuclear complexes **17** and **18**. A ratio of 1:0.3:1 = [Ag-Ag]:[Ag-Au]:[Au-Au] immediately after the generation is obtained. If the mixture is measured after one week under exclusion of light the ratio of the gold complex **18** increases to 1.5 due to decomposition of the Ag complex **17** under release of Ag(0).

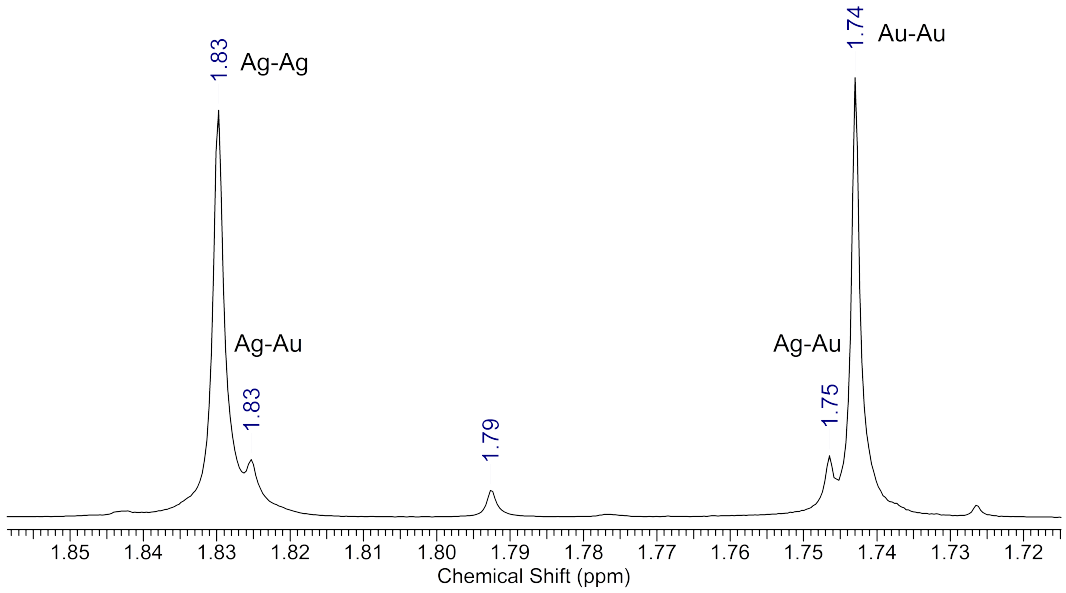

Figure 37: ^{1}H NMR spectrum (detail): *tert*-butyl group (signal at 1.79 ppm: *t*Bu signal of **2a**.)

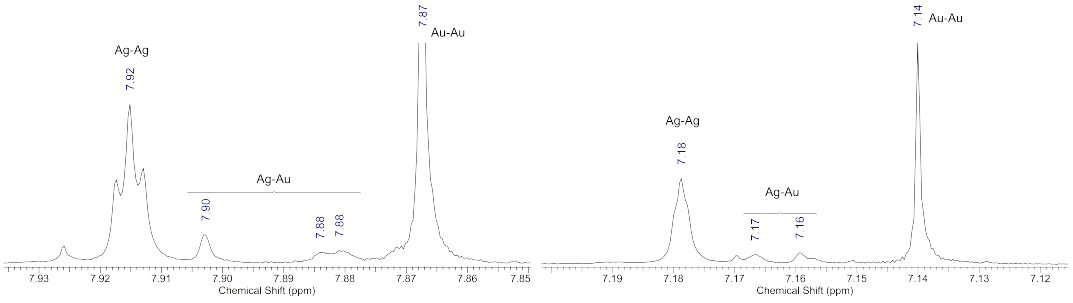

(a) signals:H-3/6 (b) signals:H-4/5

Figure 38: ^{1}H NMR spectrum: detail H-3/6 and H-4/5.

The generation of complex **20** was also tried by adding $AgBF_4$ to a solution of the gold complex **18** in acetonitrile, but only the signals for the gold complex **18** were detected in the ^{1}H NMR spectrum. The white suspension turned grey quickly and on the next day a black precipitation was observed. This might be due to the more stable Au-carbene bond and different reaction conditions.

It is possible to shift the equilibrium of the reaction to the product side (mixed complex **20**) by heating the reaction mixture at 60 °C overnight. The new ratio (measured at

room temperature) is 1:0.7:1 (**17**:**20**:**18**). Experiments from my master thesis reveal that the doublet at 7.88 results from a Ag-H coupling ($^{6}J_{\mathrm{AgH}}$ = 1.5 Hz) and not from a $^{4}J_{\mathrm{AgH}}$ coupling which had been confirmed with a ^{109}Ag,^{1}H-HSQC (CD_3CN) experiment. This explains why the doublet is next to the signal for the Au-NHC complex **18** and not next to the Ag-NHC complex **17**.[114]

To see whether the equilibrium is solvent dependent, dichloromethane was used as a solvent. The synthesis routes A and B to form the mixed complex **20** were also carried out in dichloromethane. Some unknown side products are produced in the less polar solvent via synthesis route A and no formation of the mixed complex **20** was observed. If synthesis route B, combining both homodinuclear complexes **17** and **18**, was carried out in CD_2Cl_2 only the signals for the homodinuclear complexes **17** and **18** were obtained but no formation of complex **20** was observed.

If synthetic route B was carried out in CD_2Cl_2, the solvent removed *in vacuo* and then the sample measured in CD_3CN, the mixture shows the formation of the heterodinuclear complex **20**. Also the signals for the homodinuclear complexes **17** and **18** are obtained in a ratio of 0.7:0.3:1 = [Ag-Ag]:[Ag-Au]:[Au-Au]. This explains that most probably a coordinating solvent like CD_3CN is necessary to kinetically favor the reaction. Adding several drops of acetonitrile to a solution of **17** and **18** in dichloromethane shows the formation of the signals of **20** in between the signals of the homodinuclear complexes **17** and **18** and a broadening of all signals. The mixed complex **20** was generated via synthesis route A in CD_3CN and confirmed by ^{1}H NMR spectroscopy. After removal of the solvent *in vacuo* the residue was dissolved in pure CD_2Cl_2 and a signal between the signals H-4/5 of the homodinuclear complexes **17** and **18** is obtained. The signals are not baseline separated. The signals belong to the mixed complex **20**.

The *in situ* generation of complex **20** via synthetic route A and B in CD_3CN is straightforward, whereas in CD_2Cl_2 the formation of complex **20** is kinetically inhibited. The formation of complex **20** is therefore solvent dependent.

A solution of complex **20** (route B) in CD_3CN was measured after four months partially exposed to light. The ^1H NMR spectrum shows a clear degradation of the intensity of all signals belonging to the silver complex **17**. This is due to the fact that silver(I) is reduced to silver(0) which can be observed in the NMR tube as black precipitation. Also each signal H-3, H-6, H-4, H-5 and *tert*-butyl groups of the mixed complex **20** merged into one broad signal. The exchange between the metal ions must be fast on the NMR timescale that no splitting of the signals occurs anymore. The ESI mass spectrum of this mixture shows the signals for the gold complex **18** and the mixed complex **20** but no longer a signal for the silver-NHC complex **17**.

Another synthetic pathway was tested to generate the heterobimetallic complex **20**. Using one equivalent of $AgBF_4$ and 0.5 equivalents of $AuClSMe_2$ should lead to the formation of AgCl and upon addition of the Li complexes (**10a** and **10a-H**) to the formation of the heterobimetallic complex **20** via transmetalation. However, this reaction did not lead to the formation of complex **20**. In all experiments the formation of only the Au complex **18** was observed. Therefore, the synthesis of a gold(I) precursor without any chloride ligands was of interest (Figure 39).

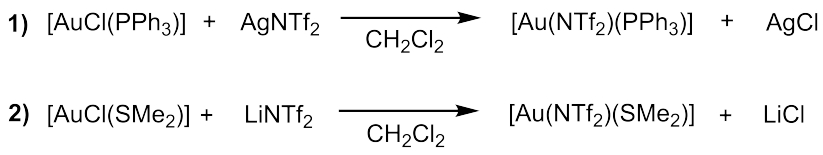

Figure 39: Literature known synthesis of $[Au(NTf_2)(PPh_3)]$ (top) and $[Au(NTf_2)(SMe_2)]$ (bottom).

The idea was to use this chloride-free precursor and a silver(I) precursor and generate the heterobimetallic complex **20** as a third and independent route C (Figure 40). Similar to a literature known synthesis of bis(trifluoromethanesulfonyl)amide triphenylphosphane gold(I) (1)[104] experiments were carried out. Instead of commercially available $AgNTf_2$ the lithium salt $LiNTf_2$ (bis(trifluoromethanesulfonyl)amide lithium(I)) was used and with the addition of $[AuCl(SMe_2)]$ the gold (I) precursor $[Au(NTf_2)(SMe_2)]$ should be gene-

rated. Both compounds were mixed together in dichloromethane and after filtering off LiCl over Celite® the resulting pale colored solution was concentrated to dryness. The elemental analysis did not indicate the formation of [Au(NTf_2)(SMe_2)]. The literature known synthesis (Figure 39) should be used to obtain a Au(I) source without chloride ligands.

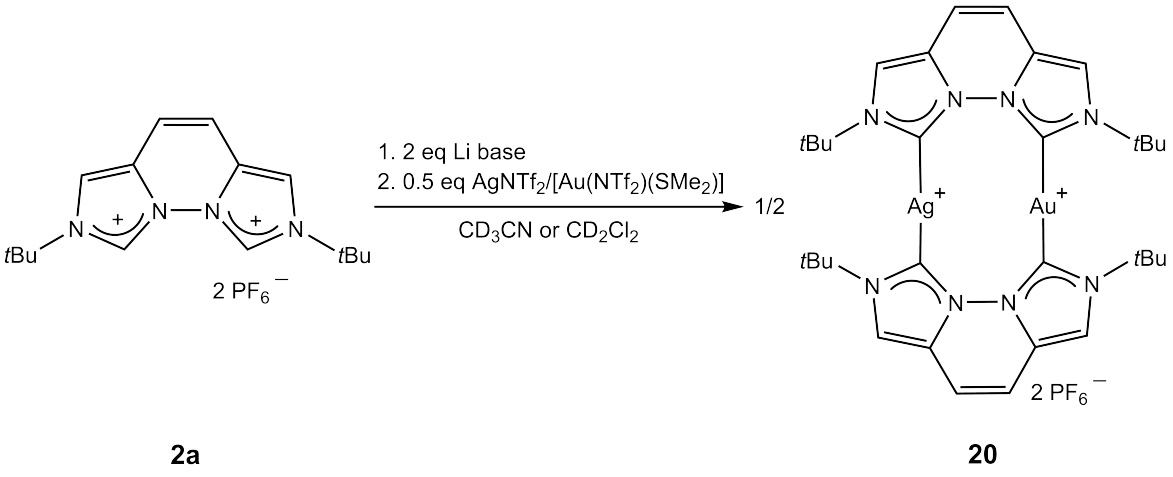

2a **20**

Figure 40: Proposed synthesis of the heterobimetallic complex **20** (route C).

5.3 Generation of the Ag-Cu complex 21

A heterodinuclear Ag-Cu-NHC complex **21** was *in situ* generated by metal ion exchange combining one equivalent of the Ag-NHC complex **17** with one equivalent of Cu-NHC complex **16** in CD_3CN (route B). The ratio is 1:2:1 = [Ag-Ag]:[Ag-Cu]:[Cu-Cu] in the ^{1}H NMR spectrum. The same ratio was found by *Denninger*.[33] The mixed complex **21** was also generated by combining one equivalent of Ag NHC complex **17** with one equivalent of CuCl in CD_3CN (route A). Signals for both homodinuclear complexes **17** and **16** and also the mixed Ag-Cu NHC complex **21** appear in the ^{1}H NMR spectrum. Achieving the same ratio by the alternative route B confirms the assumption of the system beeing in its equilibrium state. When I repeated route B, I obtained a ratio of 1:3:2 = [Ag-Ag]:[Ag-Cu]:[Cu-Cu] but K is identical.

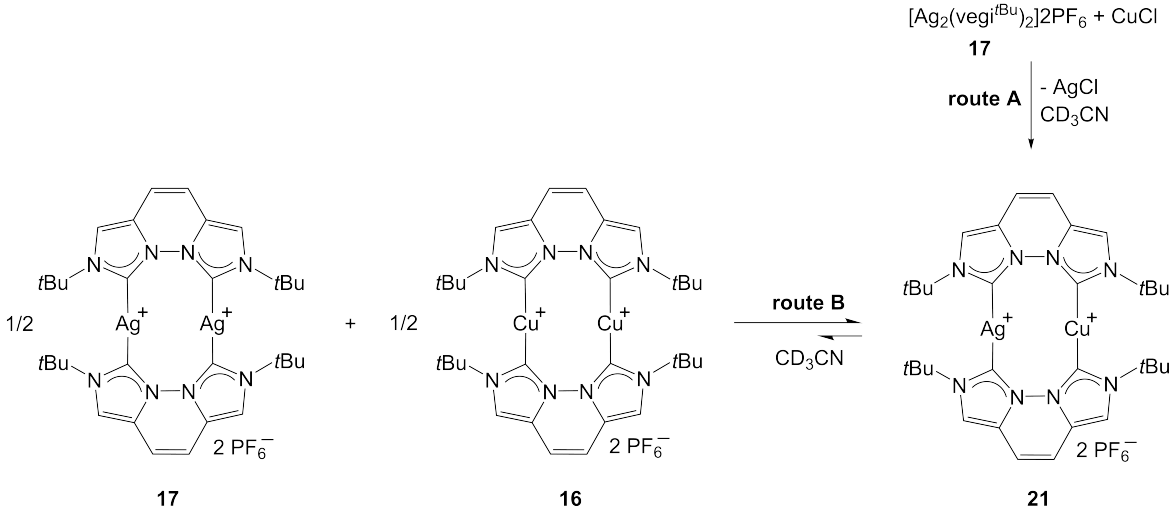

Figure 41: Synthesis of **16**, **17** and **21**.

In contrast to the Ag-Au complex **20** the ^{1}H NMR spectrum of **21** reveals only a symmetric species. The expected double set of the signals for the asymmetric complex **21** was not observed in the ^{1}H NMR spectrum which can be explained by a fast exchange of the metal ions. The spectroscopic data of the mixed complex **21** are shown in Table 12. The metal ion exchange has to be fast (on the NMR timescale) so that only three signals are observed for the mixed complex **21**.

Table 12: ^{1}H NMR data of complexes **16**, **17** and **21** in CD_3CN.

	^{1}H (NMR) [ppm]		
	H-3/6	H-4/5	*t*Bu
Ag complex **17**	7.92, "t", $^{4}J_{\mathrm{AgH}} = 1.7$	7.18, s	1.74, s
Cu complex **16**	7.87, s	7.16, s	1.70, s
Ag-Cu complex **21**	7.89, s	7.17, s	1.72, s

Both synthetic routes A and B form the mixed complex **21** were also carried out in dichloromethane. The same ^{1}H NMR spectrum with the same ratio as in acetonitrile was obtained. Synthetic route B was carried out in acetonitrile and after removal of the solvent and dissolving the residue in dichloromethane the same product ratio was obtained. No solvent dependency occurred forming complex **21**.

The generation of the heterodinuclear gold-copper complex by the reaction of the gold complex **18** with the copper complex **16** was also investigated. Heating the reaction mixture overnight at 50 °C has not led to the formation of a Au-Cu NHC complex. Only the signals for the gold complex **18** and copper complex **16** were observed in the ^{1}H NMR spectrum. The addition of small amounts of copper(I) chloride as a catalyst only lead to broadening of the signals of the homodinuclear complexes **16** and **18**. This indicates a fast exchange of the metal ions. No clear formation of an Au-Cu NHC complex has occurred in the ^{1}H NMR spectrum. The high-resolution FT-ICR mass spectrum of this mixture shows both homodinuclear complexes **16** and **18** as well as a signal at m/z 945.228938 (calcd 945.228678) indicating the formation of a Au-Cu NHC complex. Probably the amount of the mixed complex is too small to be detected in the ^{1}H NMR spectrum or the signals for the mixed complex are covered by the signals for the homodinuclear complexes **18** or **16**.

In conclusion the *in situ* generation of heterobimetallic coinage metal complexes (**20** and **21**) can be obtained via two different synthetic routes. Both reactions are in their thermodynamic equilibrium. The formation of the Ag-Cu complex **21** shows a statistical distribution with a ratio of 1:2:1. While the Ag-Au complex **20** shows a ratio of 1:0.3:1. The complex **20** is less stable than the homodinuclear complexes **17** and **18**.

6 Synthesis of group 10 vegi^{R} complexes

In this chapter the synthesis of group 10 metal vegi^{R} complexes is presented. It is usually achieved by a deprotonation reaction of **2a,b** with a slight excess of alkali-metal base followed by a transmetalation with a group 10 metal precursor.

6.1 Synthesis of nickel vegi^{R} complexes

6.1.1 Synthesis of nickel(0) NHC complexes

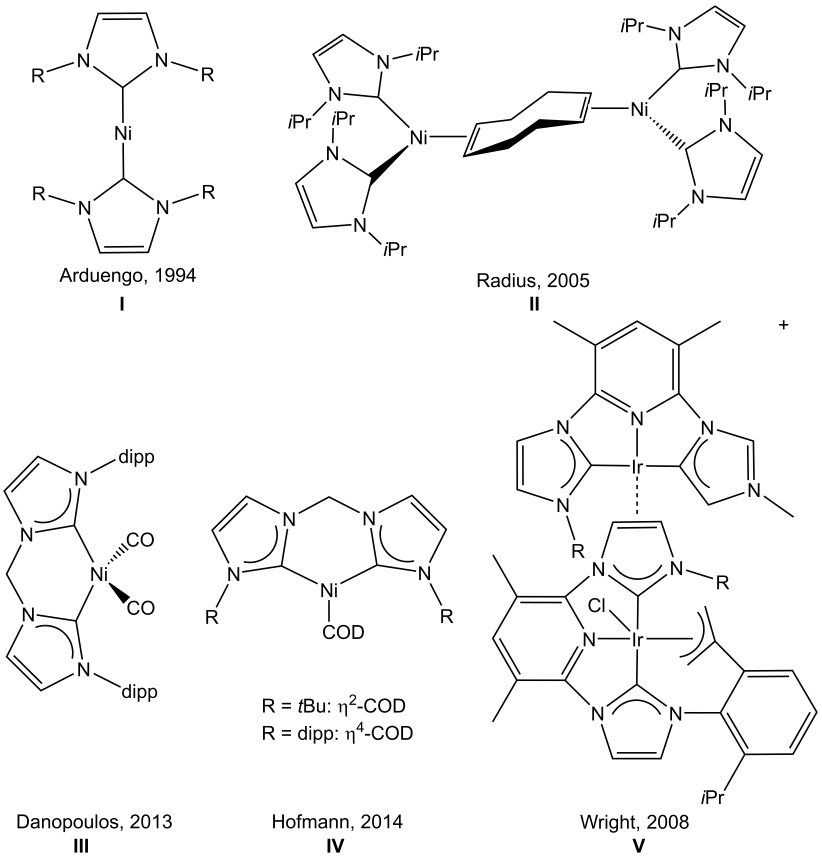

Figure 42: Selection of literature known Ni(0)-NHC complexes and an Ir(I)/Ir(III) NHC complex.

Most nickel(0)-NHC complexes are synthesized by the reaction of an isolated or an *in situ* generated free carbene with a nickel(0) precursor such as bis(1,5-cyclooctadiene)nickel(0) ([Ni(COD)$_2$]) or by reduction of Ni(II)- or Ni(I)NHC complexes.

The first Ni(0)-NHC complex was synthesized as a 14-electron homoleptic Ni(0) complex via the free carbene and [Ni(COD)$_2$] in THF (Figure 42 **I**).[126] *Hofmann et al.* obtained a chelate bis(NHC) complex (**IV**) with a η^2-coordination or a η^4-coordination of the COD ligand, depending on the steric bulk of the NHC ligand, which adopts a chair confirmation (Figure 42 **IV**). The corresponding bis(imidazolium) salt is deprotonated *in situ* with LiHMDS and [Ni(COD)$_2$] is added at room temperature in THF.[127] Ni(0)-bis(NHC) complexes bearing two CO ligands are also known (Figure 42 **III**).[128] In general Ni(NHC) complexes serve as catalysts in various reactions such as cross coupling reactions.[129] The high abundance and low cost of nickel compared to palladium makes nickel an attractive metal to work with.

Ni(COD)$_2$ is a yellow compound that must be stored at -20 °C or below. A freshly mixed solution of Ni(COD)$_2$ in THF-d$_8$ shows only signals of Ni(COD)$_2$ at 2.12 and 4.31 ppm in the ^{1}H NMR spectrum. The compound is unstable in solution and after several hours turns darker and additional signals of non-coordinated cyclooctadiene (2.33 and 5.50 ppm) are detected.

The aim was the synthesis of a Ni(0)-vegi^{R} complex (Figure 43). The bis(imidazolium) salt **2a** was therefore deprotonated with 2.2 equivalents of KHMDS in THF-d$_8$, forming *in situ* the K-vegi$^{t\mathrm{Bu}}$ complex, followed by a transmetalation with Ni(COD)$_2$ and analyzed by NMR spectroscopy.

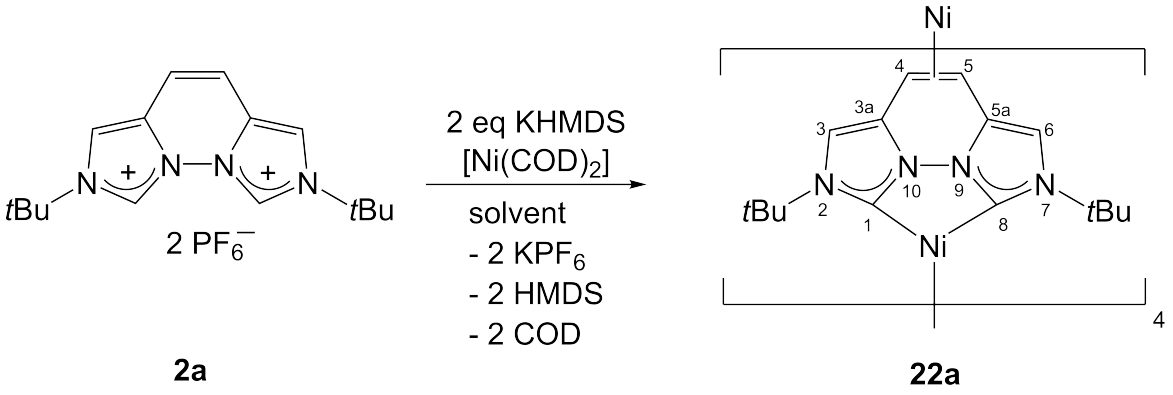

Figure 43: Synthesis of the [Ni(vegi$^{t\mathrm{Bu}}$)]$_4$ **22a,b**.

The ^{1}H NMR spectrum of the red brown solution shows three singlets at 6.57 ppm, 2.57 ppm and 1.60 ppm (filled circle) and another set of three singlets at 6.49 ppm ,

2.55 ppm and 1.59 ppm (square) in a 1:1.5 ratio. Additional signals for HMDS, COD and Ni(COD)$_2$ were also detected. The $^{13}C\{^1H\}$ NMR spectrum shows signals for the *tert*-butyl groups at 31.6 ppm and 57.0 ppm. The carbene signal is detected at 176.8 ppm, the signal for C-3/6 at 105.2 ppm and the signal C-4/5 upfield shifted at 22.9 ppm. The signals for the second species are at 21.7, 31.7, 57.3 and 105.9 ppm in the $^{13}C\{^1H\}$ NMR spectrum, the carbene signal could not be detected. The complex is stable for up to one week in solution.

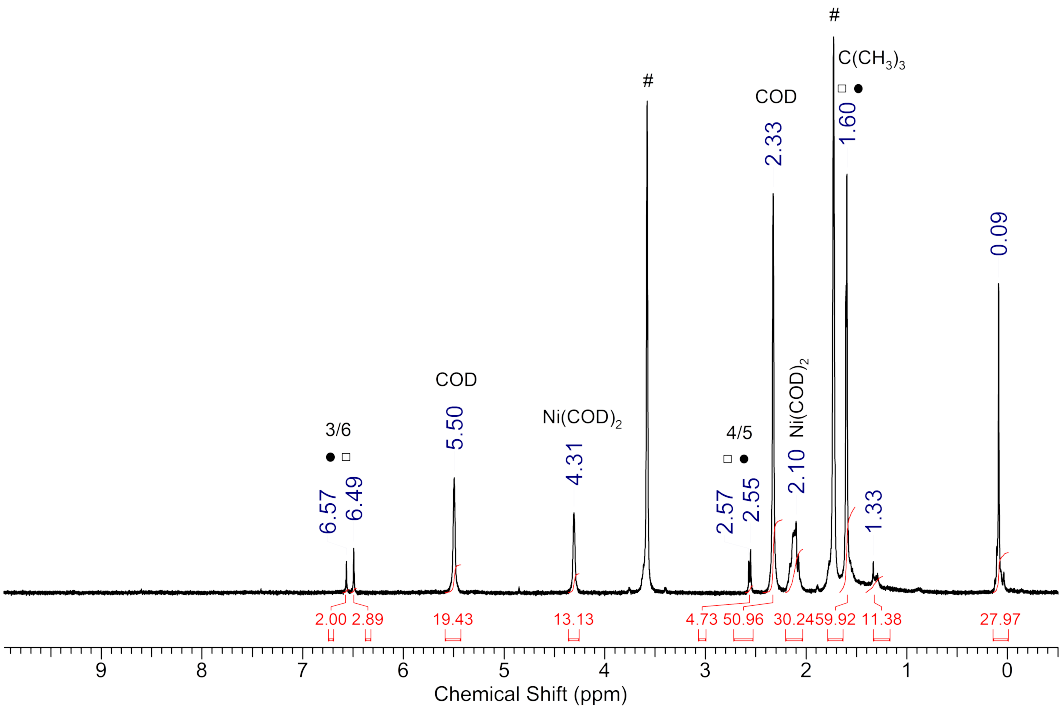

Figure 44: ^{1}H NMR of [Ni(vegi$^{t\mathrm{Bu}}$)]$_4$ complex (**23a**) (THF-d$_8$, #) .

It was expected that the Ni(0)-vegi complex would have a similar structure to **IV** obtained by *Hofmann*,[127] but the strong high-field shifts of the signal H-4/5 (2.57 as well as 2.55 ppm) in the ^{1}H NMR and 22.9 ppm of C-4/5 in the $^{13}C\{^1H\}$ NMR spectrum indicate that another complex must have formed. Red crystals suitable for X-ray structure analysis were grown at room temperature from a saturated THF-solution. The crystals were unfortunately not of optimal quality therefore, the structure serves only as a connectivity proof. The crystals of **22a** belong to the triclinic space group $P\bar{1}$. The

asymmetric unit contains two molecules of **22a** and a cocrystallized strongly disordered THF molecule within the cycle. The X-ray structure analysis confirms that the tetranuclear macrocycle [Ni(vegi$^{t\mathrm{Bu}}$)]$_4$ was formed, in which one Ni(vegi$^{t\mathrm{Bu}}$) fragment coordinates to the pyridazine double bond C-4/5 of the next Ni(vegi$^{t\mathrm{Bu}}$) moiety. This tetramer displays a very rare C_{4h} symmetry. The geometry around the nickel atom (d^{10}) of this 16 electron complex is square planar. The nickel atom favors the coordination to the double bond C4-C5 of the vegi$^{t\mathrm{Bu}}$ ligand over coordination to the more electron rich double bond of the COD ligand. This can be explained with the strong electron-donating character of the dicarbene which causes a very high electron density at the nickel center. The strong up-field shifts of H-4/5 and C-4/5 support the coordination of the double bond to the Ni atom. It is known that the coordination of olefins to a metal center results in a high-field shift of the signals versus those of the free olefin.[127] The additional signal set mentioned earlier must belong to another symmetric Ni complex which is similar to the obtained tetramer complex. For example, five vegi$^{t\mathrm{Bu}}$ fragments could form a cycle with five nickel-vegi moieties. This unique coordination resembles one example from the research group of *Danopoulos*, in which a pyridine-dicarbene-Ir(I) complex coordinates to the unsaturated backbone of imidazolin-2-ylidene (Figure 42, **V**).[130]

The coordination mode of the C4-C5 bond to the nickel atom can be regarded as anything in between a η^2-coordination of the C4-C5 double bond to the nickel atom and a metallacycle formation via a formed oxidative addition. To get insights into the bond situation the bond lengths and the hybridization need to be taken into account. The C4-C5 bond length measure an average 1.455(9) Å in complex **22a**. Due to the not optimal quality of the measured crystal, calculations on a model system regarding the bond distance have been made by *Kunz*. The obtained values match those found experimentally suggesting a pronounced single bond character. Additionally, the $^1J_{\mathrm{CH}}$ coupling constant was examined and detected via a ^{13}C ^{1}H HSQC NMR experiment. The $^1J_{\mathrm{CH}}$ coupling (H-4/5) in complex **22a** of 155 Hz is smaller than the $^1J_{\mathrm{CH}}$ coupling constant of the ligand precursor **2a** of 181 Hz. Suggesting a decrease of s-character upon coordination favors a pronounced metallacyclic contribution to the coordinative

bond in **22a**. However, it has to be taken into account that the value of the coupling constant is influenced, e.g. by electronegative substituents on the carbon atom, that change the effective nuclear charge[131] as well as geometric rearrangement in the vegi-ligand due to chelation. Therefore, determining the hybridization only by means of the $^{1}J_{CH}$ coupling constant is more reliable for pure hydrocarbons.

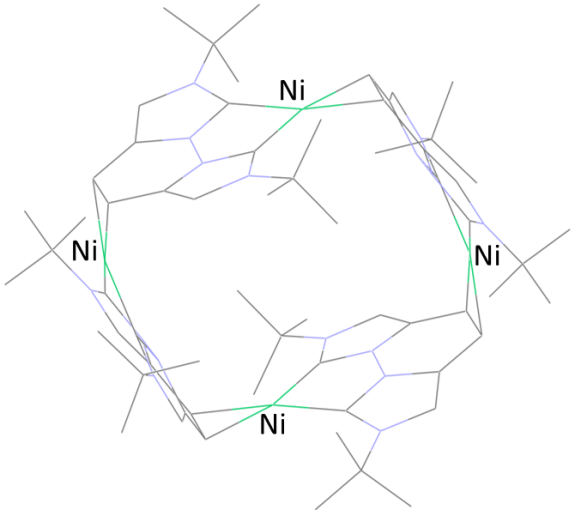

Figure 45: Molecular structure of macrocycle [Ni(vegi$^{t\mathrm{Bu}}$)]$_4$ **22a**. Hydrogen atoms as well as one disordered THF-molecule are omitted for clarity, depiction in wireframe style for reasons of clarity.

The reaction was repeated on a larger scale and the suspension filtered over Celite®. The resulting pink filtrate was concentrated to dryness. Only the signals of decomposition products are detected in the ^{1}H NMR spectrum. In another isolation attempt, the reaction was carried out in THF. By removing the solvent and washing the residue with *n*-pentane, Ni(COD)$_2$ and HMDS can be removed. Residual COD could be removed by additional washing steps with *n*-pentane and the [Ni(vegi$^{t\mathrm{Bu}}$)]$_4$ complex was isolated, however, it still contains KPF_6.

Influence of base and solvent:
The same results have been obtained by using LiHMDS instead of KHMDS under otherwise identical conditions. To see whether the used solvent has any influence on the reaction the experiment was repeated in toluene-d$_8$. After addition of KHMDS

to a suspension of **2a** in toluene the ^{1}H NMR spectrum was measured to see whether the K-vegi$^{t\mathrm{Bu}}$ complex was formed and thus the deprotonation of **2a** was successful. Then Ni(COD)$_2$ was added to the light brown suspension and only one signal set was detected in the ^{1}H NMR spectrum at 1.56 ppm, 2.98 ppm and 6.53 ppm. The signals of free COD, HMDS and for Ni(COD)$_2$, which was not fully consumed were also observed. In toluene one symmetric complex of vegi$^{t\mathrm{Bu}}$ was obtained, as confirmed by the singlets at 1.56, 2.98 and 6.53 ppm. Toluene-d$_8$ was then removed and THF-d$_8$ added, to obtain the identical two signal sets as before, when the reaction was carried out in THF-d$_8$. Heating of the orange-pink suspension at 100 °C for 2 hours increased the amount of free COD. When the reaction mixture was heated overnight, new signals at 5.81, 5.77 ppm arose (both broad singlets, each with an integral of about three, hardly baseline separated) and a broad singlet at 1.39 ppm with an integral of 19. The signals of [Ni(COD)$_2$] vanished completely and instead the signals of COD increased further. Most likely a new symmetric vegi$^{t\mathrm{Bu}}$ complex formed that is not coordinated to the C-4/5 double bond.

With the precursor **2b** an analogous Ni(0) complex can be generated, when the ligand precursor **2b** is deprotonated with KHMDS in THF-d$_8$ and then Ni(COD)$_2$ is added. The ^{1}H NMR spectrum of the brown solution reveals the generation of one symmetric vegi$^{n\mathrm{Pr}}$complex, with the signals H-3/6 at 6.29 ppm and H-4/5 at 2.81 ppm. The signals for the *n*-propyl group are detected at 3.82 ppm (NCH_2), 1.80 ppm (CH_2) and 0.97 ppm (CH_3). Signals of free COD, HMDS, [Ni(COD)$_2$] and KHMDS are also observed. In comparison to the formation of [Ni(vegi$^{t\mathrm{Bu}}$)]$_4$ only one complex is obtained. Most likely the same tetrameric structure forms as with vegi$^{t\mathrm{Bu}}$, due to better similarity of the signal of H-4/5 at 2.81 ppm. So far, suitable single crystals for X-ray analysis could not be obtained.

Nickel catalyzed - vinylcyclopropane rearrangement (VCPR)

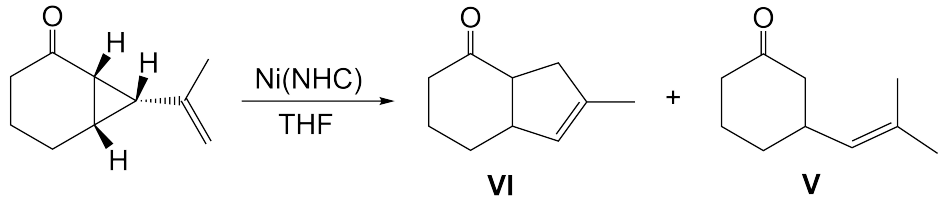

Figure 46: Reaction pathway of the vinylcyclopropane rearrangement

The vinylcyclopropane rearrangement is a ring expansion of a vinyl-substituted cyclopropane ring into a cyclopentene ring. The very first example of a thermal vinylcyclopropane rearrangement was published by *Neureiter* in 1959. He took 1,1-dichloro-2,2-dimethylcyclopropane and under pyrolysis conditions discovered a rearrangement to 4,4-dichlorocyclopentene.[132] The rearrangement reaction has become a key preparation route for cyclopentene rings in complex natural product synthesis. The research group of *Laschat* works with Nickel mono(NHC) catalysts for the VCPR. In a cooperation, the chelating complexes Ni(0)vegi$^{t\mathrm{Bu}}$ and Ni(0)vegi$^{n\mathrm{Pr}}$ were tested as catalysts in the VCPR to see whether the desired bicyclic product **VI** could be obtained. In initial independent experiments two stoichometric reactions were carried out. The vegi$^{t\mathrm{Bu}}$ salt and KHMDS were mixed in THF-d_8, after 20 minutes Ni(COD)$_2$ was added. After confirmation of the formation of the Ni(0)vegi$^{t\mathrm{Bu}}$-tetramer via ^{1}H NMR spectroscopy (Figure 47, spectrum 1) the substrate (isopropenyl-bicyclo[3.1.0]heptenone), which was synthesized in the *Laschat* group, was added at room temperature (Figure 47, spectrum 2). A solid (yellow to pink) precipitated from the pink solution. The reaction mixture was measured after 17 hours at room temperature, new signals were obtained (Figure 47, spectrum 3) at 5.81 (s), 5.78(s), 4.78 (s), 4.73 (s), 2.27 (m), 2.20 (m), 1.94 (m), 1.88 (s), 1.86 (s). After another 17 h at room temperature the signals shifted slightly down-field. Noteworthy is that the signals at 4.78 ppm and 4.73 ppm form multiplets with a coupling constant of about 1 Hz and also the signals at 1.88/1.86 start to split and show a small coupling constant of 1 Hz and 6 Hz. In addition the signals of [Ni(COD)$_2$] start to vanish.

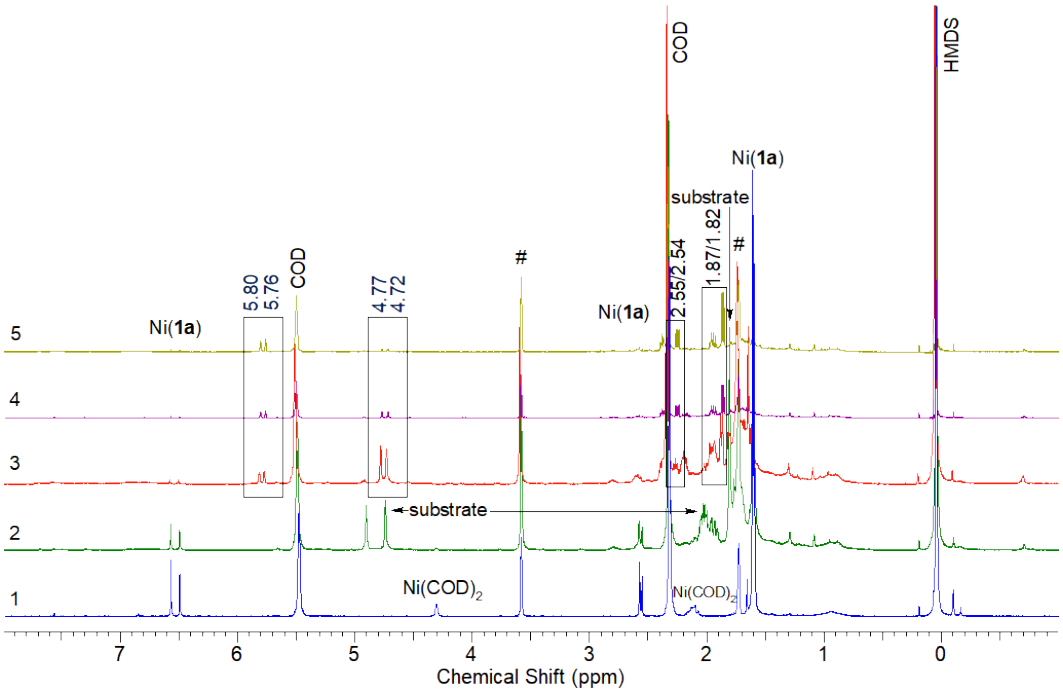

Figure 47: ^{1}H NMR spectra: 1) Ni-complex **22a**; 2) addition of substrate; 3) after 17 h at room temperature; 4) + 17 h; 5) + 30 h.

The isomerisation product **V** with two characteristic singlets at 5.80 pm and 5.76 ppm for the olefinic protons and two singlets for the methyl groups at 1.87 ppm and 1.85 ppm was likely formed during the synthesis. The desired bicyclic product **VI** can be excluded as it would lead to only one singlet for a methyl group. Since many signals are obtained in the spectrum of the reaction mixture it is difficult to detect the signals of the desired product **VI** during the reaction. Also the multiplets of the aliphatic protons are hard to identify. The *Laschat* group measured a GC/MS spectrum from the reaction mixture and found a signal at m/z = 150 (retention time 13.18 min) which is the molecular weight of the desired product, but also for the isomerisation product.

The same reaction was repeated at 100-120 °C because the *Laschat* group obtained the desired bicycle **VI** at 120 °C in toluene. To see whether this also happens in THF the reaction was repeated at higher temperatures. All compounds were mixed together and an orange to pink suspension formed. The mixture turned dark brown after heating at 100 °C overnight. In addition the mixture was heated for 3 h at 120 °C. The

brown suspension was filtered over Celite® and a ^{1}H NMR spectrum was measured (Figure 48, spectrum 2). For comparison the ^{1}H NMR spectrum of the catalyst **22a** can be seen in Figure 48, spectrum 1. The signals at 5.80, 5.76, 4.90, 4.77, 1.87 and 1.85 ppm are identical to those from the experiment at room temperature. The signal at 7.37 ppm and the very broad signal at 5.26 ppm are new. The isomerisation product **V** along with other still unknown products was formed at higher temperatures in THF.

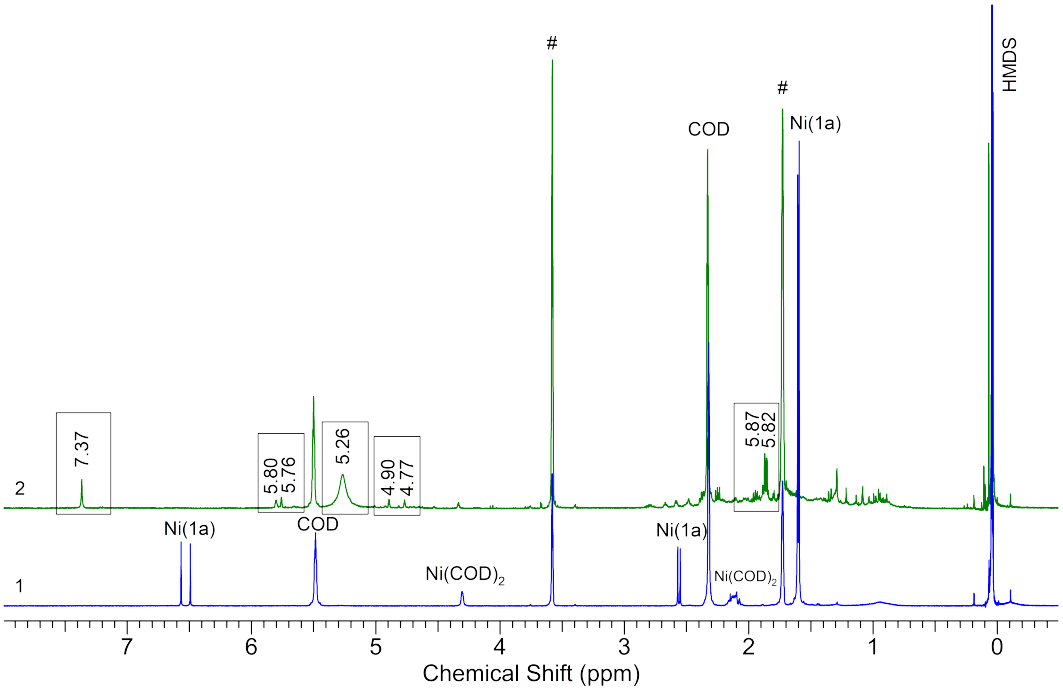

Figure 48: ^{1}H NMR spectra: 1) Ni-complex **22a**; 2) addition of substrate.

The proposed mechanisms starts with the addition of the Ni(0)-vegi$^{t\mathrm{Bu}}$ complex to the substrate, most likely forming the η^2-vinycyclopropane complex **I** that undergoes an oxidative addition to form the vinylmetallacyclobutane species **II** (Figure 49). This complex **II** can isomerize to the intermediate **III**. Complex **III** can undergo a β-H elimination, followed by reductive elimination to release the isomer **V**.

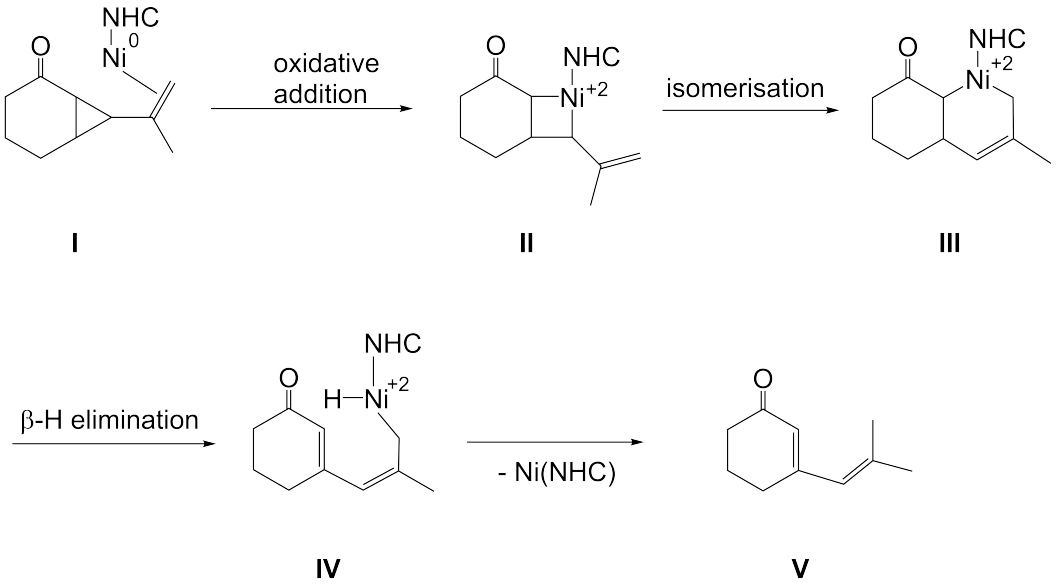

Figure 49: Proposed mechanism of VCPR; Ni(0)NHC = **22a** (monomer).

6.1.2 Synthesis of Nickel(II) vegi^{R} complexes

Nickel(II)-NHC complexes can either be synthesized by substitution of weaker donor ligands, e.g. phosphines, by NHCs or by using basic Ni(II) precursors such as $Ni(OAc)_2$. The nickel(II)–NHC complexes represent the biggest class of nickel-NHC complexes. Nickel-NHC are very prominent homogenous catalysts for C-C and C-N bond formation reactions[129], for example in the Kumada cross coupling reaction of aryl chlorides and bromides with aryl magnesium chloride under mild conditions.[133]

There are two main synthesis pathways: transmetalation or direct synthesis. In the transmetalation path a Ag(I)- or Cu(I)-NHC complex reacts with a suitable Ni(II) precursor namely, $[Ni(DME)Cl_2]$ or $[NiCl_2(PPh_3)_2]$. In the direct method, an imidazolium salt or a free carbene reacts with a suitable Ni(II) precursor.[129]

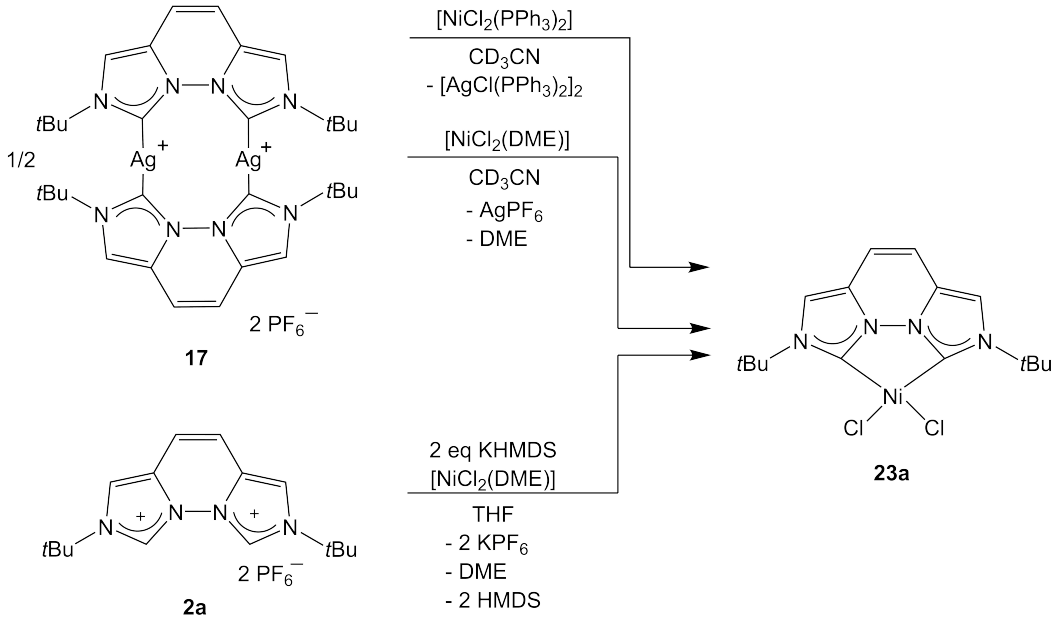

Figure 50: Synthesis of [$NiCl_2$(vegi^{tBu})] via different synthesis pathways.

A nickel complex of type [$NiCl_2$(vegi^{tBu})] can be synthesized via transmetalation from the *in situ* generated K-vegi^{tBu} complex with [$NiCl_2$(DME)] in THF or from the silver complex **17** with [$NiCl_2$(DME)] or [$NiCl_2(PPh_3)_2$].

[$NiCl_2$vegi^{tBu}] generation via silver complex **17**:

My first experiments to obtain a [$NiCl_2$(vegi^{tBu})] complex were carried out via transmetalation of the ligand from the silver complex **17** to [$NiCl_2$(DME)]. Immediately after mixing all the starting materials in acetonitrile a white solid precipitated from a light pink solution. The ^{1}H NMR spectrum of the pink filtrate shows only the signals of the silver complex **17** and for the bis(imidazolium) salt **2a** in low concentration. At room temperature pink single crystals formed that were analyzed by X-ray diffraction. The molecular structure shows a distorted tetrahedral geometry around the nickel atom. The d^8-configuration (Ni^{2+}) in a tetrahedral geometry leads to a paramagnetic 16 electron compound, which explains the absence of the signals in the ^{1}H NMR spectrum. The sterically demanding *tert*-butyl groups force the nickel atom into this geometry. The bite angle (C8-Ni1-C1) measures 84.22°. This value is higher than that of other

known chelating vegi^{R} complexes (usually around 81°). The average Ni-C(carbene) bond (2.047 Å) is shorter than the Ni-Cl bond with an average bond length of 2.231 Å. Compared to the values reported in literature for a paramagnetic Ni(II)Br_2-dicarbene complex (Ni-C(carbene) 1.976 Å) the Ni-C(carbene) bond length is longer for **23a**.[128] Typically, Ni(II) bis(NHC) complexes obtain a 1:2 metal-to-ligand stoichiometry with a square planar geometry. The preferred 1:1 metal-to-ligand stoichiometry in complex **23a** can be ascribed to the steric bulk of the ligand **2a**.[129] Mainly, neutral Ni(II)-di(NHC)-dichlorido complexes obtain a distorted square planar geometry.[134,135]

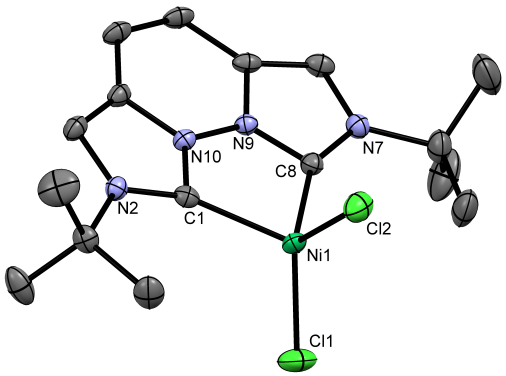

Figure 51: Molecular structure of the [$NiCl_2$vegi^{tBu}] complex **23a**. Atoms are shown with anisotropic atomic displacement parameters at the 50% probability level. Hydrogen atoms as well as two cocrystallized acetonitrile molecules and a second independent molecule of **23a** are omitted for clarity. Selected bond lengths (Å) and angles (deg) of one molecule: Ni1-C8 2.046(2), Ni1-C1 2.048(2), Ni1-Cl2 2.2269(7), Ni1-Cl1 2.2359(6), N9-N10 1.360(2), C4-C5 1.352(3), C1C8 2.742, C8-Ni1-C1 84.22(8), C8-Ni1-Cl2 109.13(6), C1-Ni1-Cl2 108.21(6), C8-Ni1-Cl1 108.19(6), C1-Ni1-Cl1 113.40(6), Cl2-Ni1-Cl1 125.78(3), N9-C8-N7 100.95(17), N10-C1-N2 100.86(18), C6-C5A-C5 139.9(2), C3-C3A-C4 140.4(2).

In another experiment the [$NiCl_2(PPh_3)_2$] precursor was used. The silver complex **17** was dissolved in acetonitrile and then the Ni(II) precursor was added. A light pink solid precipitated from the light pink solution. The ^{1}H NMR spectrum of the solution shows the signals of triphenylphosphane and some small signals resulting from residual bis(imidazolium) salt **2a**. The solid was filtered off, washed with acetonitrile, dried *in*

vacuo and dissolved in $CDCl_3$. The ^1H NMR spectrum shows two broad signals around 15 ppm and 8 ppm (close to $CDCl_3$ signal). From the choloroform solution pink single crystals formed within days at room temperature. They revealed the structure of **23a** as well. Colorless crystal also formed and turned out to be the already known $[AgCl(PPh_3)_2]_2$.[136] The broad signals and down-field shift to 15 ppm indicated the formation of a paramagnetic compound.

$[NiCl_2vegi^{tBu}]$ generation via deprotonation of vegi^{tBu} with base:
The complex **23a** was also synthesized via the *in situ* generation of the K-vegi^{tBu} complex from **2a** with KHMDS in THF. After 30 min the suspension was filtered. $[NiCl_2(DME)]$ was added to the filtrate and the ^1H NMR spectrum of the pink solution showed the same spectrum that was obtained from the the former experiments.

The reaction was repeated on a preparative scale to isolate the desired complex **23a**. **2a** was deprotonated with KHMDS in THF and then $[Ni(DME)Cl_2]$ was added to the brown filtrate which resulted in a pink solution. The solution was dried *in vacuo* and the residue separated from solid KPF_6 by extraction with dichloromethane. The pink solution was dried *in vacuo* and washed with *n*-pentane to obtain a pink solid. The elemental analysis of the dark pink compound still showed impurities of KPF_6 (1.05).

Although the Ni complex is a paramagnetic compound an analyzable ^1H NMR spectrum was obtained when the chemical shift range was increased. In CD_3CN signals at 15.10 ppm with an integral of 19 (very broad) and two relatively sharp signals at 8.98 ppm and 22.65 ppm with each an integral of one can be found. The acetonitrile solution was concentrated to dryness *in vacuo* and the residue measured in THF-d_8. The signals now appear at 22.70, 14.36 and 13.09 ppm and all are very broad. After four weeks the signals are still present, but additional signals of **2a** are obtained. The ^1H NMR measurements in THF-d_8 were repeated with an even broader sweep width. Signals at 113.50, 35.05 (br s), 22.18, 13.30 and -125.1 ppm were found. In addition this mixture showed signals for HMDS, DME and small amounts of **2a**. When the mixture was cooled down to -45 °C the signals shifted to 151.70, 49.13, 28.17 and 18.27

ppm. Another down-field shift can be observed when cooling to -95 °C. The NMR measurements clearly revealed the formation of paramagnetic Ni(II)-vegi complexes. The assignment of the signals to the Ni(II) complexes is difficult, as the integral do not match and due to the paramagnetic nature. Additional evidence for the formation of complex **23a** was obtained using mass spectrometry with peaks at m/z 363.1 (100) $[M\text{-}Cl]^+$ and 289.2 (71) $[M\text{-}Ni\text{-}2Cl\text{-}H]^+$.

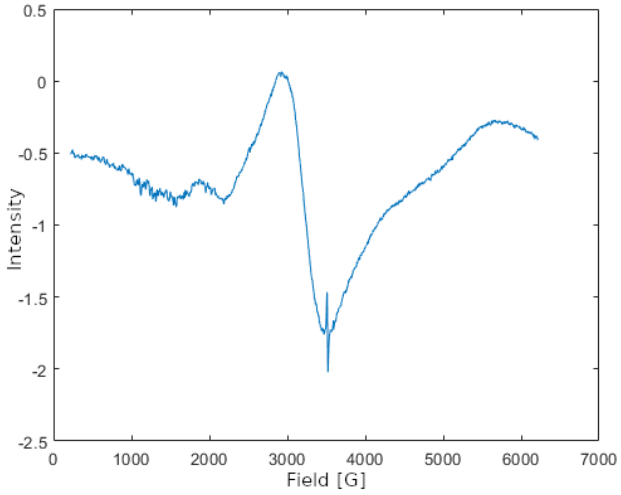

Figure 52: EPR spectrum; measured at room temperature of a solid sample of **23a**.

Because of the paramagnetism of the Ni(II) complex an EPR spectrum was also measured. The experimental g-value for the Ni(II) complex **23a** of a solid sample is 2.180. Any hyperfine couplings were not resolved in the spectrum. The signal observed in the EPR spectrum is a clear evidence for the formation of a paramagnetic compound. The smaller signal (g = 2.003) most likely results from SiO radicals from the glass.

In order to form a $[Ni(vegi^{tBu})_2Cl_2]$ complex, a reaction with one equivalent of **2a**, 2.2 equivalents of KHMDS and one equivalent of $[NiCl_2(DME)]$ was carried out. Long red, very thin needles were obtained. The single crystals reveal the formation of a Ni(II) tetracarbene complex **24** (Figure 53). The molecular structure serves only as a connectivity proof due to the limited crystal quality obtained. The geometry around the nickel atom is distorted tetrahedral. One vegi^{tBu} tilts towards the *tert*-butyl group of the second vegi^{tBu} ligand. The structure shows similarities with the calculated second

minimum structure by *Kunz* of the homoleptic vegi^{tBu} Li complex, in which the ligands coordinate in a C_2-symmetric butterfly conformation.[42] The spectrum indicates the formation of a paramagnetic compound. All signals are very broad. The broadening could also result from the suspension which forms. The formation of two equivalents of KCl instead of KPF_6 must occur in this reaction to form $[Ni(vegi^{tBu})_2](PF_6)_2$. The formation of a 1:2 metal-to-ligand complex **24** is possible with the sterically demanding ligand **2a**, which is usually obtained for Ni(II) bis(NHC) complexes.[129]

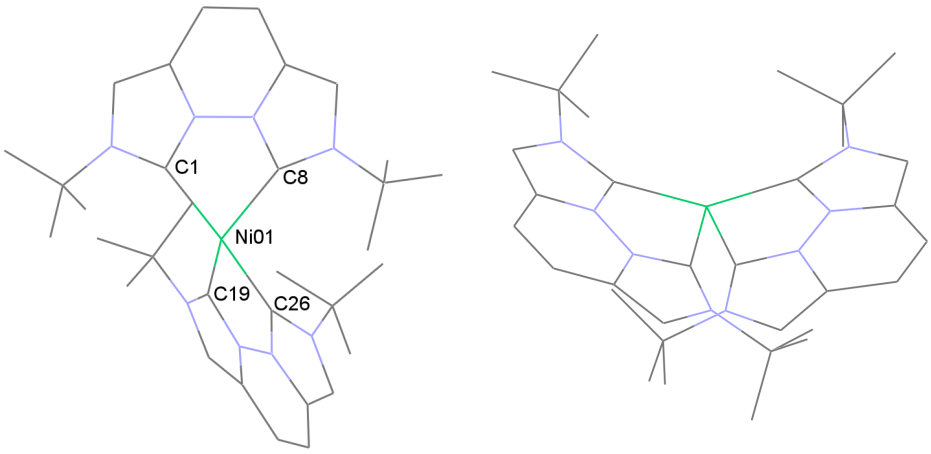

(a) The view from above. (b) The view perpendicular to C_2 axis.

Figure 53: Molecular structure of the $[Ni(vegi^{tBu})_2](PF_6)_2$ complex **24**. Hydrogen atoms as well as the two PF_6^- molecules are omitted for clarity.

Attempts to synthesize the desired $[Ni(vegi^{tBu})_2](PF_6)_2$ by a Ag–NHC transfer reaction had been unsuccessful and led to the formation of $[NiCl_2(vegi^{tBu})]$. The silver complex **17** and $[Ni(DME)Cl_2]$ were mixed in a 1:1 ratio in acetonitrile. The grey suspension turned light pink after a few minutes. The ^{1}H NMR spectrum shows signals of the silver complex **17**, **2a** and signals at 15.08 and 22.05 ppm which are very broad. Pink crystals were obtained which match according to their diffraction pattern with $[NiCl_2(vegi^{tBu})]$ and not the tetracarbene Ni complex **24**. Homoleptic nickel(II) NHC complexes with two chelating dicarbene ligands are known and can be prepared by the reaction of anhydrous $Ni(OAc)_2$ with diazolium diiodide.[137] With the sterically less demanding vegi^{nPr}, the formation of Ni (II) tetracarbene complexes should be more

easily achieved. A nickel tetracarbene complex with bromide as the counteranion which was generated via the transmetalation of a silver complex is known in literature.[138] All Ni(II) tetracarbene complexes reported in the literature show a square planar geometry. To the best of my knowledge no distorted tetrahedral complexes are known.

Because the formation of a paramagnetic Ni(II) compound was attributed to the steric bulk of the ligand, the less sterically hindered salt **2b** was tested as a ligand for a Ni(II) complex as well to see whether a diamagnetic complex would form with a square planar geometry around the nickel atom. **2b** was suspended in THF-d_8 and 2.2 equivalents of KHMDS were added. After 15 min [$NiCl_2$(DME)] was added to the brown suspension. The color turned even darker. The ^{1}H NMR spectrum indicates to formation of most likely two diamagentic complexes or an unsymmetric complex with signals of low intensity in the aromatic region (singlets at 7.89, 7.77, 7.47 and doublets at 6.96 and 6.85).

A black solid precipitated from the yellow solution. The black solid was filtered off and measured in acetonitrile. The ^{1}H NMR spectrum in acetonitrile is depicted in Figure 54 and looks different than the spectrum in THF-d_8. It is evident that diamagnetic compounds are formed with the less sterically hindered **1b** ligand.

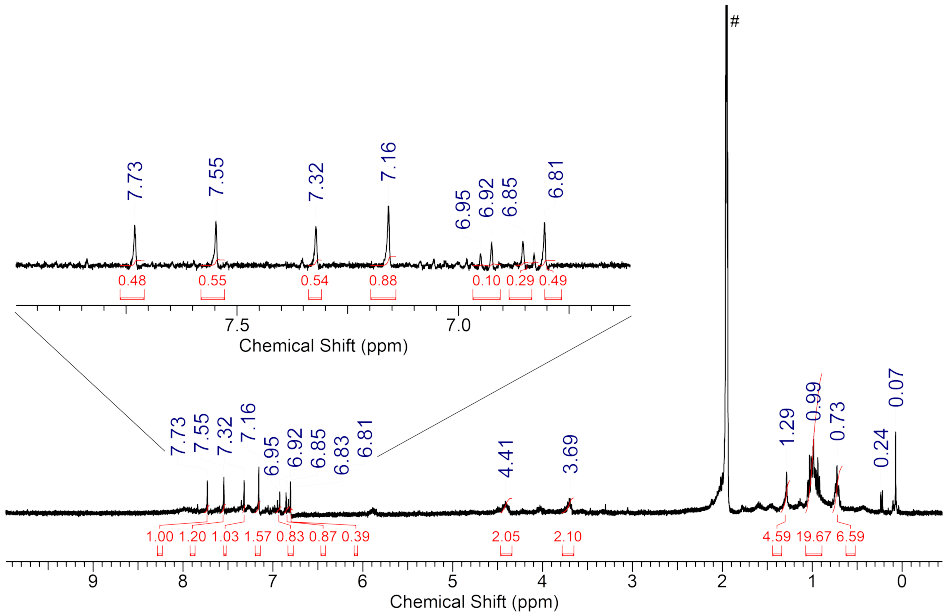

Figure 54: ^{1}H NMR spectrum of the formed solid (CD_3CN, #).

A ^{1}H NMR spectrum of the acetonitrile mixture was measured again with a broader sweep width to check the formation of any paramagnetic compounds. Additional signals at 15.77 and 42.88 ppm were detected. Both signals shift down-field to 61.66, 22.70 ppm when measuring the ^{1}H NMR spectrum at -45 °C. Contrary to expectations this confirms the formation of a paramagnetic complex bearing the vegi$^{n\mathrm{Pr}}$ ligand.

With the sterically demanding ligand **2a** a dichlorido-Ni(II) complex **23a** can be synthesized with a 1:1 metal-to-ligand ratio which is rare, usually complexes with a 1:2 metal-to-ligand ratio are obtained with dicarbene NHC ligands. In one reaction a Ni(II) complex **24** with two ligands **2a** was formed. When the preparation of complex **24** intentionally was attempt, only crystals of complex **23a** formed. The ^{1}H NMR measurement of **23a** revealed the formation of probably more than one complex. Presumably paramagnetic species like **23a** and **24** are present in the mixture and only in one case crystals of **24** were obtained. Due to steric reasons the complexes **23a** and **24** are not square planar and therefore paramagnetic. The nature of the Ni(II)-vegi$^{n\mathrm{Pr}}$ **23b** complex must also be paramagnetic as the signals in the ^{1}H NMR measurement confirmed.

6.2 Synthesis of Palladium vegi^{R} complexes

A large number of palladium-NHC complexes have been reported.[139,140] They have been investigated for applications in homogeneous catalysis.[141] A wide range of applications like C-C coupling reactions, hydroamination or hydrosilylation has been reported.[8–10] They are especially useful in Suzuki-Miyaura cross-coupling reactions.[142–146]

6.2.1 Synthesis of Palladium vegi^{R} dimethyl complexes

At first, the [Pd(CH$_3$)$_2$(TMEDA)] precursor was synthesized according to literature (Figure 55).[147] Methyllithium in diethyl ether and commercially available [PdCl$_2$(TMEDA)] were combined to form 47 % of [Pd(CH$_3$)$_2$(TMEDA)] as a white solid. The tetramethylethylendiamine ligand has labile Pd-N bonds. Therefore, it can be exchanged by stronger coordinating ligands such as NHCs to form Pd(NHC)-dichlorido complexes or Pd(NHC)-dimethyl complexes.[128,148]

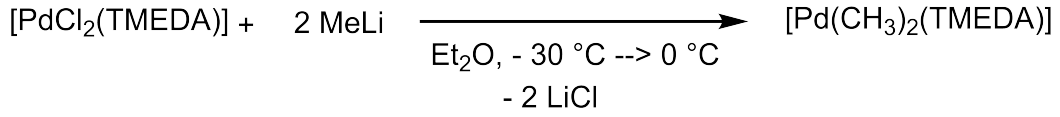

Figure 55: Literature known synthesis of [Pd(CH$_3$)$_2$(TMEDA)]

For the generation of [Pd(CH$_3$)$_2$(vegi$^{t\mathrm{Bu}}$)] the vegi$^{t\mathrm{Bu}}$·2HPF$_6$ salt (**2a**) was deprotonated with 2.2 equivalents of LiHMDS in THF followed by addition of one equivalent of the metal precursor [Pd(CH$_3$)$_2$(TMEDA)](Figure 56).

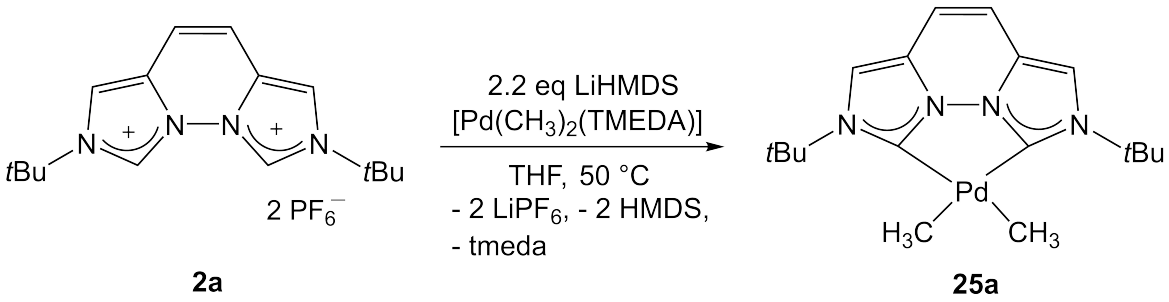

Figure 56: Synthesis of **25a**.

The immediate measurement of a ^{1}H NMR spectrum of the brown-red solution showed the formation of a new symmetric complex due to the three singlets and additionally, the signals for the lithium-complexes **10a** and **10a-H**. After 5 h at 5 °C the reaction was completed and the signals for the Li-complexes **10a** and **10a-H** have vanished. In the ^{1}H NMR spectrum the signals of the [Pd(CH$_3$)$_2$(vegi$^{t\mathrm{Bu}}$)] **25a** complex and the signals of TMEDA and HMDS are detected. The backbone signals for the vegi$^{t\mathrm{Bu}}$ ligand of **25a** appear at 7.51 (H-3/6) and 6.89 ppm (H-4/5) in THF-d$_8$, and that of the *tert*-butyl signal is at 1.79 ppm. The signal of the methyl ligands is shifted upfield to 0.26 ppm. The carbene signal of the complex **25a** is detected at 180.0 ppm in THF-d$_8$ in the ^{13}C NMR spectrum. The formation of the complex can also be confirmed by ESI mass spectrometry, with peaks at *m/z* 391.1 (69) ([M - CH$_3$]$^+$) and 463.2 (100) ([M - CH$_3$]$^+$ + THF).

Several experiments to obtain a clearer reaction have been carried out. Two equivalents of formed LiPF$_6$, TMEDA and HMDS during the reaction have to be removed. The following workup attempts always led to the decomposition of the complex **25a**. First the suspension was filtered, followed by a precipitation in acetonitrile with diethyl ether. The beige solid showed signals of the side products and decreased signals of TMEDA . All the other byproducts such as the Pd precursor, HMDS and traces of LiHMDS were still present. Also filtration over Celite®, neutral alox or simple filtration did not lead to the isolation of the product.

The synthesis of a [Pd(CH$_3$)$_2$(vegi$^{n\mathrm{Pr}}$)] complex **25b** was realized with KHMDS as a base and [Pd(CH$_3$)$_2$(TMEDA)] as the precursor.

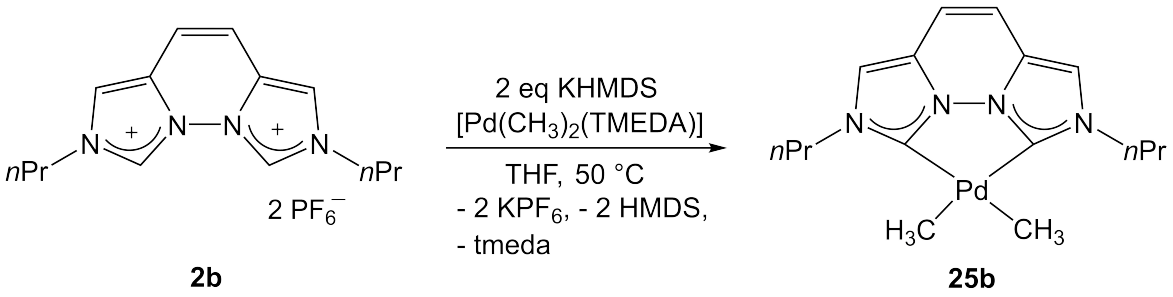

Figure 57: Synthesis of **25b**.

2a was deprotonated with KHMDS in THF and after 15 min [Pd(CH_3)$_2$TMEDA] was added to the brown suspension. The mixture was stirred overnight at 50 °C. The suspension was concentrated and the double amount of *n*-pentane was added. The suspension was filtered, and the dark remaining solid was washed twice with 1.5 mL each of a 1:1 mixture of THF/*n*-pentane. Then the solid was extracted with THF/toluene 1:1 and the extract dried in *vacuo* to obtain a beige solid. The ^{1}H NMR spectrum shows the formation of the product **25b** without any side products. The backbone signals for [Pd(CH_3)$_2$(vegi^{nPr})] are detected at 7.22 (H-3/6) and 6.94 ppm (H-4/5) in THF-d_8. The methyl groups coordinated to the palladium are shifted upfield to 0.16 ppm. In the ^{13}C NMR spectrum the carbene signal of the complex **25b** appears at 177.7 ppm in THF-d_8. In the ESI mass spectrum signals at *m/z* 347.0 (59) ([M - CH_3 - CH_4]$^+$) and 363.0 (100) ([M - CH_3]$^+$) were found.

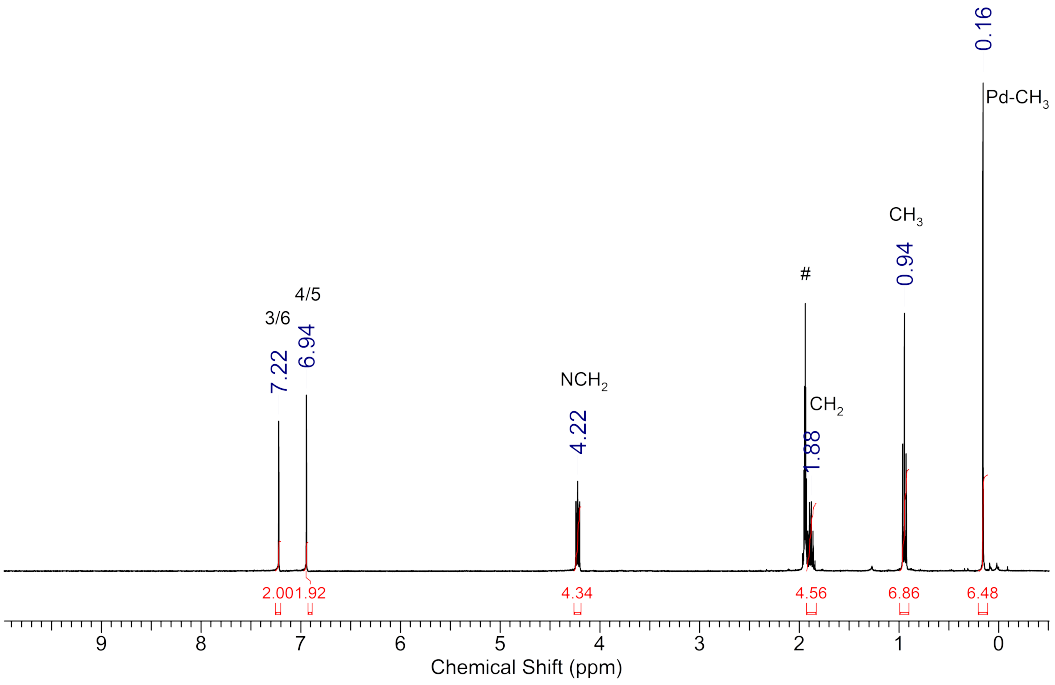

Figure 58: ^{1}H NMR spectrum of [Pd(CH$_3$)$_2$(vegi$^{n\mathrm{Pr}}$)] **25b** (CD$_3$CN, #).

Interestingly the synthesis of the dimethyl-vegi$^{n\mathrm{Pr}}$ Pd complex via KHMDS or LiHMDS in THF and [Pd(CH$_3$)$_2$(TMEDA)] lead to the formation of small amounts of methane and ethane after the mixture was heated at 50 °C overnight, which is not observed in the case of complex **25a** bearing the vegi$^{t\mathrm{Bu}}$ ligand. The sterically less hindered dimethyl-vegi$^{n\mathrm{Pr}}$ Pd complex must promote a C-H activation in this complex. Further experiments regarding the thermal stability of the isolated dimethyl complexes **25a** and **25b** in solution would be necessary to analyze this C-H activation in more detail.

6.2.2 Synthesis of Palladium vegi^{R} dichlorido complexes

Palladium(II)-NHC complexes can be obtained from the reaction of basic Pd(II) precursors such as Pd(OAc)$_2$ with imidazolium salts. Dichlorido-Pd complexes are accessible by the reaction of the isolated or *in situ* generated carbene with [PdCl$_2$(TMEDA)], PdCl$_2$ or [Pd(CH$_3$CN)$_2$Cl$_2$]. Dihalido-Pd NHC complexes are known in literature and are active catalysts in cross coupling reactions. Dichloridopalladium(II) complexes of the type [Pd(bis(NHC)Cl$_2$)] from the corresponding bis(imidazolium) salts are known.[149,150] In this chapter cis-Pd-dihalido-vegi^{R} complexes are discussed.

First experiments to obtain a vegi$^{n\mathrm{Pr}}$ halido Pd complex were made by *Gierz*.[31] She reacted vegi$^{n\mathrm{Pr}} \cdot 2\mathrm{HPF_6}$ with $\mathrm{Pd(OAc)_2}$ in acetonitrile and added NaI at 50 °C. After 20 h the mixture was filtered off. The red-brown solid was washed with acetonitrile and *n*-pentane. The remaining solid was only soluble in DMSO, and in the ^{1}H NMR spectrum a double signal set was observed. *Gierz* postulated an equilibrium between a $[\mathrm{PdI_2(vegi}^{n\mathrm{Pr}})]$ complex and its dimer. The use of chlorido instead of iodido ligands should suppress the formation of the dimer as she postulated.

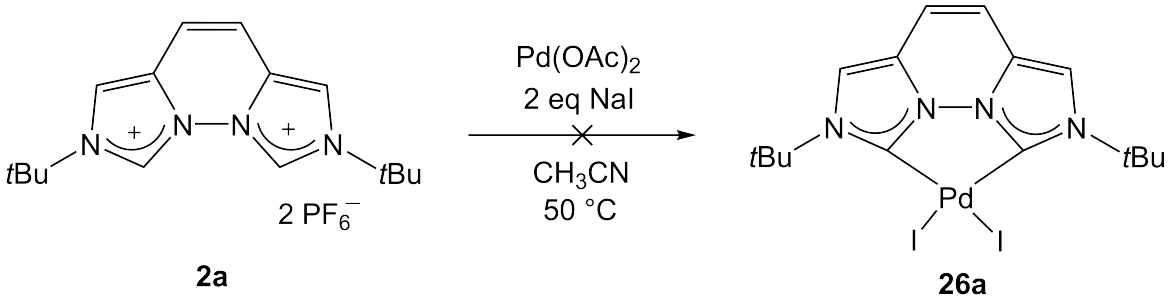

Figure 59: Proposed synthesis of **26a**.

An analogous reaction with vegi$^{t\mathrm{Bu}}$ instead of vegi$^{n\mathrm{Pr}}$ was tested (Figure 59). **2a** and $\mathrm{Pd(OAc)_2}$ were dissolved in acetonitrile. NaI was added to the orange solution, which turned black immediately. The mixture was heated at 50 °C overnight and the obtained yellow-orange suspension was filtered. The yellow residue was washed with *n*-pentane, THF and acetonitrile. It was not possible to measure a ^{1}H NMR spectrum in DSMO or any other solvent as the residue was insoluble. Therefore, the solution was examined and dried *in vacuo*. The ^{1}H NMR spectrum in $\mathrm{CD_3CN}$ showed a large number of signals (Figure 60). The obtained signals suggests the formation of an unsymmetric complex.

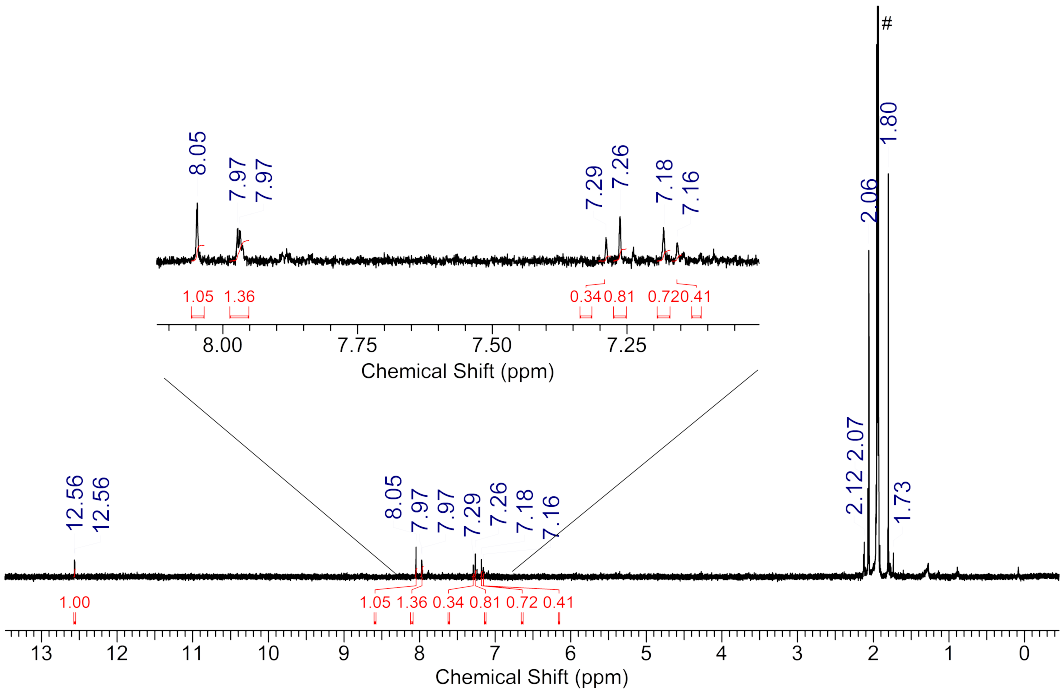

Figure 60: ^{1}H NMR spectrum of **27** (CD_3CN, #).

At -30 °C red needles were grown from that solution. The X-ray diffraction analysis reveals the formation of compound **27** (Figure 61). The signals obtained in the ^{1}H NMR spectrum (Figure 60) match to this compound. The crystals of **27** belong to the mono-clinic space group $P2_1/c$. The asymmetric unit contains one molecule of **27** and two cocrystallized acetonitrile molecules of which one is disordered. The Pd(II) center has a square planar geometry. The imidazolium moiety (N7-C8-N9) has an angle of 107.1(4)° upon coordination to the metal the angle decreases up to 102.7(3)°. The C5-C4 bond distance (1.338(6) Å) is shorter than the N9-N10 bond (1.381(5) Å). The C1-Pd1-I2 angle is almost linear (174.70(11)°). The Pd1-C1 bond distance (1.996(4) Å) is shorter than the Pd-iodide bond. The ^{1}H NMR spectrum (Figure 60) matches well with the result obtained from the X-ray analysis is of the crystals. The formation of [Pd(vegi$^{t\mathrm{Bu}}$H)I_3] is probably due to a substoichiometric reaction between **2a** and $Pd(OAc)_2$. The selective synthesis of this unsymmetric complex could be of interest to form heterobimetallic complexes by further addition of base and another metal precursor. A monopalladium vegi$^{n\mathrm{Pr}}$ complex bearing chlorido and phosphino ligands is known and was generated by *Raible*.[45]

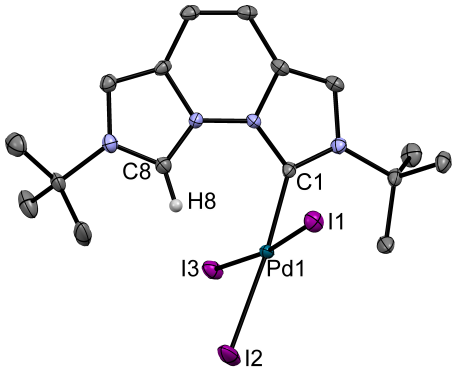

Figure 61: Molecular structure of [Pd(vegi$^{t\mathrm{Bu}}$H)I_3] (**27**). Atoms are shown with anisotropic atomic displacement parameters at the 50% probability level. Hydrogen atoms (except H-8) as well as two cocrystallized acetonitrile molecules (one of it disordered) are omitted for clarity. Selected bond lengths (Å) and angles (deg): C1-C8 3.061, Pd1-C1 1.996(4), I1-Pd1 2.6240(5), Pd1-I3 2.6232(5), Pd1-I2 2.6314(5), N9-N10 1.381(5), C5-C4 1.338(6), C8-H8 0.9500, N2-C1-N10 102.7(3), N7-C8-N9 107.1(4), C3-C3A-C4 135.4(4), C6-C5A-C5 135.0(4), C1-Pd1-I2 174.70(11), I3-Pd1-I1 173.132(16), C1-Pd1-I3 89.81(11), C1-Pd1-I1 85.86(11), I3-Pd1-I2 90.788(14), I1-Pd1-I2 93.035(14).

The next aim was to synthesize a [$PdCl_2$(vegi$^{t\mathrm{Bu}}$)] complex. As precursors [$PdCl_2$(TMEDA)], $PdCl_2$ and $Pd(OAc)_2$ with additional NaCl were used.

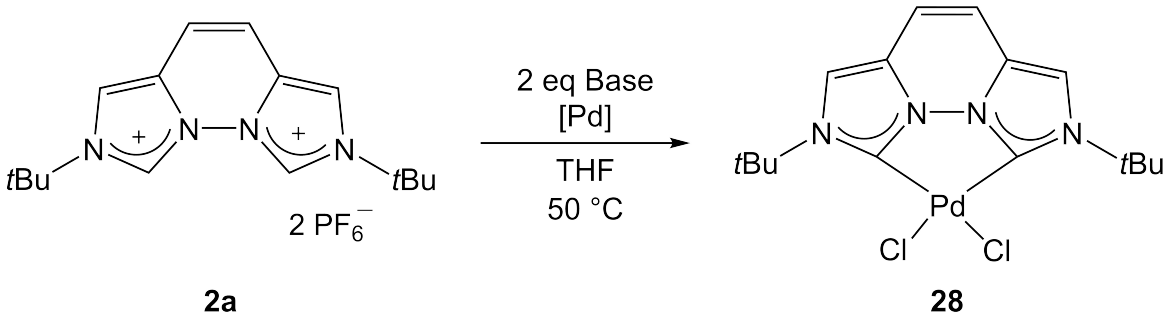

Figure 62: General synthesis of [Pd(vegi$^{t\mathrm{Bu}}$)Cl_2] (**28**).

The Pd precursor, [$PdCl_2$(TMEDA)], was added to a brown-red solution of the *in situ* generated Li complexes from **2a** with LiHMDS in THF-d_8. The precursor is poorly soluble in THF. The reaction takes place in a yellow suspension. When the ^{1}H NMR

spectrum was measured immediately after the compounds had been mixed together, signals for the Li complexes, the precursor **2a**, TMEDA, HMDS, LiHMDS and another set of three signals were observed. The mixture was heated at 50 °C overnight. The signals for the Li complexes vanished. The symmetric complex shows three signals at 7.80, 7.06 and 1.62 ppm. Because of the similar chemical shifts of the signals of the product and the Li complexes **10a** and **10a-H**, a ^{13}C NMR and a HMBC spectrum of the mixture were recorded. Unfortunately, no carbene signal was detected. All other signals have very similar chemical shifts to the Li complexes **10a** and **10a-H**. No definite statement can be made without the characteristic carbene signal. Filtration over Celite® resulted in the formation of the unsymmetric compound **30** (Figure 64).

The experiment was repeated and the solid which precipitates in THF was washed in *n*-pentane and measured in CD_3CN. The CD_3CN suspension shows three singlets and additional signals of TMEDA and the Pd precursor. The chemical shifts at 1.58, 7.01 and 7.60 ppm indicate a symmetric complex. When CD_3CN was removed and THF-d_8 added the signals shifted back to 1.62, 7.06 and 7.80 ppm. Additional peaks of various unkown species are also found. The separated THF-solution was dried *in vacuo*. Precipitation with diethyl ether from a solution in acetonitrile formed a light brown solid. The solid was washed with *n*-pentane. In the ^{1}H NMR spectrum of the residue only signals of TMEDA and HMDS were detected. From the acetonitrile/diethyl ether solution, orange single crystals formed at room temperature after several days. The dimeric structure **29** was obtained (Figure 63). The crystals of **29** belong to the orthorhombic space group *Aba2*. The asymmetric unit contains one molecule of **29**.

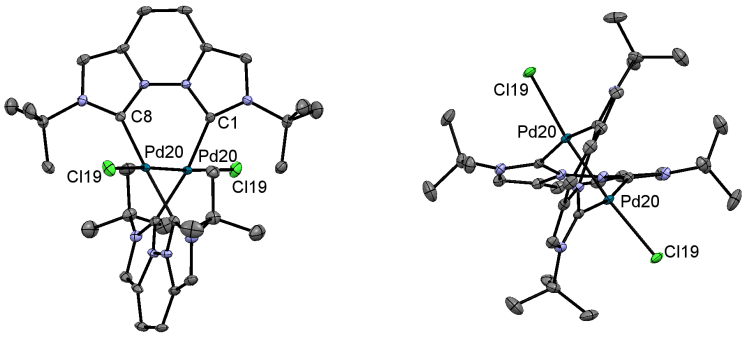

(a) Side view. (b) Top view.

Figure 63: Molecular structure of the [PdCl(vegi$^{t\mathrm{Bu}}$)]$_2$ complex **29**. Atoms are shown with anisotropic atomic displacement parameters at the 50% probability level. Hydrogen atoms are omitted for clarity. Selected bond lengths (Å) and angles (deg): C1-C8 3.008, C1-Pd20 2.039(2), N9-N10 1.379(3), C4-C5 1.345(4), Pd20-Pd20 2.4676(3), Pd20-Cl19 2.4921(6), N2-C1-N10 101.33(19), N9-C8-N7 101.4(2), C3-C3A-C4 135.7(2), C6-C5A-C5 135.6(2), C1-Pd20-C8 168.38(9).

This bridged Pd(I) NHC complex **29** is a very rare example of a Pd(I) NHC complex. Both palladium atoms have a d^9 configuration and form a σ-bond with a bond length of 2.47 Å which is smaller than the sum of the van der Waals radii (3.26 Å). The palladium-carbene bond length measures 2.039(2) Å and lies in the region of the other known dinuclear Pd(I) NHC complex by *Gardiner*.[151]
The formation of the Pd(I) complex can be explained with a comproportionation between a Pd(0) and a Pd(II) complex (Figure 64). A base could deprotonate the acidic imidazolium proton followed by the coordination of Pd(0) to the carbene carbon. Simultaneously a chloride-palladium bond must form while the Pd(0) gets oxidized to Pd(I).

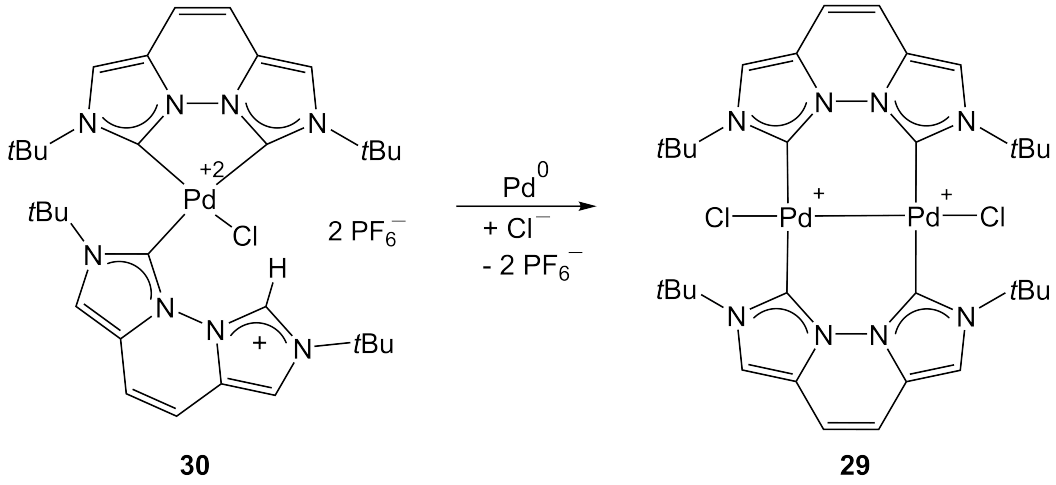

Figure 64: The proposed and simplified formation of **29**.

Because amines are often involved in the reduction of Pd(II) to Pd(I) or Pd(0), they were excluded in a further experiment to see whether a chelating Pd(II) complex could be obtained. The TMEDA-containing Pd(II) precursor was replaced with $PdCl_2$ and MeLi was used instead of LiHMDS. The ^{1}H NMR spectrum in THF-d_8 again shows three signals at 1.63, 7.06 and 7.80 ppm for a symmetric complex and are comparable to the chemical shifts obtained from the reaction of [$PdCl_2$(TMEDA)] and LiHMDS. Therefore, the product must form independently from amines, such as TMEDA and HMDS. From a saturated THF-d_8 solution, colorless crystals formed at room temperature which showed the unsymmetric Pd-complex structure **30**. The crystal had not optimal quality, but the molecular structure shows clearly the protonolysis product for which eight aromatic H-signals, four *tert*-butyl group signals and one signal shifted to low-field for H-19 are expected. In the ^{1}H NMR spectrum some small impurities are visible, which could fit the signals of the unsymmetric complex **30**.

The synthesis of Pd(I) complexes are of interest because they are relevant intermediates in Pd-catalysis.[141,152] Therefore, complex **29** should be selectively synthesized. The synthesis of a Pd(I) complex via a comproportionation reaction was tested with one equivalent of $PdCl_2$ and $Pd_2(dba)_3$ each and *in situ* generated vegi^{tBu} ligand. KHMDS is used as the base. After heating at 80 °C overnight the ^{1}H NMR spectrum of the brown suspension showed the signals of K-vegi^{tBu} complex **12a** as the main product

and some small signals, most likely signals of **30**.

In another experiment KHMDS and toluene instead of THF were tested. Ideally, the desired complex [Pd_2Cl_2(vegi^{tBu})$_2$] precipitated in the unpolar solvent toluene and could have then been easily isolated. The precursor **2a** was suspended in toluene, and KHMDS was added. After 15 min [$PdCl_2$(TMEDA)] was added to the brown suspension and the suspension turned lighter. The mixture was heated to 50 °C overnight. The yellow solution and the beige solid were separated by filtration and dried *in vacuo*. The ^{1}H NMR spectrum in THF-d_8 of the beige solid shows resonances at 1.63, 7.06 and 7.78 ppm. These chemical shifts are comparable with those obtained previously with the same metal precursor. Although the chemical shifts are very similar to the one for the Li complexes **10a** and **10a-H**, the formation of the Li complexes can be excluded as in this reaction KHMDS was used instead of LiHMDS. HMDS and two equivalents of KPF_6 which were formed during the reaction still remained in the mixture, only TMEDA was removed. An ESI mass spectrum in acetonitrile shows a signal at 342.1 [**30**-2PF_6^-]$^{2+}$. An elemental analysis of the beige product after washing with toluene to remove KPF_6 salts, confirmed the formation of [$PdCl_2$(vegi^{tBu})] (**28**) instead of [Pd_2Cl_2(vegi^{tBu})$_2$] (**29**).

From a reaction of **2a**, LiHMDS and [$PdCl_2$(TMEDA)] colorless crystals suitable for X-ray structure analysis were grown at room temperature from a saturated THF-solution. The crystals were unfortunately not of optimal quality. Therefore, the structure serves only as a connectivity proof. The crystals of **30** belong to the triclinic space group $P\bar{1}$ (Figure 65). The asymmetric unit contains two molecules of **30** and four cocrystallized strongly disordered THF molecules. The formation of this complex is unexpected, as full deprotonation of the precursor was confirmed. The preferred square planar geometry for Pd(II) is realized in complex **30**. Dispersion interactions (also observed in the Li complexes **10a** and **10a-H**) between the *tert*-butyl group and the aromatic tricycle could be one reason for the formation of this complex.

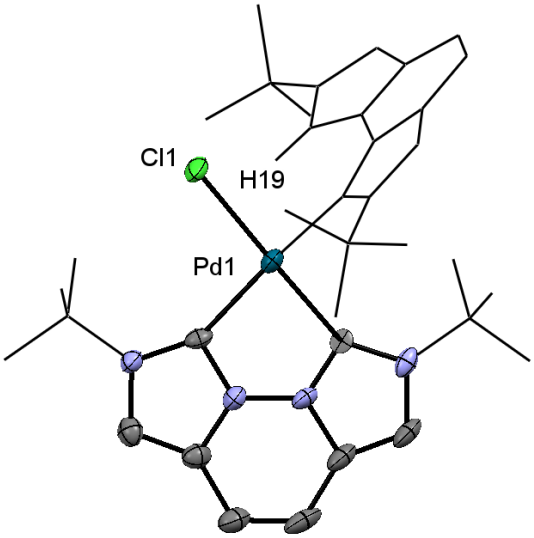

Figure 65: Molecular structure of the unsymmetric compound **30**. Atoms are shown with anisotropic atomic displacement parameters at the 50% probability level. Hydrogen atoms (except for H-19) and two PF_6^- anions are omitted for clarity.

The use of $Pd(OAc)_2$ as a basic metal precursor was advantageous. When **2a**, $Pd(OAc)_2$ and two equivalents of NaCl were dissolved in DSMO-d_6, the ^{1}H NMR spectrum showed the signals for **2a**, acetic acid and additional signals of a symmetric compound (Figure 66).

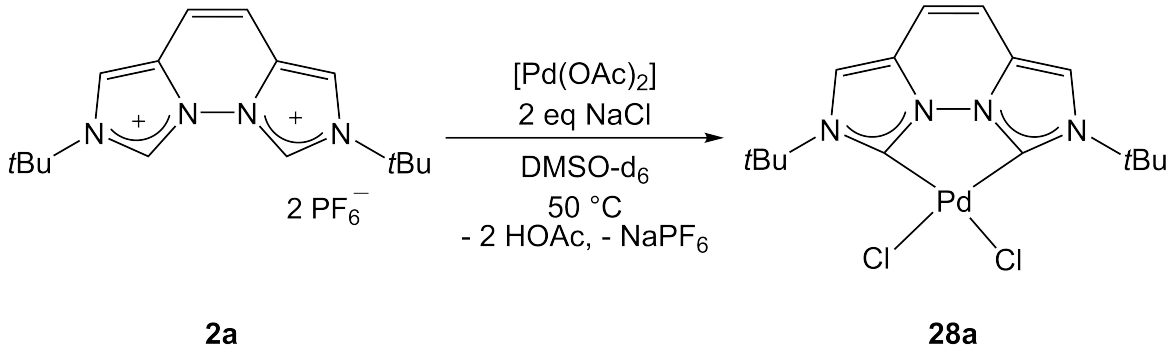

Figure 66: Synthesis of **28a**.

The mixture must be heated overnight at 50 °C for completeness of the reaction (Figure 67). Precipitation of the product with diethyl ether and washing with acetonitrile removed acetic acid, but $NaPF_6$ remained. An ESI$^+$ mass spectrum confirms the for-

mation of the [$PdCl_2$(vegi^{tBu})] complex. Signals at 413.1 (24) [M - Cl]$^+$) and 471.0 (39) [M + Na]$^+$ are found. The product in solution is inert against water and air and stable for several days. The carbene signal is detected at 142.8 ppm.

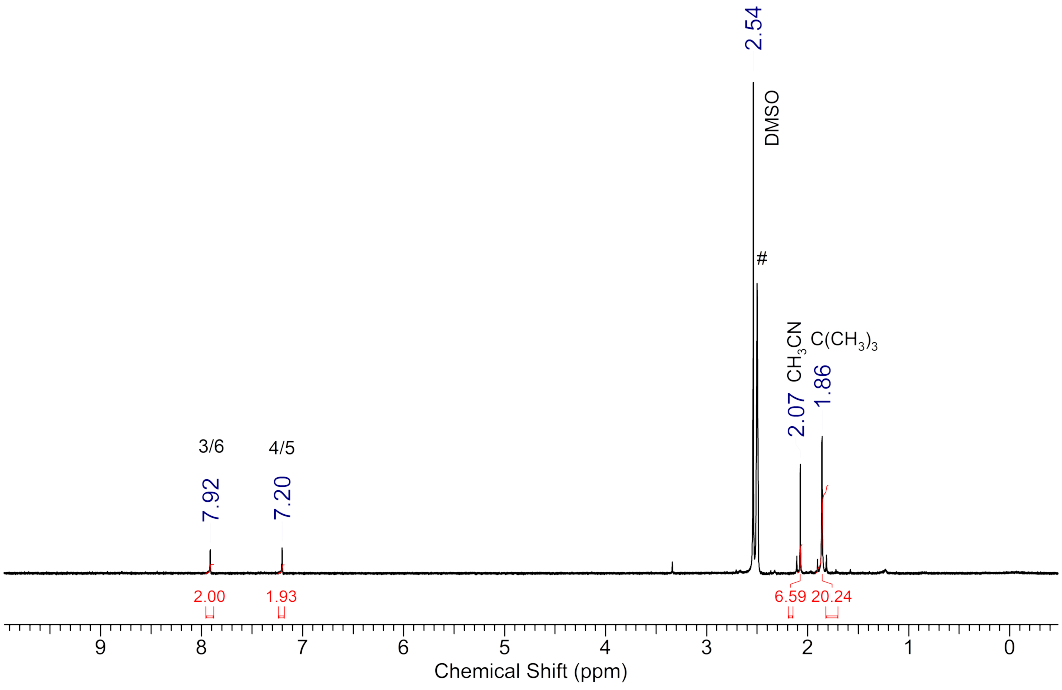

Figure 67: ^{1}H NMR spectrum of **28a** in DMSO-d_6 (#).

Without the addition of two equivalents of NaCl a DMSO-coordinated palladium complex was expected. **2a** and $Pd(OAC)_2$ dissolved in DMSO-d_6 gave a yellow solution. Upon standing for three weeks, palladium black formed slowly.

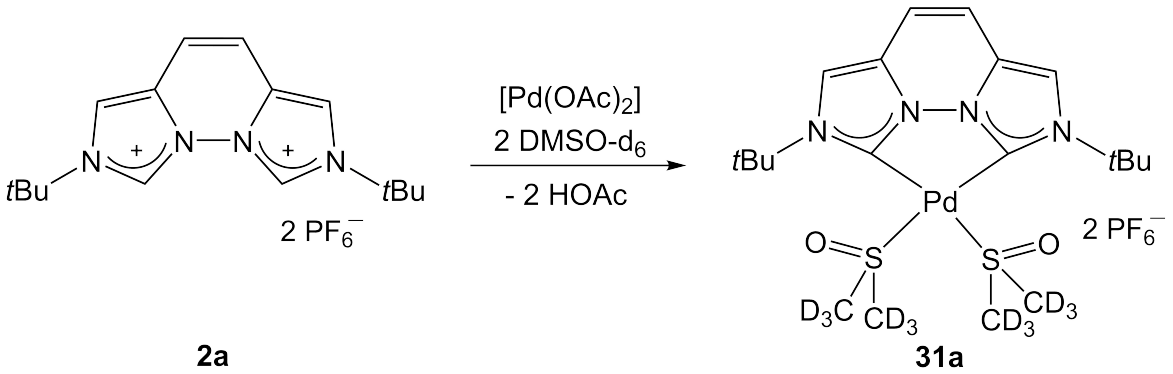

2a **31a**

Figure 68: Synthesis of **31a**.

The ^{1}H NMR spectrum shows the signals of bis(imidazolium) salt **2a**, the acetic acid

and of a symmetric complex at 1.70, 7.23 and 7.87 ppm. After heating the mixture to 50 °C overnight the spectrum did not change and even after the solution was heated at 100 °C overnight the signals for **2a** were still visible. The coordination chemistry of DMSO depends on the metal. Soft metals prefer the coordination via the soft sulfur atom, e.g. in $[Pd(DMSO)_2Cl_2]$.[153]

Instead of DMSO, acetonitrile could be used as a solvent to obtain the corresponding acetonitrile complex **32a**. In general complexes of type $[Pd(bis(NHC))(CH_3CN)_2]PF_6$ show catalytic activity.[149,154]

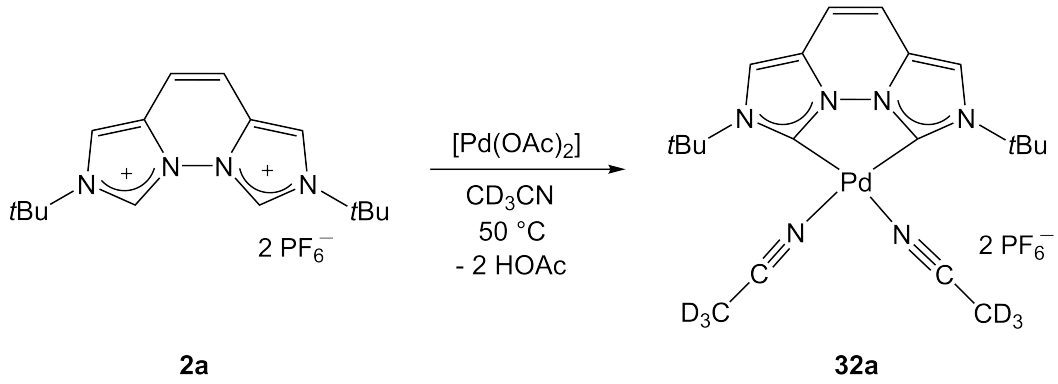

2a **32a**

Figure 69: Synthesis of **32a**.

2a and $Pd(OAc)_2$ were dissolved in acetonitrile and heated to 50 °C overnight. The yellow-brown solution and black solid were measured. The ^{1}H NMR spectrum of the solution shows the signals for the bis(imidazolium) salt, acetic acid an a symmetric new complex at 2.39 ppm, 7.09 ppm and 8.11 ppm. Heating for 60 °C overnight did not change the spectrum. Another experiment was carried out with 1.2 equivalents of $Pd(OAc)_2$ instead of one. The identical ^{1}H NMR spectrum was obtained. As the reaction was carried out in acetonitrile, the NMR spectra were measured in deuterated acetonitrile, the coordinated acetonitrile could exchange and thus no signal in the ^{1}H NMR spectrum for the coordinated acetonitrile is observed.

With the sterically less hindered vegi$^{n\mathrm{Pr}} \cdot 2HPF_6$ salt **2b** a $[PdCl_2(\mathrm{vegi}^{n\mathrm{Pr}})]$ complex could be generated as well. Different Pd precursors have been tested to obtain this

complex. In a first NMR experiment MeLi as the base and $PdCl_2$ were used. The deprotonation was confirmed by ^{1}H NMR spectroscopy then $PdCl_2$ was added. At room temperature, the reaction did not take place. Therefore, the brown-red suspension was heated overnight at 50 °C, however the ^{1}H NMR only showed signals of decomposition products. In another experiment the use of LiHMDS as the base and [$PdCl_2$(TMEDA)] was tested. Again the brown-red suspension was heated overnight at 50 °C which led to decomposition. Since $Pd(OAc)_2$ showed advantages in the synthesis of Pd-vegi^{tBu} complexes it was also tested for the vegi^{nPr} ligand.

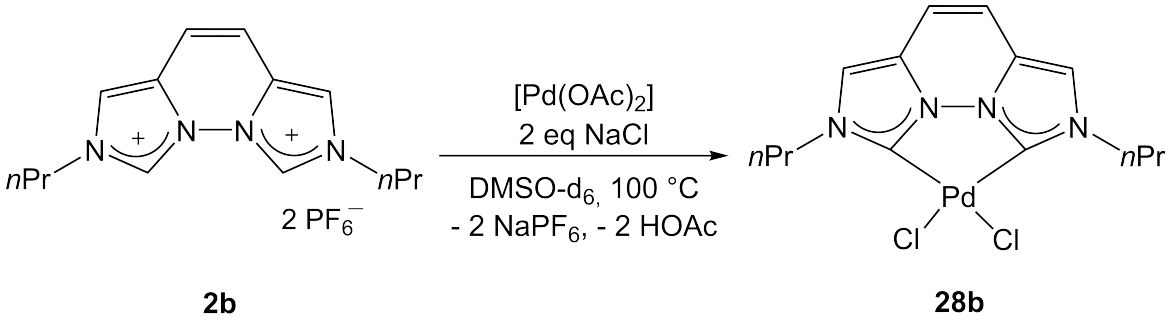

2b **28b**

Figure 70: Synthesis of **28b**.

Two experiments, one with two equivalents of NaCl added and one without addition of NaCl, were carried out in DMSO under otherwise identical conditions. After only a few hours at room temperature the ^{1}H NMR spectra of both experiments showed the formation of one or more unsymmetric species containing the vegi^{nPr} ligand. The presence of NaCl accelerated this process, which might be due to a more facile dissociation of the acetate induced by the chloride ions. After heating the mixture containing NaCl, the signals in the ^{1}H NMR spectrum decreased and the bis(imidazolium) salt vegi^{nPr}·2HPF$_6$ and $Pd(OAc)_2$ signals vanished completely. New signals for **28b** and acetic acid appeared. An ESI mass spectrum confirms the formation of a [$PdCl_2$(vegi^{nPr})] complex with a signal at m/z = 442.9 (75) which is the positively charged sodium adduct. Acetic acid and $NaPF_6$ can be removed by precipitation of **28b** with diethyl ether and washing with acetonitrile. Traces of $NaPF_6$ most likely remained.

Without added NaCl **31b** was obtained and identified with a carbene signal at 131.8

ppm. Also some minor unknown sideproducts were formed and signals for acetic acid were detected.

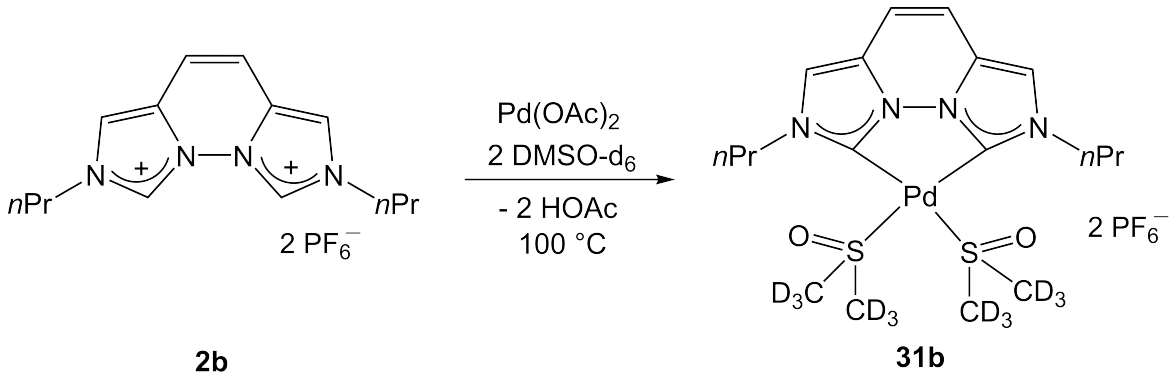

2b **31b**

Figure 71: Synthesis of **31b**.

The same reaction that lead to **32a** was repeated to synthesize the complex **32b** (Figure 72). At room temperature the ^{1}H NMR spectrum shows the signals of acetic acid and **2b** as well as of a symmetric complex as a main product, which could match those of an acetato palladium complex.

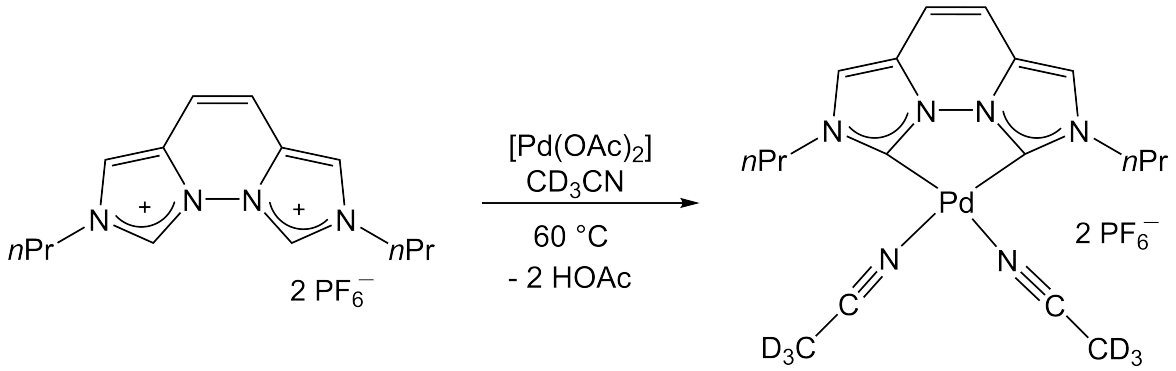

2b **32b**

Figure 72: Synthesis of **32b**.

After heating the yellow solution overnight at 60 °C the color changed to yellow-greenish. The ^{1}H NMR spectrum shows signals for acetic acid, and a symmetric complex. The carbene signal is detected at 135.5 ppm which is 69 ppm upfield shifted compared to the free carbene vegi^{nPr} **1b**. The carbene signal is in the range of literature

known complexes of type [Pd(bis(NHC))$(CH_3CN)_2$]X_2 (X = PF_6, BF_4) considering a constant influence of the metal fragment an thus a constant chemical shift difference to the free carbene.[26,149,155] The signals of the acetonitrile ligand are neither obtained in the ^{1}H nor the ^{13}C NMR spectrum. Possibly due to fast exchange process with the solvent at room temperature. From the diffusion of diethyl ether into an acetonitrile solution at -30 °C white needles formed. The X-ray structure analysis confirms a square planar complex with a cocrystallized acetonitrile molecule. The structure of [Pd$(CD_3CN)_2$(vegi$^{n\mathrm{Pr}}$)] only serves as a connectivity proof and was refined as a 2-component twin.

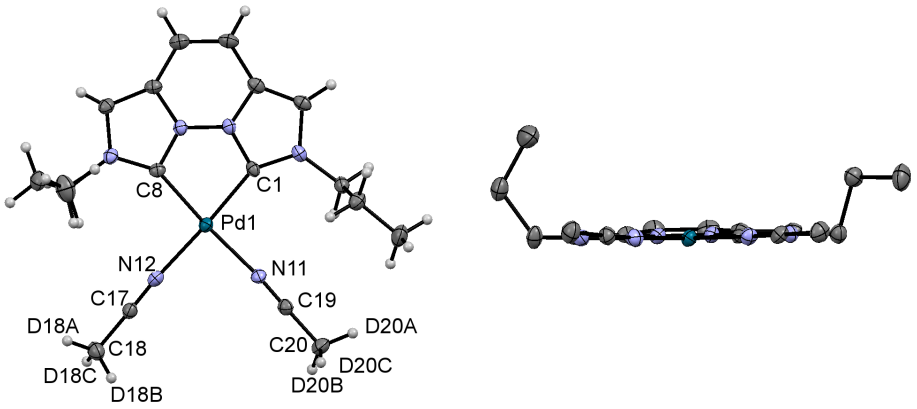

(a) Top view. (b) Side view.

Figure 73: Molecular structure of **32b**. One acetonitrile molecule and two PF_6^- anions are omitted for clarity. Atoms are shown with anisotropic atomic displacement parameters at the 50% probability level.

The reaction was repeated at a larger scale in CD_3CN. The ^{1}H NMR spectrum of the yellow solution indicates the formation of side products. A black solid formed in the NMR tube. Side products are formed, another symmetric complex most likely an acetato complex and some smaller impurities of unsymmetric compounds.

The solvent was changed to DMSO-d_6. The mixture was heated for five days at 60 °C. A ^{1}H NMR spectrum, measured on the next day, indicates the formation of

the [Pd(DMSO-d_6)$_2$(vegi$^{n\mathrm{Pr}}$)](PF$_6$)$_2$ complex which was generated before. The exchange of the solvent ligands from CD_3CN to DMSO might be due to a preferred soft-soft interaction between palladium and the sulfur atom as well as the excess of DMSO in solution. Two equivalents of NaCl were added. The ^{1}H NMR spectrum showed signals for complex [Pd(DMSO-d_6)$_2$(vegi$^{n\mathrm{Pr}}$)](PF$_6$)$_2$ (**31b**) and acetic acid and another unknown compound. After heating overnight at 100 °C signals for complex [PdCl$_2$(vegi$^{n\mathrm{Pr}}$)] (**28b**) and acetic acid were visible in the ^{1}H NMR spectrum.

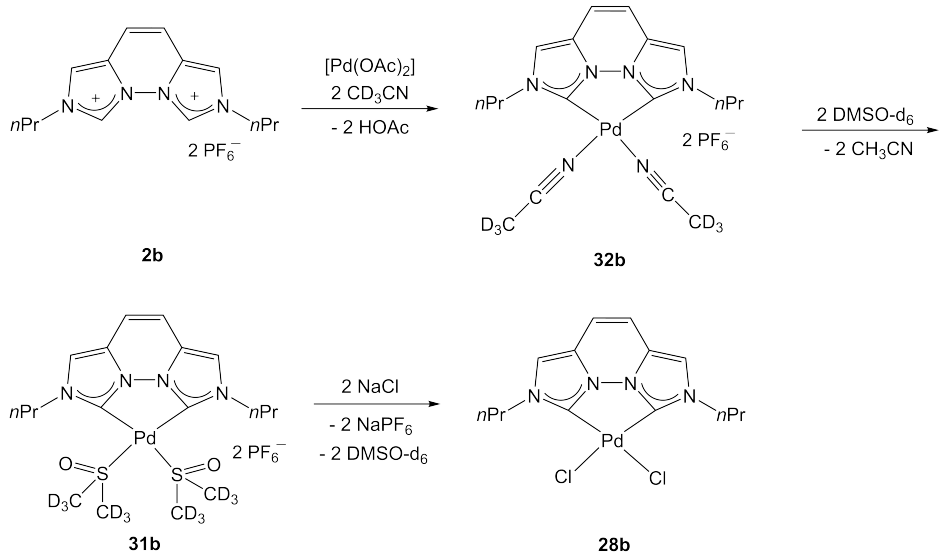

Figure 74: Reaction pathway to different Pd(II) vegi$^{n\mathrm{Pr}}$ complexes.

The formation of [Pd(DMSO-d_6)$_2$(vegi$^{n\mathrm{Pr}}$)](PF$_6$)$_2$ (**31b**) via Pd(OAc)$_2$ in DMSO-d_6 forms some unkown byproducts, whereas the formation of **31b** from **32b** via ligand substitution is straightforward.

6.3 Synthesis of Platinum vegi^{R} complexes

Platinum complexes contain the NMR active nucleus ^{195}Pt (I= 1/2, 33.8% natural abundance) that provides useful structural information due to the coupling with carbon or hydrogen nuclei.

6.3.1 Synthesis of Platinum vegi^{R} dimethyl complexes

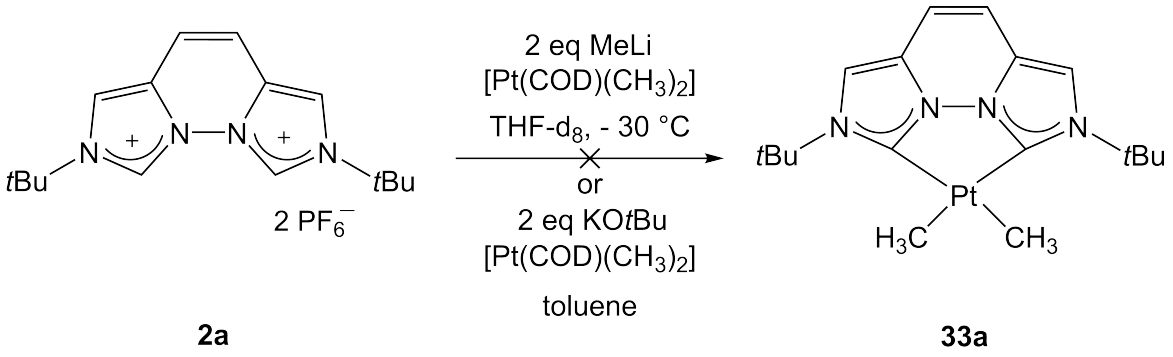

Figure 75: Synthesis with $[Pt(COD)(CH_3)_2]$ does not form **33a**.

In the first experiments $[Pt(COD)(CH_3)_2]$ was used as the Pt precursor. In one experiment MeLi was tested as the base in THF-d_8 and after 15 min the Pt precursor was added. The ^{1}H NMR spectrum shows the signals of an unsymmetric complex as well as of the Pt precursor, free COD and methane. The signals of the unsymmetric carbene complex are at 1.43 and 1.79 ppm (for both *tert*-butyl groups), 7.14 (d, J = 9.6 Hz), 8.19 d (J = 9.6 Hz), 8.34 (J = 1.9 Hz), 8.59 and 9.78 ppm (J = 1.9 Hz). The brown suspension is stable for up to two weeks.
The same Pt precursor was tested in a further experiment. **2a** was deprotonated with KO*t*Bu in toluene and then $[Pt(COD)(CH_3)_2]$ was added. The ^{1}H NMR spectrum shows also the formation of an unsymmetric vegi^{tBu} species and signals for the Pt-precursor. The mixture is also stable for up to two weeks, the unsymmetric complex remains the final product.

Probably the deprotonation reaction with methyl lithium of both imidazolium protons was not complete, as the signal at 9.78 ppm indicates. Hence, no symmetric Pt complex was generated after adding the Pt precursor. In the second experiment it is unclear whether KO*t*Bu led to a fully deprotonated vegi^{tBu} ligand in toluene. The reaction to a symmetric Pt complex with $[Pt(COD)(CH_3)_2]$ did not work. The formed unsymmetric Pt vegi^{tBu} species most likely is a mono platinum vegi^{tBu} complex with a multiple bonded platinum atom.

2a **33a**

Figure 76: Synthesis of **33a**.

Then I switched to $[Pt(CH_3)_2(DMSO)_2]$ as the Pt precursor. DMSO can easily be subsituted by NHC ligands, resulting in $[Pt(NHC)(CH_3)_2]$ complexes.

The $[Pt(CH_3)_2(vegi^{tBu})]$ **33a** can be obtained from a transmetalation of the ligand from the *in situ* generated Li complex to $[Pt(CH_3)_2(DMSO)]$. After the filtration over neutral alumina the yellow filtrate was dried *in vacuo* and washed with *n*-pentane. The product is obtained as a beige solid. The ESI mass spectrum also clearly indicates the formation of complex **33a** with a signal at m/z = 521.1 (100) $[M\text{-}CH_3+CH_3CN]^+$ and 480.1 (18) $[M\text{-}CH_3]^+$.

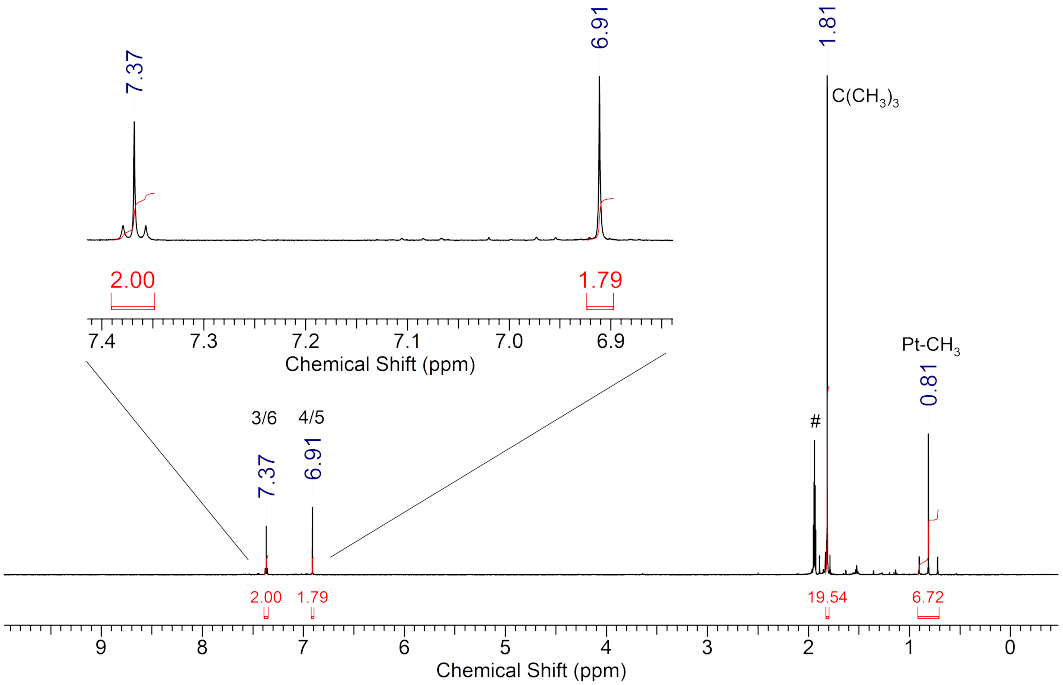

Figure 77: ^{1}H NMR spectrum **33a** (#, CD_3CN).

The presence of two methyl ligands in **33a** is also supported by a singlet in the ^{1}H NMR spectrum at 0.81 ppm, which is flanked by ^{195}Pt NMR satellites ($^{2}J_{PtH}$ = 73.1 Hz) (Figure 77). The resonances of the backbone protons are at 7.37 (singlet with Pt-satellites: $^{4}J_{PtH}$ = 8.7 Hz) and 6.91 ppm. In the ^{13}C NMR spectrum the carbene signal is detected at 172.2 ppm and the methyl signal at -3.3 ppm. The chemical shift of the carbene signal is shifted high-field compared to the free vegi^{tBu} carbene (202.6 ppm), this chemical shift difference is similar to the ones found in literature for similar complexes.[73,156,157] The resonance in the ^{195}Pt NMR spectrum can be found at -3805.9 ppm. From a saturated solution of complex **33a** in CH_3CN and Et_2O at –30 °C colorless crystals suitable for X-ray structure analysis were grown. The molecular structure confirms the expected square planar geometry around the platinum(II) center. The [Pt$(CH_3)_2$(vegi^{tBu})] complex can be heated to 100 °C over the weekend without decomposition. The crystals of **33a** belong to the orthorhombic space group *Pnma*. The asymmetric unit contains one molecule of **33a** and two cocrystallized disordered acetonitrile molecules.

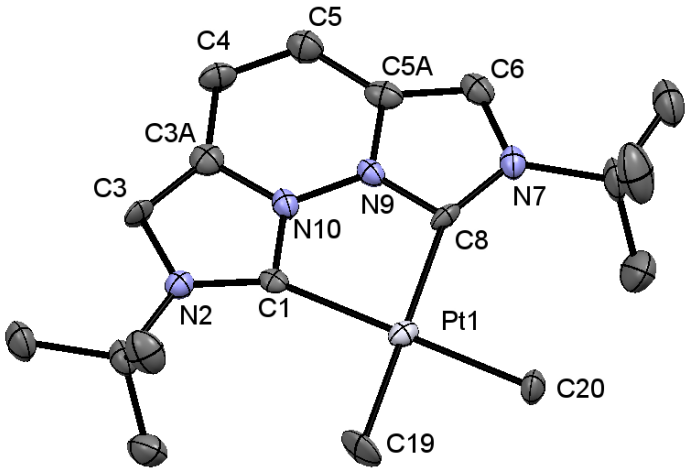

Figure 78: Molecular structure of **33a**. Atoms are shown with anisotropic atomic displacement parameters at the 50% probability level. Hydrogen atoms, two cocrystallized CH_3CN molecules (strong disorder) are omitted for clarity. Selected bond lengths (Å) and angles (deg): Pt1-C1 2.112(5), Pt1-C8 2.127(5), Pt1-C20 2.122(5), Pt1-C19 2.096(5), N9-N10 1.356(5), C4-C5 1.358(7), C3-C3A-C4 140.1(5), C6-C5A-C5 139.3(5), N9-C8-N7 100.2(4), N10-C1-N2 100.1(4), C19-Pt1-C20 79.7(2), C1-Pt1-C8 80.12(17).

The platinum-carbene bonds (2.112(5)Å (C1-Pt1), 2.086(4)Å (Pt1-C8)) and platinum-CH_3 bond lengths (2.122(5)Å (Pt1-C20), 2.096(5)Å (Pt1-C19)) are in the range of known dimethyl platinum(II) NHC complexes.[73,156] The bite angle (C1-Pt1-C1) measures
80.12(17)° which is in the typical range found for chelating vegi^{R} complexes.[79]

The **2b** ligand precursor was also tested in the synthesis of [Pt$(CH_3)_2$(vegi$^{n\mathrm{Pr}}$)].

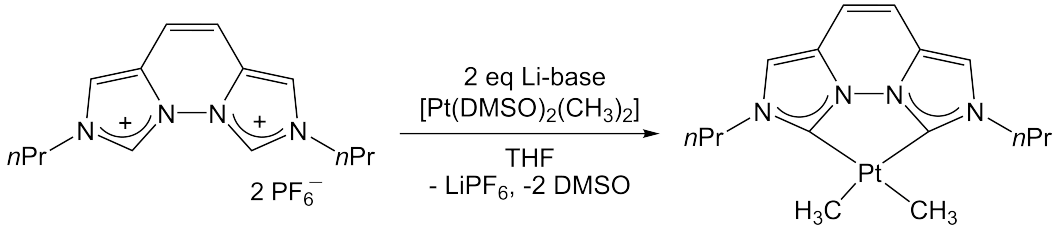

2b **33b**

Figure 79: Synthesis of **33b**.

The [Pt$(CH_3)_2$(vegi$^{n\mathrm{Pr}}$)] complex is also accessible from the reaction of **2b** with MeLi and [Pt$(CH_3)_2$(DMSO)$_2$] in THF-d_8 (Figure 79). After only 20 minutes the ^{1}H NMR spectrum showed the signals of a symmetric product and signals for [Pt$(CH_3)_2$(DMSO)$_2$] and free DMSO. Because no Li complex signals of **10b** were left, remaining Pt precursor signals are due to weighing errors. The presence of two methyl ligands in complex **33b** is also supported by a singlet resonance in the ^{1}H NMR spectrum (CD_3CN) at 0.90 ppm, which is flanked by the ^{195}Pt NMR satellite signal ($^2J_{\mathrm{PtH}} = 74.4$ Hz) that is overlapping with the triplet of the methyl protons of the *n*-propyl group (Figure 80). The resonances of the backbone protons are found at 7.11 (Pt-satellites: $^4J_{\mathrm{PtH}} = 8.0$ Hz) and 6.89 ppm. In the ^{13}C NMR spectrum the carbene signal is detected at 171.9 (no satellite signals are detected), the CH_3-signal at -10.5 (Pt-satellites: $^2J_{\mathrm{PtC}} = 662.5$ ppm) and the signal C-3/6 at 116.1 ppm (Pt-satellites: ($^3J_{\mathrm{PtH}} = 17.3$)). The ESI mass spectrum indicates clearly the formation of complex **33b** with a signal at m/z = 493.0 (100) [M-CH_3+CH_3CN]$^+$.

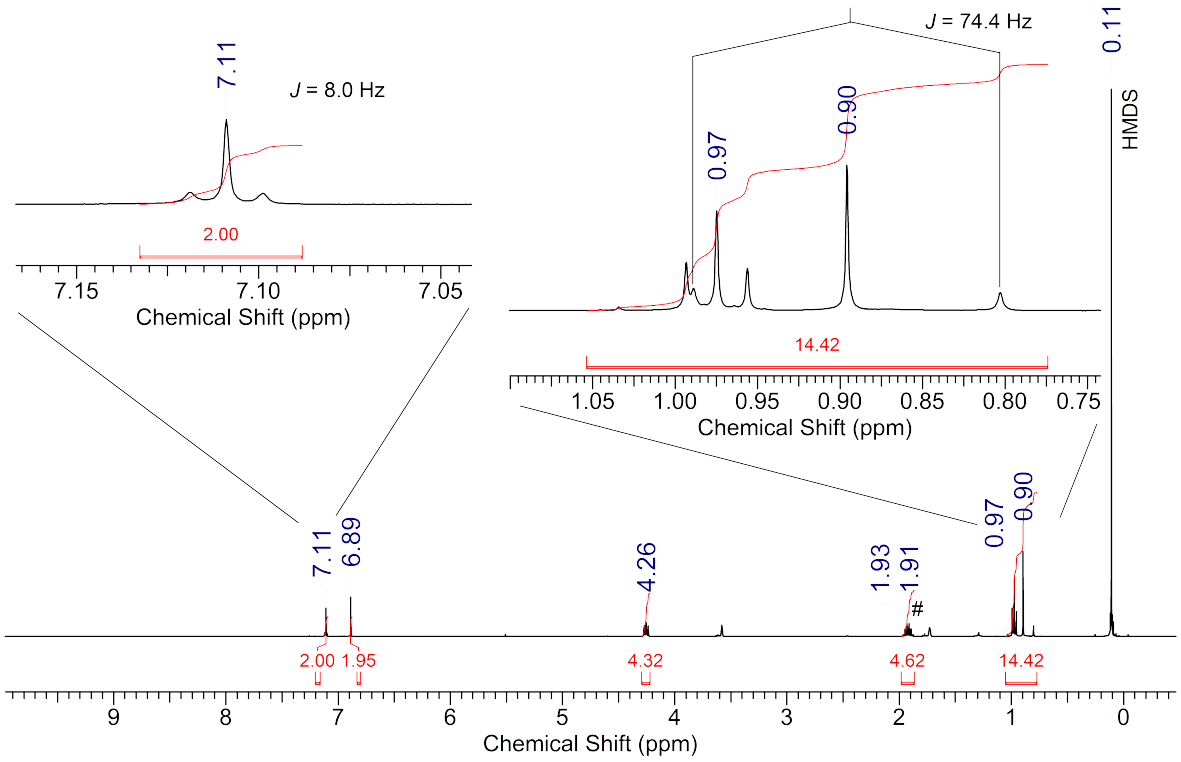

Figure 80: ^{1}H NMR of **33b** (#, CD_3CN).

Two experiments have been tested to scale-up the reaction. One with methyl lithium as the base and the other one with LiHMDS. Both experiments were done analogously to the previous reported experiment. Both mixtures were filtered over neutral alumina. $^{19}F\{^{1}H\}$ and $^{31}P\{^{1}H\}$ NMR spectroscopy confirmed the complete removal of the PF_6^- salts via filtration. The yellow filtrate was dried *in vacuo* and washed with *n*-pentane to remove HMDS and methane. Washing with *n*-pentane was more successful when the product was first dissolved in acetonitrile and then extracted with *n*-pentane. HMDS could be removed this way. After drying *in vacuo* the complex was obtained as a beige solid that was poorly soluble in acetonitrile, THF, toluene and *n*-pentane. The ^{1}H NMR spectrum proofed the formation of the complex along with some minor impurities, whose signals could match to an unsymmetric Pt-complex. Four singlets were obtained in the aromatic region which could belong to the backbone of the vegi ligand. Additionally, one triplet at 4.59 ppm was observed and could belong to the *n*-propyl group.

As this side product was not obtained in the NMR experiment, it might stem form the

filtration over alumina, when MeLi was used, the side product was obtained in a ratio **33b**:sideprodcut = 3:1 and for LiHMDS 15:1.

Colorless crystals suitable for X-ray structure analysis were grown at room temperature from a saturated solution in THF. The crystals of **33b** belong to the trigonal space group $P3_121$. The asymmetric unit contains half a molecule of **33b**. The platinum-carbene bond measures 2.070(5)Å and the platinum-methyl bond 2.086(4)Å. The values are similar to those found in **33a**.

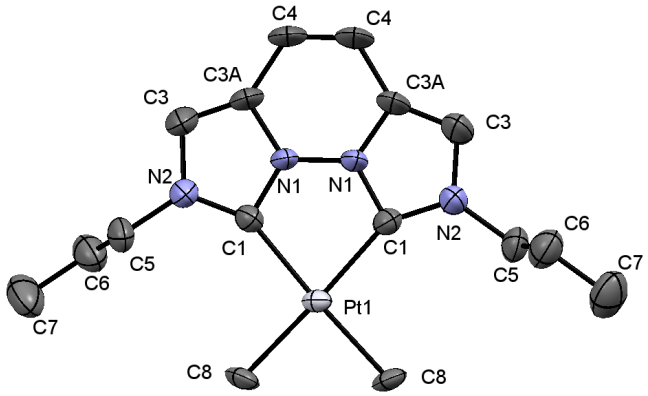

Figure 81: Molecular structure of the [Pt(CH$_3$)$_2$(vegi$^{n\mathrm{Pr}}$)] complex **33b**. Atoms are shown with anisotropic atomic displacement parameters at the 50% probability level. Hydrogen atoms are omitted for clarity. Selected bond lengths (Å) and angles (deg): C1-Pt1 2.070(5), Pt1-C8 2.086(4), N1-N1 1.355(10), C4-C4 1.306(16), N1-C1-N2 99.9(4), C3-C3A-C4 142.5(6), C1-Pt1-C1 80.8(3), C1-Pt1-C8 96.5(2), C1-Pt1-C8 174.8(3), C1-Pt1-C8 174.8(3), C1-Pt1-C8 96.5(2), C8-Pt1-C8 86.5(3).

6.3.2 Synthesis of platinum vegi^{R} dichlorido complexes

[Pt(bis(NHC))X$_2$] (X = Cl, Br, I) complexes can be synthesized by reacting the bis(imidazolium) salt with base and subsequent addition of a [Pt(II)X$_2$L$_2$] precursor.[8,158] Alternatively, basic platinum(II)-acetylacetonate can be reacted with bis(imidazolium) halides.[154,159]. The aim was to synthesize *cis*-dichlorido vegi$^{t\mathrm{Bu}}$ and vegi$^{n\mathrm{Pr}}$

complexes. Therefore, $[Pt(C_2H_4)_2Cl_2]$, $[Pt(COD)Cl_2]$ and $[Pt(acac)_2]$ were tested as precursors.

When **2a** was deprotonated with LiHMDS and subsequently reacted with $[Pt(C_2H_4)_2Cl_2]_2$ in THF-d_8 the ^{1}H NMR spectrum showed signals of the Li complex and a symmetric species. The suspension was filtered over Celite® and the yellow filtrate was dried *in vacuo* and washed twice with *n*-pentane. The ^{1}H NMR spectrum in THF-d_8 showed signals of an unsymmetric complex **36a** and a symmetric species (7.66, 7.08 and 1.92 ppm). The formation of this unsymmetric complex was often observed in various experiments aiming the synthesis of $[Pt(vegi^{R})_2(Cl)_2]$.
The ^{1}H NMR spectrum of the residue (which was separated from the solution in the beginning via filtration) showed many signals of most likely the unsymmetric complex and other formed unkown species. Complex **36a** shows the same geometry as the palladium complex **31a**. From an acetonitrile mixture colorless single crystals at -30 °C suitable for X-ray diffraction were obtained. They reveal the structure of the sideproduct **34** (Figure 82) which was unknown so far.

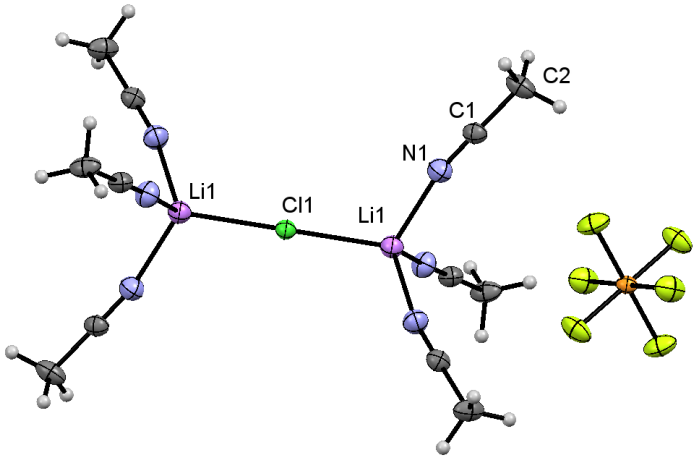

Figure 82: Molecular structure of **34**. Atoms are shown with anisotropic atomic displacement parameters at the 50% probability level.

In the next experiments the $[Pt(COD)Cl_2]$ precursor was tested to generate a symmetric $[PtCl_2(vegi^{tBu})]$ complex.

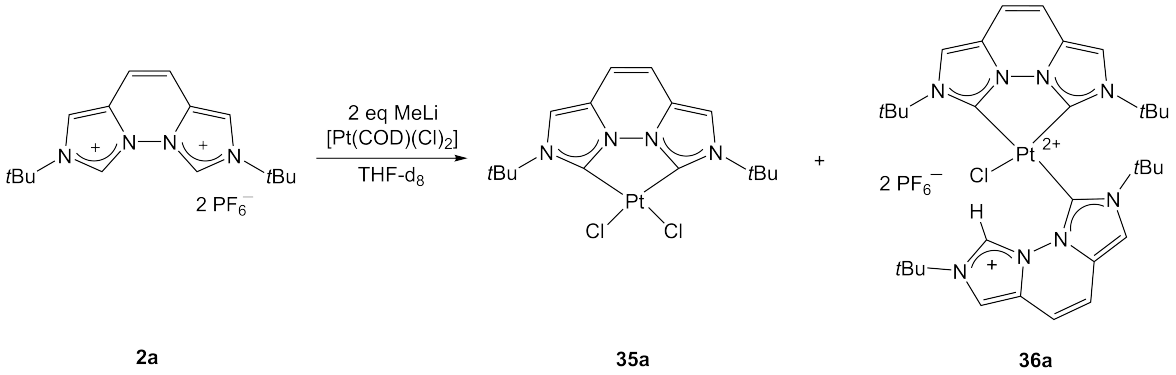

Figure 83: Synthesis of **35a** and **36a**.

The ^{1}H NMR spectrum showed many signals of unidentified species. Especially in the down-field region many signals are obtained at 11.07 ppm, 12.05 ppm and 12.36 ppm. Light yellow single crystals formed in the NMR tube were analyzed by X-ray diffraction refinement and reveal the protonolysis product **36a** (Figure 84).

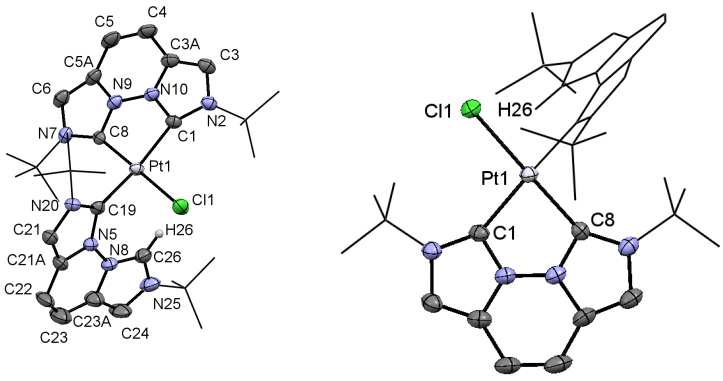

(a) The viev from above. (b) The view from the side.

Figure 84: Molecular structure of the [PtClH(vegi$^{t\mathrm{Bu}}$)$_2$]2PF$_6$ complex **36a**. Atoms are shown with anisotropic atomic displacement parameters at the 50% probability level. Hydrogen atoms (except for H-26), 4 cocrystallized THF molecules (strong disorder) and two PF_6^- anions are omitted for clarity. Selected bond lengths (Å) and angles (deg): C1-C8 2.710, C19-C26 3.062, H26-Cl1 2.732, C1-Pt1 2.105(5), Cl1-Pt1 2.3425(14), C19-Pt1 2.004(5), C8-Pt1 2.059(5), C26-H26 0.9500, C4-C5 1.343(9), N10-N9 1.349(6), C22-C23 1.312(10), N5-N8 1.383(6), C19-Pt1-C8 97.38(18), C19-Pt1-C1 170.48(19), C8-Pt1-C1 81.20(19), C19-Pt1-Cl1 83.25(14), C8-Pt1-Cl1 176.10(13), C1-Pt1-Cl1 98.82(14), N5-C19-N20 102.7(4), N25-C26-N8 107.0(5), C6-C5A-C5 140.5(5), C3-C3A-C4 139.7(5), C24-C23A-C23 135.4(6), C21-C21A-C22 135.0(5), N5-C19-N20 102.7(4), N25-C26-N8 107.0(5), N10-C1-N2 101.0(4), N9-C8-N7 101.3(4).

The crystals of **36a** belong to the triclinic space group $P\bar{1}$. The asymmetric unit contains one molecule of **36a** and four cocrystallized strongly disordered THF molecules. The Pt(II) complex has a square planar geometry around the platinum atom. Upon coordination the C1-C8 distance is shortened to 2.710 Å. The bite angle (C8-Pt1-C1) measures 81.20(19)° and lies in the region of other known chelating vegi complexes. The C8-Pt1-Cl1 angle is almost linear (176.10(13)°). The N25-C26-N8 angle of the imidazolium moiety measures 107.0(5)°. Upon carbene formation and coordination to the platinum this angle gets more acute (101.0(4)° (N10-C1-N2), 101.3(4)° (N9-C8-N7) and 102.7(4) (N5-C19-N20)).

The reaction was repeated with LiHMDS instead of MeLi with the aim to isolate the crystals and characterize the product **36a** further. After several days colorless crystals were formed at -30 °C from the orange solution in THF/diethyl ether. The X-ray structure analysis confirmed the formation of the protonolysis product **36a**. The crystals were dissolved in CD_3CN and ^{1}H, ^{13}C and 2D NMR spectra were measured.

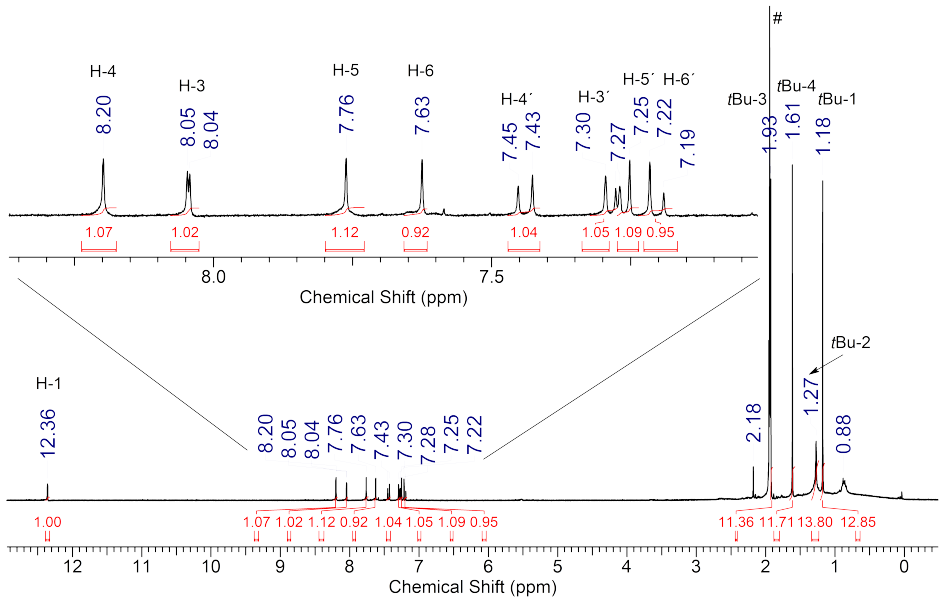

Figure 85: ^{1}H NMR spectrum of **36a** (#, CD_3CN).

Regardless, whether MeLi, LiHMDS or *n*-BuLi were used as a base, the ^{1}H NMR spectra in THF-d_8 of the orange suspension were identical and indicated the formation of a symmetric complex with signals at 7.68, 7.11 and 1.96 ppm and the formation of the protonolysis product **36a** in a ratio 1:0.2 (symmetric complex:**36a**) (Figure 86, spectrum 2). The signals for free COD are still present.

The mixture with MeLi as a base was measured after two days. The unsymmetric species is barely visible (Figure 86, spectrum 1). The signals of the symmetric product are detected at 7.68, 7.11 and 1.97 ppm. The signals for the unsymmetric complex vanished overnight. The rather low-field shift of the *tert*-butyl signal (1.97 ppm) is similar to that signal of the palladiumdichlorido vegi^{tBu} complex **28a**. Therefore, it is most likely that the platinumdichlorido vegi^{tBu} complex **35a** formed in this reaction.

The low-field shift of the *tert*-butyl signal can be explained by interactions between the hydrogen atoms from the *tert*-butyl groups with the chlorido ligands.

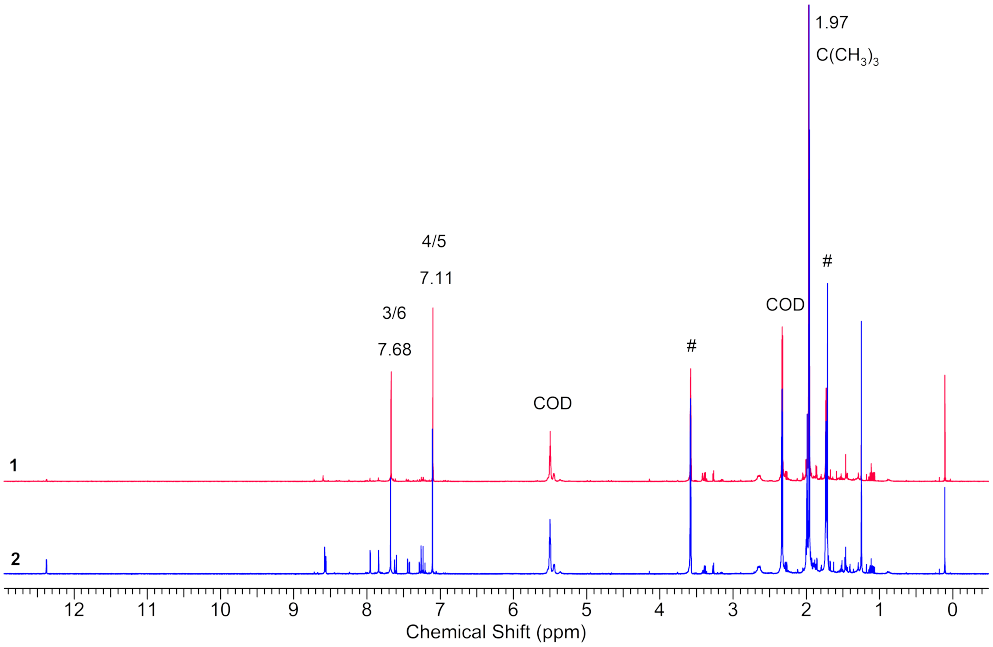

Figure 86: ^{1}H NMR spectrum (#, THF-d$_8$): 1) **35a**, 2) **35a** and **36a**.

In the next experiment the goal was to generate the protonolysis product **36a** intentionally, generated by using two equivalents of **2a**, 3.5 equivalents of methyl lithium and one equivalent of [Pt(COD)Cl$_2$]. The ^{1}H NMR spectrum in THF-d$_8$ does not show the signals for the desired complex **36a**. As a main product [PtCl$_2$(vegi$^{t\mathrm{Bu}}$)] was obtained at 1.96, 7.11 and 7.68 ppm and another unkown unsymmetric side product.

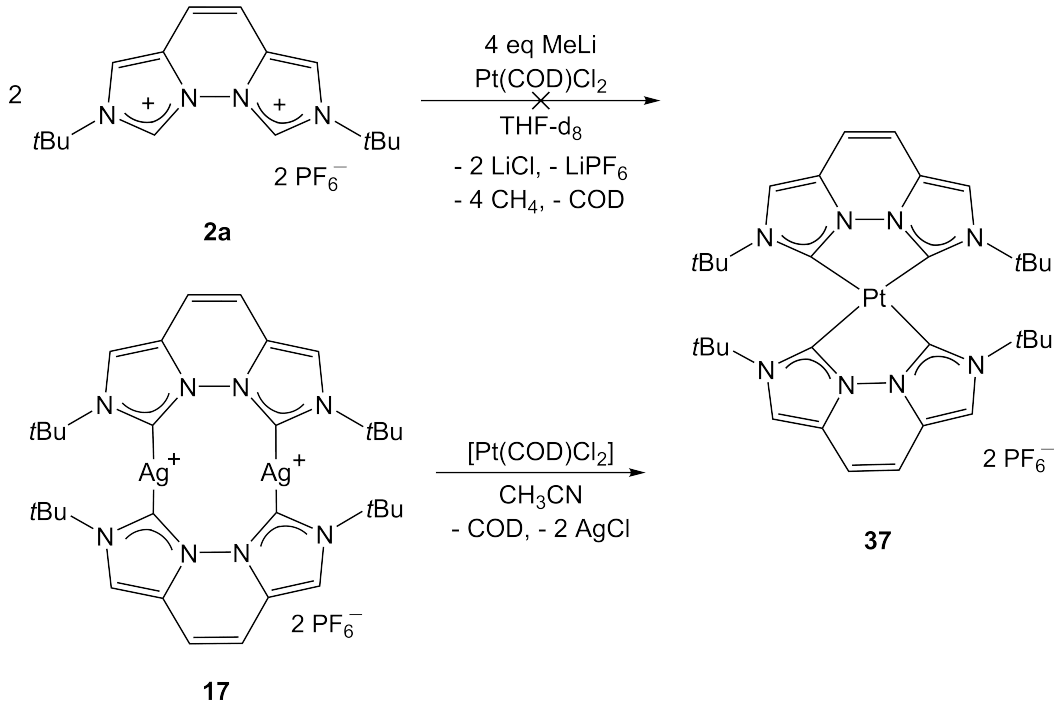

Figure 87: Synthesis of **37**.

To see whether a Pt(II)vegi$^{t\mathrm{Bu}}$ tetracarbene complex is accessible two different pathways have been tested.

The reaction of **2a**, two equivalents of MeLi and half an equivalent of [Pt(COD)Cl_2] could lead to the desired Pt-tetracarbene complex **37**. The ^{1}H NMR spectrum in THF-d_8 shows free COD and additional signals which could not yet be attributed to a defined species (bis(imidazolium) salt and probably some minor amounts of signals of the protonolysis product **36a**). Crystals of the protonolysis product **36a** were obtained as well.

The other reaction pathway starts from the silver complex **17** that is reacted with the Pt precursor. A Pt-tetracarbene complex **37** could form along with two equivalents of AgCl. The ^{1}H NMR spectrum in CD_3CN shows signals for the silver complex **17** (Figure 88, marked with stars) free COD and signals at 7.63, 7.61 and 7.17 ppm for the vegi$^{t\mathrm{Bu}}$ backbone and 1.92 and 1.82 ppm for the *tert*-butyl groups. This is not indicative for the Pt-tetracarbene complex **37** (Figure 88), which should produce only one signal for the *tert*-butyl groups. It is unclear if complex **37** formed during the reaction or another unkown product. Pt(II) favors a square planar geometry therefore, a tetra-

hedral tetracarbene is not favored, while the protonolysis product **36a** remains in the favored square planar geometry. The steric hindrance of the ligands are likely why the synthesis of a Pt(II) tetracarbene complex with vegi^{tBu} as the ligand was not successful.

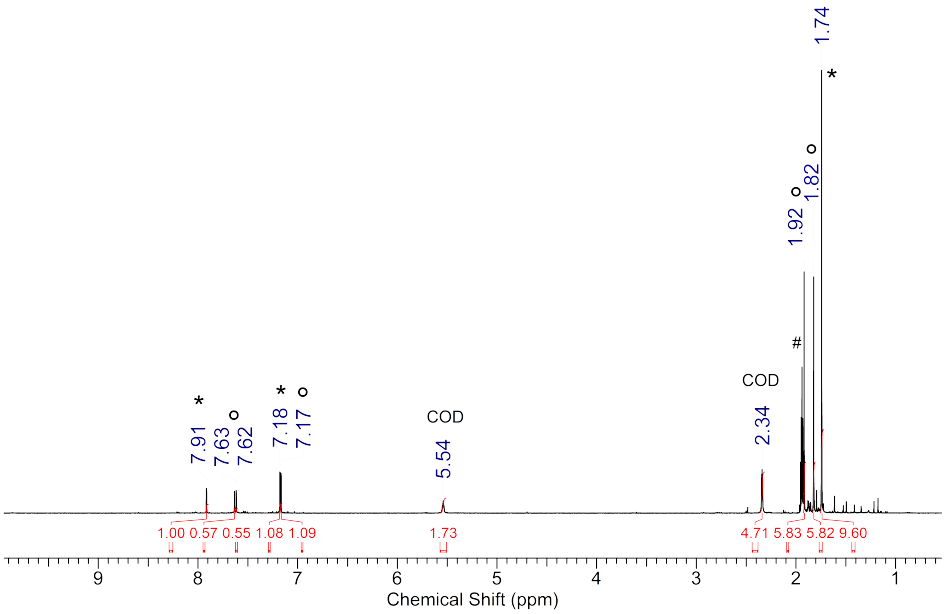

Figure 88: ^{1}H NMR spectrum (CD_3CN, #) of the reaction of **17** with [Pt(COD)Cl_2] (stars: **17**; circles: new signals)

The synthesis of [Pt(vegi$^{n\mathrm{Pr}}$)Cl_2] was also of interest. First [Pt(COD)Cl_2] and [Pt(C_2H_4)Cl_2]$_2$ were tested as metal precursors.

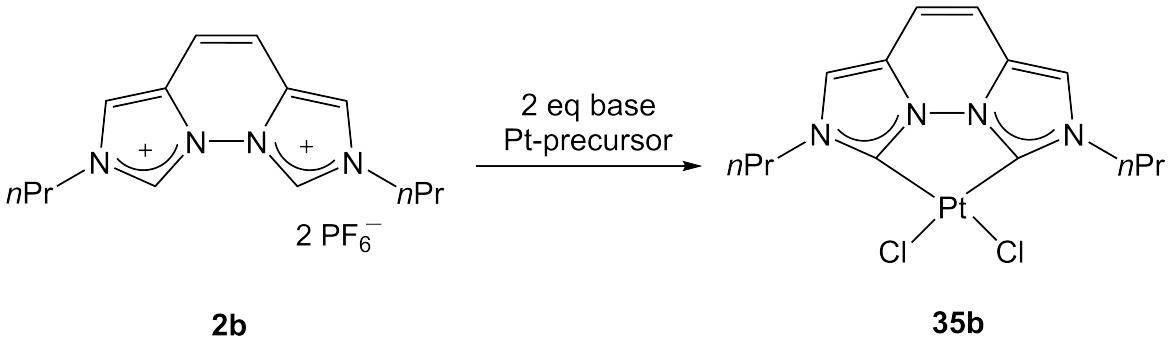

2b **35b**

Figure 89: Synthesis of **35b**.

The deprotonation was carried out in THF-d_8 with MeLi and was confirmed by ^{1}H NMR

spectroscopy. Then [Pt(COD)Cl_2] was added, and a yellow solution over a brown solid formed. The ^{1}H NMR spectrum in THF-d_8 shows two sharp and two broad signals in the aromatic region and additional signals for methane, COD and the precursor. When the spectrum was measured after 24 h additional signals in the aromatic region appeared and no main product could be elucidated. The exact same reaction was repeated with LiHMDS and showed the same signal set.

[Pt(C_2H_4)Cl_2]$_2$ was also used as a metal precursor. The ^{1}H NMR spectrum shows the signals for a symmetric complex as the main product and also those of some minor unknown sideproducts. The ratio of the sideproducts was lower compared to the reaction with [Pt(COD)Cl_2] and did not increase after five days. THF-d_8 was removed and DMSO-d_6 was added to the solid. In the ESI mass spectrum in acetonitrile a peak at m/z 584.0 indicates a +2 cations. Based on the isotope pattern it contains one platinum and two chloride atoms. A peak that would fit to a Pt complex with two vegi$^{n\mathrm{Pr}}$ ligands was not observed. In the ^{13}C NMR the characteristic carbene signal is detected at 130.0 ppm.

An alternative access to **35b** was required. In the literature [Pt(acac)$_2$] was used as a basic metal precursor that was reacted with a bis(imidazolium) chloride.[159]

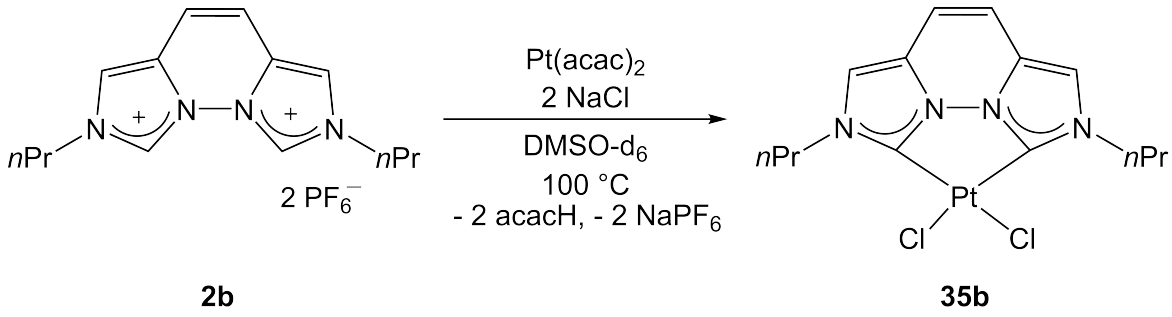

2b **35b**

Figure 90: Alternative synthesis of **35b**.

In the case of **2b** two equivalents of NaCl have to be added as a chloride source. In an NMR experiment **2b**, [Pt(acac)$_2$] and two equivalents of NaCl were mixed in DMSO and heated at 100 °C overnight. The ^{1}H NMR spectrum after one night indicated full

consumption of **2b** and [Pt(acac)$_2$] (Figure 91). New signals of complex [PtCl$_2$(vegi^{nPr})] **35b**, acetylacetone and some other unidentified side products are detected. In the ^{13}C NMR spectrum (DMSO-d$_6$) the carbene signal detected at 130.0 ppm shifted 74.5 ppm upfield compared to the free dicarbene **1b**. This is comparable with the literature known chelating platinumdichlorido dicarbene complexes.[158]

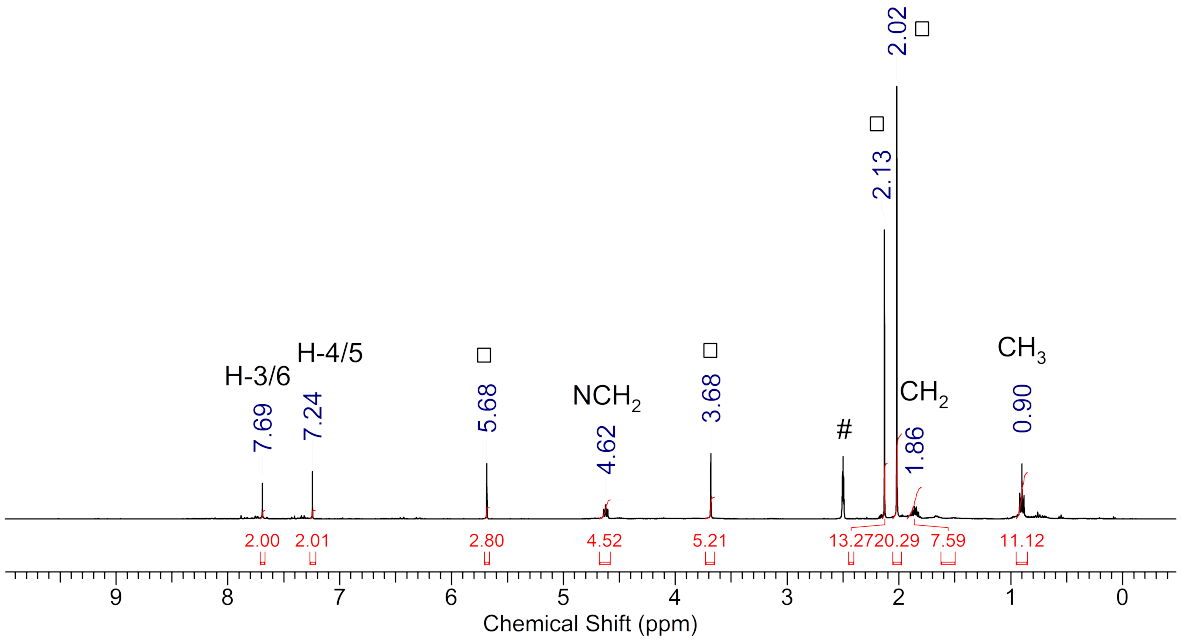

Figure 91: ^{1}H NMR spectrum of **35b** (CD$_3$CN, ; square = acetylacetone).

According to the ^{1}H NMR spectra in DMSO-d$_6$ of this experiment and the one in which [(Pt(C$_2$H$_4$)Cl$_2$)$_2$] was used, the desired complex **35b** was obtained as the main product in both cases. In case of [Pt(acac)$_2$] a smaller amount of side products has been obtained than using MeLi and [(Pt(C$_2$H$_4$)Cl$_2$)$_2$].

The experiment was repeated on a preparative scale in DMSO. The purification of the product was achieved by precipitation with *n*-pentane, followed by filtration. A ^{1}H NMR spectrum (CD$_3$CN) revealed decomposition and a white solid formed. The solid was filtered off and measured in DMSO-d$_6$, only signals of the complex **35b** are observed.

One sideproduct formed in this reaction could be a Pt-vegi^{nPr} complex with DMSO

ligands (similar to [Pd(DMSO-d_6)$_2$(vegi^{nPr})](PF$_6$)$_2$ (**31b**)) generated via a exchange of the metal-bound chloride ligand for DMSO molecules, which was already observed in a mesoionic dicarbene platinum complex in the literature.[158]

Figure 92: Synthesis of **38**.

Another experiment was carried out without adding NaCl as the chloride source. The ^{1}H NMR spectrum after 17 hour at 100 °C showed signals for **2b** and in addition signals (7.74, 7.32, 5.84, 4.37, 2.06, 1.85 and 0.91 ppm) in a 1:4 ratio. [Pt(acac)$_2$] is fully consumed, and signals for acetylacetone are detected. In addition there were two singlets at 5.84 and 2.06 ppm which fit, based on their integral ratio of the other signals, to the complex [Pt(acac)(vegi^{nPr})]PF$_6$ **38**. Additional signals at 6.06 and 2.18 ppm can be assigned to [Pt(acac)(DMSO)]PF$_6$. In the ESI mass spectrum a peak at m/z = 536.0 can be assigned to the [Pt(acac)(vegi^{nPr})]$^{+}$ cation. The chemical shifts are in the region of comparable complexes.[160] Coordinated DMSO could not be confirmed due to the use of DMSO-d_6. The integral ratio of the identified species (complex **38**, acetylacetone, **2b** and [Pt(acac)(DMSO-d_6)]PF$_6$ does not fit the stoichometry shown in Figure 92. Probably other Pt species are generated which are not observed in the ^{1}H NMR spectrum.

Because product **38** is a potential precursor to obtain various Pt-vegi^{R} complexes two equivalents of NaCl were added and the reaction mixture heated for 17 h at 100 °C. Before the mixture was heated the intensity of the signals of [Pt(acac)(DMSO-d_6)$_2$]PF$_6$ decreased already, which is attributable to the exchange of acetylacetone and chloride. After heating overnight the ^{1}H NMR spectrum matched the signals of [Pt(vegi^{nPr})Cl$_2$]

35b. It can be postulated that complex [Pt(acac)(vegi$^{n\mathrm{Pr}}$)]PF_6 **38** can be considered as an intermediate in the generation of [$PtCl_2$(vegi$^{n\mathrm{Pr}}$)] **35b** via [Pt(acac)$_2$].

For the first time, the Ni(II) vegi^{R} complexes have been prepared, which have tetrahedral geometry and thus are paramagnetic. In comparison the Pd(II) and Pt(II) vegi^{R} complexes show the preferred square planar structure. The palladiumdimethyl complexes **26a** and **26b** show resonances in the ^{13}C NMR spectrum at 180.0 (**26a**, in THF-d_8) and 177.7 ppm (**26b**, in THF-d_8). Both signals are shifted lowfield in comparison with the palladiumdichlorido complexes **29a** and **29b** which show resonances at 142.8 (**29a**, in DMSO-d_6) and 142.3 (**29b**, in DMSO-d_6). The same trend was observed for the platinum vegi^{R} complexes. The platinumdimethyl vegi^{R} complexes show resonances at 172.3 (THF-d_8, vegi$^{n\mathrm{Pr}}$ **35b**) and 172.2 ppm (CD_3CN, vegi$^{t\mathrm{Bu}}$ **35a**), while the signal is upfield shifted to 130.0 ppm (DMSO-d_6) in the dichlorido platinum vegi$^{n\mathrm{Pr}}$ complex **35b**. The difference in the chemical shifts of the carbene signal of the dimethyl versus dichlorido complexes are due to the weaker *trans*-influence of the chlorido ligands, which is also displayed by the shorter bond in the carbene metal, whereas the stronger σ-donor character of the methyl group weakens the metal-carbene bond.

7 Metal complexes of mani^{R} ligand

7.1 Alkali-metal complexes of mani^{R} ligand

The bis(imidazolium) salts mani^{R} · 2HPF$_6$ (**3a,b**) synthesized by *Steimann*[41] are interesting ligands for alkali metal complexes. The C1-C10 distance in **3b** measures 3.05 Å (X-ray).[41] In Table 13 the ^{1}H NMR chemical shifts of **3a** and **3b** are listed.

Table 13: ^{1}H NMR data [ppm] and coupling constants [Hz] of **3a** and **3b**.

	solvent	^{1}H NMR [ppm]						
		H-1/10	H-3/8	H-4/7	H-5/6	R		
3a	CD_3CN	9.68	8.47	8.04 (d, $^3J_{HH}$ = 9.4)	7.77 (d, $^3J_{HH}$ = 9.4)	1.91		
	DMSO[41]	10.34	8.97	8.15 (d, $^3J_{HH}$ = 9.5)	7.91 (d, $^3J_{HH}$ = 9.5)	1.88		
3b	CD_3CN	9.77	8.34	8.10 (d, $^3J_{HH}$ = 9.5)	7.83 (d, $^3J_{HH}$ = 9.5)	4.64	2.14	1.03
	DMSO[41]	10.66	8.79	8.27 (d, $^3J_{HH}$ = 9.5)	7.95 (d, $^3J_{HH}$ = 9.5)	4.68	2.08	0.97

The ligand precursor mani$^{n\mathrm{Pr}}$ **3b** was deprotonated with 2.2 equivalents of base in THF-d$_8$.

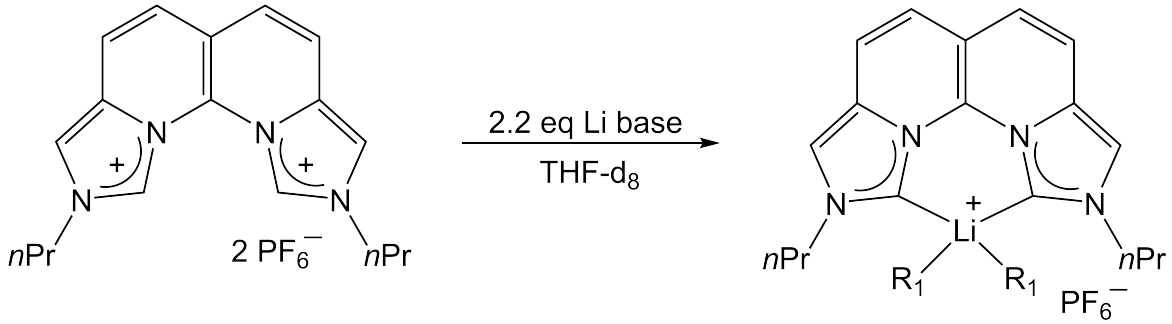

3b **39b**

R_1 = THF, 1/2 mani$^{n\mathrm{Pr}}$, PF_6^-

Figure 93: Synthesis of **39b**.

The use of MeLi resulted in a brown suspension and the ^{1}H NMR spectrum indicated full deprotonation of the acidic protons H-1/10 of **3b** and the formation of two symmetric complexes in a ratio of 1:0.7. The deprotonation with LiHMDS at -30 °C formed a dark brown suspension. The ^{1}H NMR spectrum confirms the deprotonation of **3b**,

however only one signal set is observed. The carbene signal is found at 198.9 ppm which indicates the formation of a Li-complex. Unusually, this is a species which was not obtained using MeLi for the deprotonation.

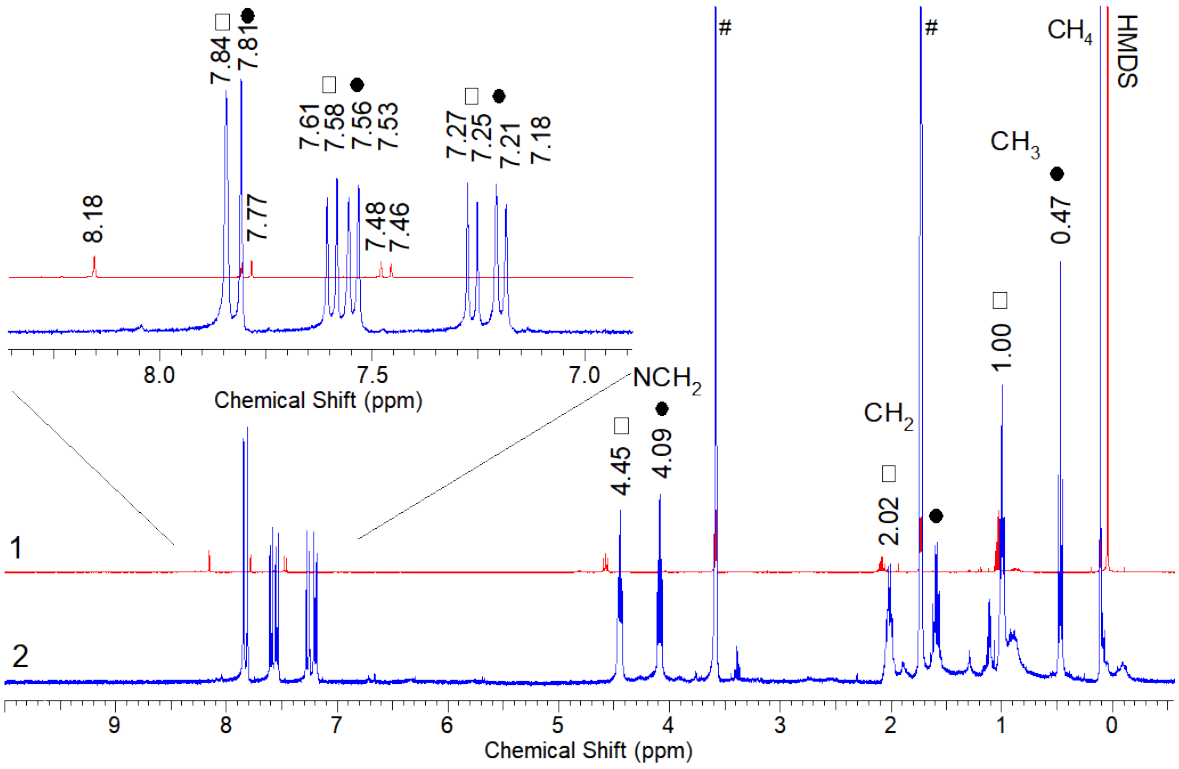

Figure 94: ^{1}H NMR spectrum of 1) Deprotonation with LiHMDS and 2) Deprotonation with MeLi.

A reason for the formation of different species could be the reaction temperature. When the deprotonation reaction with LiHMDS was repeated at -30 °C also two species were found, whose signals are almost identical with those obtained with MeLi (Figure 94, spectrum 2), with the same ratio (1:0.7). The THF-d_8 sample was measured at -80 °C; the signals H-3/8 of the two species drift apart while the signals for 4/7 and 5/6 converge. The ratio changed to 1:0.8. Heating the mixture up to 60 °C the signals H-3/8 merged while the signals for H-4/7 and H-5/6 remain separated. The ^{7}Li NMR spectrum at room temperature shows four signals: one broad signal at -0.59 ppm which can be assigned to $LiPF_6$, that is formed during the reaction and residual LiHMDS at 0.20 ppm (small signal), one broad signal at 1.79 ppm and one sharp signal at 2.85 ppm. Upon cooling to -80 °C all signals become baseline separated. The integrals of

the peaks at -0.41, 1.90 and 2.89 ppm show a ratio of 1, 0.3 and 0.1.

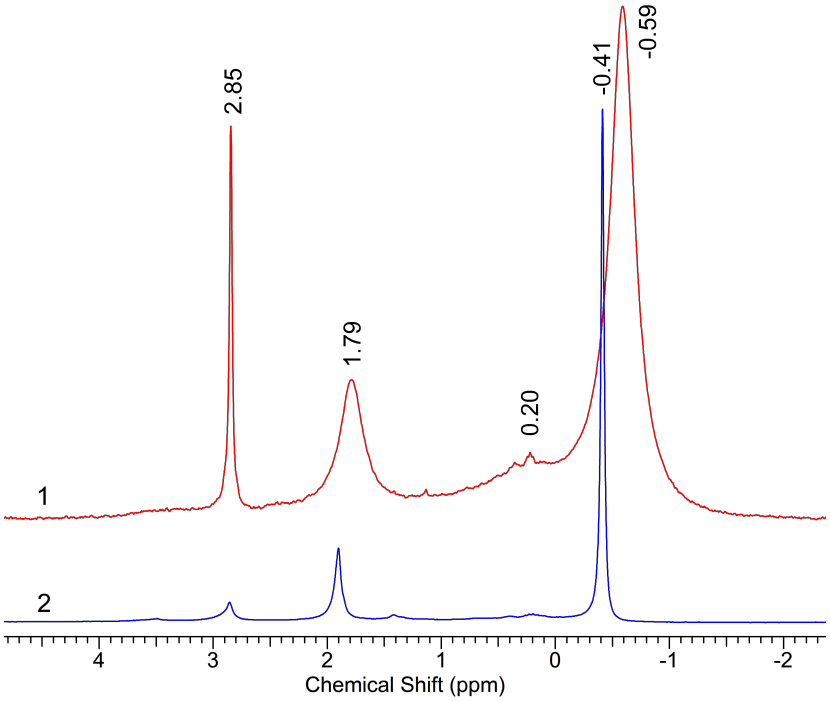

Figure 95: ^{7}Li NMR spectrum of 1) 26 °C, 2) -80 °C.

The $^{13}C\{^{1}H\}$ NMR spectrum at (Figure 96) -80 °C confirms the formation of two carbene Li complexes. In analogy to the LiC coupling in **10a** and **10a-H** here also one 1:1:1:1 quartet was obtained for each Li complex with coupling constants of 21.8 and 24.5 Hz .

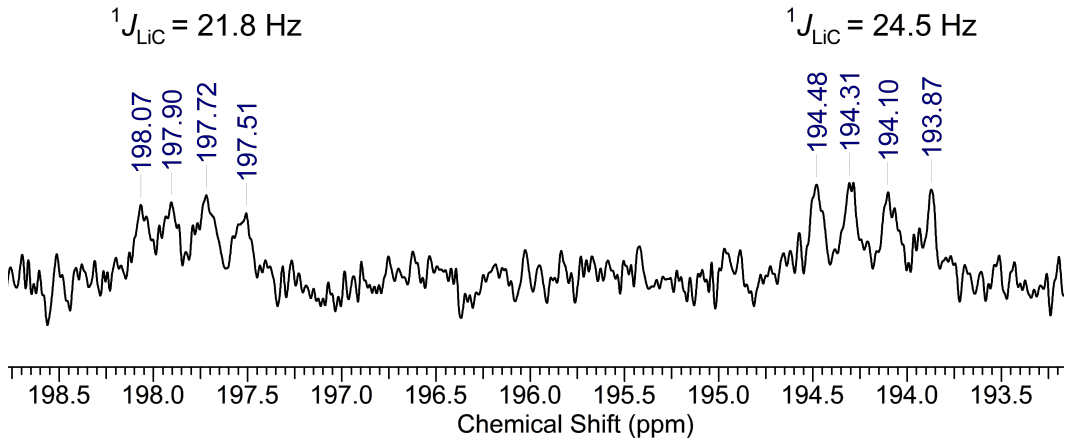

Figure 96: $^{13}C\{^{1}H\}$ NMR spectrum at -80 °C in THF-d_8: carbene signals.

The ligand precursor mani$^{n\mathrm{Pr}}$ **3b** can not be deprotonated with NaHMDS, KHMDS and P_4-*t*Bu, neither at room temperature nor at -30 °C in THF-d_8. The ^{1}H NMR spectra showed many signals in the aromatic region with very low intensity. No major product signals were obtained.

The synthesis of a Ag(I) complex was tested with mani$^{n\mathrm{Pr}}$ **3b** in dichloromethane and acetonitrile via the basic Ag_2O route. The reactions did not lead to formation of a Ag(I) complex. The deprotonation with a Li-base followed by transmetalation with $AgBF_4$ was also unsuccessful. The sterical demand of the ligand might be a reason why no dinuclear silver complex with a linear coordination of the Ag(I) cation forms.

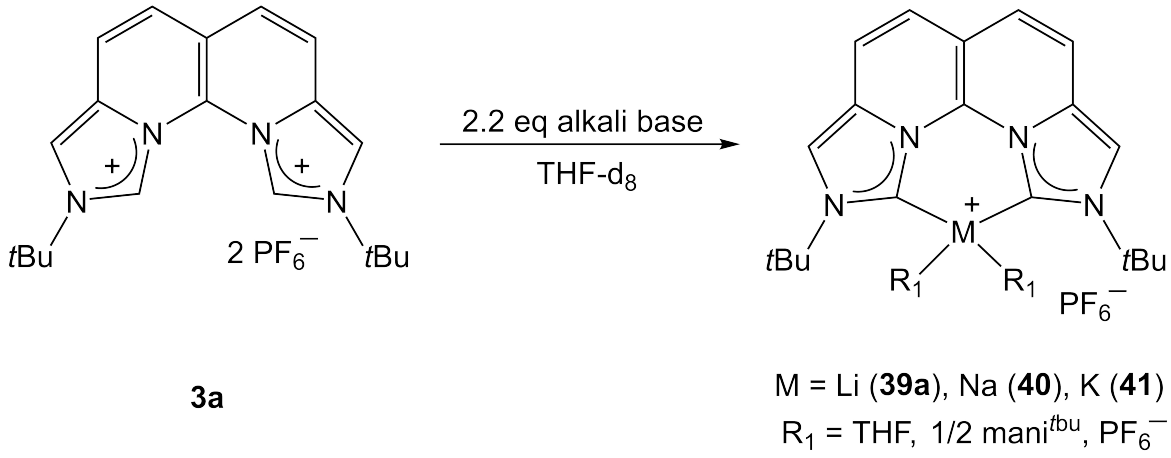

Figure 97: Synthesis of **39a**, **40** and **41**.

The bulkier ligand precursor **3a** was also tested in deprotonation reactions. The deprotonation with LiHMDS at -30 °C formed a yellow solution and a brown solid. The ^{1}H NMR spectrum of the solution shows two signal sets in a ratio 0.4:1. The deprotonation with NaHMDS at -30 °C led to a brown suspension and the ^{1}H NMR spectrum indicated the formation of one single compound. The same is observed using KHMDS. In the ^{1}H NMR spectra small signals of unknown byproducts are obtained. The deprotonation of **3a** with LiHMDS in CD_3CN led only to one signal set.

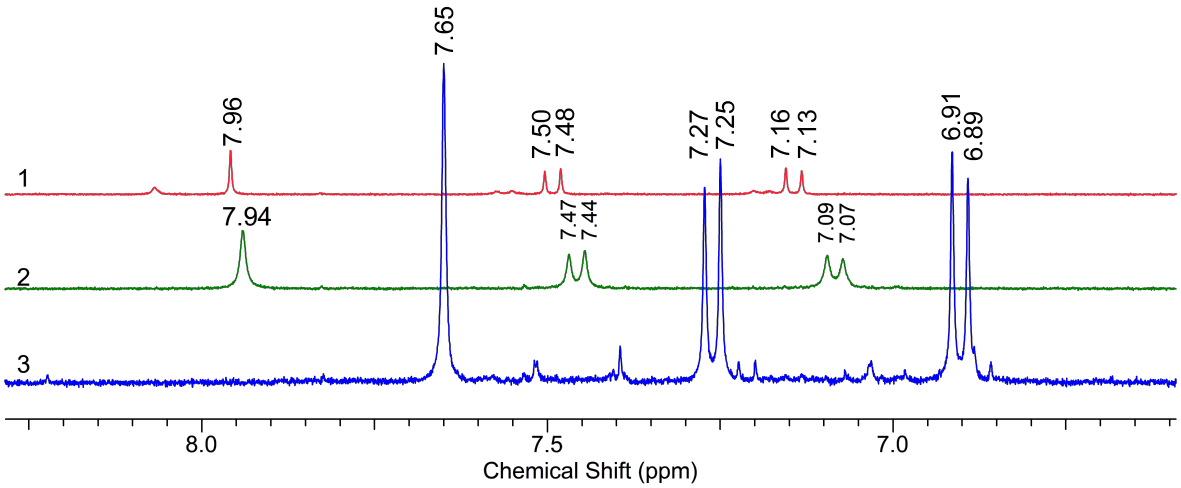

Figure 98: ^{1}H NMR spectra (detail, aromatic region) in THF-d$_8$. 1) Deprotonation with LiHMDS (**39a**) 2) Deprotonation with NaHMDS **40** 3) Deprotonation with KHMDS **41**.

The deprotonation with KHMDS shows the strongest high field shift of the aromatic proton signals in comparison with the Na and Li complexes (Figure 98). This trend was also obtained with the vegi^{R} alkali-metal complexes. The large difference of the chemical shifts of the signals for **41** compared to **39a** and **40** could also indicate the formation of the free dicarbene instead of the K-mani^{tBu} complex **41**. Unfortunately, no carbene signal was detected in the ^{13}C NMR spectrum for all three complexes, most likely due to the precipitation of the complexes in the THF over time.

7.2 Platinum mani$^{n\mathrm{Pr}}$ complex

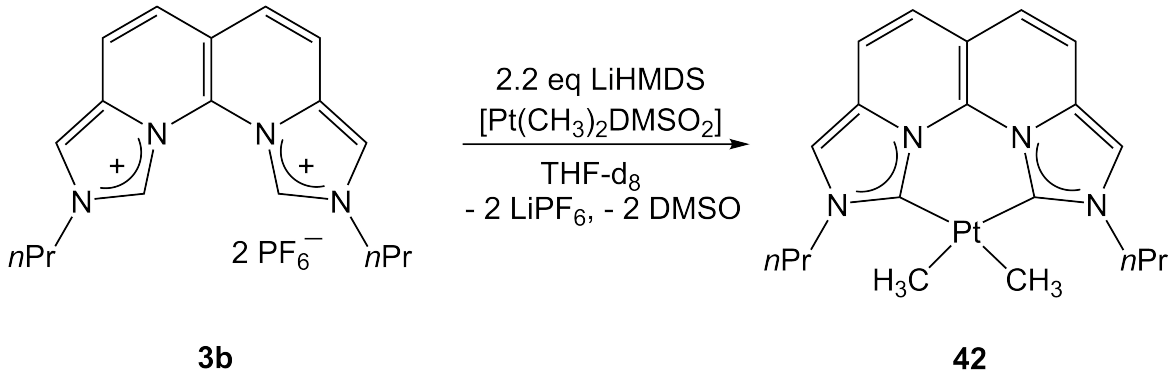

3b **42**

Figure 99: Synthesis of **42**.

The deprotonation with 2.2 equivalents of LiHMDS and transmetalation with [Pt(CH$_3$)$_2$DMSO] in THF led to the formation of [Pt(CH$_3$)$_2$(mani$^{n\mathrm{Pr}}$)]. The mixture was stirred for 2 h at room temperature then the brown suspension was filtered over neutral alumina. The yellow solution was dried and washed with *n*-pentane to yield the product as a yellow solid. The carbene signal can be detected at 171.5 ppm. The signal for the methyl groups at the platinum atom is at 0.35 ppm and show satellites ($^2J_{\mathrm{PtH}} = 65.7$ Hz).

In conclusion the less sterically hindered mani$^{n\mathrm{Pr}}$ ligand precursor can only be deprotonated by Li bases, while the N-*tert*-butyl substituted ligand can be deprotonated with Li-, Na- and KHMDS. Most likely the corresponding alkali-metal complexes are formed, which could be proved by the detection of the carbene signal in the ^{13}C{^{1}H} NMR spectrum. Until now it is unclear why the less sterically hindered mani$^{n\mathrm{Pr}}$ ligand does not lead to clean deprotonation products with Na- and KHMDS.

8 Summary and Outlook

In the first part, I showed that the deprotonation of the bis(imidazolium) salts **2a** and **2b** with alkali-metal bases leads to very stable chelate complexes of lithium, sodium and potassium ions. The lithium **10a,b** and **10a,b-H** and sodium **11a,b** complexes are stable enough to even withstand chelation by the respective crown ethers of the cations. In contrast the addition of [18]-crown-6 to the potassium complex **12a,b** leads to the liberation of the free dicarbene **1a,b**. The stability of the lithium **10a,b** and **10a,b-H** and sodium complexes **11a,b** could further be investigated towards the addition of cryptands which could lead to the free dicarbene **1a,b** and the respective cryptate. In the case of lithium and the bulkier vegi$^{t\mathrm{Bu}}$ an equilibrium between the heteroleptic **10a** and the homoleptic **10a-H** complex is observed. This can be explained by enhanced dispersion in **10a-H** due to the bulky *N*-*tert*-butyl substituents. A closer examination of the Li vegi$^{n\mathrm{Pr}}$complex showed to also form a homoleptic complex **10b-H**.
For both lithium complexes **10a** and **10a-H** direct Li-C coupling constants in the ^{13}C NMR spectrum are observed. In addition to the low-field chemical shifts of the obtained ^{7}Li NMR signals this confirms an enhanced covalent contribution in the Li-carbene bond. The generation of the free dicarbenes **1a,b** was also realized using the strong metal-free phosphazene base P$_4$-*t*Bu. Due to the very similar chemical shifts obtained in the ^{1}H and ^{13}C NMR spectra of the deprotonation of **2a,b** with CsHMDS it is yet unclear whether a Cs-vegi complex **14a,b** or the free dicarbene **1a,b** is formed. The deprotonation in toluene shows a promising isolation route. If the dicarbene **1a,b** forms it should remain in the unpolar toluene solution while a formed Cs-vegi complex **14a,b** should precipitate together with $CsPF_6$. Single crystals should be obtained and measured (X-ray crystallography) to determine the exact molecular structure.
A straightforward isolation of the free dicarbene would be a great benefit for the synthesis of other vegi metal complexes by simple coordination, instead of transmetalation. An unsymmetric selenium adduct of vegi$^{t\mathrm{Bu}}$ **9a** was also obtained.

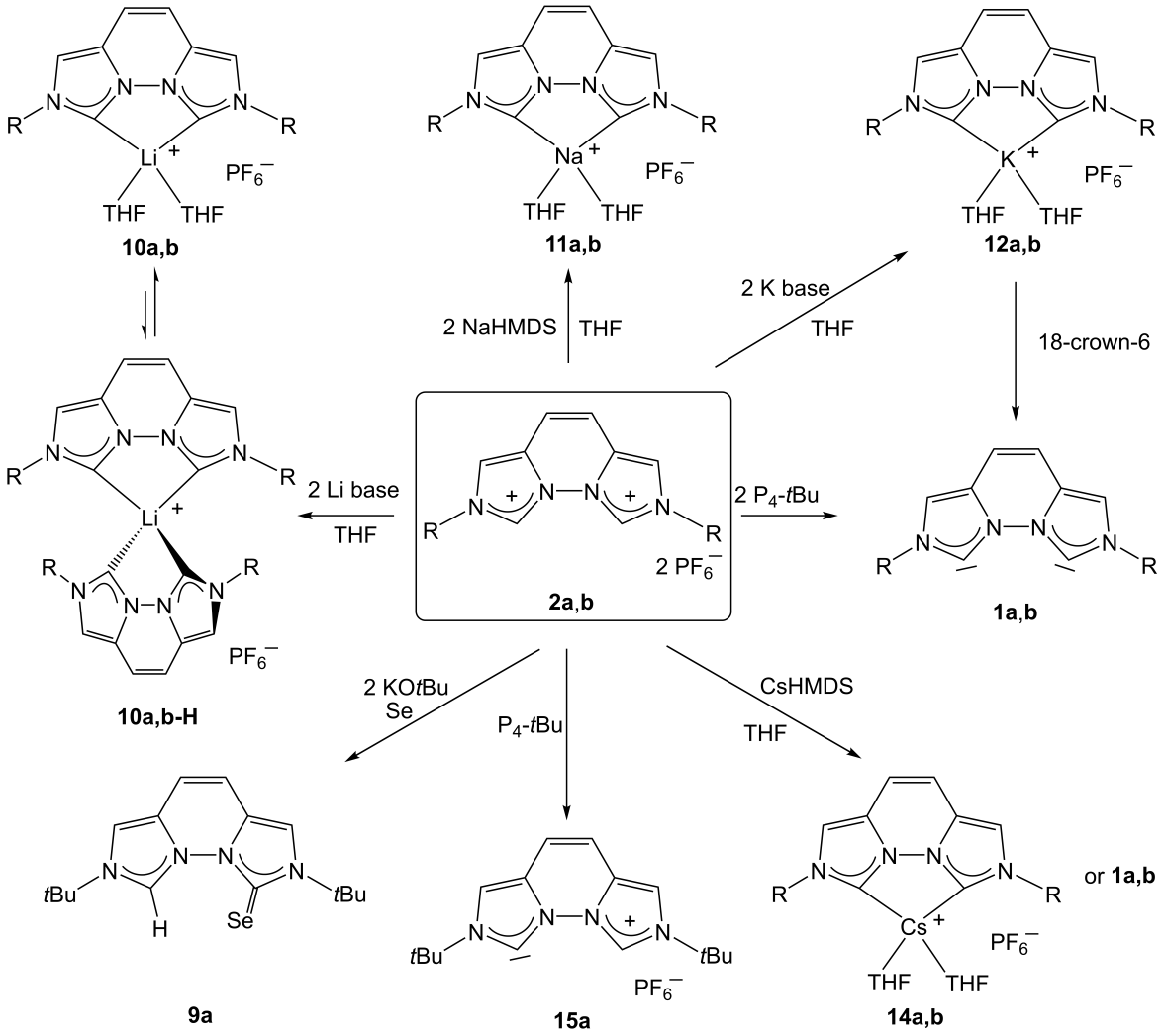

Figure 100: Reactivity of **2a,b**.

In the next chapter two new synthesis pathways were described to obtain the known dinuclear Ag(I) and Au(I) complexes **17a** and **18a**.[30] The molecular structure of the dinuclear Cu(I) complex **16a** was elucidated by X-ray crystallography and compared with the molecular structures of all coinage vegi$^{t\mathrm{Bu}}$ complexes.

The Ni(0) complexes **22a,b** were synthesized. The sensitive compound **22a** decomposed in isolation attempts during the filtration over Celite®. The removal of the solvent followed by simple washing with *n*-pentane could remove all sideproducts but KPF_6. An application of the *in situ* generated compound **22a** was to test its catalytic activity in the vinylcyclopropane rearrangement. First experiments showed no forma-

tion of a bicyclic product, but rather the formation of an isomerization product. The molecular structure of **22a** showed that the C-C bond of the pyridazine moiety acts as an additional bridging coordination site. The electron rich complex **22a** could be a catalyst in various C-C coupling reactions. Ni(II) dichlorido complexes **23a,b** could be synthesized and **23a** also structurally characterized. The tetrahedral complex **23a** is paramagnetic which was confirmed by NMR and EPR measurements.

Chelating dimethyl palladium complexes **25a,b** can be synthesized with $[Pd(CH_3)_2(TMEDA)]$. **25a** was successfully isolated and structurally characterized. The corresponding cis-dichlorido complexes **28a,b** were synthesized with $[Pd(OAc)_2]$ and two equivalents of NaCl which suppressed the formation of the protonolysis product **30a,b**, which are stable towards air and moisture. The generation of all mentioned palladium vegi complexes requires elevated temperatures whereas the synthesis of the platinum vegi complexes can be performed at room temperature. Dimethyl platinum complexes **33a,b** were synthezised and isolated (for **33a**). The corresponding dichlorido platinum complex **35a** could only be synthesized along with the protonolysis product **36**. The use of $[Pt(acac)_2]$ with two equivalents of NaCl instead of $[Pt(COD)Cl_2]$ was advantageous and led to the formation of onyl **35a** in DMSO.
Reactivity studies of the dimethyl platinum and palladium complexes **23a,b** and **25a,b** toward C-H activation would be interesting. Only with the dimethyl vegi$^{n\mathrm{Pr}}$ palladium complex **25b** the formation of small amounts of methane and ethane was observed after heating at 50 °C overnight.

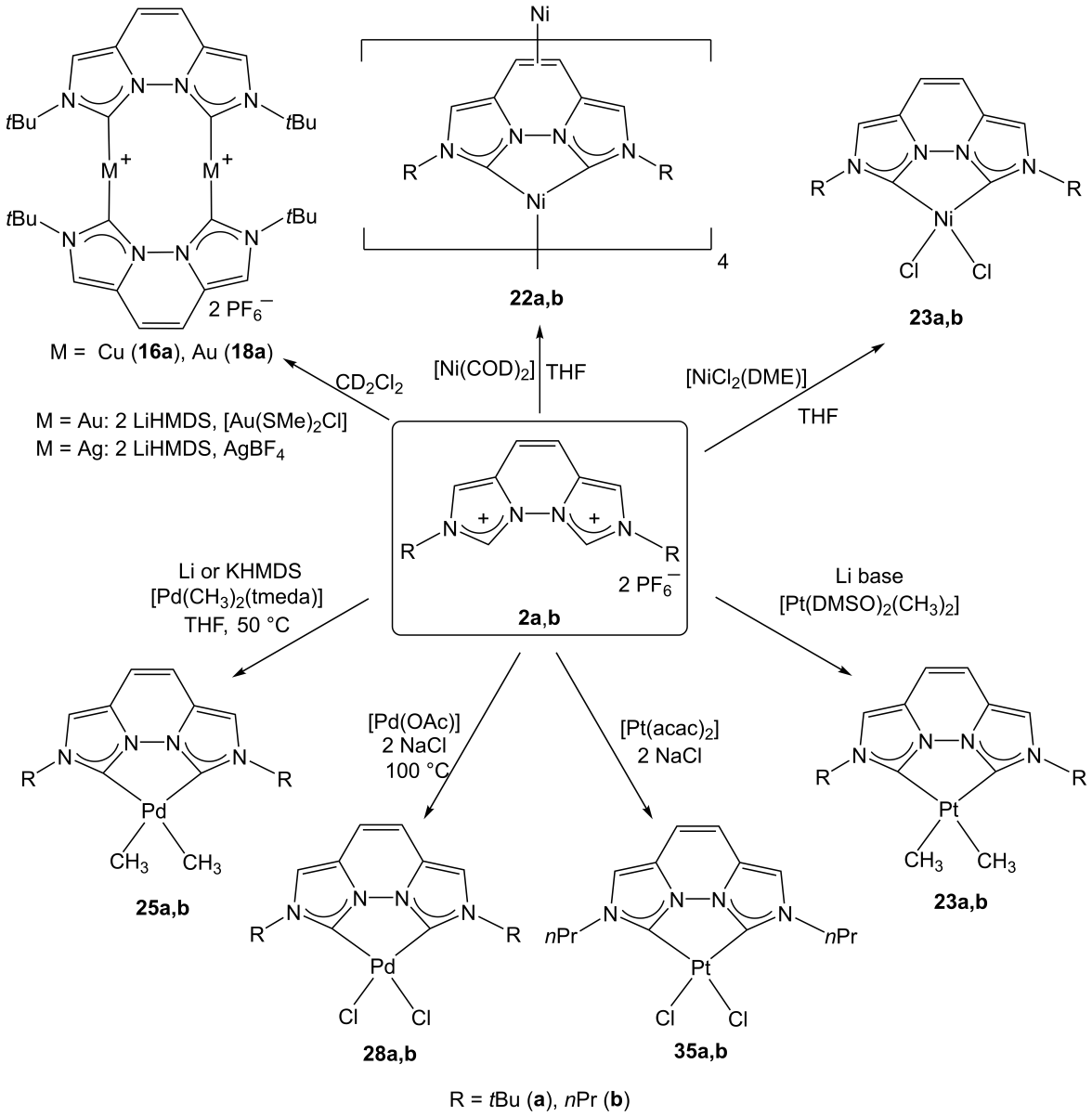

Figure 101: Synthesis of transition metal vegi complexes.

In the last chapter of this thesis the generation of alkali-metal complexes of mani^R is described. Compared to mani$^{t\mathrm{Bu}} \cdot 2\mathrm{HPF}_6$ **3a** the less sterically hindered mani$^{n\mathrm{Pr}}$ ligand precursor **3b** can only be deprotonated by Li bases whereas the *N*-*tert*-butyl-substituted precursor **3a** can be deprotonated with Li-, Na- and KHMDS. The ^{1}H NMR chemical shifts of the corresponding complexes reveal the formation of **39a,b**, **40** and **41**. Di- or homonuclear Ag(I) complexes of mani$^{n\mathrm{Pr}}$ could not be obtained via Ag_2O or transmetalation with $AgBF_4$ from the *in situ* generated Li complex. Probably

due to steric effects, no Ag(I) complex forms.

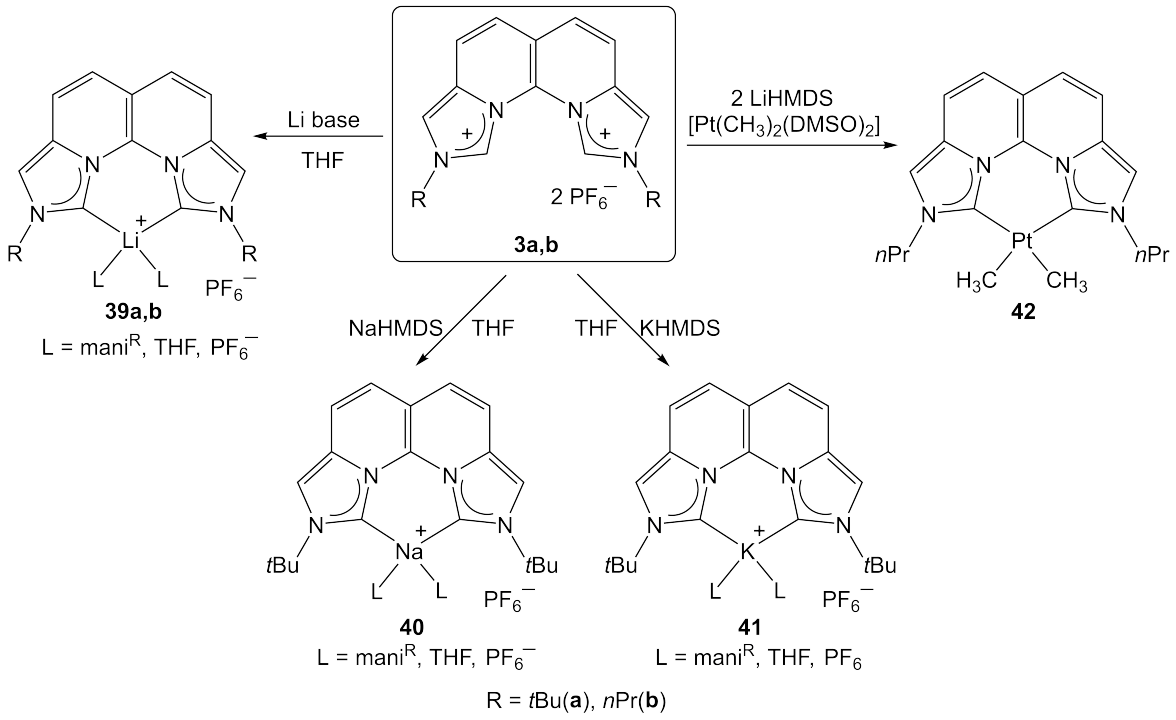

Figure 102: Synthesis of alkali-metal and platinum mani complexes.

In this work the unusual geometric flexibility of the vegi dicarbene ligand **1a,b** could be shown. The ligand does not only act as a chelating or bridging ligand, but also showed an unexpected coordination of the backbone C-C double bond. The influence of the ligands vegi$^{t\mathrm{Bu}}$ versus vegi$^{n\mathrm{Pr}}$ on the geometry of the obtained metal complexes was featured by London dispersion which were more pronounced in vegi$^{t\mathrm{Bu}}$ complexes. Due to the strong electron donor character of the vegi ligand the nucleophilicity as well as the basicity of the metal complex are enhanced, which should prove in catalysis.

9 Experimental section

9.1 General Methods

All experiments were carried out under an argon atmosphere using a glovebox or standard Schlenk techniques. Argon 5.0 from the *Westfalen* company served as the inert gas. Non-deuterated solvents were purchased from Sigma-Aldrich, dried, and degassed using an *MBraun*-SPS-800 solvent purification system. All other chemicals used were purchased from commercial suppliers and used without further purification. Deuterated solvents were dried with standard techniques.[161] Solvents were degassed by the Freeze-Pump-Thaw method. For solvent transfer the syringe- or septum-cannula technique was used. The filter paper used for filtrations was purchased from *Whatman*™ company. Glass frits or syringe filter (minisart SRP 15 0.45 μm company *Sartorius*) were also used. The *Young*® NMR tubes were bought from the company *Deutero*.
The chemicals were purchased from *Sigma Aldrich*, *ABCR*, *Merck* and *Acros*. Methyllithium was bought as a diethyl solution and dried *in vacuo* to remove the solvent and stored in the glove box fridge. P_4-*t*Bu was bought as a hexane solution and dried in vacuo to remove the solvent.

9.2 Characterization methods

NMR spectroscopy:
NMR spectra were recorded on a Bruker AVII+400 or 500 spectrometer (at 26 °C, if not otherwise mentioned). ^{1}H and ^{13}C NMR spectra were calibrated to TMS on the basis of the relative chemical shift of the respective solvent signal as an internal standard (THF-d_7 δ = 1.73, 3.58; CHD_2CN δ = 1.94, $CHCl_3$ δ = 7.26, DMSO-d_5 δ = 2.50. $^{13}C\{^1H\}$ standard signals: THF-d_8 δ = 25.31, 67.21; CD_3CN δ = 1.32, 118.26; $CDCl_3$ δ = 77.16; DMSO-d_6 δ = 39.5; CD_2Cl_2 = 53.8 ppm.) ^{7}Li NMR chemical shifts are reported in ppm and calibrated to a LiCl solution (H_2O) as external standard. All chemical shifts are reported in ppm and coupling constants in Hertz. The assignment of the signals is based on ^{1}H,^{13}C-HMBC-, ^{1}H,^{13}C-HSQC- and ^{1}H,^{1}H-COSY-spectra. The multiplicity is abbreviated as follows: s (singlet), br s (broad singlet), d (doublet),

t (triplet), q (quartet) sept (septet).

Melting point:
Melting points were measured on samples in sealed capillaries on a *Büchi* Melting Point M 560 apparatus.

Elemental analysis (EA):
Were carried out using a *Vario* MICROCube by the EA section at the Institut für Anorganische Chemie.

EPR spectroscopy:
The EPR spectrum was collected using 4 mm O.D. Wilmad quartz (CFQ) EPR tube on a continuous wave X-band Bruker EMXmicro spectrometer, and are referenced to the Bruker Strong Pitch standard $g_{iso} = 2.0028$.

Mass spectrometry:
Were carried out using a *Bruker* Esquire 3000 plus or *Bruker* HR-ESI-TOF (or Daltonics APEX II FT-ICR) at the mass spectrometry section of the Institut für Anorganische Chemie.

X-ray structure analysis:
Single crystals were measured at a *Bruker* APEX II CCD DUO diffractometer. The X-ray source was graphite monochromated Mo-K_α radiation ($\lambda = 0.71073$ Å) from a sealed tube or microfocus source. The structures were solved and refined with SHELXS and SHELXL.[162–164]

9.3 Experimental Procedure

9.3.1 3,6-Dimethylpyridazine (4a)[34,43]

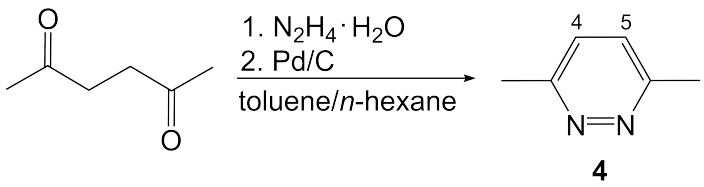

4

Synthesis according to literature.[34,43]

^{1}H NMR values match with the literature known data.

9.3.2 3,6-Bis(chlormethyl)pyridazine (5)[31]

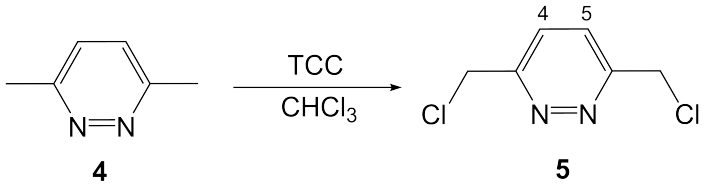

4 **5**

Synthesis according to literature.[31]

^{1}H NMR values values match with the literature known data.

9.3.3 3,6-Bis(*tert*-butylaminomethyl)pyridazine (6a)[31]

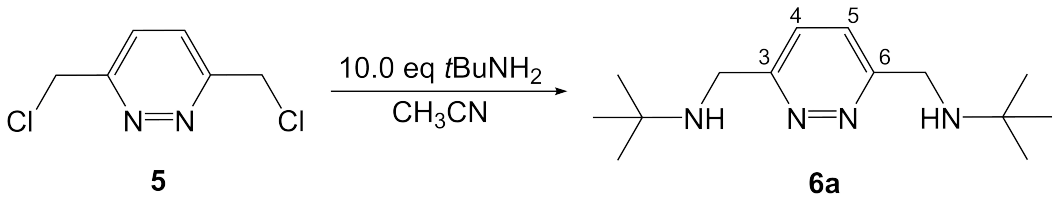

5 **6a**

Synthesis according to literature.[31]

^{1}H NMR values match with the literature known data.

9.3.4 3,6-Bis(*n*-propylaminomethyl)pyridazine (6b)[31]

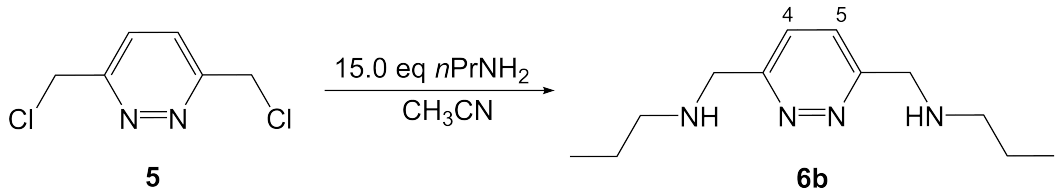

5 **6b**

Synthesis according to literature.[31]

^{1}H NMR values match with the literature known data.

9.3.5 3,6-Bis(*tert*-butylformamidomethyl)pyridazine (7a)[31,33]

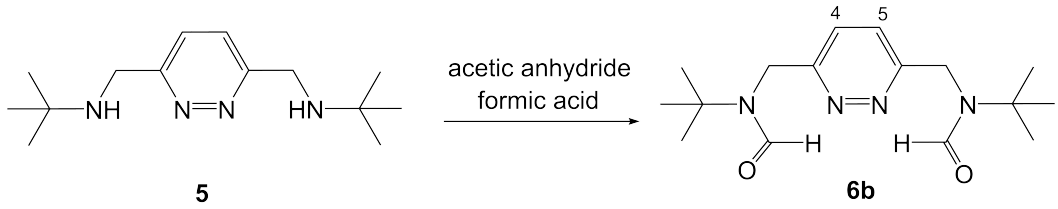

5 **6b**

Synthesis according to literature.[31]

^{1}H NMR values match with the literature known data.

9.3.6 3,6-Bis(*n*-propylformamidomethyl)pyridazine (7b)

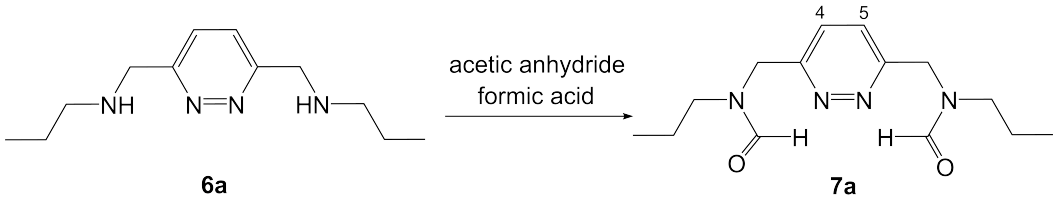

6a 7a

Synthesis according to literature.[31]

^{1}H NMR values values match with the literature known data.

9.3.7 *N*,*N*'-Di(*tert*-butyl)bisimidazo[1,5-*b*:5',1'-*f*']pyridazindiium bis(hexafluorphosphate) (2a)[31,33]

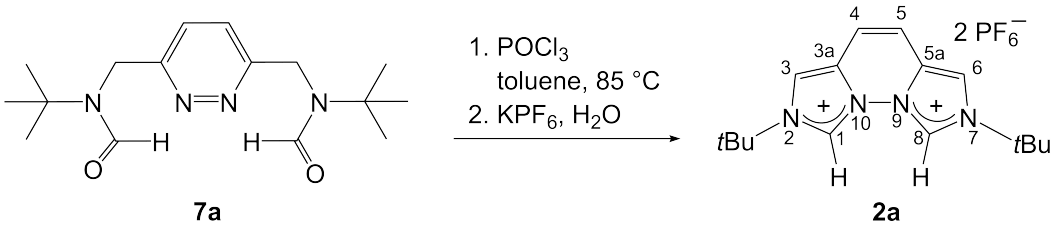

Synthesis according to literature.[31]

^{1}H NMR values match with the literature known data.

New data:

^{1}H NMR (400.13 MHz, THF-d_8):
δ = 1.79 (s, 18H, $C(CH_3)_3$), 7.46 (s, 2H, H-4/5), 8.34 (s, 2H, H-3/6), 10.27 (s, 2H, H-1/8).

Anal. Calcd for $C_{16}H_{24}N_4F_{12}P_2$:
Calcd.: C, 34.17; H, 4.30; N, 9.96.
Found: C, 34.14; H, 4.36; N, 9.79.

9.3.8 *N*,*N*'-Di(*n*-propyl)bisimidazo[1,5-*b*:5',1'-*f*']pyridazindiium bis(hexafluorphosphate) (2b)[31]

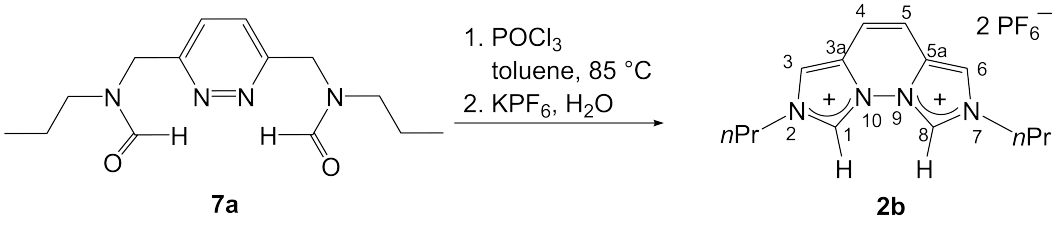

Synthesis according to literature.[31]

^{1}H NMR values match with the literature known data.

New data:

^{1}H NMR (400.13 MHz, THF-d_8):
δ = 1.06 (t, $^3J_{HH}$ = 7.4 Hz, 6H, CH_3), 2.06 (tq, $^3J_{HH}$ = 7.2 Hz, $^3J_{HH}$ = 7.4 Hz, 4H, CH_2), 4.48 (t, $^3J_{HH}$) = 7.2 Hz, 4H, NCH_2), 7.54 (s, 2H, H-4/5), 8.19 (d, $^4J_{HH}$ = 1.5 Hz, 2H, H-3/6), 10.05 (d, $^4J_{HH}$ = 1.5 Hz, 2H, H-1/8).

9.3.9 *N*,*N*'-Di(*tert*-butyl)bisimidazo[1,5-*b*:5',1'-*f*']pyridazindiiumbis(chloride) (8)

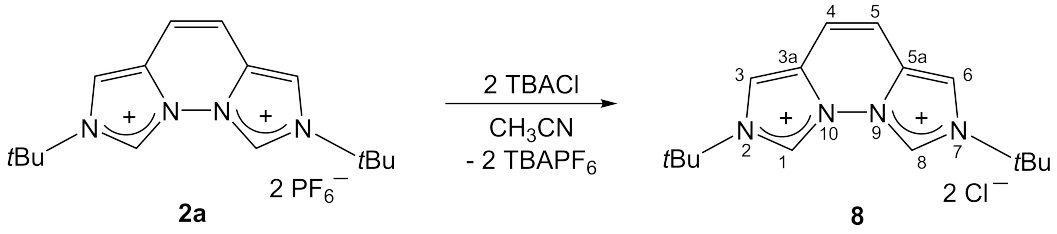

2a (90.0 mg, 262 μmol) and TBACl (90.0 mg, 323 μmol) are stirred in acetonitrile (5 ml) for 2.5 h at room temperature. The mixture is concentrated and the suspension filtered. The residue is washed with acetonitrile (3 x 0.8 mL) and dried. The product is obtained as a off-white solid with impurities of compounds containing PF_6^-.

^{1}H NMR (400.13 MHz, $DMSO_6$):
δ = 1.76 (s, 18H, $C(CH_3)_3$), 7.68 (s, 2H, H-4/5), 8.87 (d, $^4J_{HH}$ = 1.7 Hz, 2H, H-3/6), 12.26 (d, $^4J_{HH}$ = 1.7 Hz, 2H, H-1/8).

^{1}H NMR (400.13 MHz, CD_3CN):
δ = 1.82 (s, 18H, $C(CH_3)_3$), 7.51 (s, 2H, H-4/5), 8.25 (d, $^4J_{HH}$ = 1.7 Hz, 2H, H-3/6), 13.09 (d, $^4J_{HH}$ = 1.7 Hz, 2H, H-1/8).

MS(ESI$^+$, CH_3CN):

m/z 416.9 [M - 2Cl$^-$ + PF_6^-]$^+$, 307.1 [M - Cl$^-$]$^+$, 271.1 [M - 2Cl$^-$ + PF_6^-]$^+$.

Anal. Calcd for $C_{16}H_{24}N_4Cl_2 \cdot 0.35\ C_{16}H_{24}N_4P_2F_{12}$:

Cacld.: C 48.03; H 6.05; N 14.00.

Found: C 47.29; H 6.78; N 13.75.

Melting point: 198 °C (decomposition)

9.3.10 Selenium vegi$^{t\mathrm{Bu}}$ adduct 9a

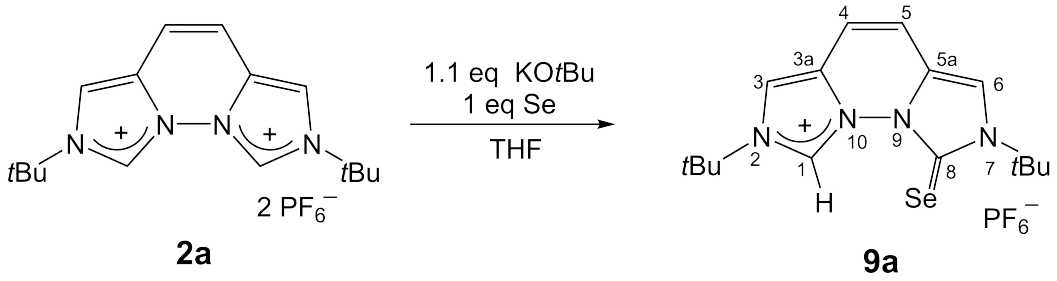

To a suspension of **2a** (100 mg, 177 μmol, 1 eq) in THF selenium (14.0 mg, 177 μmol, 1 eq) is added. The mixture was cooled to -35 °C, then a solution of KOtBu (21.0 mg, 187 μmol, 1.1 eq) in THF was added and stirred for 30 min. The mixture was slowly heated to room temperature and stirred overnight. The grey suspension was filtered over Celite® and the yellow filtrate was dried.

^{1}H NMR (400.13 MHz, CD_3CN):
δ = 1.69 (s, 9H, C(CH_3)$_3$), 1.90 (s, 9H, C(CH_3)$_3$), 6.92 (d, $^{3}J_{HH}$ = 10.6 Hz, 1H, H-4 or H-5), 7.06 (d, $^{3}J_{HH}$ = 10.2 Hz, 1H, H-4 or H-5), 7.69 (br s, 1H, H-6), 7.79 (d, $^{4}J_{HH}$ = 1.8 Hz, 1H, H-3), 13.02 (s, 1H, H-1).

^{13}C{^{1}H} NMR (125.76 MHz, CD_3CN):
δ = 28.2 (s, C(CH_3)$_3$), 29.8 (s, C(CH_3)$_3$), 64.6 (s, C(CH_3)$_3$), 65.3 (s, C(CH_3)$_3$), 111.8 (s, C-5), 113.7 (s, C-3), 115.2 (s, C-6), 117.2 (s, C-4), 121.1 (s, C-6), 126.3 (s, 3a or 5a), 126.4 (s, 3a or 5a), 128.3 (s, C-1), 212.8 (s, C-8).

^{77}Se NMR (47.70 MHz, CD_3CN):
δ = 250 (s, C-8).

9.3.11 *In situ* generation of Li-vegi^{tBu} 10a and 10a-H complexes

In THF-d_8, with LiHMDS:

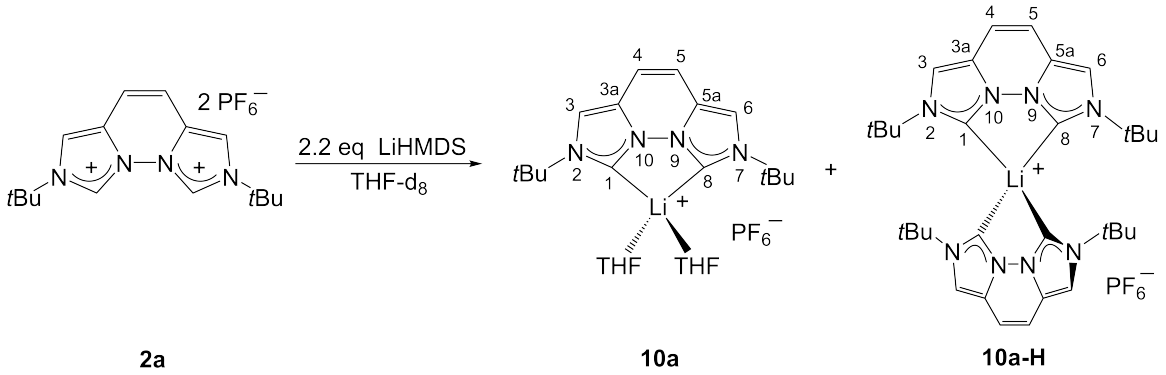

LiHMDS (5.4 mg, 32 μmol, 2.2 eq) was added to a suspension of **2a** (7.6 mg, 14 μmol, 1 eq) in 0.5 mL of THF-d_8 and stirred for 20 min at room temperature. The ^{1}H NMR spectrum of the brown-red solution indicates the deprotonation of **2a**. In all cases the formation of complexes **10a** and **10a-H** in a ratio of 1:0.5 was observed.

10a:

^{1}H NMR (500.13 MHz, THF-d_8, –80 °C):

δ = 1.69 (s, 18H, C(CH$_3$)$_3$), 7.16 (s, 2H, H-4/5), 8.03 (s, 2H, H-3/6).

^{1}H NMR (500.13 MHz, THF-d_8):

δ = 1.68 (s, 18H, C(CH$_3$)$_3$), 7.02 (s, 2H, H-4/5), 7.77 (s, 2H, H-3/6).

^{1}H NMR (400.11 MHz, CD$_3$CN):

δ = 1.64 (s, 18H, C(CH$_3$)$_3$), 6.96 (s, 2H, H-4/5), 7.57 (s, 2H, H-3/6).

^{13}C{^{1}H} NMR (125.76 MHz, THF-d_8, –80 °C):

δ = 31.1 (s, C(CH$_3$)$_3$), 58.9 (s, C(CH$_3$)$_3$), 113.3 (s, C-4/5), 115.0 (s, C-3/6), 124.3 (s, C-3a/5a), 182.2 (q, $^1J_{CLi}$ = 24.2 Hz, C-1/8).

$^{13}C\{^1H\}$ NMR (125.76 MHz, THF-d_8):
δ = 31.3 (s, C(CH_3)$_3$), 58.9 (s, C(CH_3)$_3$), 113.2 (s, -4/5), 114.5 (s, C-3/6), 124.6 (s, C-3a/5a), 184.1 (br s C-1/8).

$^7Li\{^1H\}$ NMR (194.37 MHz, THF-d_8, –80 °C):
δ = 1.51 (s).

10-H:

^1H NMR (500.13 MHz, THF-d_8, –80 °C):
δ = 1.53 (s, 18H, C(CH_3)$_3$), 7.18 (s, 2H, H-4/5), 7.99 (s, 2H, H-3/6).

^1H NMR (500.13 MHz, THF-d_8):
δ = 1.51 (s, 18H, C(CH_3)$_3$), 7.04 (s, 2H, H-4/5), 7.75 (s, 2H, H-3/6).

$^{13}C\{^1H\}$ NMR (125.76 MHz, THF-d_8, °C):
δ = 31.1 (s, C(CH_3)$_3$), 58.9 (s, C(CH_3)$_3$), 113.3 (C-4/5), 115.0 (C-3/6), 123.9 (C-3a/5a), 184.3 (q, $^1J_{CLi}$ = 22.7 Hz, C-1/8).

$^{13}C\{^1H\}$ NMR (125.76 MHz, THF-d_8):
δ = 31.3 (s, C(CH_3)$_3$), 58.9 (s, C(CH_3)$_3$), 113.2 (s, C-4/5), 114.2 (s, C-3/6), 124.4 (s, C-3a/5a), 185.7 (q, $^1J_{CLi}$ = 22.6 Hz, C-1/8).

$^7Li\{^1H\}$ NMR (194.37 MHz, THF-d_8, –80 °C):
δ = 3.16 (s).

In benzene-d_6, with LiHMDS:

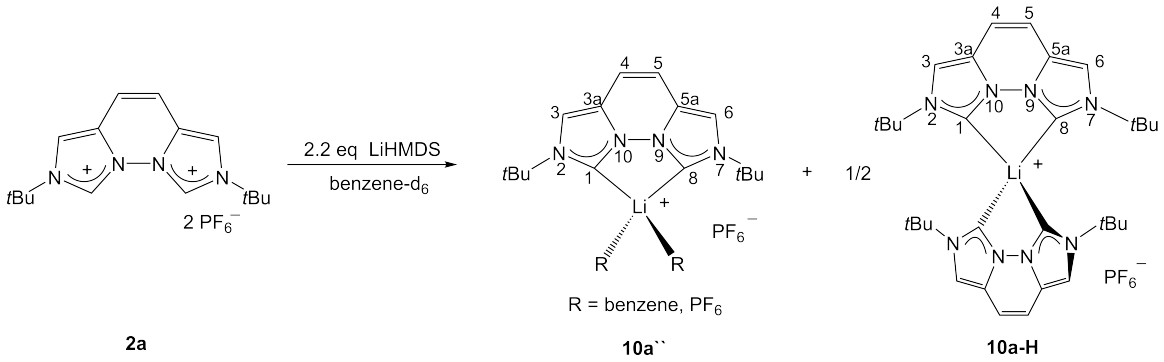

LiHMDS (3.9 mg, 23 μmol, 2.1 eq) was added to a suspension of **2a** (6.0 mg, 11 μmol, 1 eq) in 0.4 mL of benzene-d_6 and stirred for 20 min at room temperature. The ^{1}H NMR spectrum indicates deprotonation of **2a** by absence of the imidazolium peak and formation of the signal sets of **10a"** and **10a-H** (ratio 1:0.5).

10a-H:

^{1}H NMR (400.11 MHz, C_6D_6):

δ = 1.22 (s, 18H, $C(CH_3)_3$), 6.37 (s, 2H, H-4/5), 6.64 (s, 2H, H-3/6).

^{7}Li{^{1}H} NMR (194.37 MHz, C_6D_6): 2.92 (br s).

10a":

^{1}H NMR (400.11 MHz, C_6D_6):

δ = 1.36 (s, 18H, $C(CH_3)_3$), 6.06 (s, 2H, H-4/5), 6.34 (s, 2H, H-3/6).

^{7}Li{^{1}H} NMR (194.37 MHz, C_6D_6):

δ = 1.43 (br s).

In toluene-d_8, with LiHMDS:

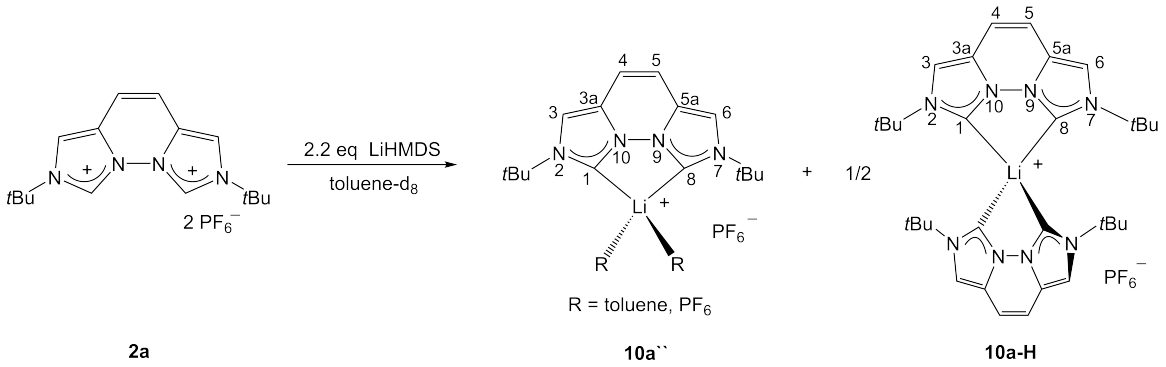

LiHMDS (3.9 mg, 23 μmol, 2.1 eq) was added to a suspension of **2a** (6.0 mg, 11 μmol, 1 eq) in 0.4 mL of toluene-d_8 and stirred for 20 min at room temperature. The ^{1}H NMR spectrum indicates deprotonation of **2a** by absence of the imidazolium peak and formation of the signal sets of two complexes **10a"** and **10a-H** in a ratio of 1:1.4.

10a-H:

^{1}H NMR (400.11 MHz, toluene-d_8):

δ = 1.23 (s, 18H, C(CH_3)$_3$), 6.38 (s, 2H, H-4/5), 6.66 (s, 2H, H-3/6).

^{7}Li{^{1}H} NMR (194.37 MHz, toluene-d_8):

δ = 2.94 (br s).

10a":

^{1}H NMR (400.11 MHz, toluene-d_8):

δ = 1.37 (s, 18H, C(CH_3)$_3$), 6.15 (s, 2H, H-4/5), 6.43 (s, 2H, H-3/6).

^{7}Li{^{1}H} NMR (194.37 MHz, toluene-d_8):

δ = 1.28 (br s).

In acetonitrile-d_3, with LiHMDS:

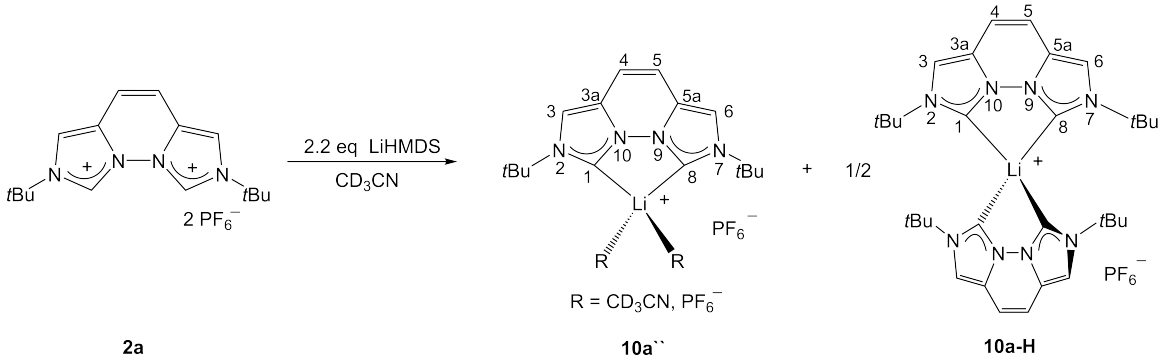

LiHMDS (7.1 mg, 43 μmol, 2.4 eq) was added to a suspension of **2a** (10 mg, 18 μmol, 1 eq) in 0.4 mL of CD_3CN and stirred for 20 min at room temperature. The ^{1}H NMR spectrum indicates the formation of two strongly superimposed signal sets for two Li-complexes **10a"** and **10a-H** (ratio 1:0.15).

^{1}H NMR (400.11 MHz, CD_3CN):
δ = 1.64 (s, 18H, $C(CH_3)_3$), 6.95/6.99 (s, 2H, H-4/5), 7.56 (s, 2H, H-3/6).

In THF-d_8, with methyllithium:

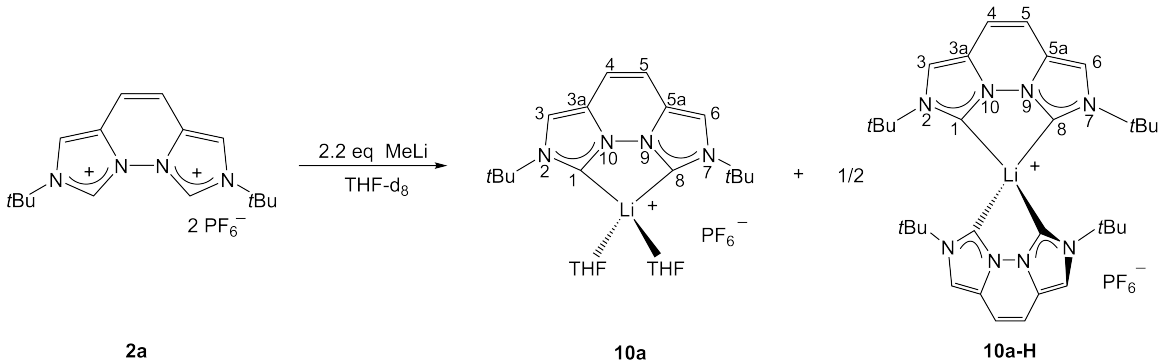

Solid methyllithium (1.1 mg, 50 μmol, 2.2 eq) was added at –30 °C to a suspension of **2a** (13 mg, 23 μmol, 1 eq) in 0.4 mL of THF-d_8. The ^{1}H NMR spectrum of the brown-red solution shows the signals of **10a** and **10a-H** (1:0.5).

In THF-d_8, with *n*-butyllithium:

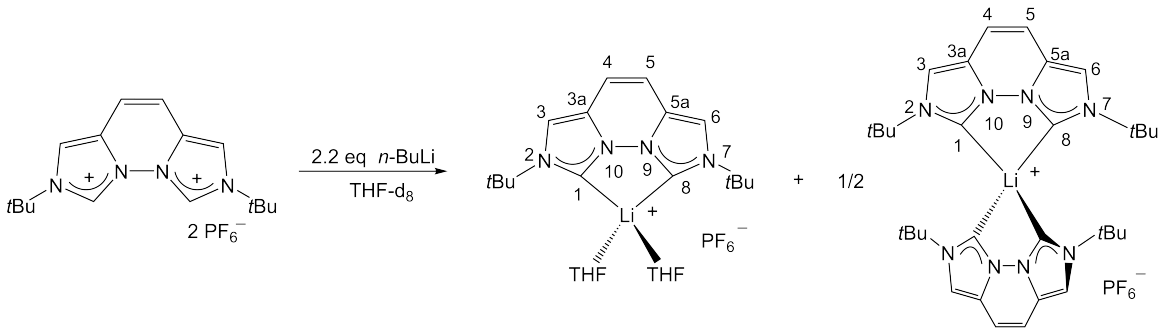

A hexane solution of *n*-butyllithium (2.5 M, 90 μL, 2.2 eq) was added to a stirred suspension of **2a** (62 mg, 0.1 mmol, 1 eq) in 3 mL of THF at -78 °C to give a dark red solution which was stirred for 30 min and another 30 min at room temperature. After drying *in vacuo*, a product mixture with $LiPF_6$ was obtained as a dark red solid. The ^{1}H NMR spectrum in THF-d_8 shows the product signals for **10a** and **10a-H** in a 1:0.5 ratio.

In C_6D_6, with methyllithium:

Solid methyllithium (1.0 mg, 41 μmol, 2.3 eq) was added to a suspension of **2a** (11 mg, 19 μmol, 1 eq) in 0.4 mL of C_6D_6. A beige suspension formed. No signals were obtained in the ^{1}H NMR spectrum. After one night the solid was precipitated and a ^{1}H NMR spectrum was measured again. The ^{1}H NMR spectrum shows the formation of one single symmetric species. Most likely a heteroleptic Li-vegi$^{t\mathrm{Bu}}$ complex with PF_6^- or solvent coordinating formed.

^{1}H NMR (400.11 MHz, C_6D_6):
δ = 1.30 (s, 18H, CH_3), 6.00 (s, 2H, H-4/5), 6.28 (s, 2H, H-3/6).

In toluene-d_8, with methyllithium:

Solid methyllithium (1.0 mg, 41 μmol, 2.3 eq) was added to a suspension of **2a** (11 mg, 19 μmol, 1 eq) in 0.4 mL of toluene-d_8. A beige suspension formed. After three days a ^{1}H NMR spectrum was measured (colorless solution and beige solid). The ^{1}H NMR spectrum shows the formation of one single symmetric species. Most likely a heteroleptic Li-vegi$^{t\mathrm{Bu}}$ complex with PF_6^- or solvent coordinating formed.

^{1}H NMR (400.11 MHz, toluene-d_8):
δ = 1.32 (s, 18H, $C(CH_3)_3$), 6.07 (s, 2H, H-4/5), 6.35 (s, 2H, H-3/6).

9.3.12 *In situ* generation of Li-vegi$^{n\mathrm{Pr}}$ complex 10b

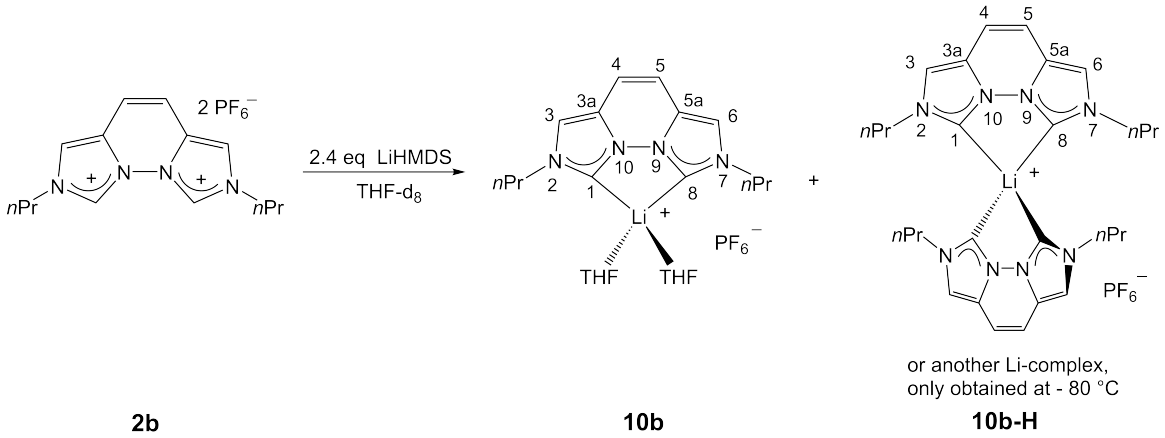

Was synthesized according to literature (with different base).[34]

In THF-d_8:
Lithium hexamethyldisilazide (7.9 mg, 47 μmol, 2.4 eq) was added to a suspension of **2b** (10 mg, 20 μmol, 1 eq) in 0.4 mL of THF-d_8. The ^{1}H, ^{13}C{^{1}H} and ^{7}Li{^{1}H} NMR spectra of the brown-red suspension confirms deprotonation of **2b** and formation of **10b** (at –80 °C signals for an additional Li-complex **10b-H** are obtained).

^{1}H NMR (400.11 MHz, THF-d_8):
δ = 0.95 (t, $^{3}J_{\mathrm{HH}}$ = 6.6 Hz, 6H, CH_3), 1.90-1.95 (m, 4H, CH_2), 4.19 (t, $^{3}J_{\mathrm{HH}}$) = 6.2 Hz, 4H, NCH_2), 7.03 (br s, 2H, H-4/5), 7.58 (br s, 2H, H-3/6).

^{7}Li{^{1}H} NMR (194.37 MHz, THF-d_8):
δ = 0.10 (br s).

^{1}H NMR (400.11 MHz, THF-d_8, –80 °C):
10b: δ = 0.93 (br s), 1.91 (br), 4.26 (br s), 7.19 (br s), 7.77 (br s).

10b-H: δ = 0.82 (br s), 1.83 (br s), 4.11 (br s), two signals superimposed by the peaks at 7.19 and 7.77.

$^{7}Li\{^{1}H\}$ NMR (194.37 MHz, THF-d_8, –80 °C):
δ = 2.42 (s, 10b-H), 1.47 (s, 10b), 0.16 (s, LiHMDS), –0.38 (s, $LiPF_6$).

In benzene-d_6

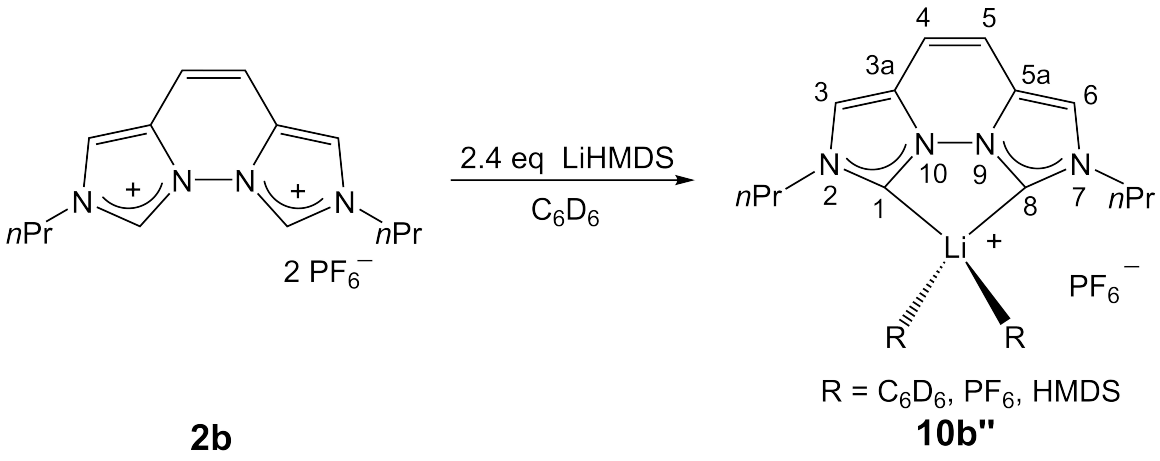

Lithium hexamethyldisilazide (7.5 mg, 43 μmol, 2.4 eq) was added to a suspension of **2b** (9.7 mg, 18 μmol, 1 eq) in 0.4 mL of benzene-d_6. The ^{1}H NMR spectrum of the brown solution indicates the deprotonation of **2b**.

^{1}H NMR (400.11 MHz, C_6D_6):
δ = 0.72 (t, $^{3}J_{HH}$ = 7.5 Hz, 6H, CH_3), 1.49-1.56 (m, 4H, CH_2), 3.98 (t, $^{3}J_{HH}$ = 7.1 Hz, 4H, NCH_2), 5.87 (s, 2H, H-4/5), 5.97 (s, 2H, H-3/6).

In toluene-d_8

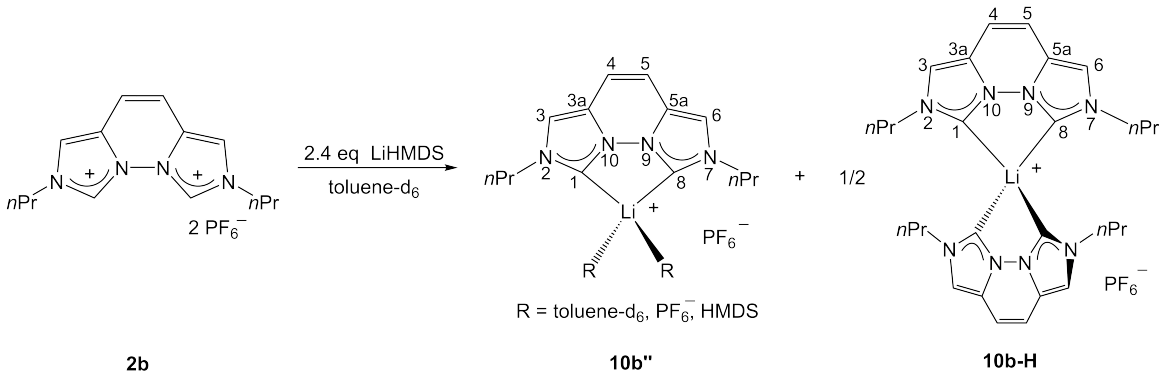

2b **10b''** **10b-H**

Lithium hexamethyldisilazide (4.0 mg, 24 μmol, 2.4 eq) was added to a suspension of **2b** (5.2 mg, 10 μmol, 1 eq) in 0.4 mL of toluene-d_8. The ^{1}H NMR spectrum of the brown solution confirms deprotonation of **2b** and the formation of two molecules A and B in a ratio of 1:3.

^{1}H NMR (400.11 MHz, toluene-d_8):
Molecule A: δ = 1.26 (br s, 6H, CH_3), 1.54-1.58 (m, 4H, CH_2), 3.99 (t, $^3J_{HH}$ = 7.2 Hz, 4H, NCH_2), 5.95 (s, 2H, H-4/5), 6.05 (s, 2H, H-3/6).

Molecule B: δ = 0.86-0.87 (m, 6H, CH_3), 1.34-1.36 (m, 4H, CH_2), 3.69-3.77 (m, 4H, NCH_2), 6.20 (br s, 4H, H-4/5 and H-3/6).

9.3.13 *In situ* generation of Na-vegi^{tBu}complex 11a

In THF-d_8:

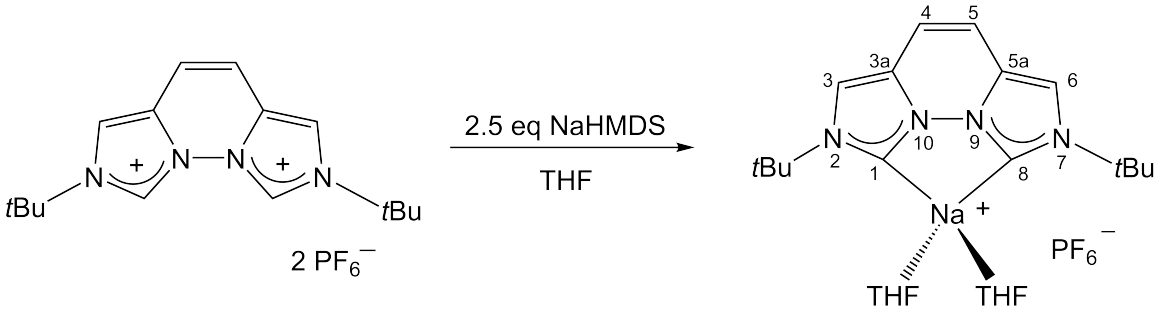

2a **11a**

Sodium hexamethyldisilazide (3.1 mg, 17 μmol, 2.5 eq) was added at –30 °Cto a stirred suspension of **2a** (3.9 mg, 6.9 μmol, 1 eq) in 0.4 mL THF-d_8 to give a light orange solution which was stirred for 15 min.

^{1}H NMR (400.11 MHz, THF-d_8):
δ = 1.64 (s, 18H, C(CH_3)$_3$), 6.92 (s, 2H, H-4/5), 7.65 (s, 2H, H-3/6).

^{13}C{^{1}H} NMR (100.61 MHz, THF-d_8):
δ = 31.4 (s, C(CH_3)$_3$), 58.7 (s, C(CH_3)$_3$), 112.7 (s, C-4/5), 113.6 (s, C-3/6), 125.0 (s, C-3a/5a), 189.3 (s, C-1/8).

^{23}Na NMR (132.29 MHz, THF-d_8):
δ = -2.39, 13.80.

In benzene-d_6:

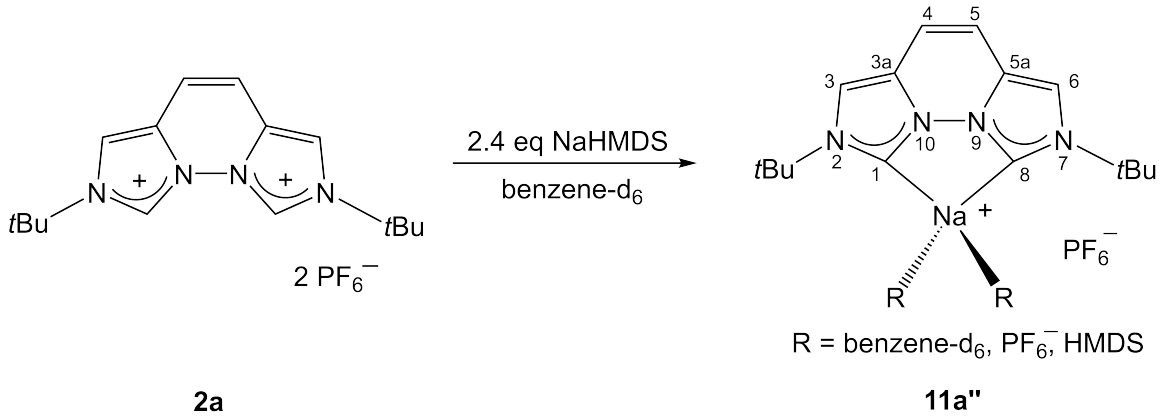

2a **11a"**

Sodium hexamethyldisilazide (3.4 mg, 19 μmol, 2.4 eq) was added to a stirred suspension **2b** (4.4 mg, 7.8 μmol, 1 eq) in 0.4 mL of benzene-d_6 to give a grey suspension which was stirred for 40 min. The ^{1}H NMR spectrum shows a signal set for a Na-complex **11b'**.

^{1}H NMR (400.11 MHz, C_6D_6):
δ = 1.35 (s, 18H, $C(CH_3)_3$), 6.08 (s, 2H, H-4/5), 6.39 (s, 2H, H-3/6).
No $^{13}C\{^1H\}$ NMR was measured due to the slowly precipitation of the product in benzene-d_6.

9.3.14 *In situ* generation of Na-vegi$^{n\mathrm{Pr}}$ complex 11b

In THF-d_8:

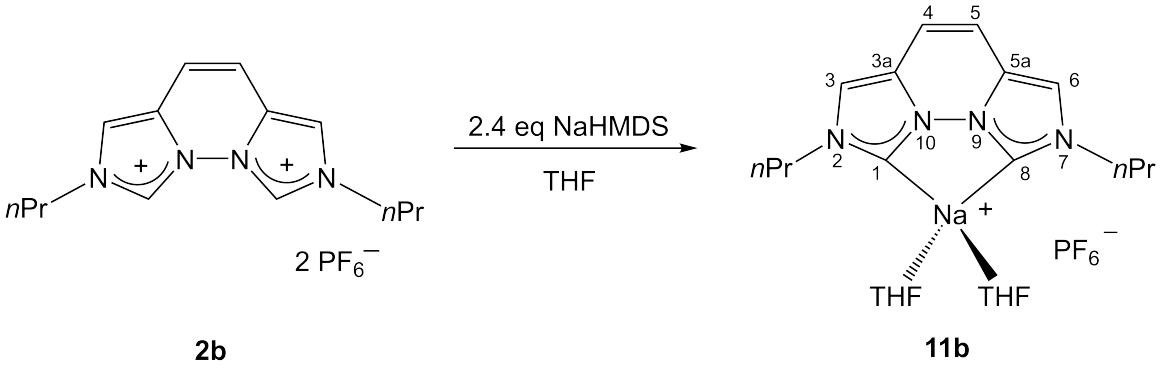

2b **11b**

Sodium hexamethyldisilazide (3.9 mg, 21 μmol, 2.4 eq) was added to a suspension of **2b** (4.7 mg, 8.8 μmol, 1 eq) in 0.4 mL of THF-d_8 and stirred for 15 min at room temperature. The ^{1}H NMR spectrum of the light brown suspension indicates formation of the Na-complex **11b**.

^{1}H NMR (400.13 MHz, THF-d_8):
δ = 0.93 (t, $^3J_{HH}$ = 7.4 Hz, 6H, CH_3), 1.88 (ps sxt, $^3J_{HH}$ = 7.2 Hz, 4H, CH_2), 4.17 (t, $^3J_{HH}$ = 7.2 Hz, 4H, NCH_2), 6.91 (s, 2H, H-4/5), 7.43 (s, 2H, H-3/6).

^{13}C{^{1}H} NMR (125.76 MHz, THF-d_8):
δ = 11.4 (s, CH_3), 24.8 (s, CH_2), 54.6 (s, NCH_2), 112.6 (s, C-4/5), 116.0 (s, C-3/6), 125.1 (s, C-3a/5a), 191.9 (s, C-1/8).

In benzene-d_6:

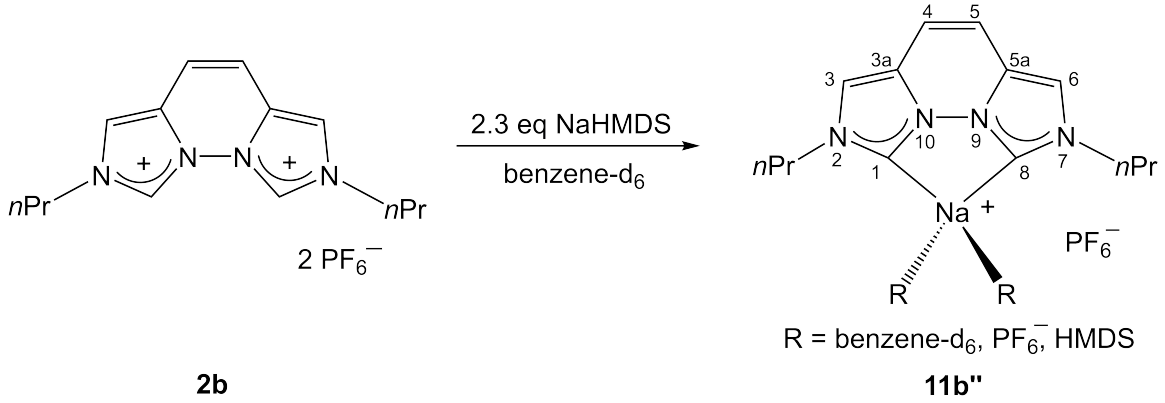

2b **11b"**

Sodium hexamethyldisilazide (3.9 mg, 21 μmol, 2.3 eq) was added to a suspension of **2b** (4.7 mg, 9 μmol, 1 eq) in 0.4 mL of benzene-d_6 and stirred for 15 min at room temperature. The ^{1}H NMR spectrum of the brown-red suspension indicates formation of **11b"**.

^{1}H NMR (400.13 MHz, C_6D_6):
δ = 0.80 (t, $^3J_{HH}$ = 7.4 Hz, 6H, CH3), 1.60 (ps sxt, $^3J_{HH}$ = 7.6 Hz, 4H, CH_2), 3.81 (t, $^3J_{HH}$ = 7.7 Hz, 4H, NCH_2), 5.97 (s, 2H, H-4/5), 6.04 (s, 2H, H-3/6).

No ^{13}C{^{1}H} NMR was measured due to the slowly precipitation of the product in benzene-d_6.
In toluene-d_8.

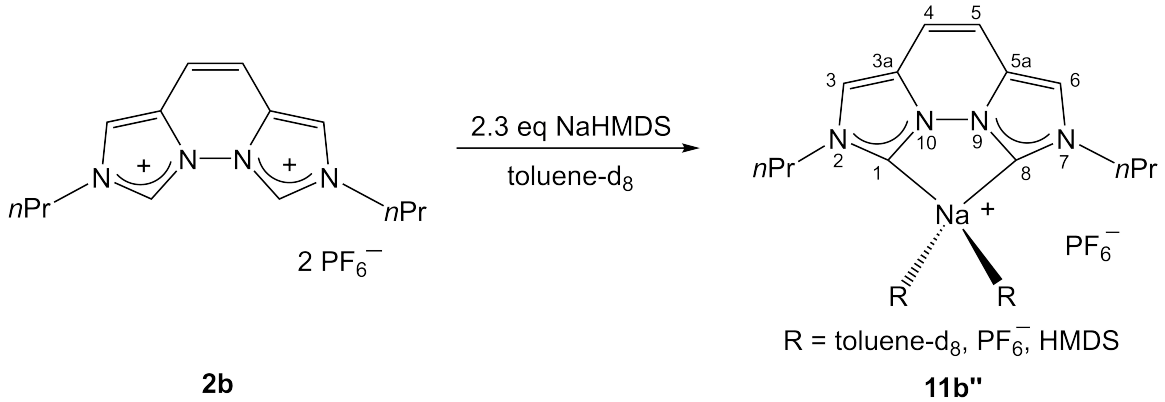

2b **11b"**

Sodium hexamethyldisilazide (3.6 mg, 6.7 μmol, 2.4 eq) was added to a suspension of **2b** (3.0 mg, 16 μmol, 1 eq) in 0.4 mL of toluene-d_8 and stirred for 15 min at room temperature. The signals in the ^{1}H NMR spectrum of the brown-red suspension indicate formation of the Na-complex **11b"**.

^{1}H NMR (400.13 MHz, toluene-d_8):

δ = 0.87 (t, $^3J_{HH}$ = 7.1 Hz, 6H, CH_3), 1.68-1.72 (m, 4H, CH_2), 3.93 (t, $^3J_{HH}$ = 7.4 Hz, 4H, NCH_2), 6.06 (s, 2H, H-4/5), 6.14 (s, 2H, H-3/6).

No $^{13}C\{^1H\}$ NMR was measured due to the slowly precipitation of the product in toluene-d_8.

9.3.15 *In situ* generation of K-vegi$^{t\mathrm{Bu}}$ complex 12a

In THF-d_8:

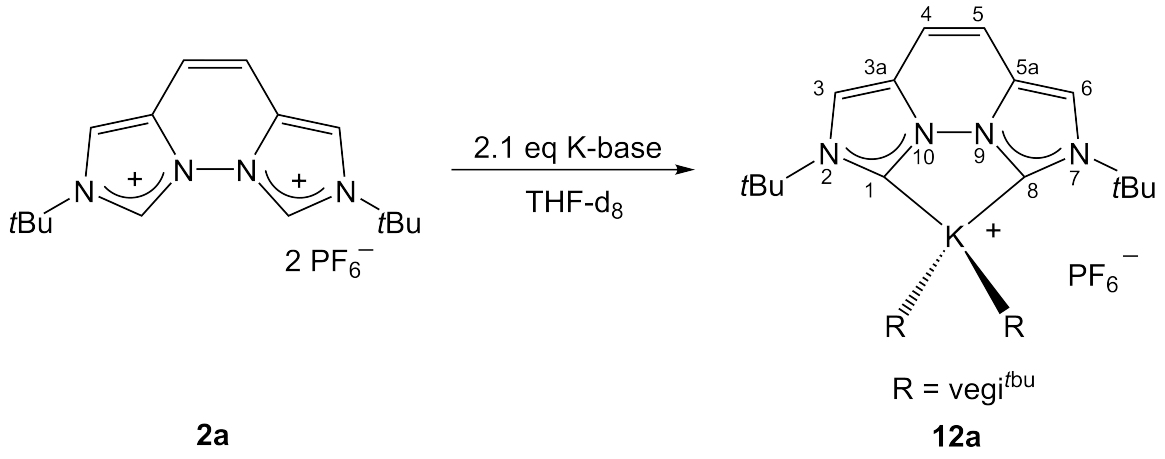

With KHMDS:

Potassium hexamethyldisilazide (27.3 mg, 137 μmol, 2.1 eq) was added at –30 °C to a stirred suspension of **2a** (37.5 mg, 66.7 μmol, 1 eq) in 2 mL of THF-d_8 to give a brown solution which was stirred for 30 min at –30 °C and at room temperature for 1.5 h. After drying *in vacuo*, the product **12a** was obtained as a light brown solid.

^{1}H NMR (400.11 MHz, THF-d_8):

δ = 1.65 (s, 18H, C(CH_3)$_3$), 6.85 (s, 2H, H-4/5), 7.57 (s, 2H, H-3/6).

^{1}H NMR (400.11 MHz, CD_3CN):

δ = 1.62 (s, 18H, C(CH_3)$_3$), 6.89 (s, 2H, H-4/5), 7.52 (s, 2H, H-3/6).

^{13}C{^{1}H} NMR (100.61 MHz, THF-d_8):

δ = 31.6 (s, C(CH_3)$_3$), 58.5 (s, C(CH_3)$_3$), 112.4 (s, C-4/5), 113.0 (s, C-3/6), 125.2 (s, C-3a/5a), 195.2 (s, C-1/8).

With K-benzyl:

K-benzyl (6.7 mg, 51 μmol, 2.1 eq) was added to a suspension of **2a** (14 mg, 25 μmol, 1 eq) in 0.4 mL of THF-d_8 to give a red solution which turns light brown. The ^{1}H NMR signals match those obtained from deprotonation with KHMDS in THF-d_8.

With KO*t*Bu:

KO*t*Bu (4.4 mg, 39 μmol, 2.2 eq) was added to a suspension of **2a** (10 mg, 18 μmol, 1 eq) in 0.4 mL of THF-d_8 to give a brown solution. The ^{1}H NMR signals match those obtained from deprotonation with KHMDS in THF-d_8.

In benzene-d_6:

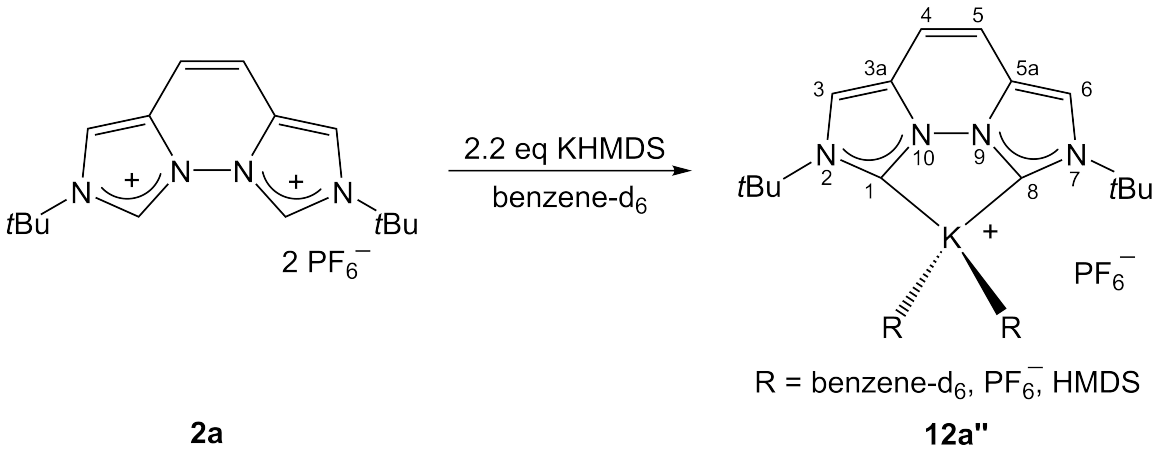

2a **12a"**

KHMDS (5.6 mg, 28 μmol, 2.2 eq) was added to a stirred suspension of **2a** (7.5 mg, 13 μmol, 1 eq) in 0.4 mL C_6D_6. The ^{1}H NMR spectrum of the beige suspension shows the signal set for the K-complex **12a"**.

^{1}H NMR (400.11 MHz, C_6D_6):

δ = 1.43 (s, 18H, $C(CH_3)_3$), 6.18 (s, 2H, H-4/5), 6.54 (s, 2H, H-3/6).

No $^{13}C\{^1H\}$ NMR was measured due to the slowly precipitation of the product in benzene-d_6.

In toluene-d_6:

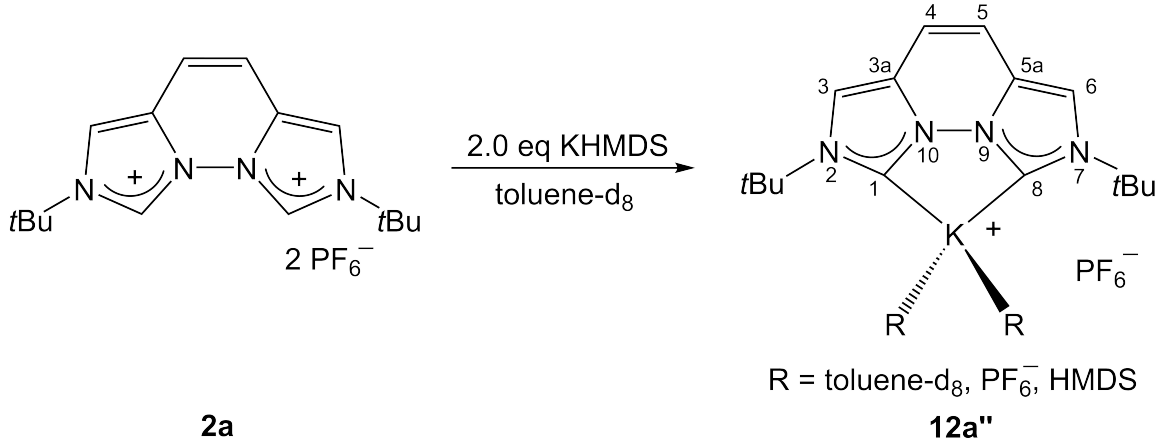

2a **12a"**

Potassium hexamethyldisilazide (3.6 mg, 18 μmol, 2.0 eq) was added to a stirred suspension of **2a** (5.0 mg, 8.9 μmol, 1 eq) in 0.4 mL toluene-d_8. The ^{1}H NMR spectrum of the light brown suspension shows the signal set for the K-complex **12a"**.

^{1}H NMR (400.11 MHz, toluene-d_6):
δ = 1.42 (s, 18H, C(CH_3)$_3$), 6.18 (s, 2H, H-4/5), 6.55 (s, 2H, H-3/6).

No ^{13}C{^{1}H} NMR was measured due to the slowly precipitation of the product in toluene-d_6.

Deprotonation of **2a** with KHMDS + 2.1 equiv of [18]-crown-6.

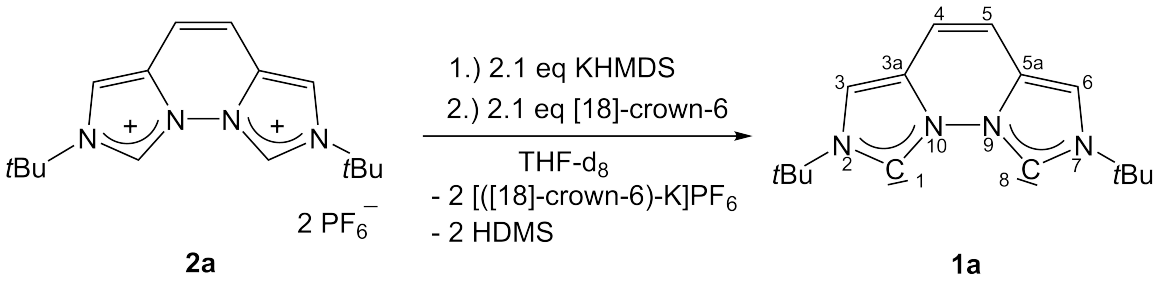

Potassium hexamethyldisilazide (7.6 mg, 38 μmol, 2.1 eq) was added to a suspension of **2a** (10.4 mg, 18.5 μmol, 1 eq) in 0.4 mL of THF-d_8. A ^{1}H NMR spectrum conrms formation of the K-complex **12a**. A solution of [18]-crown-6 in toluene (0.95 M, 40 μL, 38 μmol, 2.1 eq) was then added to the brown suspension. The formation of more solid is recognized and the ^{1}H and ^{13}C{^{1}H} NMR spectra show the peaks of dicarbene **1a**.

^{1}H NMR (400.11 MHz, THF-d_8):
δ = 1.65 (s, 18H, C(CH_3)$_3$), 6.75 (s, 2H, H-4/5), 7.42 (s, 2H, H-3/6).

^{13}C{^{1}H} NMR (125.76 MHz, THF-d_8):
δ = 31.7 (s, CH_3)$_3$), 57.5 (s, C(CH_3)$_3$), 112.0 (s, C-4/5 and C-3/6), 125.2 (s, C-3a/5a), 202.9 (s, C-1/8).

9.3.16 *In situ* generation of K-vegi$^{n\mathrm{Pr}}$ complex 12b

In THF-d_8:

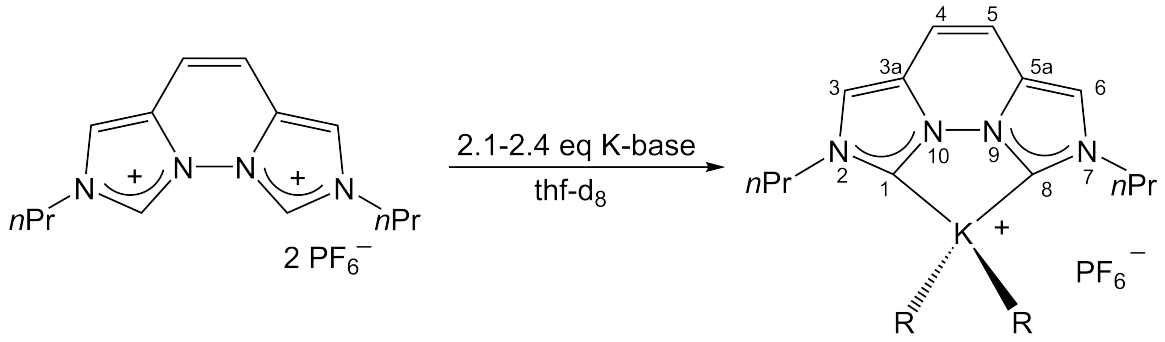

2b **12b** (R = vegi$^{n\mathrm{Pr}}$)

With KHMDS:

KHMDS (3.6 mg, 6.7 μmol, 2.4 eq) was added to a suspension of **2b** (3.0 mg, 16 μmol, 1 eq) in 0.4 mL THF-d_8 at –78 °C. The reaction mixture was stirred for 15 min, warmed up to room temperature within 30 min and stirred for 1 h.

^{1}H NMR (400.13 MHz, THF-d_8):

δ = 0.95 (br s, 6H, CH_3), 1.89 (ps sxt, $^3J_{HH}$ = 7.3 Hz, 4H, CH_2), 4.16 (br s, 4H, NCH_2), 6.86 (s, 2H, H-4/5), 7.37 (s, 2H, H-3/6).

^{13}C{^{1}H} NMR (125.76 MHz, THF-d_8):

δ = 11.4 (s, CH_3), 26.0 (s, CH_2), 54.6 (s, NCH_2), 112.5 (s, C-4/5), 115.5 (s, C-3/6), 125.4 (s, C3a/5a), 196.3 (s, C-1/8).

With KO*t*Bu:

KO*t*Bu (4.2 mg, 37 μmol, 2.2 eq) was added to a suspension of **2b** (9.0 mg, 17 μmol, 1 eq) in 0.4 mL of THF-d_8 to give a brown solution. The ^{1}H NMR signals match with the received signals with KHMDS as a base in THF-d_8.

With K-benzyl:

K-benzyl (4.0 mg, 31 μmol, 2.1 eq) was added to a suspension of **2b** (7.8 mg, 15 μmol, 1 eq) in 0.4 mL of THF-d_8 to give a dark brown suspension. The ^{1}H NMR signals match with the received signals with KHMDS as a base in THF-d_8.

In benzene-$_6$.

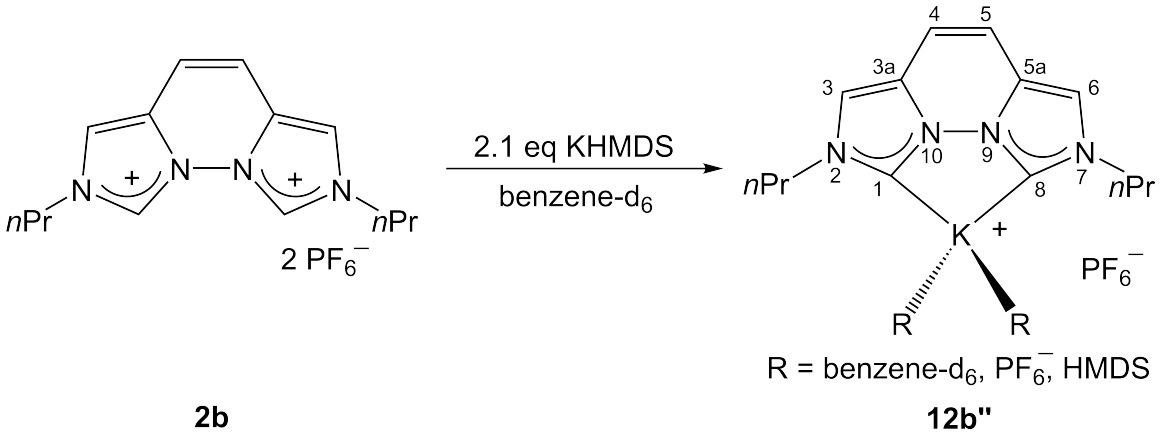

2b **12b"**

Potassium hexamethyldisizalide8.0 mg, 40 μmol, 2.1 eq) was added to a suspension of **2b** (10.4 mg, 19 μmol, 1 eq) in 0.4 mL benzene-d_6 and stirred for 15 min at room temperature. The ^{1}H NMR spectrum of the brown-red suspension shows the signals of complex **12b"**.

^{1}H NMR (400.13 MHz, C_6D_6):

δ = 0.82 (t, $^3J_{HH}$ = 7.4 Hz, 6H, CH_3), 1.63 (ps sxt, $^3J_{HH}$ = 7.9 Hz, 4H, CH_2), 3.90 (t, $^3J_{HH}$ = 8.0 Hz, 4H, NCH_2), 6.02 (s, 2H, H-4/5), 6.10 (s, 2H, H-3/6).

No $^{13}C\{^1H\}$ NMR was measured due to the slowly precipitation of the product in benzene-d_6.

Deprotonation of **2a** with KHMDS + 2.1 eq of [18]-crown-6.

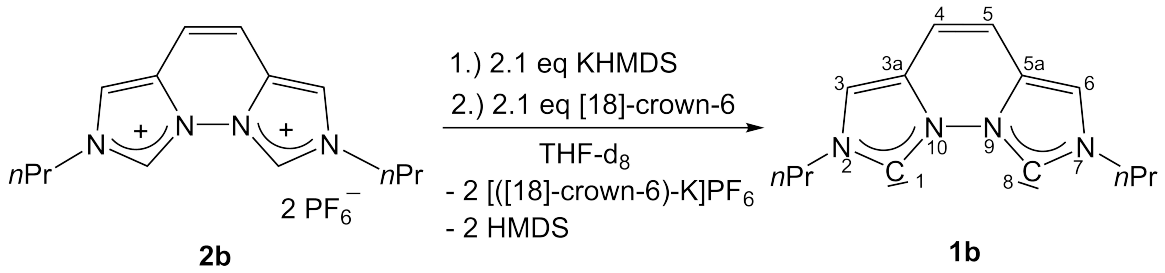

In THF-d_8.

Potassium hexamethyldisilazide (17.3 mg, 86.7 mol) was added to a suspension of **2b** (22.1 mg, 41.4 mol) in 0.4 mL of THF-d_8. A ^{1}H NMR spectrum conrmed formation of the K-complex **12a**. A solution of [18]-crown-6 in toluene (0.95 M, 93 L, 87.0 mol, 2.1 eq) was then added to the brown-red solution. The ^{1}H and ^{13}C{^{1}H} NMR spectrum showed the signals of the dicarbene **1b**.

^{1}H NMR (400.11 MHz, THF-d_8):

δ = 0.95 (br s, 6H, CH_3), 1.90 (br s, 4H, CH_2), 4.10 (br s, NCH_2), 6.75 (s, 2H, H-4/5), 7.24 (s, 2H, H-3/6).

^{13}C{^{1}H} NMR (125.76 MHz, THF-d_8):

δ = 11.7 (CH_3), 26.0 (CH_2), 54.7 (NCH_2), 112.2 (C-4/5), 115.2 (C-3/6), 125.5 (C3a/5a), 202.1 (C-1/8).

9.3.17 CsHMDS[89]

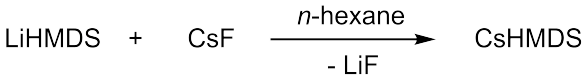

Lithium hexamethyldisilazide (550 mg, 3.28 mmol, 1 eq) and CsF (449 mg, 3.28 mmol, 1 eq) were suspended in *n*-hexane (20 mL). The mixture was refluxed for 16 h. The white suspension was cooled to ambient temperature, the solvent removed under a vacuum, and toluene (15 mL) was added. The reaction was filtered and the solid washed with toluene (2 x 1 mL). The solvent of the colorless solution was removed under a vacuum and the resultant white powder was sublimated at 200 °C ($3 \cdot 10^{-4}$ bar, -80 °C). The product is obtained as a off-white solid (60%, 0.57 g).

^{1}H NMR (400.13 MHz, C_6D_6):
$\delta = 0.21$ (s, CH_3)

$^{13}C\{^{1}H\}$ NMR (100.61 MHz, C_6D_6):
$\delta = 7.6$ (s, CH_3) .
(Values match with the literature known data.)

9.3.18 *In situ* generation of Cs-vegi$^{t\mathrm{Bu}}$ 14a

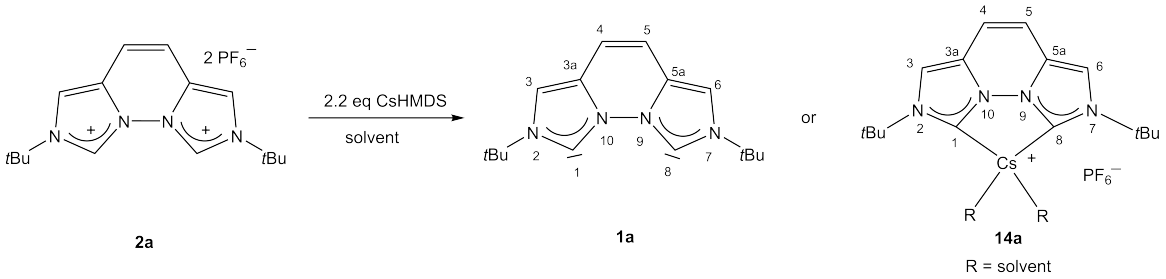

2a **1a** **14a**

In THF-d_8:

Cesium hexamethyldisilazide (17.2 mg, 58.6 μmol, 2.2 eq) was added to a suspension of **2a** (15.0 mg, 26.7 μmol, 1 eq) in THF-d_8. The color turns light brown. The ^{1}H NMR was measured after 20 min and shows the signals for a symmetric compound.

^{1}H NMR (400.13 MHz, THF-d_8):

δ = 1.57 (s, 18H, C(CH_3)$_3$), 6.80 (s, 2H, H-4/5,), 7.48 (s, 2H, H-3/6).

^{13}C{^{1}H} NMR (100.61 MHz, THF-d_8):

δ = 31.7 (s, C(CH_3)$_3$), 58.2 (s, C(CH_3)$_3$), 112.2 (s, C-4/5), 112.3 (s, C-3/6), 125.3 (s, C-3a/5a), 201.7 (s, C-1/8).

^{19}F{^{1}H} NMR (376.48 MHz, THF-d_8)

δ = -72.5 (d, $^1J_{\mathrm{PF}}$ = 710 Hz, PF_6^-).

^{31}P{^{1}H} NMR (161.97 MHz, THF-d_8)

δ = -144.1 (sept, $^1J_{\mathrm{PF}}$ = 710 Hz, PF_6^-).

In benzene-d_6:

Cesium hexamethyldisilazide (11.5 mg, 39.2 μmol, 2.2 eq) was added to a suspension of **2a** (10.0 mg, 17.8 μmol, 1 eq) in benzene-d_6. The color turns light brown and a brown solid forms. The ^{1}H NMR was measured after 20 min and shows the signals for a symmetric compound.

^{1}H NMR (400.13 MHz, benzene-d_6):

δ = 1.45 (s, 18H, C(CH_3)$_3$), 6.25 (s, 2H, H-4/5), 6.61 (s, 2H, H-3/6).

In toluene-d_8:

CsHMDS (11.5 mg, 39.2μmol, 2.2 eq) was added to a suspension of **2a** (10.0 mg, 17.8 μmol, 1 eq) in toluene-d_8. The color turns light brown and a brown solid forms. The ^{1}H NMR was measured after 20 min and shows the signals for a symmetric compound.

^{1}H NMR (400.13 MHz, toluene-d_8):

δ = 1.44 (s, 18H, C(CH_3)$_3$), 6.23(s, 2H, H-4/5), 6.61 (s, 2H, H-3/6).

9.3.19 *In situ* generation of Cs-vegi$^{n\mathrm{Pr}}$ 14b

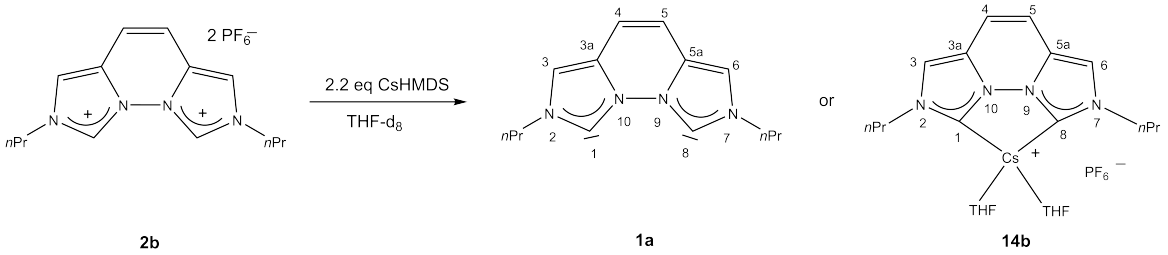

2b **1a** **14b**

CsHMDS (18.1 mg, 61.7 μmol, 2.2 eq) was added to a suspension of **1b** (15.0 mg, 28.1 μmol, 1 eq) in THF-d_8. The color turns dark brown. The ^{1}H NMR was measured after 20 min and shows the signals for a symmetric compound.

^{1}H NMR (400.11 MHz, THF-d_8):
δ = 0.89 (t, $^3J_{\mathrm{HH}}$ = 7.48 Hz, 6H, CH_3) 1.84 (q, $^3J_{\mathrm{HH}}$ = 7.2 Hz, 4H, CH_2), 4.08 (br s, 4H, NCH_2), 6.80 (s, 2H, H-4/5), 7.20 (s, 2H, H-3/6).

^{13}C{^{1}H} NMR (100.61 MHz, THF-d_8):
δ = 11.6 (s, CH_3), 25.3 (s, CH_2, under THF-signal), 54.7 (s, NCH_2), 112.2 (s, C-4/5), 114.9 (s, C-3/6), 125.6 (s, C-3a/5a), 202.8 (s, C-1/8).

9.3.20 Generation of the free dicarbene 1a

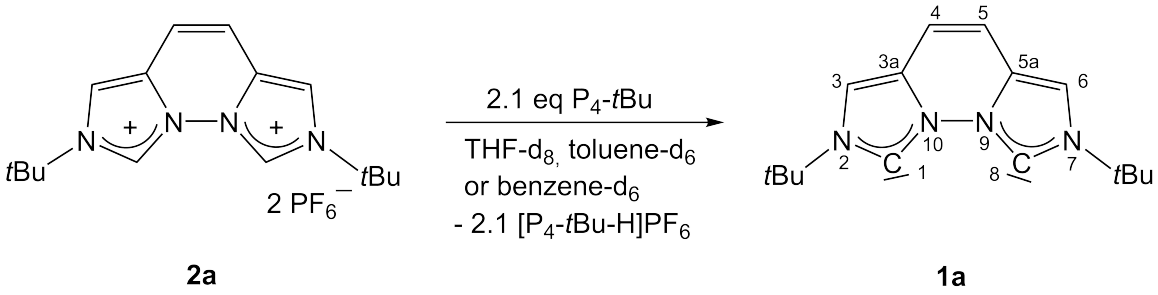

In THF-d_8:

P_4-*t*Bu (29.8 mg, 47.0 μmol, 2.1 eq) was added to a suspension of **2a** (12.6 mg, 22.4 μmol, 1 eq) in 0.4 mL of THF-d_8 and the reaction mixture turns immediately into a light brown solution of **1a**.

^{1}H NMR (400.11 MHz, THF-d_8):

δ = 1.64 (s, 18H, $C(CH_3)_3$), 6.77 (s, 2H, H-4/5), 7.47 (s, 2H, H-3/6).

$^{13}C\{^1H\}$ NMR (125.76 MHz, THF-d_8):

δ = 31.7 (s, $C(CH_3)_3$), 58.0 (s, $C(CH_3)_3$), 112.1 (s, C-4/5 and C-3/6), 125.3 (s, C-3a/5a), 202.6 (s, C-1/8).

In benzene-d_6:

P_4-*t*Bu (21 mg, 33 μmol, 2.4 eq) was added to a suspension of **2a** (7.8 mg, 14 μmol, 1 eq) in 0.4 mL of C_6D_6 and a dark brown solution of **1a** containing brown oily droplets forms which is stable for 3 days at room temperature.

^{1}H NMR (400.11 MHz, C_6D_6):

δ = 1.49 (s, 18H, $C(CH_3)_3$), 6.33 (s, 2H, H-4/5), 6.71 (s, 2H, H-3/6).

In toluene-d_8:

P_4-*t*Bu (12 mg, 19 μmol, 2.2 eq) was added to a suspension of **1a** (4.8 mg, 8.5 μmol, 1 eq) in 0.4 mL of toluene-d_8 and a colorless solution of 5b forms.

^{1}H NMR (400.13 MHz, toluene-d_8):

δ = 1.48 (s, 18H, $C(CH_3)_3$), 6.31 (s, 2H, H-4/5), 6.71 (s, 2H, H-3/6).

9.3.21 Generation of the free dicarbene(1b)

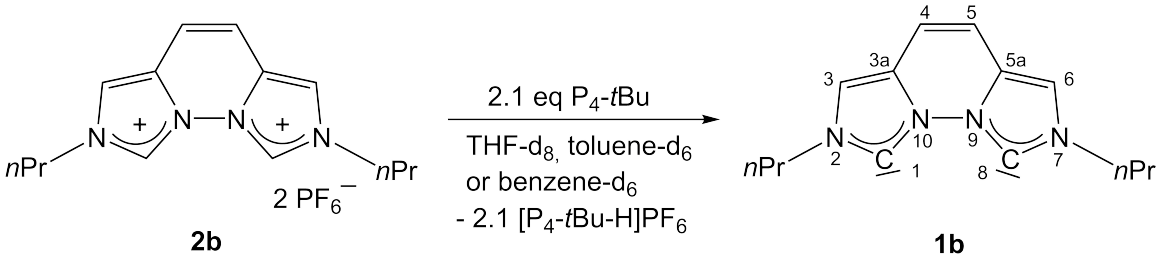

In THF-d_8:

P_4-*t*Bu (30.3 mg, 47.8 μmol, 2.1 eq) was added to a suspension of **2b** (12.8 mg, 22.8 μmol, 1 eq) in 0.4 mL of THF-d_8. The suspension turns dark brown immediately. The ^{1}H NMR shows full conversion of the imidazolium salt **2b** into the dicarbene **1b** and the signals of the protonated P_4-*t*Bu base.

^{1}H NMR (400.11 MHz, THF-d_8):

δ = 0.94 (t, $^3J_{HH}$ = 7.4 Hz, 6H, CH_3), 1.90 (ps sxt, $^3J_{HH}$ = 7.1 Hz, 4H, CH_2), 4.10 (t, $^3J_{HH}$ = 7.1 Hz, 4H, NCH_2), 6.79 (s, 2H, H-4/5), 7.33 (s, 2H, H-3/6).

^{13}C{^{1}H} NMR (125.76 MHz, THF-d_8):

δ = 11.7 (s, CH_3), 54.7 (s, NCH_2), 112.1 (s, C-4/5), 114.8 (s, C-3/6), 125.7 (s, C3a/5a), 204.5 (s, C-1/8). The signal for methylene carbon (CH_2) is covered by the THF-d_8 signal at 25 ppm. The carbene signal at 204.5 ppm was detected via a ^{1}H,^{13}C HMBC NMR experiment.

^{1}H NMR (400.11 MHz, THF-d_8, –80 °C):

δ = 0.92 (br s, 6H, CH_3), 1.86 (br s, 4H, CH_2), 4.16 (br s, 4H, NCH_2), 6.97 (br s, 2H, H-4/5), 7.23 (br s, 2H, H-3/6).

^{13}C{^{1}H} NMR (125.76 MHz, THF-d_8, –80 °C):

δ = 11.9 (s, CH_3), 54.3 (s, NCH_2), 112.3 (s, C-4/5), 115.6 (s, C-3/6), 125.5 (s, C-3a/5a), 202.3 (s, C-1/8). The signal for methylene carbon (CH2) is covered by the THF-d_8

signal at 25 ppm.

In benzene-d_6:
P_4-*t*Bu (15 mg, 23 μmol, 2.1 eq) was added to a suspension of **2b** (5.8 mg, 11 μmol, 1 eq) in 0.4 mL of C_6D_6 and a dark brown solution of **1b** containing brown oily droplets forms.

^{1}H NMR (400.11 MHz, C_6D_6):
δ = 0.71 (t, $^3J_{HH}$ = 7.4 Hz, 6H, CH_3), 1.64 (m, 4H, CH_2), 3.83 (t, $^3J_{HH}$ = 7.1 Hz, 4H, NCH_2), 6.25 (s, 2H, H-4/5), 6.36 (s, 2H, H-3/6).

In toluene-d_8:
P_4-*t*Bu (25 mg, 40 μmol, 2.2 eq) was added to a suspension of **2b** (9.7 mg, 18 μmol, 1 eq) in 0.4 mL of toluene-d_8 and a dark brown oil forms. The ^{1}H NMR spectrum confirms full conversion of the imidazolium salt (**2b**) into the dicarbene **1b**.

^{1}H NMR (400.13 MHz, toluene-d_8):
δ = 0.74 (t, $^3J_{HH}$ = 9.1 Hz, 6H, CH_3), 1.67 (m, 4H, CH_2), 3.81 (t, $^3J_{HH}$ = 7.2 Hz, 4H, NCH_2), 6.25(s, 2H, H-4/5), 6.37 (s, 2H, H-3/6).

9.3.22 Generation of the monocarbene 15b

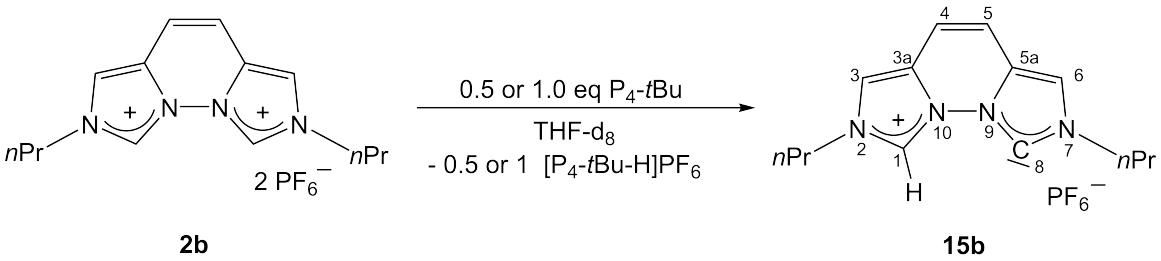

2b **15b**

In THF-d_8 with 0.5 eq of base:

P_4-*t*Bu (2.0 mg, 3.2 μmol, 0.5 eq) was added to a suspension of **2b** (3.7 mg, 6.9 μmol, 1 eq) in 0.4 mL of THF-d_8. The ^{1}H NMR spectrum of the orange mixture shows the formation of two species, the monocarbene **15b** and one (possibly decomposition) byproduct.

^{1}H NMR (400.11 MHz, THF-d_8):

δ = 1.04 (t, $^3J_{HH}$ = 7.5 Hz, 6H, CH_3), 2.06 (ps sxt, $^3J_{HH}$ = 7.1 Hz, 4H, CH_2), 4.49 (t, $^3J_{HH}$ = 7.1 Hz, 4H, NCH_2), 7.57 (s, 2H, H-4/5), 8.21 (s, 2H, H-3/6), 10.67 (s, 1H, H-1 or H-8).

In THF-d_8 with 1 eq of base:

P_4-*t*Bu (5.2 mg, 8.2 μmol, 1 eq) was added to a suspension of **2b** (4.4 mg, 8.2 μmol, 1 eq) in 0.4 mL of THF-d_8. The ^{1}H NMR spectrum of the brown solution shows the formation of monocarbene (**15b**) and one unknown side product.

^{1}H NMR (400.11 MHz, THF-d_8):

δ = 0.91 (s, 6H, CH_3), 1.02 (s, 4H, CH_2), 4.49 (s, 4H, NCH_2), 7.59 (s, 2H, H-4/5), 8.19 (s, 2H, H-3/6).

Side product:

δ = 0.91 (s, 6H, CH_3), 1.02 (s, 4H, CH_2), 4.49 (s, 4H, NCH_2), 6.30 (s, 2H, H-4/5), 7.37 (s, 2H, H-3/6). All peaks are very broad.

9.3.23 Generation of the monocarbene 15a

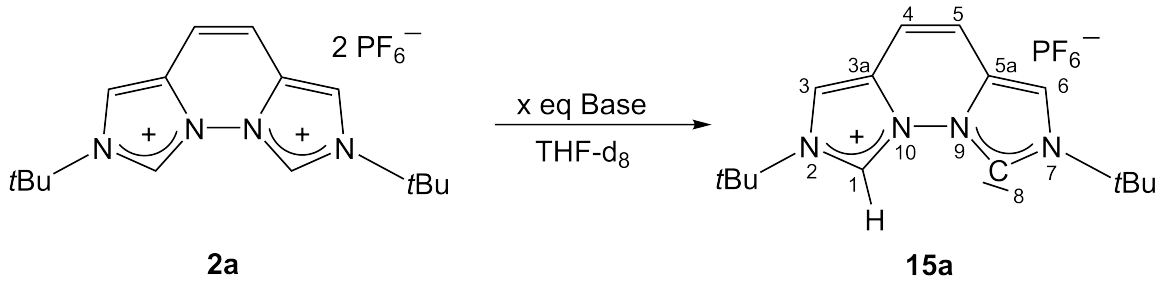

With P_4-*t*Bu:

In THF-d_8 with 0.4 eq of base:

P_4-*t*Bu (4.1 mg, 6.5 μmol, 0.4 eq) was added to a suspen-sion of **2a** (90 mg, 16 μmol, 1 eq) in 0.4 mL of THF-d_8. The ^{1}H NMR spectrum of the beige suspension shows the formation of two species. One main species, the monocarbene **15a** and one byproduct, a decomposed species.

^{1}H NMR (400.11 MHz, THF-d_8): Monocarbene:

δ = 1.76 (s, 18H, $C(CH_3)_3$), 7.18 (s, 2H, H-4/5), 8.17 (s, 2H, H-3/6), 10.02 (s, 1H, H-1 or H-8).

In THF-d_8 with 1.0 eq of base:

P_4-*t*Bu (11.7 mg, 18.0 μmol, 1.0 eq) was added to a suspension of **2a** (10.4 mg, 18 μmol, 1.0 eq) in 0.4 mL of THF-d_8. The ^{1}H NMR spectrum of the light pink solution shows the formation of the monocarbene **15a**. The solution is stable over several days. At room temperature, a fast exchange of the imidazolium proton leads to a symmetric species.

^{1}H NMR (400.11 MHz, THF-d_8):

δ = 1.75 (s, 18H, $C(CH_3)_3$), 7.31 (s, 2H, H-4/5), 8.17 (s, 2H, H-3/6), 10.08 (s, 1H, H-1 or H-8).

^{1}H NMR (400.11 MHz, THF-d_8, –80 °C):
δ = 1.75 (br s, 18H, C(CH_3)$_3$), 7.22 (s, 1H, H-4 or H-5), 7.48 (s, 1H, H-4 or H-5), 8.14 (s, 1H, H-3 or H-6), 8.36 (s, 1H, H-3 or H-6), 10.34 (br s, 1H, H-1 or H-8).

^{13}C{^{1}H} NMR (125.76 MHz, THF-d_8, –80 °C):
δ = 29.6 (s, C(CH_3)$_3$), 31.2 (s, C(CH_3)$_3$), 59.5 (s, C(CH_3)$_3$), 62.4 (s, C(CH_3)$_3$), 111.1, 115.8, 117.4, 123.9, 125.7, 127.4, 197.7 (C-1/8).
The chemical shifts cannot all be assigned.

In THF-d8 with 1.5 eq of base:
P_4-*t*Bu (16 mg, 26 μmol, 1.5 eq) was added to a suspension of **2a** (9.7 mg, 17 μmol) in 0.4 mL of THF-d8. The ^{1}H NMR spectrum of the brown solution shows the formation of the monocarbene **15a**. The solution is stable over the weekend at room temperature. Only one signal set is observed, whose peaks lie in between those of monocarbene **15a** and dicarbene **1a**.

^{1}H NMR (400.11 MHz, THF-d8):
δ = 1.70 (s, 18H, C(CH_3)$_3$), 7.15 (s, 2H, H-4/5), 8.04 (s, 2H, H-3/6), 10.27 (s, 1H, H-1 or H-8).

With DBU:

In THF-d_8 with 2.1 eq DBU:

DBU (4.8 mg, 32 μmol, 2.1 eq) was added to a suspension of **2a** (8.5 mg, 15 μmol) in THF-d8 to give a beige solution. The ^{1}HNMR spectrum shows the formation of monocarbene **15a**.

^{1}H NMR (400.11 MHz, THF-d_8):

δ = 1.75 (s, 18H, C(CH_3)$_3$), 7.30 (s, 2H, H-4/5), 8.15 (s, 2H, H-3/6), 10.50 (s, 2H, H-1/8).

In THF-d_8 with 4.8 eq DBU

DBU (6.9 mg, 45 μmol, 4.8 eq) was added to a THF-d_8 suspension of **2a** (5.3 mg, 9.4 μmol, 1 eq) to give a beige solution.

The ^{1}H NMR spectrum shows only the formation of the monocarbene **15a**.

^{1}H NMR (400.11 MHz, THF-d_8):

δ = 1.75 (s, 18H, C(CH_3)$_3$), 7.30 (s, 2H, H-4/5), 8.14 (s, 2H, H-3/6), 10.79 (br s, 2H, H-1/8).

In benzene-d_6 with 2.2 eq DBU:

DBU (6.80 μL, 44.6 μmol, 2.2 eq) was added to a suspension of **2a** (11.4 mg, 20.3 μmol) in THF-d_8 to give a beige solution and a dark oil forms. The ^{1}H NMR spectrum shows the formation of monocarbene **15a**.

^{1}H NMR (400.11 MHz, THF-d_8):

δ = 1.54 (s, 18H, C(CH_3)$_3$), 7.27 (s, 2H, H-4/5), 7.82 (s, 2H, H-3/6).

In THF-d_8 with 4.2 eq DBU:

DBU (11.2 μL, 74.69 μmol, 4.2 eq) was added to a suspension of **2a** (10 mg, 17.78 μmol, 1 eq) in THF-d8 to give a beige solution. The ^{1}H NMR spectrum shows the formation of monocarbene **15a**.

^{1}H NMR (400.11 MHz, THF-d_8):
1.75 (s, 18H, C(CH_3)$_3$), 7.30 (s, 2H, H-4/5), 8.15 (s, 2H, H-3/6), 10.50 (s, 2H, H-1/8).

In THF-d_8 with 4.8 eq DBU:
DBU (6.9 mg, 45 μmol, 4.8 eq) was added to a THF suspension of **2a** (5.3 mg, 9.4 μmol, 1 eq) to give a beige solution.
The ^{1}H NMR spectrum shows only the formation of the monocarbene **15a**.

^{1}H NMR (400.11 MHz, THF-d_8):
δ = 1.75 (s, 18H, C(CH_3)$_3$), 7.29 (s, 2H, H-4/5), 8.14 (s, 2H, H-3/6), 11.06 (br s, 2H, H-1/8).

With P_1-*t*Bu:
In THF-d_8 with 2.2 eq P_1-*t*Bu:
P_1-*t*Bu (12 μL, 39 μmol, 2.2 eq) was added to a suspension of **2a** (10 mg, 18 μmol, 1 eq) in THF-d_8 to give a light brown solution. The ^{1}H NMR spectrum shows the formation of monocarbene **15a**.
^{1}H NMR (400.11 MHz, THF-d_8):
δ = 1.75 (s, 18H, C($_3$)$_3$), 1.78 (s, 18H, C(CH_3)$_3$), 7.28 (s, 2H, H-4/5), 8.12 (s, 2H, H-3/6), 9.96 (br s, 1H, H-1/8).

In THF-d_8 with 4.4 eq P_1-*t*Bu:
P_1-*t*Bu (24 μL, 78.24 μmol, 4.4 eq) was added to a suspension of **2a** (10.0 mg, 17.78 μmol, 1 eq) in THF-d8 to give a light brown solution. The ^{1}H NMR spectrum shows the formation of monocarbene **15a**.

^{1}H NMR (400.11 MHz, THF-d_8):
δ = 1.75 (s, 18H, C(CH_3)$_3$), 1.77 (s, 18H, C(CH_3)$_3$), 7.28 (s, 2H, H-4/5), 8.13 (s, 2H, H-3/6), 9.99 (br s, 1H, H-1/8).

In THF-d_8 with Verkades base:

Triisobutylphosphatrane (11 mg, 31 μmol, 2.2 eq) was added to a suspension of **2a** (8.0 mg, 14 μmol, 1 eq) in THF-d_8 to give a beige solution. The ^{1}H NMR spectrum shows the formation of monocarbene **15a**.

^{1}H NMR (400.11 MHz, THF-d_8):

δ = 1.72 (s, 18H, C(CH_3)$_3$), 7.24 (s, 2H, H-4/5), 8.10 (s, 2H, H-3/6), 10.13 (br s, 1H, H-1/8).

In THF-d_8 with 1.1 eq. LiHMDS:
LiHMDS (3.9 mg, 23 μmol, 1.1 eq) was added to a suspension of **2a** (12 mg, 21 μmol, 1 eq) in THF-d8 to give a beige solution. The ^{1}H NMR spectrum shows the formation of monocarbene **15a**.

^{1}H NMR (400.11 MHz, THF-d8):
δ = 1.74 (s, 18H, C(CH_3)$_3$), 7.27 (s, 2H, H-4/5), 8.11 (s, 2H, H-3/6), 9.94 (br s, 1H, H-1/8).

^{1}H NMR (500.11 MHz, THF-d_8, –80 °C):
δ = 1.74 (br s, 9H, C(CH_3)$_3$), 1.81 (br s, 9 H, C(CH_3)$_3$), 7.20 (s, 1H, H-4 or H-5), 7.46 (s, 1H, H-4 or H-5), 8.12 (s, 1H, H-3 or H-6), 8.31 (s, 1H, H-3 or H-6), 10.34 (br s, 1H, H-1 or H-8).

^{7}Li{^{1}H} NMR (194.37 MHz, THF-d_8, –80 °C):
δ = - 2.14 (s), 0.15 (s).

^{13}C{^{1}H} NMR (125.76 MHz, THF-d_8, –80 °C):
δ = 197.8 (s, C-1/8).
The carbene signal at –80 °C could be detected at 197.8 ppm. Because the ^{13}C{^{1}H} NMR measurement was of a probe with sideproducts, all other signals are not discussed.

9.3.24 Monocyclic product 13

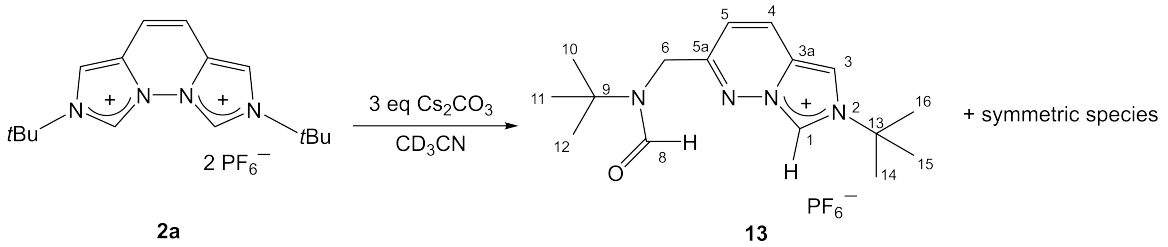

2a 13

2a (4.0 mg, 7.1 μmol, 1.0 eq) is solved in acetonitrile (0.4 mL). Then Cs_2CO_3 (7.0 mg, 21 μmol, 3.0 eq), is added to the colorless solution. After 4 h the ^{1}H NMR spectrum shows full conversion to the monocyclic **13**.

^{1}H NMR (400.13 MHz, CD_3CN):
δ = 1.41 (s, $C(CH_3)_3$, H-(10-12)), 1.73 (s, $C(CH_3)_3$, H-(14-16)), 4.7 (s, 2H, H-6) 7.06 (d, $^4J_{HH}$ = 9.8 Hz, H-4), 7.97 (s, 1H, H-3), 8.07 (d, $^4J_{HH}$ = 9.8 Hz, 1H, H-5) 8.6 (s, 1H, COH), 9.33 (br s, H-1, 1H).

^{13}C{^{1}H} NMR (125.76 MHz, CD_3CN):
δ = 29.8(s, $C(CH_3)_3$, C-(10-12)), 30.0 (s, $C(CH_3)_3$, C-(14-16)), 57.1 (s, ($C(CH_3)_3$, C-9), 63.2 (s, $C(CH_3)_3$, C-13), 113.0 (s, C-3), 119.2 (s, C-4), 125.7 (s, C-3a), 128.1 (s, C-5), 128.3 (s, C-1), 161.7 (s, C-5a), 163.5 (s, C-8).

MS(ESI$^+$, CH_3CN):
m/z 289.17 (100) [M - PF_6^-]$^+$.

Symmetric species:
^{1}H NMR (400.13 MHz, CD_3CN):
δ = 1.72 (s, $C(CH_3)_3$, 18H), 7.21 (s, 2H), 7.83 (s, 2H).

Generation of the free dicarbene **1a** and addition of $LiPF_6$.

In THF-d_8 with 0.5 eq. of $LiPF_6$.
P_4-*t*Bu (20 mg, 31 μmol 2.1 eq) was added to a suspension of **2a** (8.3 mg, 15 μmol, 1eq) in 0.4 mL of THF-d_8 to give a light brown solution, and $LiPF_6$ (11 mg, 7.2 μmol, 0.5 eq) was added. The ^{1}H NMR spectrum showed one signal set, whose broad peaks lie between those of complexes **10a** and **10a-H**.

^{1}H NMR (400.11 MHz, THF-d_8):
δ = 1.62 (s, 18H, $C(CH_3)_3$), 6.78 (br s, 2H, H-4/5), 7.49 (br s, 2H, H-3/6).

In THF-d_8 with 1.0 equiv of $LiPF_6$.
P_4-*t*Bu (8.9 mg, 14 μmol, 2.2 eq) was added to a suspension of **2a** (3.3 mg, 5.9 μmol, 1 eq) in 0.4 mL of THF-d_8 to give a light brown solution, and $LiPF_6$ (0.9 mg, 5.9 μmol, 1 eq) was added. The ^{1}H NMR spectrum showed full conversion into the Li complexes **10a** and **10a-H** in a ratio of 0.6:1. The backbone signals were broad and were not baseline separated.

^{1}H NMR (500.13 MHz, THF-d_8):
δ = 1.69 (s, 18H, $C(CH_3)_3$), 7.05 (s, 2H, H4/5), 7.77 (s, 2H, H-3/6); 2b-H, 1.51 (s, 18H, $C(CH_3)_3$), 7.05 (s, 2H, H-4/5), 7.77 (s, 2H, H-3/6).

In THF-d_8 with 2.0 eq of $LiPF_6$.

P_4-*t*Bu (16 mg, 25 μmol, 2.2 eq) was added to a suspension of **2a** (5.8 mg, 10 μmol, 1 eq) in 0.4 mL of THF-d_8 to give a light brown solution, and $LiPF_6$ (31 mg, 20 μmol, 2 eq) was added. The ^{1}H NMR spectrum showed one signal set of broad peaks that lie between those of **10a** and **10a-H**.

^{1}H NMR (400.11 MHz, THF-d_8):
δ = 1.56 (br s, 18H, $C(CH_3)_3$), 7.01 (br s, 2H, H-4/5), 7.75 (br s, 2H, H-3/6).

In benzene-d_6.

P_4-tBu (21 mg, 33 μmol) was added to a suspension of **2a** (7.8 mg, 14 μmol) in C_6D_6 to give a colorless solution and a brown oil. $LiPF_6$ (22 mg, 14 μmol) was added to the solution. The ^{1}H NMR spectrum showed no shift of the signals.

^{1}H NMR (400.11 MHz, C_6D_6):

δ = 1.49 (s, 18H, $C(CH_3)_3$), 6.32 (s, 2H, H-4/5), 6.70 (s, 2H, H-3/6).

Generation of the free dicarbene **1a** and addition of KPF_6.

In THF-d_8 with 0.5 eq of KPF_6.
P_4-*t*Bu (11 mg, 17 μmol, 2.1 eq) was added to a suspension of **2a** (3.9 mg, 6.9 μmol, 1 eq) in 0.4 mL of THF-d_8 to give a light brown solution, and KPF_6 (0.6 mg, 3.3 μmol, 0.5 eq) was added. The ^{1}H NMR spectrum showed the signals for the dicarbene **1a**.

^{1}H NMR (400.11 MHz, THF-d_8):
δ = 1.63 (s, 18H, $C(CH_3)_3$), 6.75 (s, 2H, H-4/5), 7.43 (s, 2H, H-3/6).

In THF-d_8 with 1.0 eq of KPF_6.
P_4-*t*Bu (17 mg, 27 μmol) was added to a suspension of **2a** (6.9 mg, 12 μmol) in THF-d_8 to give a light brown solution, and KPF_6 (2.3 mg, 12 μmol, 1.0 eq) was added. The ^{1}H NMR spectrum showed full conversion into the K-complex **12a**.

^{1}H NMR (400.11 MHz, THF-d_8):
δ = 1.64 (s, 18H, $C(CH_3)_3$), 6.86 (s, 2H, H-4/5), 7.57 (s, 2H, H-3/6).

In THF-d_8 with 1.5 eq. of KPF_6.
Carbene **1b** was generated from P_4-*t*Bu (11 mg, 17 μmol, 2.1 eq) and **2a** (3.9 mg, 6.9 μmol, 1 eq) in 0.4 mL of THF-d_8, and KPF_6 (1.8 mg, 9.8 μmol, 1.5 eq) was added. The ^{1}H NMR spectrum showed full conversion to complex **12a**.

^{1}H NMR (400.11 MHz, THF-d_8):
δ = 1.64 (s, 18H, $C(CH_3)_3$), 6.85 (s, 2H, H-4/ 5), 7.57 (s, 2H, H-3/6).

9.3.25 Cu-Cu vegi$^{t\mathrm{Bu}}$ complex (16)[33]

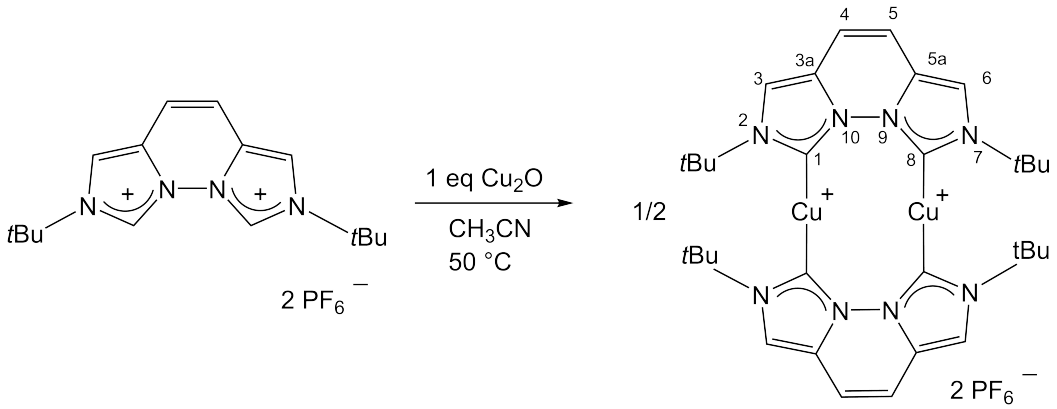

2a **16**

Synthesis according to literature.[31]

^{1}H NMR values match with the literature known data.

9.3.26 Ag-Ag vegi$^{t\mathrm{Bu}}$ complex (17)[31,33]

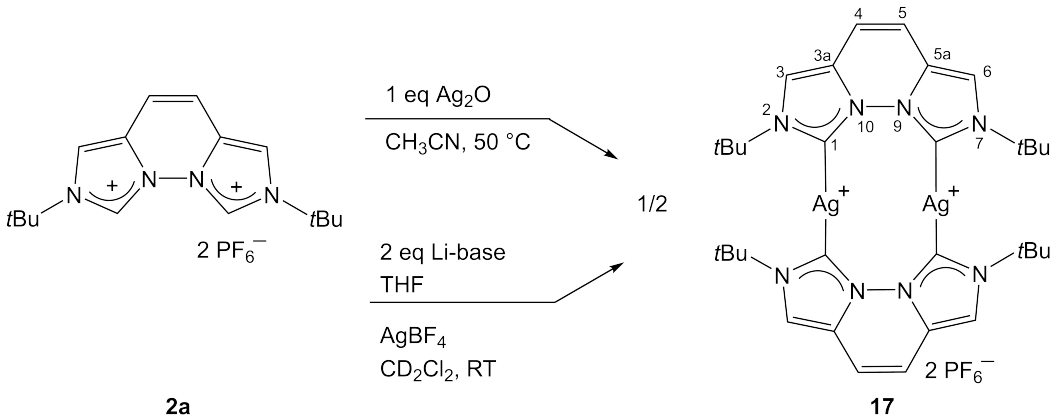

2a **17**

Synthesis of Route A according to literature.[31,33]

^{1}H NMR values values match with the literature known data.[114]

Route B:

$[Li(vegitBu)_2]PF_6$ (1.8 mg, 2.1 μmol) and $AgBF_4$ (1.0 mg, 5.1 μmol) were solved in dichloromethane-d_2. After 15 min a ^{1}H NMR spectrum was measured of the brown solution. It shows a full conversion to complex **17**.

^{1}H NMR (CD_2Cl_2, 400.11 MHz):
δ = 1.80 (s, 36H, $C(CH_3)_3$), 7.24 (s, 4H, H-4/5), 7.86 (s, 4H, H-3/6).

9.3.27 Au-Au vegi$^{t\mathrm{Bu}}$ complex (18)[33]

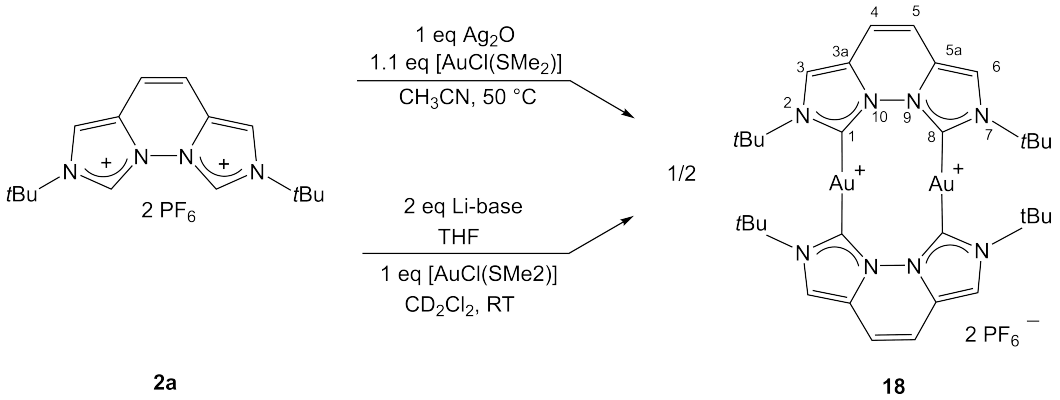

Synthesis of Route A according to literature.[31,33]

^{1}H NMR values match with the literature known data.[31,33]
Route B:

[Li(vegitBu)$_2$]PF$_6$ (1.8 mg, 2.0 μmol, 1 eq) and AuClSMe$_2$ (0.6 mg, 2.0 μmol, 1 eq) were mixed in dichloromethane-d$_2$. After 15 min a ^{1}H NMR spectrum was measured of the brown suspension. It shows a full conversion to complex **18**.

^{1}H NMR (CD_2Cl_2, 400.11 MHz):
δ = 1.88 (s, 36H, C(CH$_3$)$_3$), 7.22 (s, 4H, H-4/5) , 7.83 (s, 4H, H-3/6).

9.3.28 Ag-Au vegi$^{t\mathrm{Bu}}$ complex 20[33]

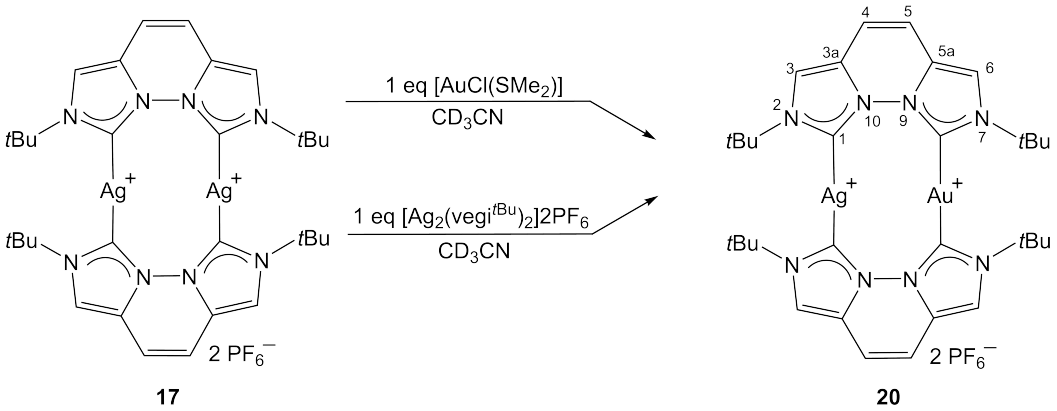

Synthesis of Route A according to literature.[31,33]

^{1}H NMR values match with the literature known data.[31,33]

The formation of a mixed Ag-Au complex was obtained in a ratio of 1:0.3:1 ([Ag-Ag]:[Ag-Au]:[Au-Au]).

9.3.29 Ag-Cu-complex 21[33]

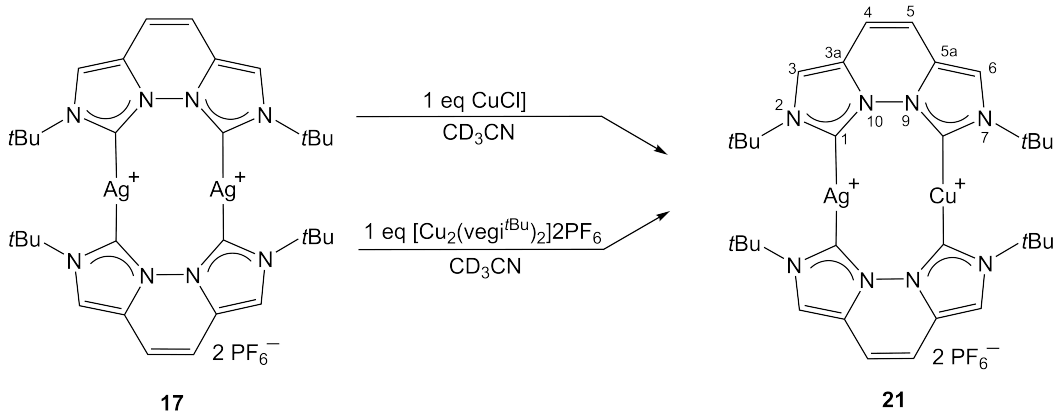

Route A:

1 eq Ag-NHC complex **17** (12.7 mg, 12.1 μmol, 1 eq) with 1 eq CuCl (1.2 mg, 12.1 μmol, 1 eq) in CD_3CN. Signals for both homodinuclear complexes **17** and **16** also a mixed Ag-Cu NHC complex **21** occur in the 1H NMR spectrum.

Route B:

The mixed complex **21** was also generated *in situ* by metal ion exchange combining 1 eq of the Ag-NHC (2.3 mg, 2.2 μmol, 1 eq) complex **17** with 1eq of Cu-NHC complex **16** (2.3 mg, 2.2 μmol, 1 eq) in CD_3CN.

The formation of a mixed Ag-Cu complex was obtained in a ratio of 1:2:1 ([Ag-Ag]: [Ag-Cu]:[Cu-Cu]).

Only the signals for the mixed Ag-Au complex are listed:

^{1}H NMR (500.13 MHz, CD_3CN):

δ = 1.72 (br s, 18H, $C(CH_3)_3$), 1.83 (br s, 18H, $C(CH_3)_3$), 7.17 (br s, 2H, H-5), 7.89 (br s, 2H, H-4).

9.3.30 [Ni(vegi$^{t\mathrm{Bu}}$)$_4$] (22a)

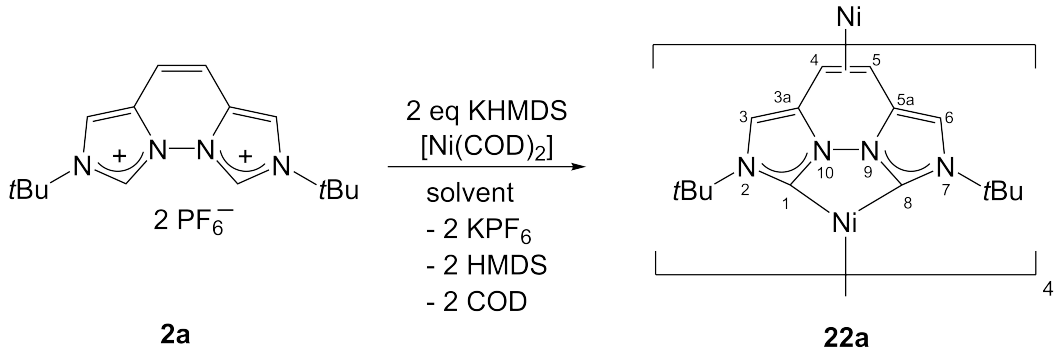

In THF-d_8:

Bis(imidazolium) salt **2a** (15 mg, 26 μmol, 1 eq) and potassium hexamethyldisilazide (11 mg, 54 μmol, 2.1 eq) were reacted in THF-d(0.5 mL) for 20 min at room temperature. After filtration [Ni(COD)$_2$] (7.3 mg, 26.54 μmol, 1 eq) was added to the brown solution upon which it turned red-brown. After stirring for 2 h at room temperature the mixture was dried *in vacuo* and washed with *n*-pentane.

The ratio of both Ni-complexes in the ^{1}H NMR spectrum is 1.5:1 (molecule A : molecule B).

^{1}H NMR (400.13 MHz, THF-d_8)

Molecule A:

δ = 1.59 (s, 18H, C(CH$_3$)$_3$), 2.55 (s, 2H, H-4/5), 6.49 (s, 2H, H-3/6).

Molecule B:

δ = 1.60 (s, 18H, C(CH$_3$)$_3$), 2.57 (s, 2H, H-4/5), 6.56 (s, 2H, H-3/6).

Molecule A:

^{13}C{^{1}H} NMR (100.61 MHz, THF-d_8):

δ = 22.9 (C-4/5), 31.6 (C(CH$_3$)$_3$), 57.0 (C(CH$_3$)$_3$), 105.2 (C-3/6), 132.0 (C-3a/5a), 176.8 (C-1/8).

Molecule B:

$^{13}C\{^{1}H\}$ NMR (100.61 MHz, THF-d_8):

δ = 21.7 (C-4/5), 31.7 (C(CH$_3$)$_3$), 57.3 (C(CH$_3$)$_3$), 105.9 (C-3/6). Carbene and C-3a/5a signals could not be detected.

In toluene-d_8:

Bis(imidazolium) salt **2a** (8.0 mg, 14 μmol, 1 eq) and potassium hexamethyldisilazide (5.9 mg, 29 μgmol, 2.1 eq) were reacted in toluene (0.5 mL) for 20 min at room temperature. [Ni(COD)$_2$] (3.9 mg, 14 μmol, 1.0 eq) was added to the dark brown suspension. The suspension turns orange and immediately pink after several minutes.

^{1}H-NMR (400.13 MHz, toluene-d_8):

δ = 1.56 (s, 18H, C(CH$_3$)$_3$), 2.98 (s, 2H, H-4/5), 6.53 (s, 2H, H-3/6).

9.3.31 $[Ni(vegi^{nPr})]_4$ 22b

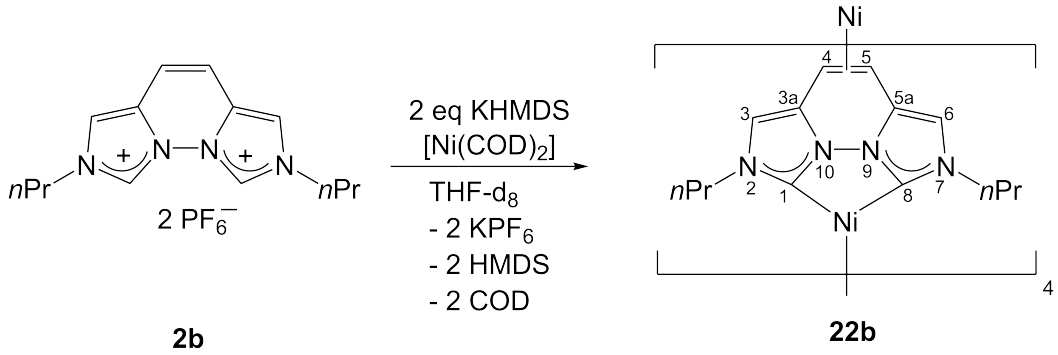

Bis(imidazolium) salt **2b** (10 mg, 19 μmol, 1 eq) and lithium hexamethyldisilazide (7.8 mg, 47 μgmol, 2.5 eq) were reacted in THF-d_8 (0.5 mL) for 20 min at room temperature. $[Ni(COD)_2]$ (5.3 mg, 19 μmol, 1 eq) was added to the dark brown suspension. The suspension turns orange and immediately pink after several minutes.

^{1}H NMR (400.13 MHz, THF-d_8):
δ = 0.97 (br s, 6 H, CH_3), 1.80 (br s, 4 H, CH_2), 2.81 (br s, 2 H, H-4/5), 3.82 (br s, 2 H, CH_2), 6.29 (s, 2H, H-3/6).

9.3.32 $NiCl_2$(vegi^{tBu})] (23a)

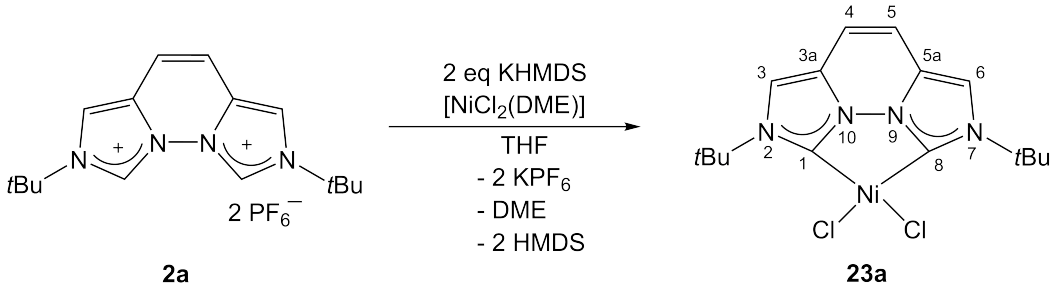

To a suspension of **2a** (100 mg, 178 μmol, 1 eq) in THF potassium hexamethyldisilazide (72.7 mg, 364 μmol, 2.1 eq) was added. After 20 min [$NiCl_2$(DME)] (39.1 g, 178 μmol, 1 eq) was added. The suspension turned pink. After 1 h the solid was filtered off and extracted with dichloromethane. The dichloromethane extract is dried and washed 5 x with *n*-pentane. The product is obtained as a paramagnetic pink solid.

^{1}H NMR (400.13 MHz, CD_3CN):
δ = 8.98 (br s), 15.10 (br s), 22.65 (br s).

^{1}H NMR (400.13 MHz, THF-d_8):
δ = 13.09 (br s), 14.36 (br s), 22.70 (br s).

^{1}H NMR (400.13 MHz, THF-d_8, -45 °C):
δ = 18.27 (s), 28.17 (s), 49.13 (br s), 151.70 (s).

^{1}H NMR (400.13 MHz, THF-d_8, -95 °C):
δ = 25.27 (br s), 35.02 (s), 69.49 (br s), 196.25 (br s).

^{19}F{^{1}H} NMR (376.48 MHz, CD_3CN)
δ = - 72.71 (d, $^1J_{PF}$ = 706 Hz, PF_6^-)

^{31}P{^{1}H} NMR (161.97 MHz, CD_3CN)
δ = - 144.63 (sept, $^1J_{PF}$ = 706 Hz,PF_6^-)

Anal. Calcd for $C_{16}H_{22}N_4NiCl_2 \cdot 1.05\ KPF_6$:

Calcd.: C 32.39; H 3.74; N 9.44

Found: C 33.49; H 4.47; N 8.04

MS(ESI^+, CH_3CN):

m/z = 363.1 (100) $[M\text{-}Cl]^+$, 289.2 (71) $[M\text{-}Ni\text{-}2Cl\text{-}H]^+$.

9.3.33 [Pd(TMEDA)Me$_2$][147]

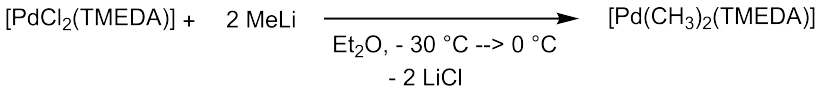

Methyllihium in diethyl ether (2.3 mL, 1.6 M, 2.1 eq) is added to a stirred suspension of [Pd(TMEDA)Cl$_2$] (0.50 g, 1.7 mmol, 1 eq) in diethy ether (5 mL) at -30 °C. The mixture was allowed to warm slowly to 0 °C and was kept for 1 h at that temperature. Iced water (2.5 mL) was added to the grey suspension. A clear diethyl ether layer and a black aqueous layer was formed. The organic layer was separated, dried over Na_2SO_4 and evaporated *in vacuo* to give a white solid as a product (205 mg, 47 %; Literature: 60-85 %[147]).

^{1}H-NMR (400.13 MHz, THF-d$_8$)
δ = -0.36 (s, 6H, PdMe), 2.39 (s, 12H, NMe2), 2.49 (s, 4H, CH_2).

Values match with the literature known data.[147]

9.3.34 $[Pd(CH_3)_2(vegi^{nPr})]$ (25b)

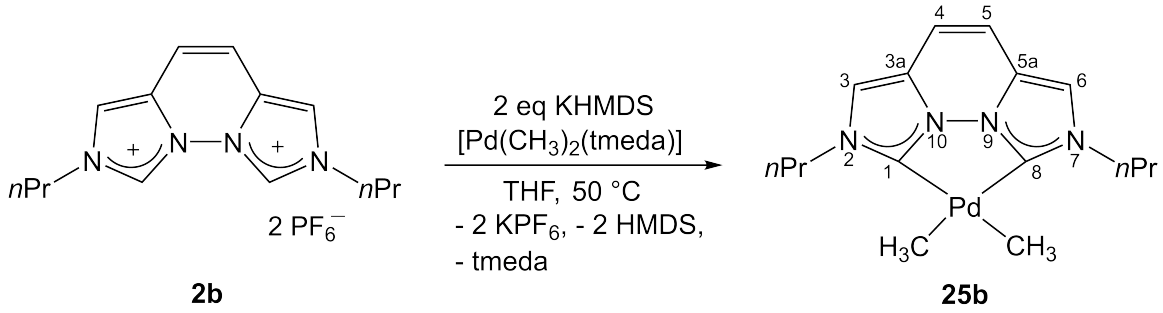

To a cooled suspension of **2b** (80.0 mg, 150 μmol, 1 eq) in THF at -30 °C potassium hexamethyldisilazide was added (65.7 mg, 329 μmol, 2.2 eq) and the suspension turned dark brown. After 15 min [Pd(TMEDA)Me_2] (37.8 mg, 150 μmol, 1 eq) is added. The dark suspension was stirred overnight at 50 °C. The suspension was concentrated and the double amount of *n*-pentane was added. The yellow *n*-pentane suspension was filtered, and the dark remaining solid was washed 2 x with 1.5 mL of a 1:1 mixture of THF/*n*-pentane. Then the solid was extracted with 3 mL of a THF/toluene 1:1 mixture and the extract dried *in vacuo*. The resulting beige solid was dried in high vacuum for 4 days (13.0 mg, 22%).

^{1}H NMR (400.11 MHz, CD_3CN):
δ = 0.16 (s, 6H, Pd-CH_3), 0.94 (t, $^3J_{HH}$ = 7.4 Hz, 6H, CH_3), 1.88 (tq, $^3J_{HH}$ = 7.4 Hz, $^3J_{HH}$ = 7.1 Hz CH_2, 4H), 4.22 (t, $^3J_{HH}$ = 7.1 Hz, 4H, NCH_2), 6.95 (s, 2H, H-4/5), 7.22 (s, 2H, H-3/6).

^{1}H NMR (400.11 MHz, THF-d_8):
δ = 0.19 (s, 6H, Pd-CH_3), 0.96 (t, $^3J_{HH}$ = 7.4 Hz, 36H, CH_3), 1.90 (tq, $^3J_{HH}$ = 7.2 Hz, $^3J_{HH}$ = 7.1 Hz CH_2, 4H), 4.24 (t, $^3J_{HH}$ = 7.1 Hz, 4H, NCH_2), 6.91 (s, 2H, H-4/5), 7.27 (s, 2H, H-3/6).

^{13}C{^{1}H} NMR (100.61 MHz, CD_3CN):
δ = -6.6 (Pd-CH_3), 11.2 (CH_3), 26.0 (CH_2), 52.5 (NCH_2), 114.0 (C-4/5), 116.5 (C-3/6),

121.1 (C-3a/5a), 175.5 (C-1/8).

$^{13}C\{^{1}H\}$ NMR (100.61 MHz, THF-d_8):
δ = -6.8 (Pd-CH_3), 11.4 (CH_3), 25.0 (CH_2), 52.5 (NCH_2), 113.6 (C-4/5), 116.2 (C-3/6), 121.1 (C-3a/5a), 177.7 (C-1/8).

MS(ESI^+, CH_3CN):
m/z 347.0 (59) ([M-CH_3-CH_4]$^+$), 363.0 (100) ([M CH_3]$^+$).

Anal. Calcd for $C_{16}H_{24}N_4Pd$:
Calcd.: C 50.73; H 6.38; N 14.79
Found.: C 49.39; H 5.78; N 14.25

Melting point: 340.6 °C (decomposition)

9.3.35 $[Pd(CH_3)_2(vegi^{tBu})]$ (25a)

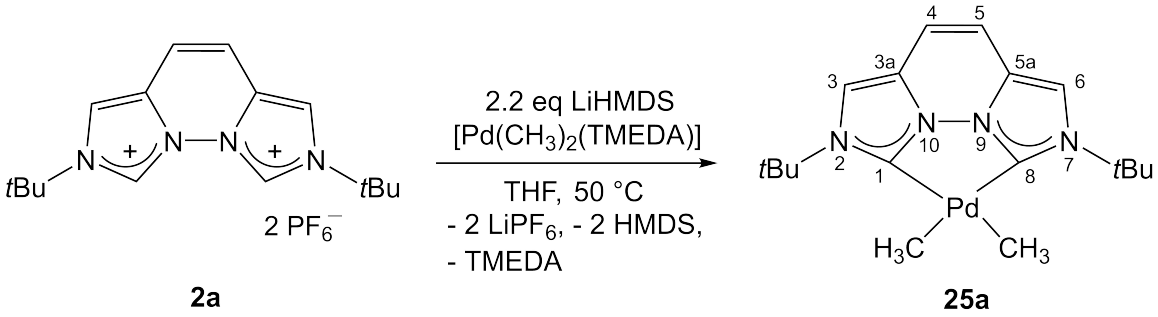

To a suspension of **2a** (18.7 mg, 33.2 μmol, 1 eq) in THF-d_8 lithium hexamethyldisilazide (13.4 mg, 80.1 μmol, 2.4 eq) was added. After 20 min [Pd(TMEDA$(Me)_2$] (8.40 mg, 33.2 μmol, 1 eq) was added to the dark brown solution and heated at 50 °C overnight. The ^{1}H NMR spectrum shows the formation of complex **25a**.

^{1}H NMR (400.11 MHz, THF-d_8)
$\delta = 0.26$ (s, 6H, CH_3), 1.79 (s, 18H, $C(CH_3)_3$)), 6.89 (s, 2H, H-4/5), 7.51 (s, 2H, H-3/6).

$^{13}C\{^1H\}$ NMR (100.61 MHz, THF-d_8):
δ = 1.0 (Pd-CH_3), 31.5 ($C(CH_3)_3$), 59.7 ($C(CH_3)_3$), 113.0 (C-4/5), 113.7 (C-3/6), 121.8 (C-3a/5a), 180.0 (C-1/8).

MS(ESI$^+$, CH_3CN):
m/z 391.1 (69) [M-CH_3]$^+$, 463.2 (100) [M-CH_3]$^+$.

9.3.36 $[PdCl_2(vegi^{tBu})]$ (28a)

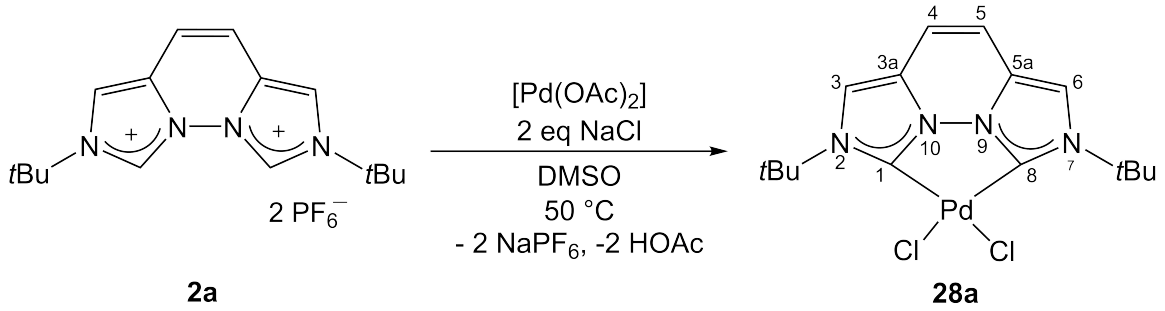

2a **28a**

To a solution of **2a** (6.0 mg, 11 μmol, 1 eq) in DMSO $Pd(OAc)_2$ (2.4 mg, 11 μmol, 1 eq) and NaCl (1.2 mg, 21 μmol, 2 eq) was added. Then the orange solution was heated at 50 °C overnight. The product was precipitated with diethyl ether, filtered off and washed with acetonitrile.

^{1}H NMR (400.11 MHz, DMSO-d_6):
δ = 1.86 (s, 18H, $C(CH_3)_3$)), 7.19 (s, 2H, H-4/5), 7.89 (s, 2H, H-3/6).

$^{13}C\{^1H\}$ NMR (100.61 MHz, DMSO-d_6):
δ = 30.5 ($C(CH_3)_3$), 61.1 ($C(CH_3)_3$), 113.7 (C-4/5), 115.6 (C-3/6), 120.1 (C-3a/5a), 142.8 (C-1/8).

MS(ESI^+, CH_3CN):
m/z = 413.1 (24) $[M\text{-}Cl]^+$, 471.0 (39) $[M+Na]^+$

9.3.37 [$PdCl_2$(vegi$^{n\mathrm{Pr}}$)] (28b)

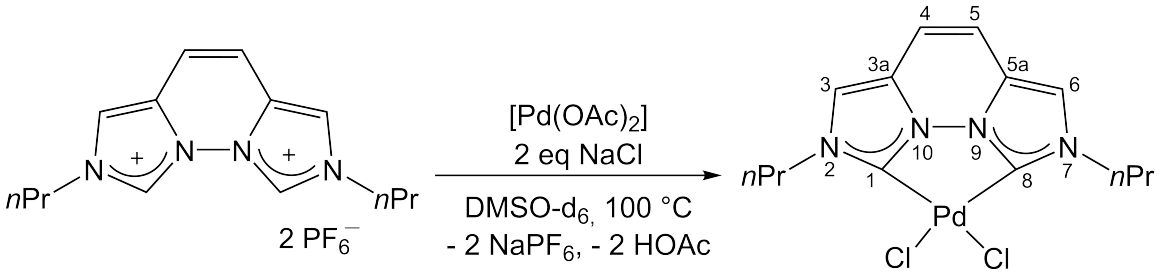

2b **28b**

2b (15.0 mg, 28.1 μmol, 1 eq), palladium(II)-acetate (6.30 mg, 28.1 μmol, 1 eq) and NaCl (3.28 mg, 56.2 μmol, 2 eq) were mixed in dimethylsulfoxide-d_6 (0.5 mL). The mixture was heated at 100 °C for 68 h. The color changed from a light to a dark yellow. The ^{1}H NMR spectrum indicates the formation of [Pd(vegi$^{n\mathrm{Pr}}$)Cl_2].

^{1}H NMR (400.11 MHz, DMSO-d_6):
δ = 0.89 (t, $^3J_{HH}$ = 7.4 Hz, 6H, CH_3), 1.84 (tq, $^3J_{HH}$ = 7.2 Hz, $^3J_{HH}$ = 7.4 Hz, 4H, CH_2), 4.62 (t, $^3J_{HH}$ = 7.2 Hz, 4H, NCH_2, 7.27 (s, 2H, H-4/5), 7.78 (s, 2H, H-3/6).

^{13}C{^{1}H} NMR (100.61 MHz, DMSO-d_6):
δ = 10.5 (CH_3), 24.6 (CH_2), 50.5 (NCH_2)), 114.5 (C-4/5), 117.5 (C-3/6), 120.3 (C-3a/5a), 142.3 (C-1/8).

MS(ESI$^+$, CH_3CN):
m/z = 442.9 (75) [M+Na]$^+$

9.3.38 [Pd(DMSO-d_6)(vegi^{tBu})]$(PF_6)_2$ (31a)

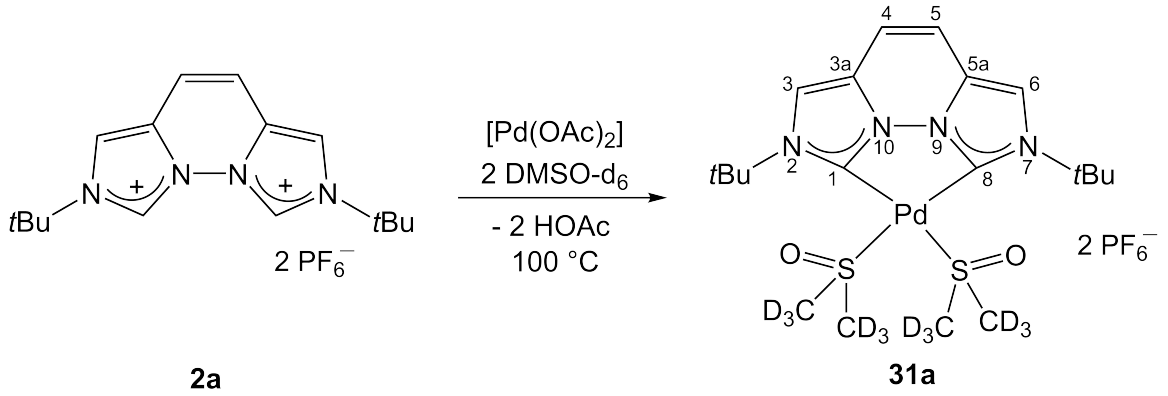

2a **31a**

2b (15.0 mg, 28.1 μmol, 1 eq) and palladium(II)-acetate (6.30 mg, 28.1 μmol, 1 eq) were mixed with dimethylsulfoxide-d_6 (0.5 mL). The mixture was heated at 100 °C for overnight. The ^{1}H NMR spectrum of the yellow solution shows the formation of **31b** and signals of actic acid and **2a**.

^{1}H NMR (400.11 MHz, DMSO-d_6):
δ = 1.70 (s, 18H, C(CH_3)$_3$), 7.23 (s, 2H, H-4/5), 7.87 (s, 2H, H-3/6).

9.3.39 [Pd(DMSO-d_6)(vegi$^{n\mathrm{Pr}}$)](PF_6)$_2$ (31b)

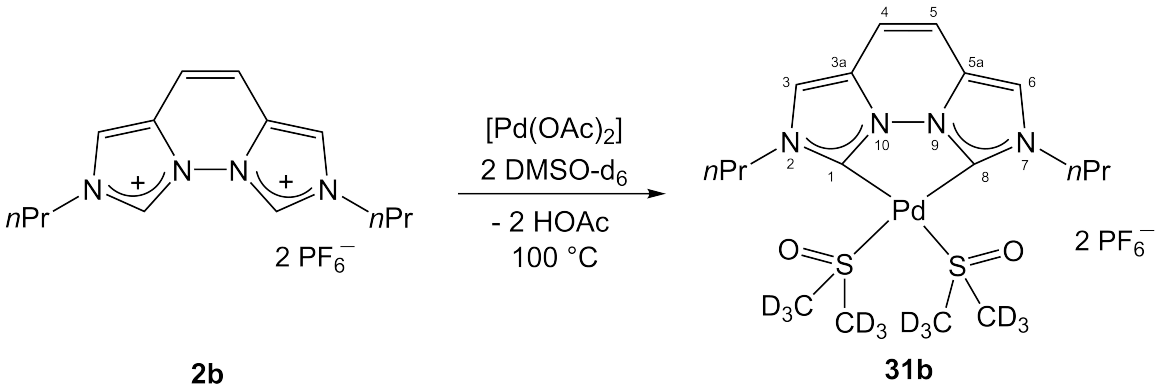

2b (15.0 mg, 28.1 μmol, 1 eq) and palladium(II)-acetate (6.30 mg, 28.1 μmol, 1 eq) were mixed with dimethylsulfoxide-d_6 (0.5 mL). The mixture was heated at 100 °C for 68 h upon which the yellow color changed to a darker yellow. The ^{1}H NMR spectrum shows the formation of **31b** and some minor unidentified side products.

^{1}H NMR (400.11 MHz, DMSO-d_6):
δ = 0.92 (t, $^3J_{HH}$ = 7.4 Hz, 6H, CH_3), 1.87 (tq, $^3J_{HH}$ = 7.1 Hz, $^3J_{HH}$ = 7.4 Hz, 4H, CH_2), 4.27 (t, $^3J_{HH}$ = 7.1 Hz, 4H, NCH_2), 7.37 (s, 2H, H-4/5), 7.87 (s, 2H, H-3/6).

^{13}C{^{1}H} NMR (100.61 MHz, DMSO-d_6):
δ = 10.5 (CH_3), 24.3 (CH_2), 51.0 (NCH_2), 115.3 (C-4/5), 118.1 (C3/6), 120.9 (C-3a/5a), 131.8 (C-1/8).

9.3.40 $[Pd(CD_3CN)_2(vegi^{tBu})](PF_6)_2$ (32a)

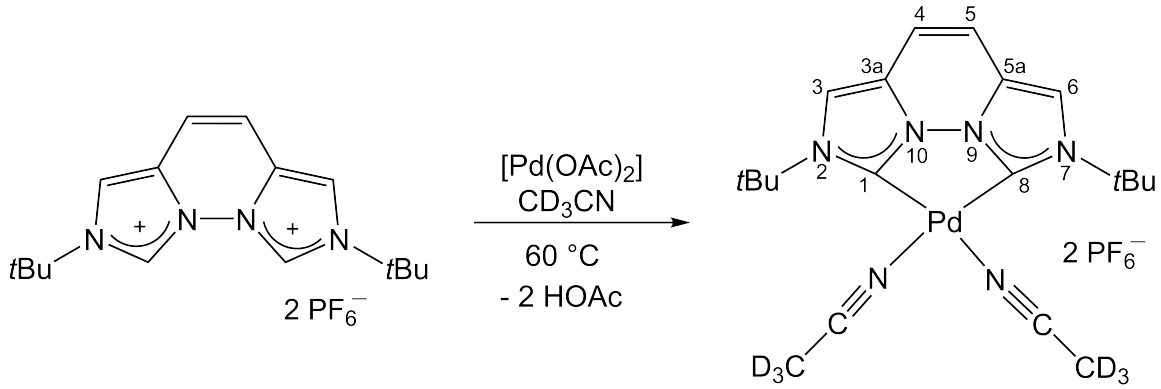

2a **32a**

2a (10 mg, 17 μmol, 1 eq) and palladium(II)-acetate (4.8 mg, 21 μmol, 1 eq) were mixed with acetonitrile-d_3 (0.5 mL). The reaction mixture was heated at 60 °C overnight. The ^{1}H NMR spectrum of the brown-yellow solution shows the signals for **32b** along with signals of acetic acid and **2a**.

^{1}H NMR (400.11 MHz, DMSO-d_6):
δ = 2.38 (s, 18H, $C(CH_3)_3$), 7.09 (s, 2H, H-4/5), 8.11 (s, 2H, H-3/6).

9.3.41 $[Pd(CD_3CN)_2(vegi^{nPr})](PF_6)_2$ (32b)

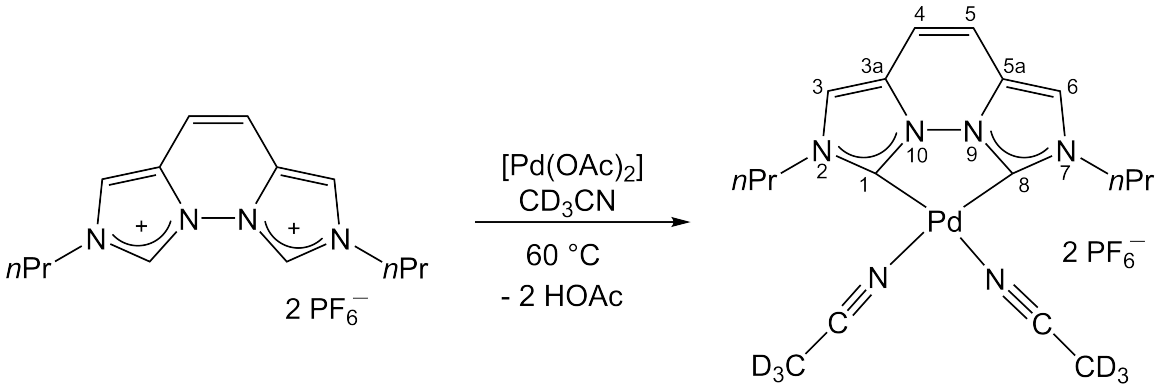

2b **32b**

2b (15.0 mg, 28.1 μmol, 1 eq) and palladium(II)-acetate (6.30 mg, 28.1 μmol, 1 eq) were mixed with acetonitrile-d_3 (0.5 mL). The reaction mixture was heated at 60 °C for 68 h. The yellow mixture turned yellow-green. The ^{1}H NMR spectrum shows the signals for **32b**.

^{1}H NMR (400.11 MHz, DMSO-d_6):
δ = 0.96 (t, $^3J_{HH}$ = 7.4 Hz, 6H, CH_3), 1.93 (tq, $^3J_{HH}$ = 7.1 Hz, $^3J_{HH}$ = 7.4 Hz, 4H, CH_2), 4.30 (t, $^3J_{HH}$ = 7.1 Hz, 4H, NCH_2), 7.29 (s, 2H, H-4/5), 7.55 (s, 2H, H-3/6).

^{13}C{^{1}H} NMR (100.61 MHz, DMSO-d_6):
δ = 10.9 (CH_3), 25.6 (CH_2), 53.4 (NCH_2), 116.3 (C-4/5), 119.3 (C-3/6), 122.5 (C-3a/5a), 135.5 (C-1/8).

9.3.42 $[Pt(CH_3)_2(vegi^{tBu})]$ (33a)

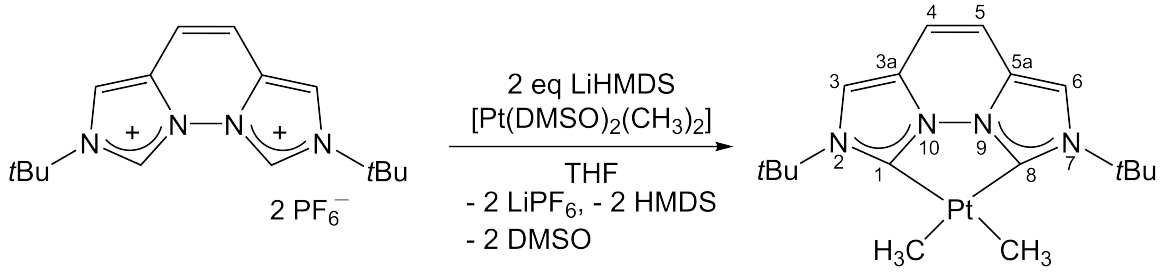

2a **34a**

Lithium hexamethyldisilazide (46.9 mg, 280 μmol, 2.2 eq) was added to a suspension of **2a** (65.7 mg, 117 μmol, 1 eq) in 3.5 mL THF. After 20 min $[Pt(CH_3)_2(DMSO)_2]$ (44.6 mg, 117 μmol, 1 eq) was added and stirred overnight. The brown suspension was filtered over neutral alumina and the residue washed twice with each 4 mL THF. The yellow filtrate was concentrated to dryness and the residue washed with *n*-pentane (3 x 2 mL). The product was obtained as a white solid (18.2 mg, 36.7 μmol, 31 %).

^{1}H NMR (400.11 MHz, THF-d_8):
δ = 0.86 (s+sat, $^2J_{PtH}$ = 74.0 Hz, 6H, Me_2Pt), 1.84 (s, 18H, $C(CH_3)_3$), 6.88 (s, 2H, H-4/5), 7.39 (s+sat, $^4J_{PtH}$ = 8.8 Hz, 2H, H-3/6).

^{1}H NMR (400.11 MHz, DMSO-d_6):
δ = 0.77 (s+sat, $^2J_{PtH}$ = 62.5 Hz, 6H, Me_2Pt), 1.77 (s, 18H, $C(CH_3)_3$), 7.05 (s, 2H, H-4/5), 7.63 (s br, 2H, H-3/6).

^{1}H NMR (400.11 MHz, CD_3CN):
δ = 0.81 (s+sat, $^2J_{PtH}$ = 73.1 Hz, 6H, Me_2Pt), 1.81 (s, 18H, $C(CH_3)_3$), 6.91 (s, 2H, H-4/5), 7.37 (s+sat, $^4J_{PtH}$ = 8.7 Hz, 2H, H-3/6).

$^{13}C\{^1H\}$ NMR (100.61 MHz, CD_3CN):
δ = -3.3 (CH_3), 31.2 ($C(CH_3)_3$), 59.9 ($C(CH_3)_3$), 113.7 (C-4/5), 114.6 (C-3/6), 121.6 (C-3a/5a), 172.2 (C-1/8).

^{195}Pt NMR (53.77 MHz, CD_3CN):

δ = - 3805.9 ppm

Anal. Calcd for $C_{18}N_4H_{28}Pt \cdot 0.05$ mol $LiPF_6$:

Calcd.: C 42.97; H 5.61; N 11.14

Found.: C 42.84; H 5.90; N 11.31

MS (ESI+, CH_3CN):

m/z = 521.1 (100) $[M\text{-}CH_3\text{+}CH_3CN]^+$, 480.1 (18) $[M\text{-}CH_3]^+$.

9.3.43 $[Pt(CH_3)_2(vegi^{nPr})]$ (33b)

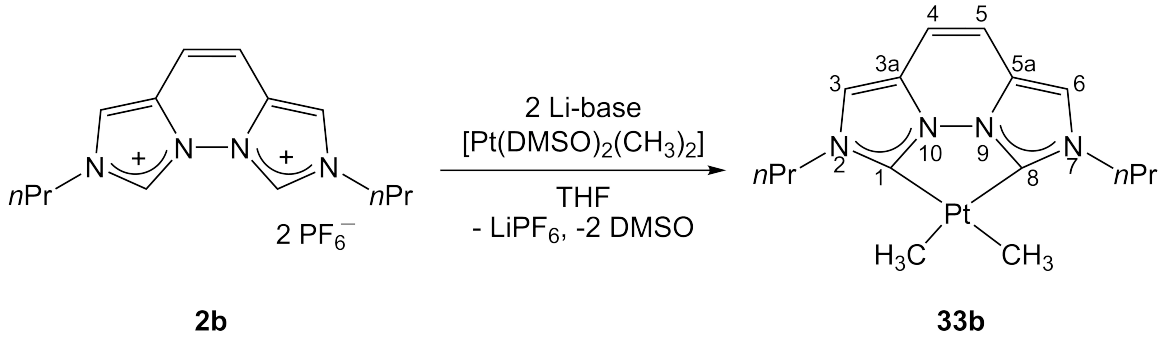

2b **33b**

Route A:

Lithium hexamethyldisilazide (90.9 mg, 539 μmol, 2.4 eq) was added to a suspension of **2b** (120 mg, 225 μmol, 1 eq) in 3.5 mL THF. After 20 min $[Pt(DMSO)_2Me_2]$ (85.7 mg, 225 μmol, 1 eq) was added and stirred overnight. The red-brown suspension was filtered over neutral alumina. The yellow solution was dried *in vauo* and the remaining solid washed with *n*-pentane (10 x 0.5 mL). The product **33b** is obtained as a beige solid (10.4 mg, 10 %) with an unkown species.

Route B:

Methyllithium (11.9 mg, 539 μmol, 2.4 eq) was added to a suspension of **2b** (120 mg, 225 μmol, 1 eq) in 3.5 mL THF at –30 °C. First an orange, then a brown-red solution formed. After 10 min $[Pt(DMSO)_2Me_2]$ (85.7 mg, 225 μmol, 1 eq) was added and stirred for 3 h. The red-brown mixture was filtered over neutral alumina. The yellow filtrate was dried *in vacuo*, the obtained brown solid dissolved in acetonitrile (1.5 mL) and washed with *n*-pentane (3 x 1 mL). After drying *in vacuo* the product was obtained as a brown solid. The ^{1}H NMR spectrum of the red-brown suspension shows the formation of complex **33b** (69.6 mg, 66 %) and an unkown species.

^{1}H NMR (400.11 MHz, THF-d_8):

δ = 0.90 (s+sat, $^2J_{PtH}$ = 73.9 Hz, 6H, Me_2Pt), 0.97 (t, $^3J_{CH}$ = 7.4 Hz, 6H, CH_3), 1.92 (tq, $^3J_{CH}$ = 7.3 Hz, $^3J_{CH}$ = 7.4 Hz, 4H, CH_2), 4.26 (t, $^3J_{CH}$ = 7.3 Hz, 4H, NCH_2), 6.89 (s, 2H, H-4/5), 7.11 (s+sat, $^4J_{PtH}$ = 7.9 Hz, 2H, H-3/6).

$^{13}C\{^{1}H\}$ NMR (100.61 MHz, THF-d_8):

δ = - 10.9 (s+sat, $^{1}J_{CPt}$ = 662.5 Hz, CH_3), 11.1 (CH_3), 25.2 (CH_2-Pr, from HSQC), 51.8 (NCH_2), 113.5 (C-4/5), 116.1 (s+sat, $^{3}J_{CPt}$ = 17.3 Hz, C-3/6), 121.5 (C-3a/5a), 172.3 (C-1/8).

Another unkown species obtained during purification:

^{1}H NMR (400.11 MHz, THF-d_8):

δ = 7.22 (s), 7.26 (s), 6.96 (s), 6.95 (s), 4.59 (t, J = 7.2 Hz).

MS (ESI^+, CH_3CN):

m/z = 493.0 (100) $[M\text{-}CH_3\text{+}CH_3CN]^+$.

9.3.44 [$PtCl_2$(vegi$^{n\mathrm{Pr}}$)] (35b)

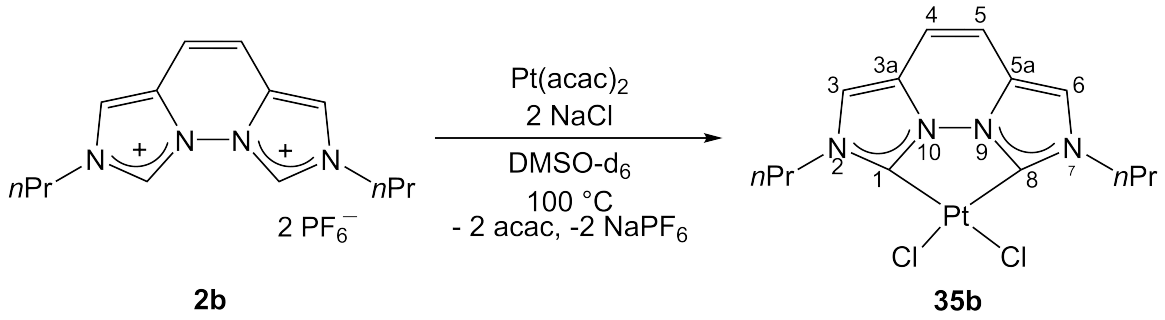

2b (15.0 mg, 28.1 μmol, 1 eq), platinum(II)-acetylacetonate (11.0 mg, 28.1 μmol, 1 eq) and NaCl (3.28 mg, 56.2 μmol, 2 eq) were suspended in dimethylsulfoxide-d_6 (0.5 mL). The mixture was heated at 100 °C for 17 h. The color turned from a light to a dark yellow. The ^{1}H NMR confirms the formation of **35b**.

^{1}H NMR (400.11 MHz, THF-d_8):
δ = 0.97 (t, $^3J_{HH}$ = 7.4 Hz, 6H, CH_3), 1.94 (sext., $^3J_{HH}$ = 7.4 Hz, 4H, CH_2-Pr), 4.73 (t, $^3J_{HH}$ = 7.4 Hz, 4H, NCH_2), 7.12 (s, 2H, H-4/5), 7.42 (s, 2H, H-3/6).

^{1}H NMR (400.11 MHz, DMSO-d_6):
δ = 0.90 (t, $^3J_{HH}$ = 7.4 Hz, 6H, CH_3), 1.85 (tq, $^3J_{HH}$ = 7.3 Hz, $^3J_{HH}$ = 7.4 Hz, 4H, CH_2-), 4.62 (t, $^3J_{HH}$ = 7.3 Hz, 4H, NCH_2), 7.24 (s, 2H, H-4/5), 7.69 (s, 2H, H-3/6).

^{13}C{^{1}H} NMR (100.61 MHz, DMSO-d_6):
δ = 10.5 (CH_3-Pr), 24.6 (CH_2-Pr), 50.1 (NCH_2-Pr), 114.8 (C-4/5), 118.1 (C-3/6), 120.0 (C-3a/5a), 130.0 (C-1/8).

9.3.45 [Pt(acac) (vegi$^{n\mathrm{Pr}}$)]$\mathbf{PF_6}$ (38b)

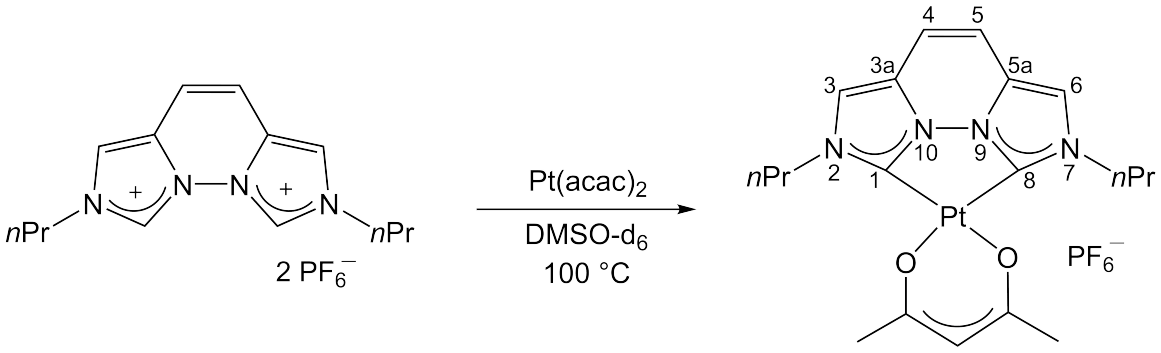

2b **38b**

2b (15.0 mg, 28.1 μmol, 1 eq) and platin(II)-acetylacetonate (11.0 mg, 28.1 μmol, 1 eq) were dissolved in dimethylsulfoxide-d_6 (0.5 mL). The mixture was heated at 100 °C for 17 h. The ^{1}H NMR spectrum shows signals of **38b**, acetylacetone and most probably [Pt(DMSO-d_6)$_2$(acac)]PF_6 as well as signals for **2b**.

^{1}H NMR (400.11 MHz, DMSO-d_6):
δ = 0.91 (t, $^3J_{HH}$ CH_2) = 7.4 Hz, 6H, CH_3), 1.85 (tq, $^3J_{HH}$ = 7.1 Hz, $^3J_{HH}$ = 7.4 Hz, 4H, CH_2), 2.06 (s, 6H, CH_3-acac), 4.37 (t, $^3J_{HH}$ = 7.1 Hz, 4H, NCH_2), 5.84 (s, 1H, CH-acac), 7.32 (s, 2H, H-4/5), 7.74 (s, 2H, H-3/6).

MS (ESI$^+$, CH_3CN):
m/z = 536.0 (100) ([10 – PF_6]$^+$).

9.3.46 Pt(vegi^{tBu})$_2$HCl)$_2$PF$_6$] (36)

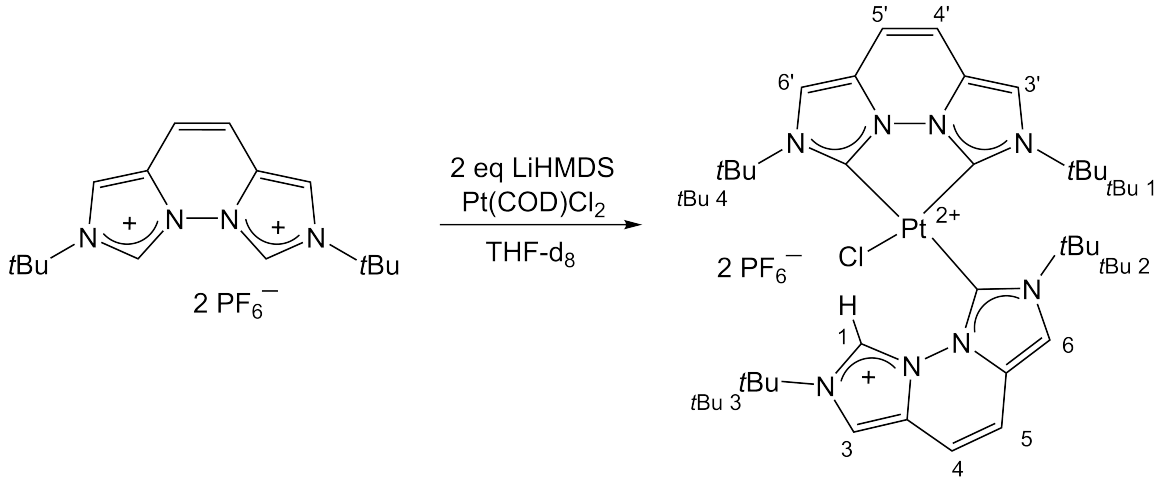

2a **36**

2a (6.0 mg, 11 μmol, 1 eq) was suspended in 0.5 mL THF-d$_8$. Then lithium hexamethyldisilazide (4.2 mg, 2.5 μmol, 2.4 eq.) was added. [Pt(COD)Cl$_2$] (4.0 mg, 11 μmol, 1 eq) was added to the red-brown solution. The color changed to orange. After several days at -30 °C colorless crystals were obtained and filtered off. The crystals were dissolved in CD$_3$CN and NMR spectra were measured. They confirm the formation of complex **36**.

^{1}H NMR (400.11 MHz, CD$_3$CN):

δ = 1.18 (s, 1H, C(CH$_3$)$_3$)-1), 1.27 (s, 1H, C(CH$_3$)$_3$)-2), 1.61 (s, 1H, C(CH$_3$)$_3$)-4), 1.96 (s, 1H, C(CH$_3$)$_3$)-3), 7.20 (d, $^2J_{HH}$ = 10.1 Hz, 1H), 7.26 (d, $^2J_{HH}$ = 7.2 Hz, 1H), 7.28 (d, $^2J_{HH}$ = 7.2 Hz, 1H), 7.44 (d, $^2J_{HH}$ = 10.1 Hz, 1H), 7.63 (s, 1H, H-6), 7.76 (s, 1H, H-5), 8.05 (d, $^4J_{HH}$ = 1.8 Hz, 1H, H-3), 8.20 (s, 1H, H-4), 12.36 (d, $^4J_{HH}$ = 1.8 Hz, 1H, 1-H).

The signal at 1.96 lies under the THF-d$_8$ signal and was detected via ^{1}H ^{13}C HSQC NMR experiment.

^{13}C{^{1}H} NMR (100.61 MHz, CD$_3$CN):

δ = 29.6 (C(CH$_3$)$_3$)-4), 30.9 (C(CH$_3$)$_3$)-2), 31.1 (C(CH$_3$)$_3$)-1), 32.1 (C(CH$_3$)$_3$)-3), 61.9

($C(CH_3)_3$)-4), 62.5 ($C(CH_3)_3$)-2), 64.5 ($C(CH_3)_3$)-1), 65.2 ($C(CH_3)_3$)-3), 113.3, 115.0, 115.7, 116.7 (C-4), 117.2, 117.4 (C-5), 118.0 (C-6), 119.7 (C-3), 124.4 (C-1).

Carbene signals were not detected. Further assignment cannot be made unambiguously.

9.3.47 *In situ* generation of Li-mani$^{n\mathrm{Pr}}$R$_2$ 39b

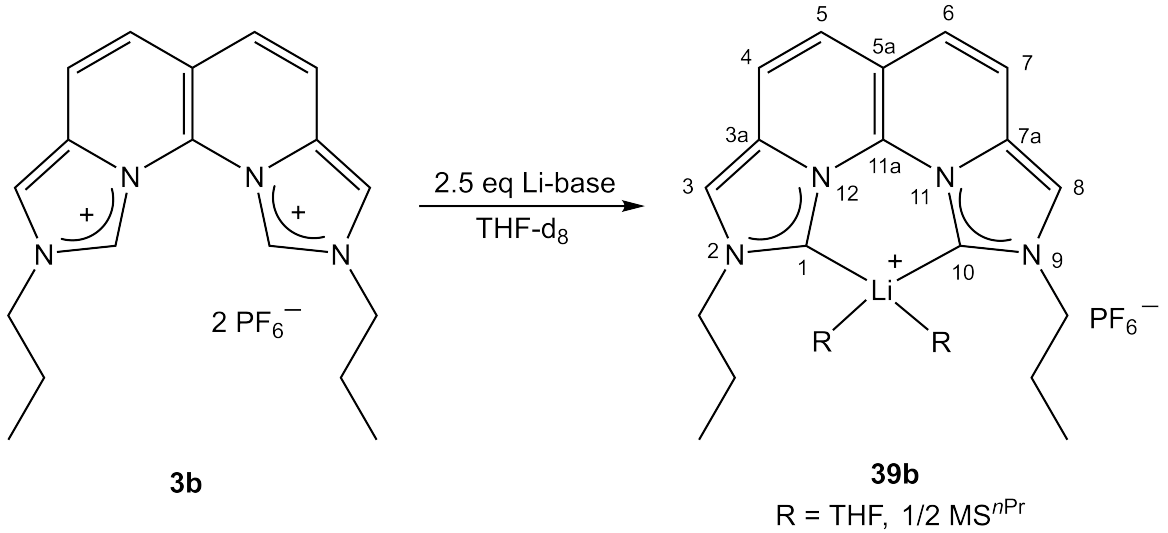

With Methyllithium:

Methyllithium (1.30 mg, 59.1 μmol, 2.5 eq) was added to a suspension of **3b** (13.5 mg, 23.1 μmol) in 0.4 mL of THF-d$_8$. The light brown suspension turned dark brown. After 2.5 h a ^{1}H NMR spectrum was measured. Two symmetric Li-complexes are obtained.

^{1}H NMR(400.13 MHz, THF-d$_8$):

Molecule A: δ = 1.00 (t, $^3J_{\mathrm{HH}}$ = 7.2 Hz, CH$_3$, 3H), 2.01 (sext., $^3J_{\mathrm{HH}}$ = 7.2 Hz, 2H, CH$_2$), 4.45 (t, $^3J_{\mathrm{HH}}$ = 7.8 Hz, 2H, NCH$_2$), 7.26 (d, $^3J_{\mathrm{HH}}$ = 9.3 Hz, 2H, H-5/6), 7.60 (d, $^3J_{\mathrm{HH}}$ = 9.3 Hz, 2H, H-4/7), 7.84 (s, 2H, H-3/8).

Molecule B:

δ = 0.47 (t, $^3J_{\mathrm{HH}}$ = 7.4 Hz, 3H, CH$_3$), 1.59 (sext., $^3J_{\mathrm{HH}}$ = 7.4 Hz, 2H, CH$_2$), 4.09 (t, $^3J_{\mathrm{HH}}$ = 7.4 Hz, 2H, NCH$_2$), 7.20 (d, $^3J_{\mathrm{HH}}$ = 9.2 Hz, 2H, H-5/6), 7.54 (d, $^3J_{\mathrm{HH}}$ = 9.2 Hz, 2H, H-4/7), 7.81 (s, 2H, H-3/8).

with LiHMDS:

Lithium hexamethyldisilazide (2.5 mg, 16 μmol, 2.01 eq) was added at -30 °C to a suspension of **3b** (4.3 mg, 7.4 μmol, 1eq) in 0.4 mL of THF-d$_8$. The light brown suspension

turned dark brown. After 45 min a ^{1}H NMR was measured. Only one deprotonated species is obtained.

^{1}H NMR(400.13 MHz, THF-d_8): one species is obtained
δ = 1.03 (t, $^{3}J_{HH}$ = 7.4 Hz, CH_3, 3H), 2.08 (sext., $^{3}J_{HH}$ = 7.4 Hz, 2H, CH_2), 4.58 (t, $^{3}J_{HH}$ = 7.4 Hz, 2H, NCH_2), 7.47 (d, $^{3}J_{HH}$ = 9.4 Hz, 2H, H-5/6), 7.77 (d, $^{3}J_{HH}$ = 9.4 Hz, 2H, H-4/7), 8.18 (s, 2H, H-3/6).

The reaction was repeated and the spectrum shows two set of signals in a ratio of 0.7:1 (A:B).

^{1}H NMR(400.13 MHz, THF-d_8):
Molecule A: δ = 0.47 (t, $^{3}J_{HH}$ = 7.4 Hz, 3H, CH_3), 1.58 (sext., $^{3}J_{HH}$ = 7.3 Hz, 2H, CH_2), 4.08 (t, $^{3}J_{HH}$ = 7.4 Hz, 2H, NCH_2), 7.26 (d, $^{3}J_{HH}$ = 9.3 Hz, 2H, H-5/6), 7.59 (d, $^{3}J_{HH}$ = 9.3 Hz, 2H, H-4/7), 7.80 (s, 2H), 7.80 (s, 2H, H-3/8)

Molecule B: δ = 0.98 (br s, CH_3, 3H, CH_3), 1.99 (br s, 2H, CH_2), 4.43 (br s, 2H, NCH_2), 7.20 (d, $^{3}J_{HH}$ = 9.2 Hz, 2H, H-5/6), 7.55 (d, $^{3}J_{HH}$ = 9.2 Hz, 2H, H-4/7), 7.85 (br s, 2H, H-3/8).

^{13}C{^{1}H} NMR (100.61 MHz, THF-d_8, -80 °C):
δ = 11.3 and 11.7 (CH_3), 25.23 (under THF-signal: both CH_2 signals), 54.6 and 54.8 (NCH_2), 112.8, 113.1, 116.7, 123.8, 194.2 (q, $^{1}J_{CLi}$ = 24.5 Hz, C-1/10), 197.8 (q, $^{1}J_{CLi}$ = 21.8 Hz, C-1/10).
All other signals could not be assigned.

^{7}Li{^{1}H} NMR (194.4 MHz, THF-d_8, -80 °C):
Molecule A and B: δ = 2.86 (br s) and 1.90 (s).

^{7}Li{^{1}H} NMR (194.4 MHz, THF-d_8):

Molecule A and B: δ = 2.85 (s) and 1.79 (br s).

9.3.48 *In situ* generation of Li-mani$^{t\mathrm{Bu}}$R$_2$ 39a

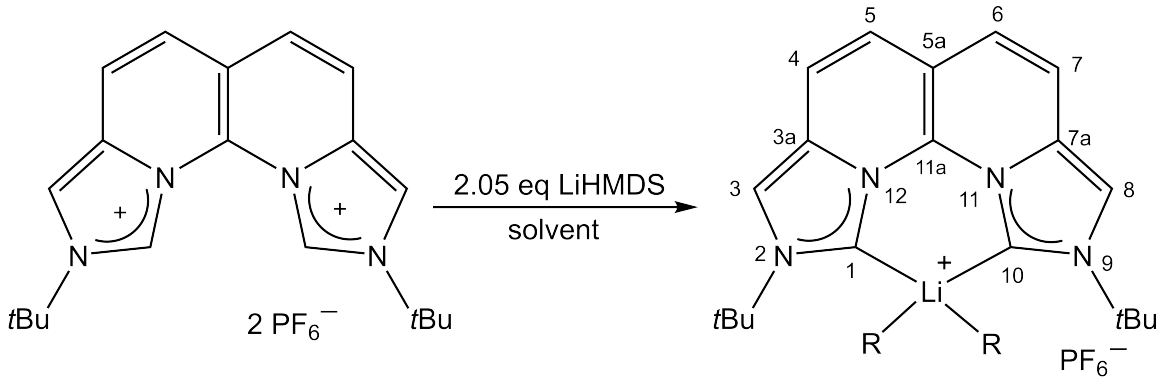

In THF-d_8:

Lithium hexamethyldisilazide (4.0 mg, 24 μmol, 2.1 eq) was added at -30 °C to a suspension of **3a** (7 mg, 11 μmol, 1eq) in 0.4 mL of THF-d_8. A ^{1}H NMR spectrum of the yellow solution and brown solid is measured after 45 min. Two species are obtained.

^{1}H NMR(400.13 MHz, THF-d_8):

Molecule A:

δ = 1.95 (s, 18H, C(CH$_3$)$_3$), 7.14 (d, $^{3}J_{\mathrm{HH}}$ = 9.3 Hz, 2H, H-5/6), 7.49 (d, $^{3}J_{\mathrm{HH}}$ = 9.3 Hz, 2H, H-4/7), 7.96 (s, 2H, H-3/8).

Molecule B:

δ = 1.81 (br s, 18H, C(CH$_3$)$_3$), 7.19 (d, $^{3}J_{\mathrm{HH}}$ = 8.8 Hz, 2H, H-5/6), 7.57 (d, $^{3}J_{\mathrm{HH}}$ = 8.8 Hz, 2H, H-4/7), 8.07 (s, 2H, H-3/8).

^{19}F{^{1}H}NMR (376.48 MHz, CD$_3$CN)

δ = - 73.85 (d, $^{1}J_{\mathrm{PF}}$ = 710 Hz, PF6$^-$)

^{31}P{^{1}H} NMR (161.97 MHz, CD$_3$CN)

δ = - 144.1 (sept, $^1J_{PF}$ = 710 Hz, $PF6^-$)

In CD_3CN:

Lithium hexamethyldisilazide (6 mg, 36 μmol, 2.1 eq) was added at -30 °C to a suspension of **3a** (10 mg, 16 μmol, 1eq) in 0.4 mL of CD_3CN. The dark brown suspension was filtered. From the filtrate a ^{1}H NMR spectrum is measured after 45 min.

^{1}H NMR(400.13 MHz, CD_3CN):

δ = 1.82 (s, 18H, $C(CH_3)_3$), 7.48 (d, $^3J_{HH}$ = 9.5 Hz, 2H, H-5/6), 7.74 (d, $^3J_{HH}$ = 9.5 Hz, 2H, H-4/7), 8.10 (s, 2H, H-3/8).

9.3.49 *In situ* generation of Na-mani$^{n\mathrm{Pr}}$ 40a

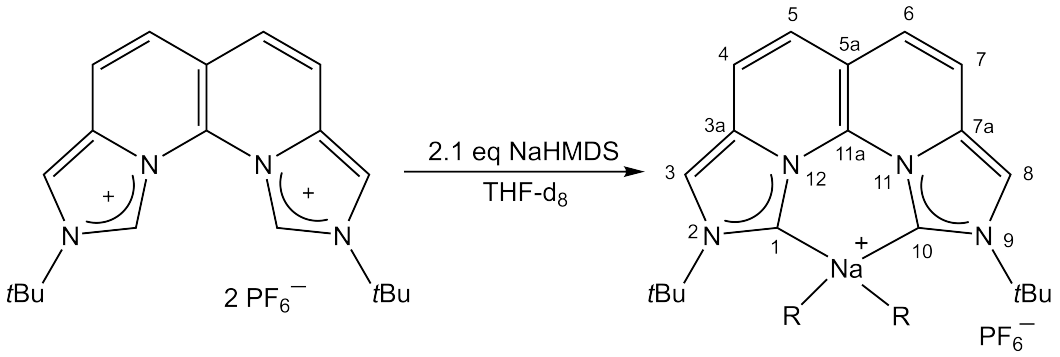

3a **40a**
R = THF, 1/2 mani$^{n\mathrm{Pr}}$

Sodium hexamethyldisilazide (4.4 mg, 24 μmol, 2.1 eq) was added at -30 °C to a suspension of **3a** (7.0 mg, 11 μmol, 1 eq) in 0.4 mL of THF-d_8. A ^{1}H NMR spectrum of the dark brown suspension is measured after 45 min.

^{1}H NMR(400.13 MHz, THF-d_8):
δ = 1.77 (s, 18H, C(CH_3)$_3$), 7.08 (d, $^3J_{HH}$ = 9.3 Hz, 2H, H-5/6), 7.46 (d, $^3J_{HH}$ = 9.3 Hz, 2H, H-4/7), 7.94 (s, 2H, H-3/8).

9.3.50 *In situ* generation of K-mani$^{n\mathrm{Pr}}$ 41a

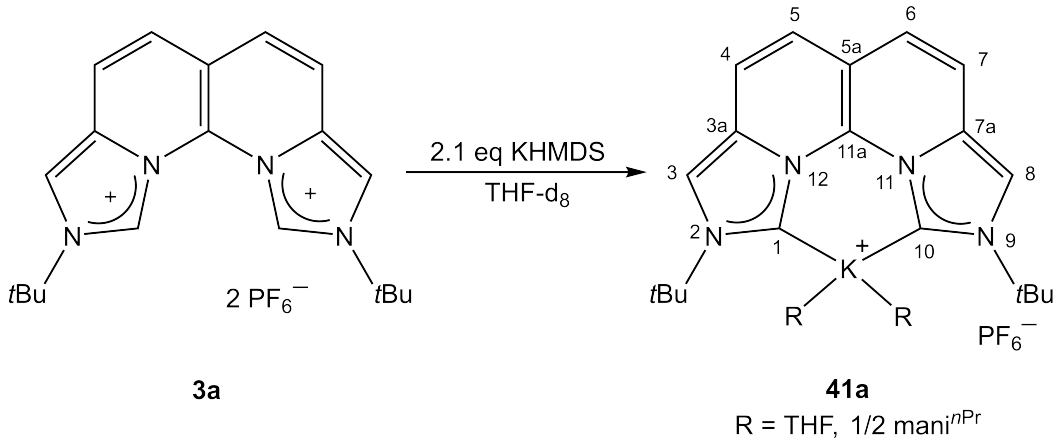

Potassium hexamethyldisilazide (4.8 mg, 24 μmol, 2.1 eq) was added at -30 °C to a suspension of **3a** (7.0 mg, 11 μmol, 1 eq) in 0.4 mL of THF-d_8. A ^{1}H NMR spectrum of the dark brown suspension is measured after 45 min.

^{1}H NMR(400.13 MHz, THF-d_8):

δ = 1.74 (s, 18H, $C(CH_3)_3$), 6.90 (d, $^3J_{HH}$ = 9.0 Hz, 2H, H-5/6), 7.26 (d, $^3J_{HH}$ = 9.0 Hz, 2H, H-4/7), 7.65 (s, 2H, H-3/8).

9.3.51 [Pt(mani$^{n\mathrm{Pr}}$)(CH_3)$_2$] 42a

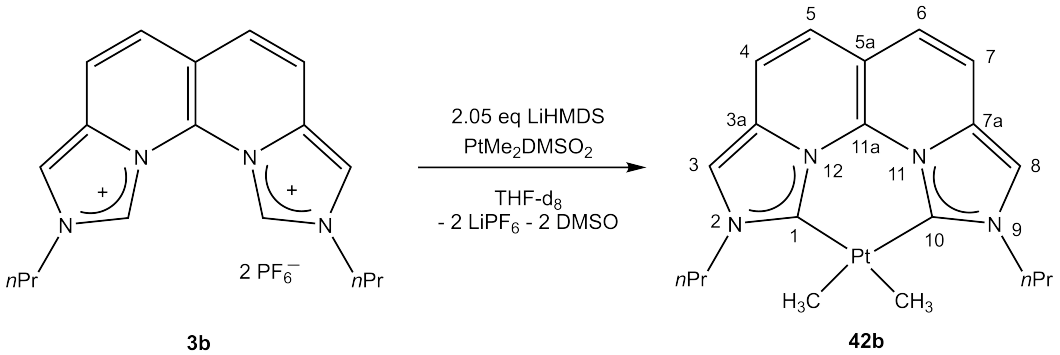

Lithium hexamethyldisilazide (30.1 mg, 170 μmol, 2.1 eq) was added to a suspension of **3a** (50.0 mg, 85.6 mol, 1 eq) in 2 mL of THF-d_8. The dark brown suspension was stirred for 20 min, [Pt(DMSO)Me_2] (32.6 mg, 85.5 μmol, 1 eq) was added. After 2 h the dark brown suspension was filtered over neutral alumina. The yellow solution was dried in vacuo and washed with *n*-pentane. The product was obtained as a yellow solid.

^{1}H NMR (400.11 MHz, THF-d_8):
δ = 0.35 (s+sat, $^2J_{\mathrm{PtH}}$ = 65.7 Hz, 3H, Pt-CH_3), 0.91 (t, $^3J_{\mathrm{HH}}$ = 14.8 Hz, 6H, CH_3), 1.89 (sext, $^3J_{\mathrm{HH}}$ = 7.5 Hz, 2H, CH_2), 4.41 (t, $^3J_{\mathrm{HH}}$ = 7.5 Hz, 3H, NCH_2), 6.89 (d, $^4J_{\mathrm{HH}}$ = 9.5 Hz, H-5/6), 7.20 (d, $^4J_{\mathrm{HH}}$ = 9.5 Hz, H-4/7), 7.44 (s+sat $^4J_{\mathrm{PtH}}$ = 7.2 Hz, 3/8).

^{13}C{^{1}H} NMR (100.61 MHz, THF-d_8):
δ = -5.1 (Pt-CH_3), 11.5 (CH_3), 25.23 (CH_2), 53.4 (NCH_2), 113.5 (C-3/8), 115.9 (C-4/7), 122.9 (C-5/6), 130.7 (C-3a/7a), 171.5 (C-1/10).
signals for C-5a/12a can not be detected.

10 Abbreviations

acac	acetylacetonate
Ac_2O	acetic anhydride
AcOH	acetic acid
Bn	benzyl-
CD_3CN	acetonitrile-d_3
CD_2Cl_2	dichloromethane-d_2
COD	cycloocta-1,5-diene
DME	1,2-dimethoxyethane
DMSO	dimethylsulfoxide
EtOH	ethanol
ESI	electrospray ionization
Eq	equivalents
HMBC	Heteronuclear Multiple Bond Correlation
HMDS	hexamethyldisilazane
HOMO	Highest Occupied Molecular Orbital
HSQC	Heteronuclear Single Quantum Coherence
iPr	*i*-propyl-
LUMO	Lowest Unoccupied Molecular Orbital
NTf	bis(trifluoromethanesulfonyl)
NMR	Nuclear Magnetic Resonance
***n*Pr**	*n*-propyl-
ppm	parts per million
rt	room temperature
***t*Bu**	*tert*-butyl-
THF	tetrahydrofurane
TMEDA	tetramethylethylendiamin

11 Crystal data

11.1 10a

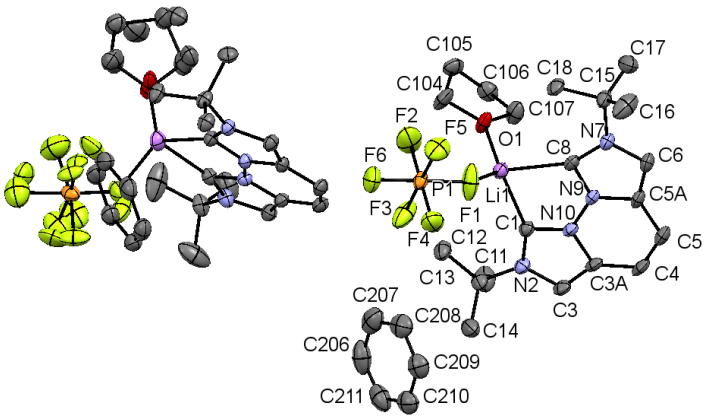

Identification code	mo_EM15_2_0ma_a_tw
Empirical formula	C_{26} H_{36} F_6 Li N_4 O P
Formula weight	572.50
Temperature	103(2) K
Wavelength	0.71073 Å
Crystal system	Monoclinic
Space group	$P2_1/n$
Unit cell dimensions	a = 24.520(7) Å $\alpha = 90°$.
	b = 9.689(3) Å $\beta = 90.279(7)°$.
	c = 24.546(7) Å $\gamma = 90°$.
Volume	5831(3) $Å^3$
Z	8
Density (calculated)	1.304 Mg/m^3
Absorption coefficient	0.158 mm^{-1}
F(000)	2400
Crystal size	0.410 x 0.106 x 0.086 mm^3
Theta range for data collection	1.171 to 29.164°

Index ranges	-33<=h<=33, -13<=k<=13, -33<=l<=33
Reflections collected	15687
Independent reflections	15687 [R(int) = 0.0835]
Completeness to theta = 25.242°	100.0 %
Absorption correction	Semi-empirical from equivalents
Max. and min. transmission	0.7458 and 0.6227
Refinement method	Full-matrix least-squares on F2
Data / restraints / parameters	15687 / 999 / 817
Goodness-of-fit on F2	1.009
Final R indices [I>2σ(I)]	R1 = 0.0604, wR2 = 0.1244
R indices (all data)	R1 = 0.1094, wR2 = 0.1456
Extinction coefficient	n/a
Largest diff. peak and hole	0.932 and -0.505 e.Å^{-3}

Table 14: Crystal data and structure refinement for **10a**.

11.2 12a

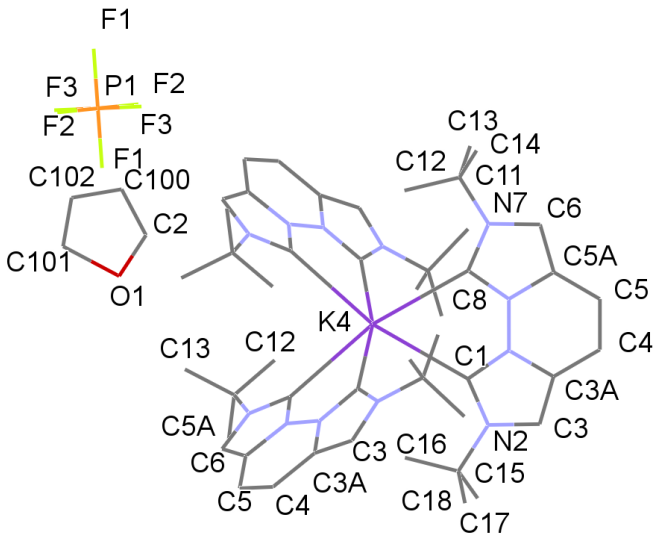

Identification code	mo_KF374_0m_numerical_monoklin final
Empirical formula	C_{56} H_{82} F_6 K N_{12} O_2 P
Formula weight	1139.40
Temperature	100(2) K
Wavelength	0.71073 Å
Crystal system	Monoclinic
Space group	$C2/c$
Unit cell dimensions	a = 25.540(2) Å $\alpha = 90°$.
	b = 14.7512(12) Å $\beta = 118.1370(10)°$.
	c = 18.080(2) Å $\gamma = 90°$.
Volume	6006.7(10) Å^3
Z	4
Density (calculated)	1.260 Mg/m^3
Absorption coefficient	0.284 mm^{-1}
F(000)	2424
Crystal size	0.176 x 0.166 x 0.103 mm^3
Theta range for data collection	1.807 to 29.201°.

Index ranges	-34<=h<=35, -20<=k<=20, -24<=24<=20
Reflections collected	38094
Independent reflections	8424 [R(int) = 0.0589]
Completeness to theta = 25.242°	100.0 %
Absorption correction	Semi-empirical from equivalents
Max. and min. transmission	0.7461 and 0.5307
Refinement method	Full-matrix least-squares on F2
Data / restraints / parameters	8424 / 508 / 410
Goodness-of-fit on F2	1.007
Final R indices [I>2σ(I)]	R1 = 0.0745, wR2 = 0.0943
R indices (all data)	R1 = 0.1299, wR2 = 0.2390
Extinction coefficient	n/a
Largest diff. peak and hole	0.569 and -0.415 e.Å^{-3}

Table 15: Crystal data and structure refinement for **12a**.

11.3 Na[15-crown-5]PF_6

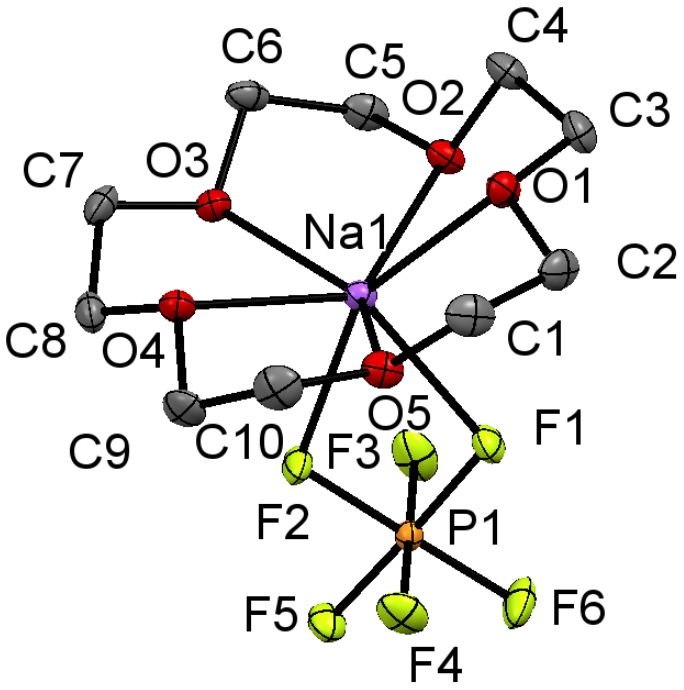

Identification code	mo_KF319_0m_final
Empirical formula	C_{10} H_{20} F_6 Na O_5 P
Formula weight	388.22
Temperature	100(2) K
Wavelength	0.71073 Å
Crystal system	Monoclinic
Space group	$P2_1/c$
Unit cell dimensions	a = 10.1653(17) Å $\alpha = 90°$.
	b = 10.2411(18) Å $\beta = 95.416(3)°$.
	c = 15.447(3) Å $\gamma = 90°$.
Volume	1601.0(5) $Å^3$
Z	4
Density (calculated)	1.611 Mg/m^3
Absorption coefficient	0.281 mm^{-1}

F(000)	800
Crystal size	0.448 x 0.120 x 0.106 mm^3
Theta range for data collection	2.012 to 28.277°.
Index ranges	-13<=h<=11, -13<=k<=13, -20<=l<=20
Reflections collected	24551
Independent reflections	3971 [R(int) = 0.0663]
Completeness to theta = 25.242°	99.7 %
Absorption correction	Semi-empirical from equivalents
Max. and min. transmission	0.7461 and 0.5307
Refinement method	Full-matrix least-squares on F2
Data / restraints / parameters	3971 / 0 / 208
Goodness-of-fit on F2	1.089
Final R indices [I>2σ(I)]	R1 = 0.0423, wR2 = 0.0915
R indices (all data)	R1 = 0.0638, wR2 = 0.0990
Extinction coefficient	n/a
Largest diff. peak and hole	0.363 and -0.488 e.$Å^{-3}$

Table 16: Crystal data and structure refinement for Na[15-crown-5]PF_6

11.4 16a

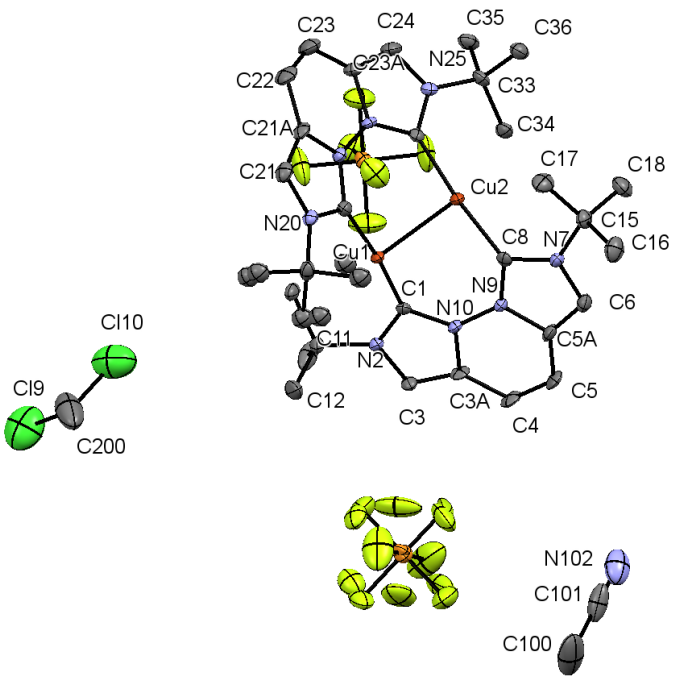

Identification code	mo_ND48_0m_final
Empirical formula	C_{35} H_{49} Cl_2 Cu_2 F_{12} N_9 P_2
Formula weight	1083.75
Temperature	100 K
Wavelength	0.71073 Å
Crystal system	Orthorhombic
Space group	*Pbca*
Unit cell dimensions	a = 19.08(2) Å $\alpha = 90°$.
	b = 17.91(2) Å $\beta = 90°$.
	c = 26.37(3) Å $\gamma = 90°$.
Volume	9011(17) $Å^3$
Z	8
Density (calculated)	1.598 Mg/m^3
Absorption coefficient	1.222 mm^{-1}
F(000)	4416

Crystal size	0.320 x 0.124 x 0.107 mm^3
Theta range for data collection	1.740 to 23.825°.
Index ranges	-21<=h<=20, -20<=k<=20, -29<=l<=29
Reflections collected	72860
Independent reflections	6920 [R(int) = 0.0948]
Completeness to theta = 23.825°	99.8 %
Absorption correction	Numerical
Max. and min. transmission	0.6765 and 0.6053
Refinement method	Full-matrix least-squares on F2
Data / restraints / parameters	6920 / 299 / 637
Goodness-of-fit on F2	1.034
Final R indices [I>2σ(I)]	R1 = 0.0567, wR2 = 0.1505
R indices (all data)	R1 = 0.0839, wR2 = 0.1700
Extinction coefficient	n/a
Largest diff. peak and hole	1.126 and -1.524 e.$Å^{-3}$

Table 17: Crystal data and structure refinement for **16a**.

11.5 19a

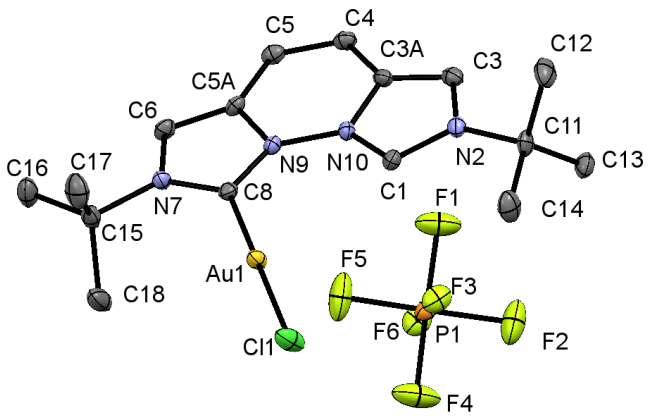

Identification code	KF77_monoklin
Empirical formula	C_{16} H_{23} Au Cl F_6 N_4 P
Formula weight	648.77
Temperature	173(2) K
Wavelength	0.71073 Å
Crystal system	Monoclinic
Space group	$P2_1/n$
Unit cell dimensions	a = 9.1818(2) Å $\alpha = 90°$.
	b = 18.7358(4) Å $\beta = 95.4300(10)°$.
	c = 12.3976(3) Å $\gamma = 90°$.
Volume	2123.17(8) $Å^3$
Z	4
Density (calculated)	2.030 Mg/m^3
Absorption coefficient	7.192 mm^{-1}
F(000)	1248
Crystal size	0.329 x 0.220 x 0.176 mm^3
Theta range for data collection	1.976 to 30.573°.
Index ranges	-13<=h<=13, -26<=k<=26, -17<=l<=17
Reflections collected	91194

Independent reflections	6502 [R(int) = 0.0685]
Completeness to theta = 25.242°	100.0 %
Refinement method	Full-matrix least-squares on F2
Data / restraints / parameters	6502 / 0 / 268
Goodness-of-fit on F2	1.018
Final R indices [I>2σ(I)]	R1 = 0.0257, wR2 = 0.0394
R indices (all data)	R1 = 0.0453, wR2 = 0.0432
Extinction coefficient	n/a
Largest diff. peak and hole	1.304 and -0.956 e.Å^{-3}

Table 18: Crystal data and structure refinement for **19a**.

11.6 23a

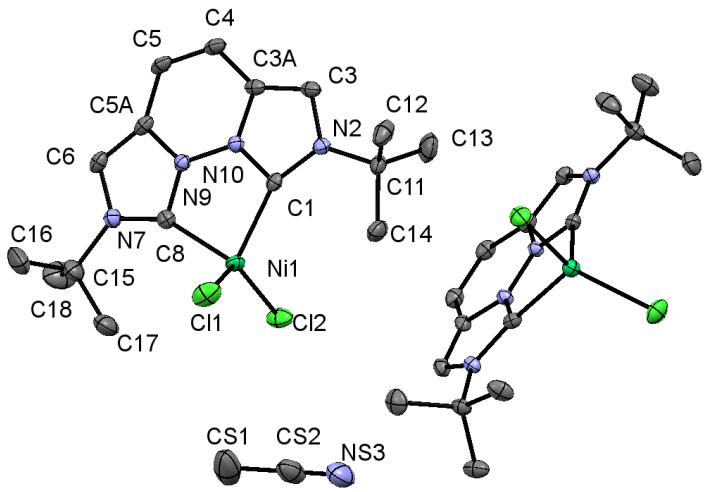

Identification code	mo_fb16_0m
Empirical formula	C_{34} H_{47} Cl_4 N_9 Ni_2
Formula weight	841.02
Temperature	150 K
Wavelength	0.71073 Å
Crystal system	Monoclinic
Space group	$P2_1/c$
Unit cell dimensions	a = 18.3309(12) Å $\alpha = 90°$.
	b = 8.9844(6) Å $\beta = 99.5790(10)°$.
	c = 23.9920(15) Å $\gamma = 90°$.
Volume	3896.2(4) $Å^3$
Z	4
Density (calculated)	1.434 Mg/m^3
Absorption coefficient	1.278 mm^{-1}
F(000)	1752

Crystal size	0.161 x 0.153 x 0.064 mm^3
Theta range for data collection	1.127 to 29.649°.
Index ranges	-25<=h<=25, -12<=k<=12, -33<=l<=30
Reflections collected	77903
Independent reflections	11028 [R(int) = 0.0781]
Completeness to theta = 25.242°	100.0 %
Absorption correction	Numerical
Max. and min. transmission	0.7459 and 0.6626
Refinement method	Full-matrix least-squares on F2
Data / restraints / parameters	11028 / 0 / 455
Goodness-of-fit on F2	1.002
Final R indices [I>2σ(I)]	R1 = 0.0388, wR2 = 0.0720
R indices (all data)	R1 = 0.0792, wR2 = 0.0858
Extinction coefficient	n/a
Largest diff. peak and hole	0.436 and -0.483 e.$Å^{-3}$

Table 19: Crystal data and structure refinement for **23a**.

11.7 22a

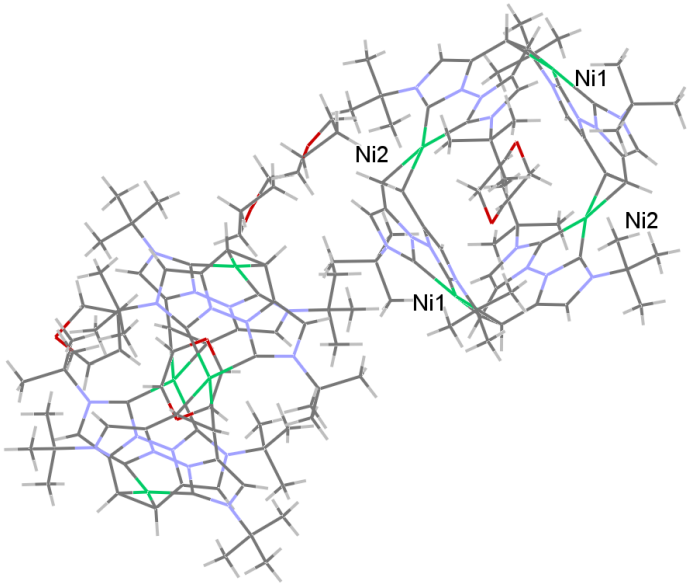

Identification code	mo_KF238_2_newfirst	
Empirical formula	C_{80} H_{115} N_{16} Ni_4 O_4	
Formula weight	1599.71	
Temperature	173(2) K	
Wavelength	0.71073 Å	
Crystal system	Triclinic	
Space group	$P\bar{1}$	
Unit cell dimensions	a = 14.1158(13) Å	$\alpha = 83.024(3)°$.
	b = 14.5624(13) Å	$\beta = 77.557(2)°$.
	c = 19.7003(18) Å	$\gamma = 80.766(2)°$.
Volume	3887.3(6) $Å^3$	
Z	2	
Density (calculated)	1.367 Mg/m^3	
Absorption coefficient	1.014 mm^{-1}	
F(000)	1702	
Crystal size	0.057 x 0.080 x 0.087 mm^3	
Theta range for data collection	1.063 to 24.430°C.	

Index ranges	-16<=h<=16, -16<=k<=16, -22<=l<=22
Reflections collected	76530
Independent reflections	12761 [R(int) = 0.1434]
Completeness to theta = 24.430°	99.5 %
Refinement method	Full-matrix least-squares on F2
Data / restraints / parameters	12761 / 927 / 958
Goodness-of-fit on F2	1.084
Final R indices [I>2sigma(I)]	R1 = 0.0728, wR2 = 0.1563
R indices (all data)	R1 = 0.1236, wR2 = 0.1796
Extinction coefficient	n/a
Largest diff. peak and hole	1.545 and -1.452 e.Å^{-3}

Table 20: Crystal data and structure refinement for **22a**.

11.8 27a

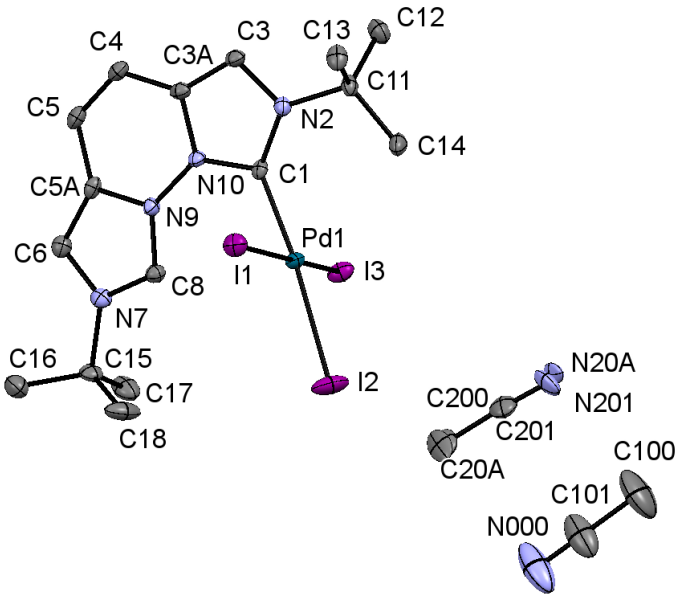

Identification code	mo_DAT7_0m-monoklin_pl
Empirical formula	C_{20} H_{29} I_3 N_6 Pd
Formula weight	840.59
Temperature	173(2) K
Wavelength	0.71073 Å
Crystal system	Monoclinic
Space group	$P2_1/c$
Unit cell dimensions	a = 15.7169(18) Å $\alpha = 90°$.
	b = 9.5344(11) Å $\beta = 98.289(2)°$.
	c = 18.638(2) Å $\gamma = 90°$.
Volume	2763.8(5) Å^3
Z	4
Density (calculated)	2.020 Mg/m^3
Absorption coefficient	4.040 mm^{-1}
F(000)	1584
Crystal size	0.924 x 0.134 x 0.129 mm^3

Theta range for data collection	2.208 to 26.518[3].
Index ranges	-19<=h<=17, -11<=k<=11, -23<=l<=23
Reflections collected	36494
Independent reflections	5711 [R(int) = 0.0374]
Completeness to theta = 25.242[3]	100.0 %
Absorption correction	Semi-empirical from equivalents
Max. and min. transmission	0.7457 and 0.5881
Refinement method	Full-matrix least-squares on F2
Data / restraints / parameters	5711 / 0 / 296
Goodness-of-fit on F2	1.097
Final R indices [I>2σ(I)]	R1 = 0.0289, wR2 = 0.0718
R indices (all data)	R1 = 0.0326, wR2 = 0.0745
Extinction coefficient	n/a
Largest diff. peak and hole	2.322 and -1.722 e.Å^{-3}

Table 21: Crystal data and structure refinement for **27a**.

11.9 29a

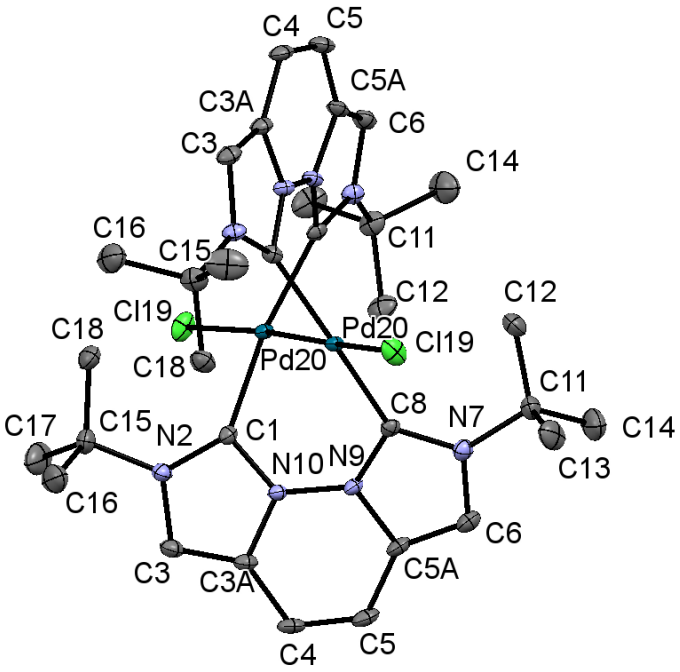

Identification code	mo_TR11a_0m_multiscana
Empirical formula	C_{32} H_{44} Cl_2 N_8 Pd_2
Formula weight	824.45
Temperature	100 K
Wavelength	0.71073 Å
Crystal system	Orthorhombic
Space group	*Aba2*
Unit cell dimensions	a = 17.984(3) Å $\alpha = 90°$.
	b = 16.898(2) Å $\beta = 90°$.
	c = 11.092(2) Å $\gamma = 90°$.
Volume	3370.9(9) $Å^3$
Z	4
Density (calculated)	1.625 Mg/m^3
Absorption coefficient	1.261 mm^{-1}
F(000)	1672

Crystal size	0.329 x 0.225 x 0.182 mm^3
Theta range for data collection	2.265 to 30.657°.
Index ranges	-25<=h<=25, -24<=k<=24, -15<=l<=15
Reflections collected	30177
Independent reflections	5176 [R(int) = 0.0273]
Completeness to theta = 25.242°	100.0 %
Absorption correction	Semi-empirical from equivalents
Max. and min. transmission	0.6586 and 0.5552
Refinement method	Full-matrix least-squares on F2
Data / restraints / parameters	5176 / 1 / 205
Goodness-of-fit on F2	1.035
Final R indices [I>2σ(I)]	R1 = 0.0182, wR2 = 0.0461
R indices (all data)	R1 = 0.0195, wR2 = 0.0468
Absolute structure parameter	0.022(8)
Extinction coefficient	n/a
Largest diff. peak and hole	0.843 and -0.278 e.$Å^{-3}$

Table 22: Crystal data and structure refinement for **29a**.

11.10 32b

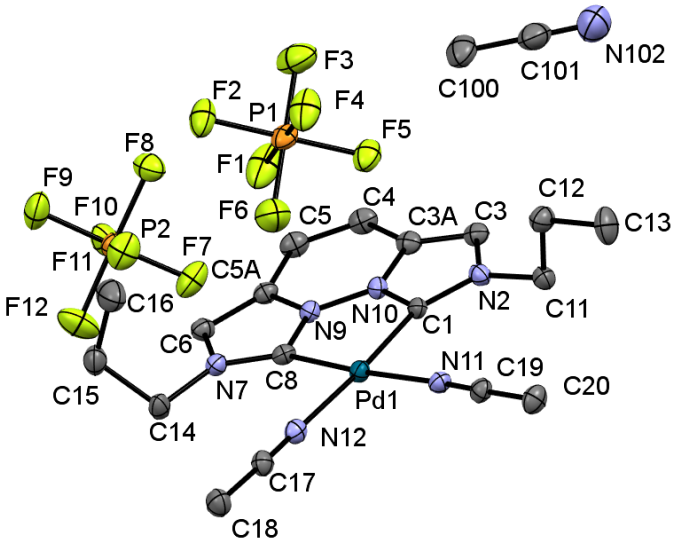

Identification code	mo_TS14_0m_numerical
Empirical formula	C_{20} H_{21} D_6 F_{12} N_7 P_2 Pd
Formula weight	767.86
Temperature	173(2) K
Wavelength	0.71073 Å
Crystal system	Triclinic
Space group	$P\bar{1}$
Unit cell dimensions	a = 9.279(5) Å $\alpha = 102.629(6)°$.
	b = 12.723(6) Å $\beta = 97.100(6)°$.
	c = 13.613(7) Å $\gamma = 110.408(5)°$.
Volume	1434.3(13) $Å^3$
Z	2
Density (calculated)	1.778 Mg/m^3
Absorption coefficient	0.862 mm^{-1}
F(000)	760
Crystal size	0.711 x 0.124 x 0.085 mm^3
Theta range for data collection	2.369 to 28.304°.

Index ranges	-12<=h<=12, -16<=k<=16, -18<=l<=18
Reflections collected	24096
Independent reflections	7015 [R(int) = 0.0746]
Completeness to theta = 25.242°	99.9 %
Refinement method	Full-matrix least-squares on F2
Data / restraints / parameters	7015 / 345 / 387
Goodness-of-fit on F2	1.039
Final R indices [I>2σ(I)]	R1 = 0.0801, wR2 = 0.2262
R indices (all data)	R1 = 0.0944, wR2 = 0.2416
Extinction coefficient	n/a
Largest diff. peak and hole	3.143 and -1.125 e.Å^{-3}

Table 23: Crystal data and structure refinement for **32b**.

11.11 33a

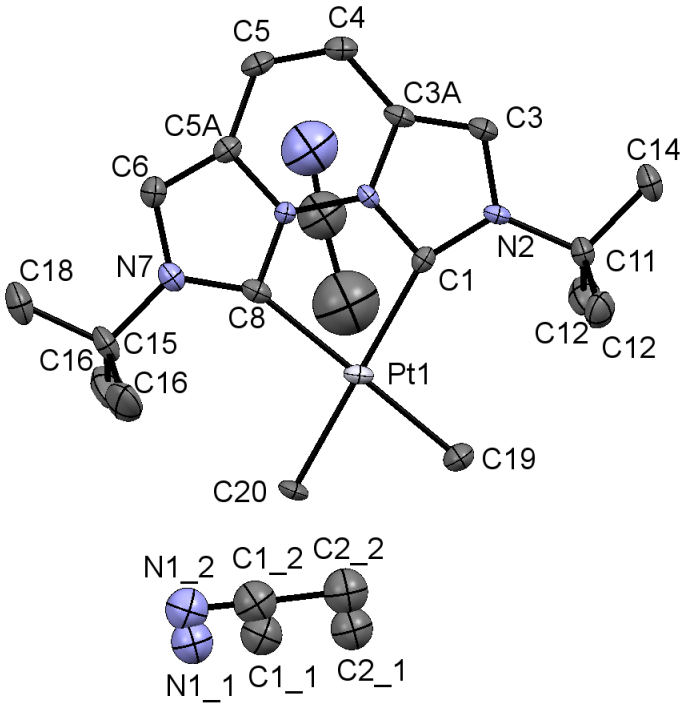

Identification code	mo_KF239_0m_Cilia
Empirical formula	C_{24} H_{43} N_7 Pt
Formula weight	104.55
Temperature	100 K
Wavelength	0.71073 Å
Crystal system	Orthorhombic
Space group	*Pnma*
Unit cell dimensions	a = 19.533(8) Å $\alpha = 90°$.
	b = 6.803(3) Å $\beta = 90°$.
	c = 18.249(7) Å $\gamma = 90°$.
Volume	2425.0(17) $Å^3$
Z	8
Density (calculated)	0.573 Mg/m^3
Absorption coefficient	5.743 mm^{-1}

F(000)	341
Crystal size	0.088 x 0.120 x 0.606 mm^3
Theta range for data collection	2.085 to 28.282°.
Index ranges	-26<=h<=26, -9<=k<=9, -24<=l<=24
Reflections collected	36667
Independent reflections	3250 [R(int) = 0.0470]
Completeness to theta = 25.242°	99.8 %
Refinement method	Full-matrix least-squares on F2
Data / restraints / parameters	3250 / 102 / 198
Goodness-of-fit on F2	1.054
Final R indices [I>2σ(I)]	R1 = 0.0287, wR2 = 0.0704
R indices (all data)	R1 = 0.0317, wR2 = 0.0721
Extinction coefficient	n/a
Largest diff. peak and hole	2.947 and -1.238 e.$Å^{-3}$

Table 24: Crystal data and structure refinement for **33a**.

11.12 33b

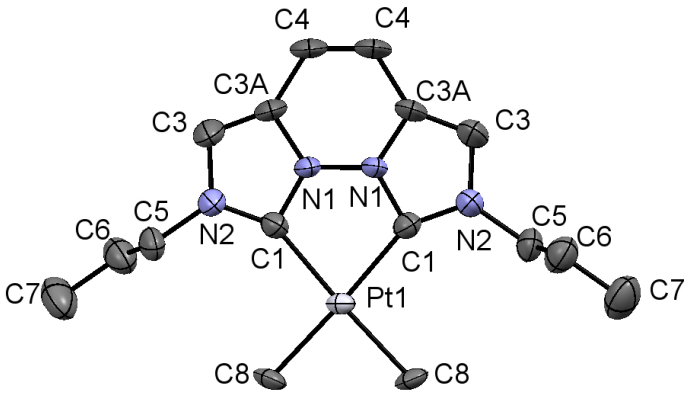

Identification code	mo_TS11_0m_multiscana
Empirical formula	C_{16} H_{24} N_4 Pt
Formula weight	467.48
Temperature	100 K
Wavelength	0.71073 Å
Crystal system	Trigonal
Space group	$P3_121$
Unit cell dimensions	a = 10.3912(17) Å $\alpha = 90°$.
	b = 10.3912(17) Å $\beta = 90°$.
	c = 14.709(3) Å $\gamma = 120°$.
Volume	1375.5(5) $Å^3$
Z	3
Density (calculated)	1.693 Mg/m^3
Absorption coefficient	7.651 mm^{-1}
F(000)	678
Crystal size	0.118 x 0.104 x 0.085 mm^3
Theta range for data collection	2.263 to 30.517°.
Index ranges	-14<=h<=14, -14<=k<=14, -20<=l<=20
Reflections collected	12833
Independent reflections	2438 [R(int) = 0.0476]

Completeness to theta = 25.242°	77.2 %
Absorption correction	Semi-empirical from equivalents
Max. and min. transmission	0.5523 and 0.3679
Refinement method	Full-matrix least-squares on F2
Data / restraints / parameters	2438 / 48 / 99
Goodness-of-fit on F2	1.035
Final R indices [I>2σ(I)]	R1 = 0.0244, wR2 = 0.0500
R indices (all data)	R1 = 0.0289, wR2 = 0.0512
Absolute structure parameter	0.005(9)
Extinction coefficient	n/a
Largest diff. peak and hole	1.205 and -1.418 e.Å^{-3}

Table 25: Crystal data and structure refinement for **33b**.

11.13 34

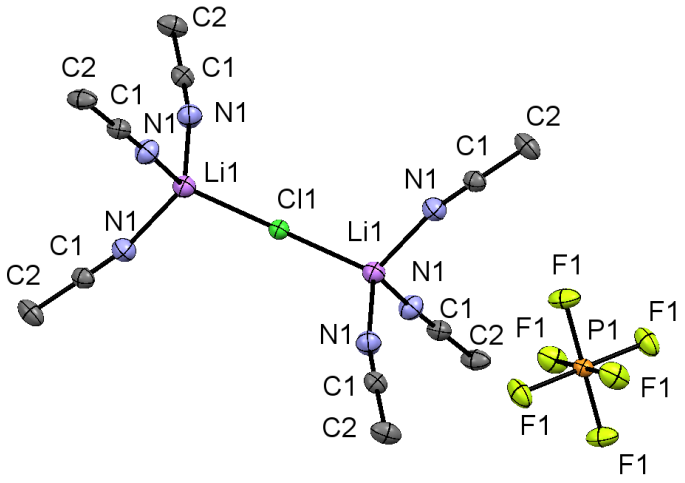

Identification code	mo_TR9b_0m_rhomohedral_3stirch
Empirical formula	C_{12} H_{18} Cl F_6 Li_2 N_6 P
Formula weight	440.62
Temperature	373(2) K
Wavelength	0.71073 Å
Crystal system	Trigonal
Space group	$R\bar{3}$
Unit cell dimensions	a = 11.308(3) Å $\alpha = 90°$.
	b = 11.308(3) Å $\beta = 90°$.
	c = 14.683(4) Å $\gamma = 120°$.
Volume	1626.0(8) $Å^3$
Z	3
Density (calculated)	1.350 Mg/m^3
Absorption coefficient	0.308 mm^{-1}
F(000)	672
Crystal size	0.406 x 0.260 x 0.187 mm^3
Theta range for data collection	2.500 to 33.929°.
Index ranges	-17<=h<=17, -17<=k<=17, -22<=l<=23

Reflections collected	13697
Independent reflections	1455 [R(int) = 0.0790]
Completeness to theta = 25.242°	99.5 %
Refinement method	Full-matrix least-squares on F2
Data / restraints / parameters	1455 / 0 / 45
Goodness-of-fit on F2	1.050
Final R indices [I>2σ(I)]	R1 = 0.0420, wR2 = 0.1061
R indices (all data)	R1 = 0.0599, wR2 = 0.1145
Extinction coefficient	n/a
Largest diff. peak and hole	0.428 and -0.563 e.Å^{-3}

Table 26: Crystal data and structure refinement for **34**.

11.14 36a

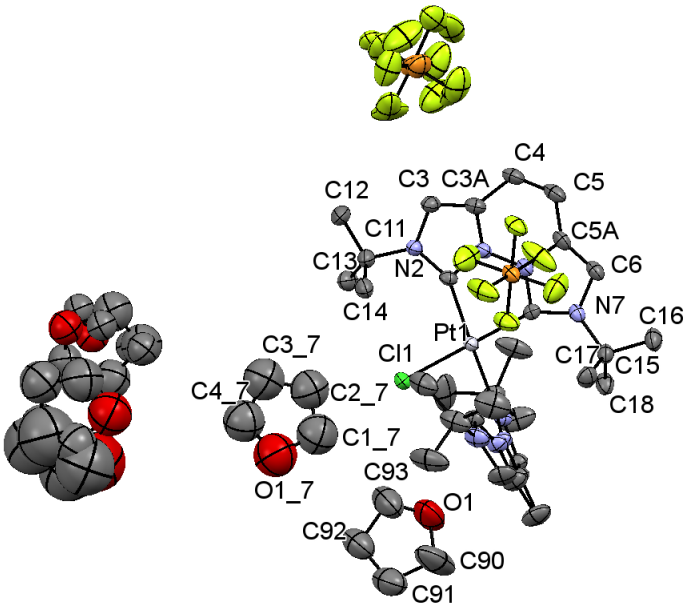

Identification code	mo_Kf192_triklin_centro
Empirical formula	C_{48} H_{77} Cl F_{12} N_8 O_4 P_2 Pt
Formula weight	1350.65
Temperature	100 K
Wavelength	0.71073 Å
Crystal system	Triclinic
Space group	$P\bar{1}$
Unit cell dimensions	a = 11.575(2) Å $\alpha = 68.414(6)°$.
	b = 15.407(3) Å $\beta = 72.082(6)°$.
	c = 18.463(3) Å $\gamma = 75.321(6)°$.
Volume	2876.5(9) $Å^3$
Z	2
Density (calculated)	1.559 Mg/m^3
Absorption coefficient	2.628 mm^{-1}
F(000)	1372
Crystal size	0.195 x 0.074 x 0.017 mm^3

Theta range for data collection	1.221 to 26.551°.
Index ranges	-14<=h<=14, -19<=k<=19, -23<=l<=23
Reflections collected	68640
Independent reflections	11851 [R(int) = 0.0738]
Completeness to theta = 25.242°	100.0 %
Absorption correction	Numerical
Max. and min. transmission	0.7454 and 0.6464
Refinement method	Full-matrix least-squares on F2
Data / restraints / parameters	11851 / 806 / 853
Goodness-of-fit on F2	1.064
Final R indices [I>2σ(I)]	R1 = 0.0417, wR2 = 0.0913
R indices (all data)	R1 = 0.0576, wR2 = 0.0972
Extinction coefficient	n/a
Largest diff. peak and hole	1.333 and -1.136 e.Å^{-3}

Table 27: Crystal data and structure refinement for **36a**.

12 List of publications

Publications

Generation of Annelated Biscarbenes and Their Alkali-Metal Chelate Complexes in Solution: Equilibrium between Hetero- and Homoleptic NHC Lithium Complexes - K. S. Flaig, B. Raible, V. Mormul, N. Denninger, C. Maichle-Mössmer, D. Kunz, *Organometallics*, **2018**, *37*, 1291-1303.

The coordinative flexibility of rigid phenantrholine-analogous di(NHC)-ligands - K. S. Flaig, D. Kunz, *Coordination Chemistry Reviews*, **2018**, *377*, 73-85.

Presentations

Synthesis of a heterodinuclear silver- and gold-NHC complex - 6th EuCheMS Chemistry Congress, Sevilla, **2016**.

Synthese und dynamisches Verhalten von Bis(NHC)-Metallkomplexen - Anorganisches Seminar, Universität Tübingen, **2018**.

Dynamisches Verhalten von chelatisierenden Bis(NHC)-Li-Komplexen - Koordinationschemietreffen, Heidelberg, **2018**.

A rigid annelated bis(NHC) ligand with unusual flexibility - 22. Tag der Organischen Chemie, TOCUS, Stuttgart, **2018**.

Posterpresentations

Synthesis and characterization of dinuclear silver- and gold-NHC-complexes, Goslar, 12. Iminiumsalztagung (IMSAT), **2015**.

Synthesis of a heterodinuclear silver- and gold-NHC complex, Sevilla, 6th EuCheMS Chemistry Congress, **2016**.

Characterization of a dinuclear silver-NHC complex and the formation of a heterodinuclear silver-gold-NHC complex, Potsdam, 13. Koordinationschemietreffen, **2017**.

Synthesis of Ni(0), Ni(II) and Pt(II) complexes with chelating bis(NHC) ligands, Conference on Organometallic Chemistry XXII (EuCOMC), Amsterdam, **2017**.

Alkali- and Group 10-Metal complexes of a Dicarbene Ligand: Dynamic Behavior and Structural Characterization, Organometallic Chemistry Gordon Research Seminar (GRS), Newport, RI, USA, **2018**.

Alkali- and Group 10-Metal complexes of a Dicarbene Ligand: Dynamic Behavior and Structural Characterization, Organometallic Chemistry Gordon Research Conference (GRC), Newport, RI, USA, **2018**.

13 Molecular directory

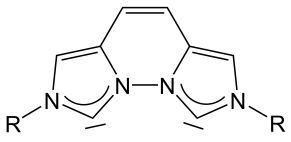

1a,**b**

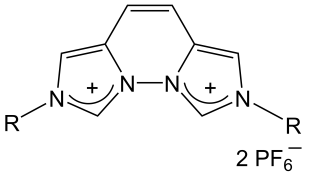

2a,**b**

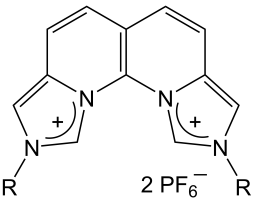

3a,**b**

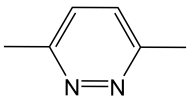

4

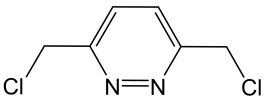

5

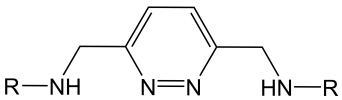

6

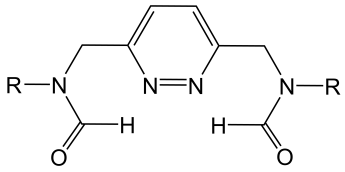

7a,b

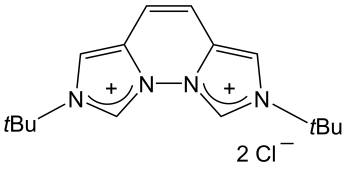

8

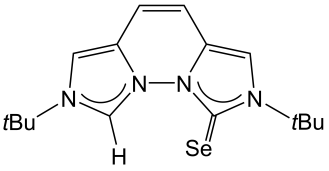

9

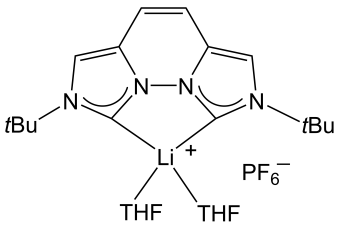

10a

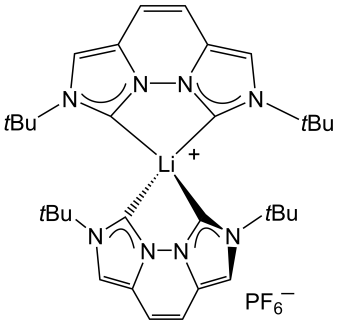

10a-H

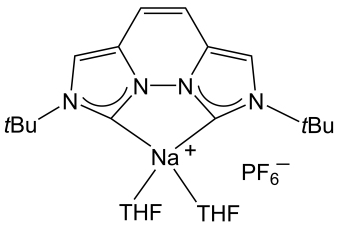

11a,b

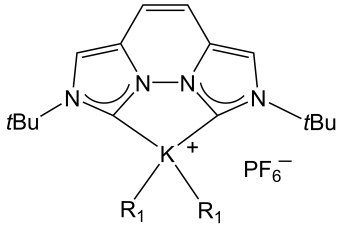

12a,b
R_1 = vegi^{tbu}

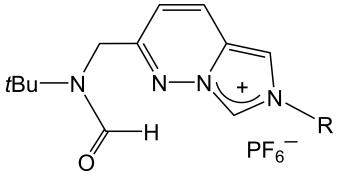

13

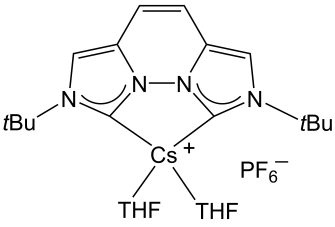

14a,b

R = *t*Bu (**a**), *n*Pr (**b**)

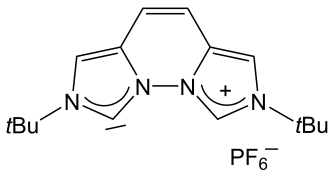

15a

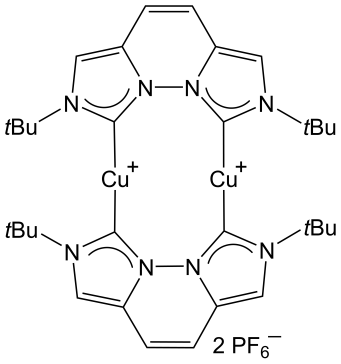

16

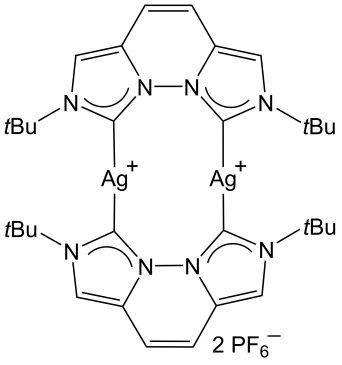

17

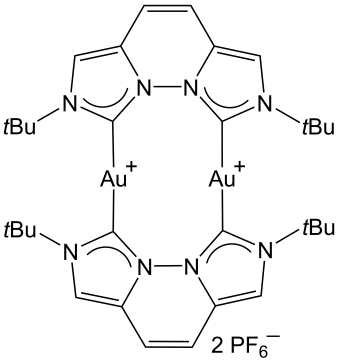

18

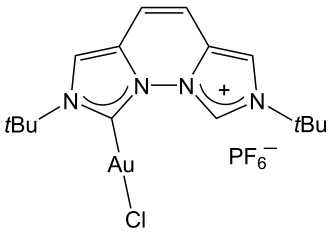

19

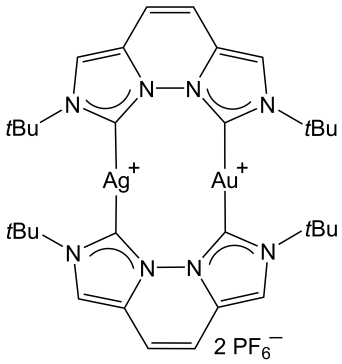

20

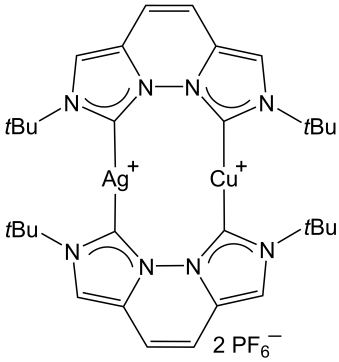

21

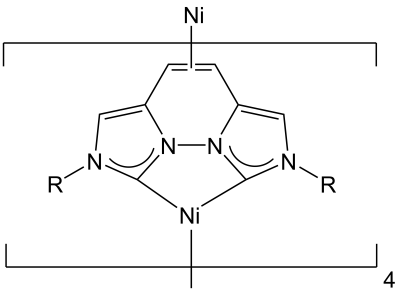

22a,b

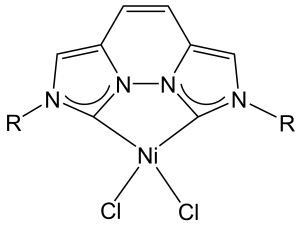

23a,b

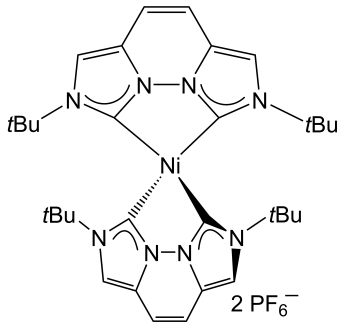

24

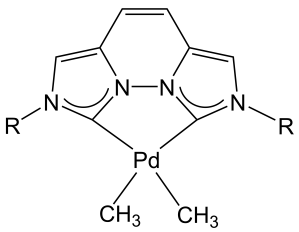

25a,b

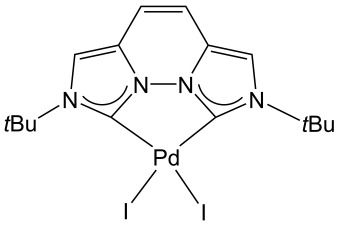

26

R = *t*Bu (**a**), *n*Pr (**b**)

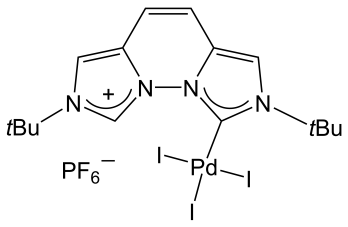

27

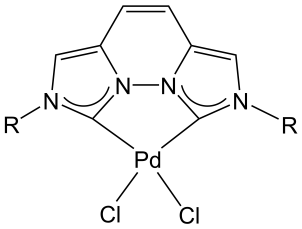

28a,b

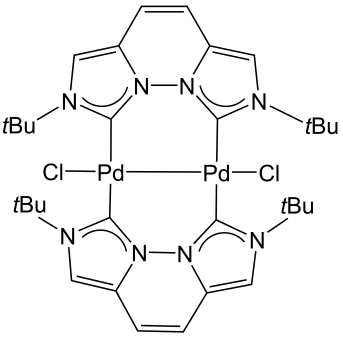

29

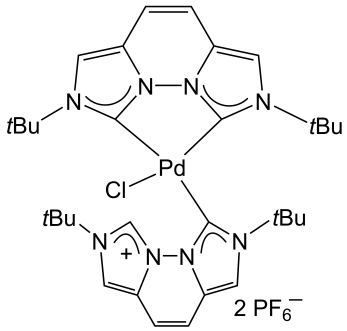

30

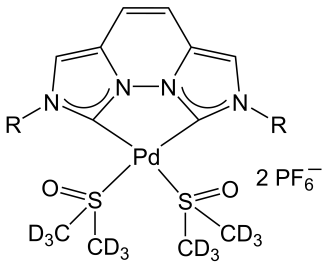

31a,b

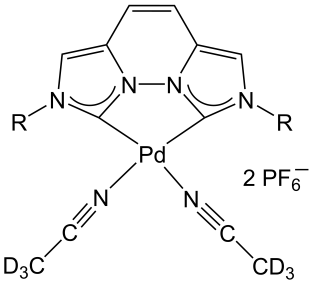

32a,b

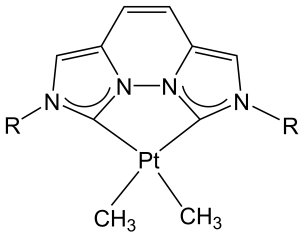

33a,b

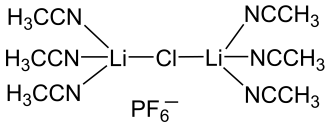

34

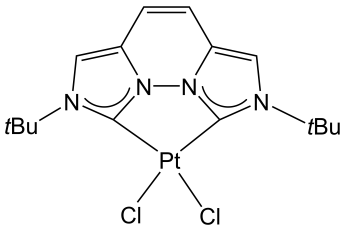

35a

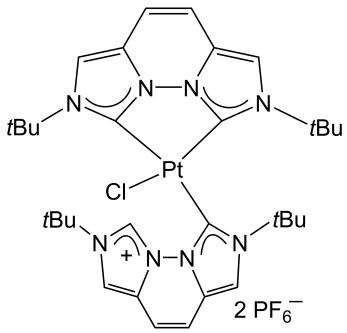

36a

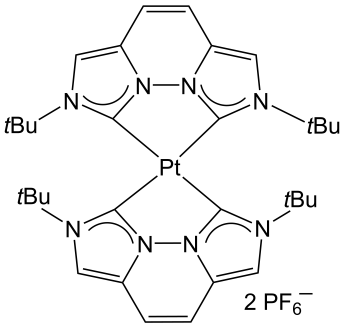

37

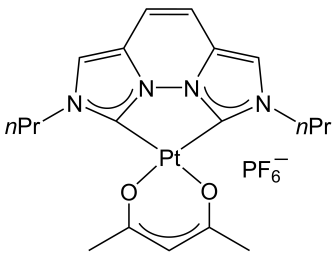

38b

R = *t*Bu (**a**), *n*Pr (**b**)

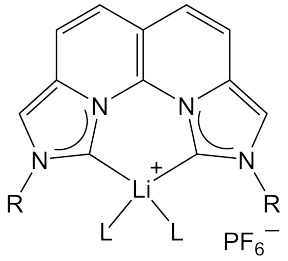

39a,b
L = mani^{R}, THF, PF_6

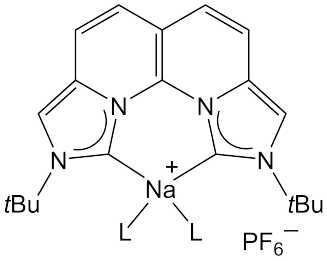

40a
L = mani^{R}, THF, PF_6

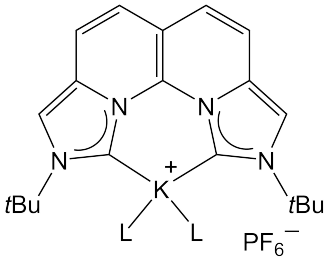

41a
L = mani^{R}, THF, PF_6

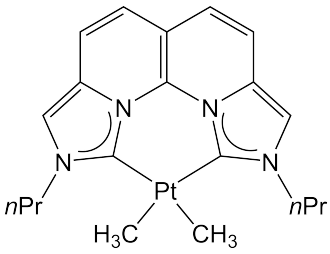

42b
L = mani^{R}, THF, PF_6

R = *t*Bu (**a**), *n*Pr (**b**)

14 Acknowledgment

I would like to thank:

Prof. Dr. Doris Kunz, for giving me the opportunity to work in her group, for providing the interesting research topic and for all of the support she has provided, both as a mentor in the lab and through the memorable dinner invitations over the years including delicious homemade meals for all of the group members.

Prof. Dr. Reiner Anwander for reviewing this thesis.

The research group members Fabio Mazzotta, Manfred Steimann, Ronja Jordan, Theo Maulbetsch, Yingying Tian, all former members and our neighbor research group Seitz for the good work atmosphere and the fun times in- and outside the lab.

All my practical students Franziska Freitag, Thomas Herster, Julian Seidel, Fabio Mazzotta, Christian Gienger, Anh Thy Dam, Khoa Linh Pham, Eric Moinet, Theresa Rieser and Tanno Schmid for their good cooperation and interesting discoveries.

Dr. Cecilia Maichle-Mössmer for helping me with the refinement of many molecular structures.

Dr. Klaus Eichele, Kristina Strohmeier, Dr. Wolfgang Leis for the special NMR measurements.

Dr. Dorothee Wistuba and Dr. Peter Haiss for the mass spectrometry, Wolfang Bock for the elemental analysis, and Paul Schuler for the EPR measurements.

Sabine Ehrlich for all administration matters.

Anna Stärz, Fabio Mazzotta, Theo Maulbetsch and Ronja Jordan for proofreading this thesis.

All my former classmates thank you for a lifetime of memories. Especially Anna Stärz for her support, the help with the cover design and our friendship.

Christopher for his loving support, all of the wonderful times and for always making me laugh.

My whole family for their love and support. Especially, my grandmother and my brother who I can always count on for honest advice.

Most of all, my loving parents for always believing in me. Words cannot express how much their encouragement and unconditional love means to me.

References

[1] W. von Eggers Doering, A. K. Hoffmann, *J. Am .Chem. Soc.* **1954**, *76*, 6162–6165.

[2] A. Igau, H. Grützmacher, A. Baceiredo, G. Bertrand, *J. Am .Chem. Soc.* **1988**, *110*, 6463–6466.

[3] H.-W. Wanzlick, H.-J. Schönherr, *Angew. Chem. Int. Ed.* **1968**, *7*, 141–142.

[4] K. J. Öfele, *Organomet. Chem.* **1968**, *12*, 42–43.

[5] D. J. Cardin, B. Cetinkaya, M. F. Lappert, *Chem. Rev.* **1972**, *72*, 545–574.

[6] M. F. Lappert, *Organomet. Chem.* **1988**, *358*, 185–213.

[7] A. J. Arduengo III, R. L. Harlow, M. Kline, *J. Am. Chem. Soc.* **1991**, *113*, 361–363.

[8] W. A. Herrmann, *Angew. Chem. Int. Ed.* **2002**, *41*, 1290–1309.

[9] F. E. Hahn, M. C. Jahnke, *Angew. Chem. Int. Ed.* **2008**, *47*, 3122–3172.

[10] S. Díez-Gonzáles, N. Marion, S. P. Nolan, *Chem. Rev.* **2009**, *109*, 3612–3676.

[11] D. Bourissou, O. Guerret, F. P. Gabbaï, G. Bertrand, *Chem. Rev.* **2000**, *100*, 39–91.

[12] H. V. Huynh, *Chem. Rev.* **2018**, *118*, 9457–9492.

[13] H. Jacobsen, A. Correa, A. Poater, C. Costabile, L. Cavallo, *Coord. Chem. Rev.* **2009**, *253*, 687–703.

[14] R. W. Alder, E. Blake, L. Chaker, J. N. Harvey, F. Paolini, J. Schütz, *Angew. Chem. Int. Ed.* **2004**, *43*, 5896–5911.

[15] S. Díez-Gonzáles, S. P. Nolan, *Coord. Chem. Rev.* **2007**, *251*, 874–883.

[16] W. A. Herrmann, M. Elison, J. Fischer, C. Köcher, G. R. J. Artus, *Angew. Chem. Int. Ed.* **1995**, *34*, 2371–2374.

[17] U. Radius, F. M. Bickelhaupt, *Coord. Chem. Rev.* **2009**, *253*, 678–686.

[18] L. A. Tschugajeff, M. S. Skanawy-Grigorjewa, A. Posnjak, *Anorg. und Allg. Chem.* **1925**, *148*, 37–42.

[19] L. A. Tschugajeff, M. S. Skanawy-Grigorjewa, *J. Russ. Physico-Chemical Soc.* **1915**, *47*, 776–777.

[20] A. Burke, A. L. Balch, J. H. Enemark, *J. Am .Chem. Soc.* **1970**, *92*, 2555–2557.

[21] G. Rouschias, B. L. Shaw, *J. Chem. Soc. Chem. Commun.* **1970**, *183*.

[22] W. A. Herrmann, M. Elison, J. Fischer, C. Koecher, G. R. J. Artus, *Chem. Eur. J.* **1996**, *2*, 722–780.

[23] M. Poyatos, W. McNamara, C. Incarvito, E. Peris, R. H. Crabtree, *Chem. Commun.* **2007**, *5*, 2267–2269.

[24] M. Poyatos, W. McNamara, C. Incarvito, E. Clot, E. Peris, R. H. Crabtree, *Organometallics* **2008**, *27*, 2128–2136.

[25] G. Guisado-Barrios, J. Bouffard, B. Donnadieu, G. Bertrand, *Organometallics* **2011**, *30*, 6017–6021.

[26] S. Schick, T. Pape, F. E. Hahn, *Organometallics* **2014**, *33*, 4035–4041.

[27] C. Jandl, A. Pöthig, *Acta Cryst. Sect. C. Struct. Chem.* **2017**, *73*, 1131–1136.

[28] C. Jandl, A. Pöthig, *Chem. Commun.* **2017**, *53*, 2098–2101.

[29] M. Poyatos, A. J. Mata, E. Peris, *Chem. Rev.* **2009**, *109*, 3677–3707.

[30] V. Gierz, *PhD thesis*, Universität Tübingen, **2012**.

[31] V. Gierz, A. Urbanaite, A. Seyboldt, D. Kunz, *Organometallics* **2012**, *31*, 7532–7538.

[32] V. Gierz, C. Maichle-Mössmer, D. Kunz, *Organometallics* **2012**, *31*, 739–747.

[33] N. Denninger, *Zulassungsarbeit*, Universität Tübingen, **2012**.

[34] B. Raible, *PhD thesis*, Universität Tübingen, **2015**.

[35] B. Raible, V. Gierz, D. Kunz, *Organometallics* **2015**, *34*, 2018–2027.

[36] B. Raible, *Diplomarbeit*, Universität Tübingen, **2011**.

[37] V. Gierz, A. Seyboldt, C. Maichle-Mössmer, K. W. Törnroos, M. T. Speidel, K. Eichele, D. Kunz, *Organometallics* **2012**, *31*, 7893–7901.

[38] J. Hahn, *Diplomarbeit*, Universität Tübingen, **2012**.

[39] D. Kunz, V. Gierz, *Metal Complexes WO 2012/079741 A1* **2010**.

[40] V. Gierz, C. Maichle-Mössmer, D. Kunz, *Organometallics* **2012**, *31*, 739–747.

[41] unpublished results, M. Steimann.

[42] K. S. Flaig, B. Raible, V. Mormul, N. Denninger, C. Maichle-Mössmer, D. Kunz, *Organometallics* **2018**, *37*, 1291–1303.

[43] R. H. Wiley, *J. Macromol. Sci. Chem.* **1987**, *24*, 1183–1190.

[44] P. D. Mayo, J. B. Stothers, M. C. Usselman, *Can. J. Chem.* **1972**, *50*, 612–617.

[45] B. Raible, *Diplomarbeit*, Universität Tübingen, **2015**.

[46] J.-R. Dormoy, B. Castro, *Tetrahedron* **1981**, *37*, 3699–3706.

[47] O. Back, M. Henry-Ellinger, C. D. Martin, D. Martin, G. Bertrand, *Angew. Chem. Int. Ed.* **2013**, *52*, 2939–2943.

[48] R. R. Rodrigues, C. L. Dorsey, C. A. Arceneaux, T. W. Hudnall, *Chem. Commun.* **2014**, *50*, 162–164.

[49] A. Liske, K. Verlinden, H. Buhl, K. Schaper, C. Ganter, *Organometallics* **2013**, *32*, 5269–5272.

[50] D. J. Nelson, F. Nahra, S. R. Patrick, D. B. Cordes, A. M. Z. Slawin, S. P. Nolan, *Organometallics* **2014**, *33*, 3640–3645.

[51] D. J. Nelson, A. Collado, S. Manzinim, S. Meiries, A. M. Z. Slawin, D. B. Cordes, S. P. Nolan, *Organometallics* **2014**, *33*, 2048–2058.

[52] D. Buck, *Diplomarbeit*, Universität Tübingen, **2013**.

[53] T. Dröge, F. Glorius, *Angew. Chem. Int. Ed.* **2010**, *49*, 6940–6952.

[54] Y. Chu, H. Deng, J.-P. Cheng, *J. Org. Chem.* **2007**, *72*, 7790–7793.

[55] A. M. Magill, K. J. Cavell, B. F. Yates, *J. Am. Chem. Soc.* **2004**, *126*, 8717–8724.

[56] T. L. Amyes, S. T. Diver, J. P. Richard, F. M. Rivas, K. Toth, *J. Am. Chem. Soc.* **2004**, *126*, 4366–4374.

[57] W. A. Herrmann, C. Köcher, *Angew. Chem. Int. Ed.* **1997**, *36*, 2162.

[58] A. J. Arduengo III, *Angew. Acc. Chem. Res.* **1999**, *32*, 913–921.

[59] P. de Frémont, N. Marion, S. P. Nolan, *Coord. Chem. Rev.* **2009**, *253*, 862–892.

[60] D. Ripin, D. Evans, *pKa tables* **2005**.

[61] F. G. Bordwell, *Acc. Chem. Res.* **1988**, *21*, 456–463.

[62] G. Boche, C. Hilf, K. Harms, M. Marsch, J. C. W. Lohrenz, *Angew. Chem. Int. Ed.* **1995**, *34*, 487–489.

[63] Z. Yoshida, H. Konishi, S. Sawada, H. Ogoshi, *J. Chem. Soc. Chem. Commun.* **1997**, 850–851.

[64] H. Konishi, S. Matsumoto, Y. Kamitori, H. Ogoshi, Z. Yoshida, *Chem. Lett.* **1978**, *7*, 241–244.

[65] R. Weiss, C. Priesner, H. Wolf, *Angew. Chem. Int. Ed.* **1978**, *7*, 446–447.

[66] V. Lavallo, Y. Ishida, B. Donnadieu, G. Betrand, *Angew. Chem. Int. Ed.* **2006**, *45*, 6652–6655.

[67] V. Lavallo, Y. Canac, B. Donnadieu, W. W. Schoeller, G. Bertrand, *Science* **2006**, *312*, 722–724.

[68] R. W. Alder, E. M. Blake, C. Bortolotti, S. Bufali, C. P. Butts, E. Linehan, J. M. Olivia, A. G. Orpen, M. J. Quayle, *Chem. Commun.* **1999**, *43*, 241–242.

[69] A. Koch, H. Goerls, S. Krieck, M. Westerhausen, *Dalton Trans.* **2017**, *46*, 9058–9067.

[70] M. S. Hill, G. Kociok-Köhn, D. J. MacDougall, *Inorg. Chem.* **2011**, *50*, 5234–5241.

[71] D. R. Armstrong, S. E. Baillie, V. L. Blair, N. G. Chabloz, J. Diez, J. Garcia-Alvarez, A. R. Kennedy, S. D. Roberston, E. Hevia, *Chem. Sci.* **2013**, *4*, 4259–4266.

[72] L. C. H. Maddock, T. Cadenbach, A. R. Kennedy, I. Borilovic, G. Aromì, E. Hevia, *Inorg. Chem.* **2015**, *54*, 9201–9210.

[73] M. Brendel, R. Engelkle, V. G. Desai, F. Rominger, P. Hofmann, *Organometallics* **2015**, *34*, 2870–2878.

[74] A. J. Arduengo, H. V. R. Dias, R. L. Harlow, M. Kline, *J. Am .Chem. Soc.* **1992**, *114*, 5530–5534.

[75] D. Tapu, D. A. Dixon, C. Roe, *Chem. Rev.* **2009**, *109*, 3385–3407.

[76] W. Bauer, W. R. Winchester, P. v. R. Schleyer, *Organometallics* **1987**, *6*, 2371–2379.

[77] C. Elschenbroich, *Organometallchemie*, B. G. Teubner, Ed.; GMW: Wiesbaden, **2008**.

[78] T. Simler, L. Karmazin, C. Bailly, P. Braunstein, A. Danopoulos, *Organometallics* **2016**, *35*, 903–912.

[79] K. S. Flaig, D. Kunz, *Coord. Chem. Rev.* **2018**, *377*, 73–85.

[80] F. H. Allen, *Acta Cryst. Sect. B: Struct. Sci.* **2002**, *58*, 380–388.

[81] B. Raible, D. Kunz, *Z. Naturforsch. B: Chem. Sci.* **2016**, *71*, 659–666.

[82] J. P. Wagner, P. R. Schreiner, *Angew. Chem. Int. Ed.* **2015**, *54*, 12274–12296.

[83] J. P. Wagner, P. R. Schreiner, *Chem. Theory Comput.* **2016**, *12*, 231–237.

[84] D. J. Liptrot, P. P. Power, *Nature Rev. Chem.* **2017**, *1*, 0004.

[85] A. L. Hawley, C. A. Ohlin, L. Fohlmeister, A. Stasch, *Chem. Eur. J.* **2017**, *23*, 447–455.

[86] S. Grimme, J. Antony, S. Ehrlich, H. Krieg, *J. Chem. Phy.* **2010**, *132*, 154104.

[87] F. Weller, H. Borgholte, H. Stenger, S. Vogler, K. Dehnicke, *Z. Naturforsch. B. Chem. Sci.* **1989**, *44*, 1524–1530.

[88] V. Nesterov, D. Reiter, P. Bag, P. Frisch, R. H. A. Porzelt, S. Inoue, *Chem. Rev.* **2018**, *118*, 9678–9842.

[89] A. I. Ojeda-Amador, A. J. Martinez, A. R. Kennedy, C. T. OHara, *Inorg. Chem.* **2016**, 5719–5728.

[90] C. Müller, A. Stahlich, L. Wirtz, C. Gretsch, V. Huch, A. Schäfer, *Inorg. Chem.* **2018**, *57*, 8050–8053.

[91] C. Boehme, G. Frenking, *J. Am .Chem. Soc.* **1996**, *118*, 2039–2046.

[92] C. Heinemann, T. Mueller, Y. Apeloig, J. Schwarz, *J. Organomet. Chem.* **1996**, *118*, 2023–2038.

[93] R. Schwesinger, H. Schlemper, C. Hasenfratz, J. Willaredt, T. Dambcher, T. Breuer, C. Ottaway, M. Fletschinger, J. Boele, H. Fritz, D. Putzas, H. W. Rotter, F. G. Bordwell, A. V. Statish, G.-Z. Ji, E.-M. Peters, K. Peters, H. G. von Schnering, L. Walz, *Liebigs Ann.* **1996**, 1055–1081.

[94] H. Schlemper, R. Schwesinger, *Angew. Chem. Int. Ed.* **1987**, *26*, 1167–1169.

[95] W. A. Herrmann, O. Runte, G. Artus, *J. Organomet. Chem.* **1995**, *501*, C1–C4.

[96] J. C. Y. Lin, R. T. W. Huang, C. S. Lee, A. Bhattacharyya, W. S. Hwang, I. J. B. Lin, *Chem. Rev.* **2009**, *109*, 3561–3598.

[97] A. J. Arduengo, H. V. R. Dias, J. C. Calabrese, F. Davidson, *Organometallics* **1993**, *12*, 3405–3409.

[98] H. M. J. Wang, I. J. B. Lin, *Organometallics* **1998**, *17*, 972–975.

[99] I. J. B. Lin, C. S. Vasam, *Coord. Chem. Rev.* **2007**, *251*, 642–670.

[100] J. C. Garrison, W. J. Youngs, *Chem. Rev.* **2005**, *105*, 3978–4008.

[101] J. Ramírez, R. Corberán, M. Sanaú, E. Peris, E. Fernandez, *Chem. Commun.* **2005**, *24*, 3056–3058.

[102] A. Melaiye, R. S. Simons, A. Milsted, F. Pingitore, C. Wesdemiotis, C. A. Tessier, W. J. Youngs, *Med. Chem.* **2004**, *47*, 973–977.

[103] S. Hase, Y., Kayaki, T. Ikariya, *Organometallics* **2013**, *32*, 5285–5288.

[104] N. Mézailles, L. Ricard, F. Gagosz, *Org. Let.* **2005**, *7*, 4133–4136.

[105] S. Díez-Gonzáles, S. P. Nolan, *Angew. Chem. Int. Ed.* **2008**, *47*, 8881–8884.

[106] T. Nakamura, T. Terashima, K. Ogata, S.-i. Fukuzawa, *Org. Lett.* **2011**, *13*, 620–623.

[107] C. Tubaro, A. Biffis, R. Gava, E. Scattolin, A. Volpe, M. Basato, M. M. Díaz-Requejo, P. Perez, *Eur. J. Org. Chem.* **2012**, 1367–1372.

[108] T. Simler, P. Braunstein, A. A. Danopoulos, *Dalton Trans.* **2016**, *45*, 5122–5139.

[109] K. Nomiya, S. Morozumi, Y. Yanagawa, M. Hasegawa, K. Kurose, K. Taguchi, R. Sakamoto, K. Mihara, N. C. Kasuga, *Inorg. Chem.* **2018**, *57*, 11322–11332.

[110] C. Boehme, G. Frenking, *Organometallics* **1998**, *17*, 5801.

[111] D. Nemcsok, K. Wichmann, G. Frenking, *Organometallics* **2004**, *23*, 3640.

[112] I. J. B. Lin, C. S. Vasam, *Can. J. Chem* **2005**, *83*, 812–825.

[113] A. A. D. Tulloch, A. A. Danopoulos, S. Kleinhenz, E. M. Hursthouse, B. M. Eastham, *Organometallics* **2011**, *20*, 2027–2031.

[114] K. S. Flaig, *Master thesis*, Universität Tübingen, **2015**.

[115] P. Pyykkö, *Chem. Rev.* **1997**, *97*, 597–636.

[116] J. Emsley, *The Elements 3rd ed.; Oxford University Press: New York* **1998**.

[117] A. Bondi, *J. Phys. Chem.* **1964**, *68*, 441–451.

[118] S. Sculfort, P. Braunstein, *Chem. Soc. Rev.* **2011**, *40*, 2741–2760.

[119] H. Schmidbaur, A. Schier, *Angew. Chem. Int. Ed.* **2015**, *54*, 746–784.

[120] R. Zhong, A. Pöthig, D. C. Mayer, C. Jandl, P. J. Altmann, W. A. Herrmann, F. E. Kühn, *Organometallics* **2015**, *34*, 2573–2579.

[121] F. Hackenberg, H. Mueller-Bunz, R. Smith, W. Streciwilk, X. Zhu, *Organometallics* **2013**, *32*, 5551–5560.

[122] T. Simler, P. Braunstein, A. A. Danopoulos, *Dalton Trans.* **2016**, *45*, 5122–5139.

[123] T. P. Pell, D. J. D. Wilson, B. W. Skelton, J. L. Dutton, P. J. Barnard, *Inorg. Chem.* **2016**, *55*, 6882–6891.

[124] V. J. Catalano, M. A. Malwitz, A. O. Etogo, *Inorg. Chem.* **2004**, *43*, 5714–5724.

[125] P. Ai, M. Mauro, C. Gourlaouen, S. Carrara, L. D. Cola, Y. Tobon, U. Giovanella, C. Botta, A. A. Danopoulos, P. Braunstein, *Inorg. Chem.* **2016**, *55*, 8527–8542.

[126] A. J. A. III, S. F. Gamper, J. C. C. F. Davidson, *J. Am. Chem. Soc.* **1994**, *116*, 4391–4394.

[127] M. Brendel, C. Braun, F. Rominger, P. Hofmann, *Angew. Chem. Int. Ed.* **2014**, *53*, 8741–8745.

[128] A. Huffer, B. Jeffery, B. J. Waller, A. A. Danopoulos, *C. R. Chimie* **2013**, *16*, 557–565.

[129] A. P. Prakasham, P. Ghosh, *Inorg. Chim. Acta* **2015**, *431*, 61–100.

[130] A. A. Danopoulos, D. Pugh, J. A. Wright, *Angew. Chem. Int. Ed.* **2008**, *47*, 9765–9767.

[131] H. Günther, *NMR Spektroskopie*, Georg Thieme Verlag Stuttgart, **1992**.

[132] N. Neureiter, *J. Org. Chem.* **1959**, *24*, 2044–2046.

[133] J. Berdig, M. Lutz, A. L. Spek, E. Bouwman, *Organometallics* **2009**, *28*, 1845–1854.

[134] T. Böttcher, B. S. Bassil, L. Zhechkov, T. Heine, G.-V. Röschenthaler, *Chem. Sci.* **2013**, *4*, 77–83.

[135] M. V. Baker, B. W. Skelton, A. H. White, C. C. Williams, *J. Chem Soc. Dalton Trans.* **2001**, 111–120.

[136] A. Cassel, *Acta Cryst. Sect. B.* **1979**, *35*, 174–177.

[137] W. A. Herrmann, M. Elison, J. Fischer, C. Koecher, G. R. J. Artus, *J. Org. Chem.* **1999**, *575*, 80–86.

[138] T. A. P. Paulose, S. C. Wu, J. A. Olson, T. Chau, N. Theaker, M. Hassler, J. W. Quail, S. R. Foley, *Dalton Trans.* **2012**, *41*, 251–260.

[139] A. Chartoire, A. Boreux, A. R. Martin, S. P. Nolan, *RSC Adv.* **2013**, *3*, 3840–3843.

[140] Q. Chen, L. Lv, M. Yu, Y. Shi, Y. Li, G. Pang, C. Cao, *RSC Adv.* **2013**, *3*, 18359–18366.

[141] G. C. Fortman, S. P. Nolan, *Chem. Soc. Rev.* **2011**, *40*, 5151–5169.

[142] S. Kozuch, J. M. Martin, *ACS Catalysis* **2011**, *1*, 246–253.

[143] M. Ghiaci, M. Zarghani, A. Khojastehnezad, F. Moeinpour, *RCS Adv.* **2014**, *4*, 15496–15501.

[144] F. Rajabi, W. R. Thiel, *Adv Synth. Catal.* **2014**, *356*, 1873–1877.

[145] Y. Takeda, Y. Ikeda, A. Kuroda, S. Tanaka, S. Minakata, *J. Am .Chem. Soc.* **2014**, *136*, 8544–8547.

[146] G. N. Marion, O. Navarro, J. Mei, E. D. Stevens, N. M. Scott, S. P. Nolan, *J. Am. Chem. Soc.* **2006**, *128*, 4101–4111.

[147] W. de Graaf, J. Boersma, W. J. J. Meets, A. L. Spek, G. van Koten, *Organometallics* **1989**, *8*, 2907–2917.

[148] S. S. Subramanium, L. M. Slaughter, *Dalton Trans.* **2009**, 6930–6933.

[149] M. G. Gardiner, W. A. Herrmann, C.-P. Reisinger, J. Schwarz, M. Spiegler, *J. Organomet. Chem.* **1999**, *572*, 239–247.

[150] J. Schwarz, V. P. W. Böhm, M. G. Gardiner, M. Grosche, W. A. Herrmann, W. Hieringer, G. Raudaschl-Sieber, *Chem. Eur. J.* **2000**, *6*, 1773–1780.

[151] P. D. W. Boyd, A. J. Edwards, M. G. Gardiner, C. C. Ho, M.-H. Lemèe-Cailleau, D. S. McGuinness, A. Riapanitra, J. W. Steed, D. N. Stringer, B. F. Yates, *Angew. Chem. Int. Ed.* **2010**, *49*, 6315–6318.

[152] C. C. C. Johansson Seechurn, T. Sperger, T. G. Scrase, F. Schoenebeck, T. J. Colacot, *J. Am. Chem. Soc.* **2017**, *139*, 5194–5200.

[153] M. J. Bennett, F. A. Cotton, D. L. Weaver, R. J. Williams, W. H. Watson, *Acta Cryst.* **1967**, *23*, 788–796.

[154] S. Ahrens, T. Strassner, *Inorg. Chim. Acta* **2006**, *359*, 4789–4796.

[155] M. G. Gardiner, C. C. Ho, F. M. Mackay, D. S. Mcguinness, M. Tucker, *Dalton Trans.* **2013**, *42*, 7447–7457.

[156] S. Jamali, D. Milic, R. Kia, Z. Mazloomi, H. Abdolahi, *Dalton Trans.* **2011**, *40*, 9362–9365.

[157] R. E. Douthwaite, D. Haüssinger, M. L. H. Green, P. J. Silcock, *Organometallics* **1999**, *18*, 4584–4590.

[158] V. Khlebnikov, M. Heckenroth, H. Müller-Bunz, M. Albrecht, *Dalton Trans.* **2013**, *42*, 4197–4207.

[159] S. Ahrens, E. Herdtweck, S. Goutal, T. Strassner, *Eur. J. Inorg. Chem.* **2006**, 1268–1274.

[160] E. E. Drinkel, L. Wu, A. Linden, R. Dorta, *Organometallics* **2014**, *33*, 627–636.

[161] W. L. F. Armarego, C. L. L. Chai, *Purification of Laboratory Chemicals*, *Vol. 5. Auflage*, Oxford, **2003**.

[162] G. M. Sheldrick, *SHELXS 97, Programm for the Solution of Crystal Strucutures*, Sheldrick, **1997**.

[163] G. M. Sheldrick, *Acta Cryst.* **1990**.

[164] G. M. Sheldrick, *SHELXTL, Bruker Analytical X-ray Division, Madison, WI*, **2001**.